Indian Institute of Technology Guwahati
Department of Physics
Ph.D. Thesis

Neutron stars and black holes: Insights from modified and EiBI gravity models

Muhammed Shafeeque

Thesis Supervisor: Dr. Malay Kumar Nandy
August 2025

Neutron stars and black holes: Insights from modified and EiBI gravity models

A Thesis submitted for the award of the degree of

Doctor of Philosophy in Physics

by

Muhammed Shafeeque

Thesis Supervisor: **Dr. Malay Kumar Nandy**

Department of Physics

Indian Institute of Technology Guwahati

Guwahati 781039 India

August 2025

Declaration

The work contained in the thesis entitled "**Neutron stars and black holes: Insights from modified and EiBI gravity models**" has been carried out at the Department of Physics, Indian Institute of Technology Guwahati, India, by me with the supervision of Dr. Malay Kumar Nandy. The material of this thesis has not been submitted elsewhere for any other degree. Works presented in the thesis are all my own unless referenced to the contrary in the text.

12 August 2025 **(Muhammed Shafeeque)**

Disclamer

The bibliography included in this thesis is by no means complete but contains the ones which are consulted thoroughly by me. I apologize for inadvertently missing out some of the research papers, review articles and other scientific documents pertaining to the focus of this thesis.

Certificate

Indian Institute of Technology Guwahati
Department of Physics
Guwahati 781039 India

Dr. Malay K. Nandy
Associate Professor
Phone: +91-(361)-258-2706, 4706
Mobile: +91-94010-86706
Email: mknandy@iitg.ac.in

This is to certify that the work contained in the thesis entitled "**Neutron stars and black holes: Insights from modified and EiBI gravity models**" has been carried out by Muhammed Shafeeque (Roll No. 196121020) with my supervision, and that this work has not been submitted elsewhere for the award of any other degree.

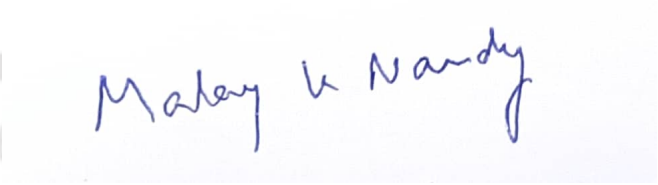

12 August 2025 (Malay K. Nandy)

To my partner

Jenny

and

to my parents

Abdul Majeed and Safiya

Acknowledgements

I would like to express my deepest gratitude to all those who have contributed to my academic journey and personal growth during my PhD in theoretical physics, focusing on black holes and neutron stars.

First and foremost, I am profoundly grateful to my supervisor, Dr. Malay Kumar Nandy, for his guidance, insightful theoretical inputs, valuable comments, suggestions, and meticulous corrections that shaped this thesis. His unwavering support—both academic and personal—helped me navigate the challenges of my doctoral work. His passion for understanding the physics of nature and his wide-ranging reading inspired me to strive for greater depth in my own research. Our stimulating discussions on various subjects, including my thesis, enriched my understanding immensely. With his deep knowledge and mastery of the subject, he consistently guided me toward achieving the best possible outcomes. He is one of the finest teachers I have known, and I learned greatly from our academic interactions, including the courses where I served as his teaching assistant. His constant encouragement brought out the researcher in me.

I gratefully acknowledge the Ministry of Education, Government of India, for financial support, and the Indian Institute of Technology Guwahati for providing the necessary infrastructure, including advanced computational facilities such as supercomputers, as well as accommodation and other amenities.

I extend my sincere thanks to my doctoral committee—Dr. Bibhas Ranjan Majhi (Chair), Dr. Meduri C. Kumar, and Prof. Sukanta Pati—for their valuable feedback and critical evaluations during my annual progress reviews and synopsis seminar. I also thank the Heads of the Department of Physics during my PhD—Prof. Subhradeep Ghosh, Prof. Alagarswami Perumal, and Prof. Basanta Ranjan Barua—for their support throughout my doctoral journey.

I further express my sincere thanks to my reviewers, Prof. S. Shankaranarayanan and Prof. Nicolas Yunes, for their valuable comments that helped improve this thesis. I also

thank my viva voce board members, Dr. Sayan Chakrabarti and Prof. Rajen K. Sinha.

I am grateful to all my physics teachers, beginning from my undergraduate studies, whose teaching laid the foundation for this journey.

I am indebted to Dr. Arun Mathew, whom I consider a brother and with whom I had the privilege of collaborating on two research works under the guidance of Dr. Nandy. Our time working together at IIT Guwahati was both academically productive and personally enriching.

I would also like to thank my research group—Bhargabi Saha, Hrisikesh Thakur, Harpreet Singh, Vishal, Nihar Ranjan Ghosh, and Surendra Gaur—for the valuable discussions, exchange of ideas, and camaraderie that made our research environment lively and inspiring. The moments of laughter we shared will remain cherished memories.

To my friends from the institute—Dr. Siva Kumar, Tanveera Ronaque Sarhadi, Dr. Esha Bhatia, Dr. Nikhil Danny Babu, Aswani K., K. Chitra, Dheeraj Paleri, Midhun Mathew, Ajaya Samadder, Al Ameen, Dr. Saraswati Devi, Ravinder Chahal, Alolika Roy, Mohammed Salim, Aditya Anand, the late Surya, Fayyad, Dr. Vivek Venugopal, Dr. Sumit Dey, Dr. Sahabub Jahedi, Tanaya Hazarika, Pranamika Doimary, Hemant Dogra, Pratik Nanda, Upasana Hazarika, Gargi Deka, Dr. Shilpa Krishnan, Dr. Adeep Hussain, Ajmal Rasaq, and many others—I am grateful for the time we shared, the insightful academic discussions, and the memorable moments that made my time at IIT Guwahati truly enriching.

I also express my sincere gratitude to the friends who inspired me to pursue a career in academia—Dr. Jayaraj K. P., Dr. Remya Ramakrishnan, Dr. Musadhique K. P., Dr. Riscob James Bright, Noushaba Nas, Ajmal V., Limseer Ali, Subair, Dr. Haris M. N., and Dr. Jabir T. K.—for their encouragement and belief in me during the early stages of my academic journey.

I am forever grateful to my parents, Abdul Majeed and Safiya, for their unwavering love, patience, and support throughout my life. They stood by me even when I could not be there for them in times of need, and their faith in me has been my strength.

Finally, I express my deepest gratitude to my partner in life, Jenny Majeed, the most important person outside of academia. Her constant love and support sustained me throughout my PhD and the years we have spent together. Her unwavering motivation inspired me to join IIT and successfully complete my thesis in theoretical physics. Through times of intense pressure and self-doubt, she was always there, encouraging me to believe in myself. She carried the burdens of the world outside my academic life so that I could focus entirely on my research. Without her, this thesis—and perhaps even my PhD journey—would not have been possible.

12 August 2025 Muhammed Shafeeque

Synopsis

This thesis provides a comprehensive investigation into the structural and stability properties of neutron stars and black holes in conventional and modified gravitaty theories. A summary of the thesis is presented below.

Neutron star with deconfined quark core

The recent observational evidences for existence massive neutron stars [2, 4, 5, 62, 128] naturally require a theoretical explanation including their stellar structure and composition of matter interior to such massive objects. However, such evidences bring about constraints on the equation of state, so that a stellar mass of $\sim 2\ M_{\odot}$ could be obtained ([197]). The nature of equation of state for the matter in the neutron star plays an important role in determining its maximal mass.

Consequently, efforts have been made to obtain an equation of state with a high degree of stiffness. In fact, high stiffness was incorporated for the high density regions of the star by removing the hyperons from the nuclear matter ([78, 84, 104]). When some of these hadronic equations of state are employed throughout the star, they violate the condition of causality ($c_s \leq c$) just before the gravitational instability sets in, so that, at ultra-high densities in the core region, the speed of sound c_s exceeds the speed of light c.

It is also important to note that, when these hadronic equations of state are employed throughout the star, in order to attain the maximal mass configurations ($M_{\rm max} \sim 2\ M_{\odot}$), the central densities turn out to be $\rho_c \sim 10\ \rho_{\rm nuc}$, where $\rho_{\rm nuc} = 2.67 \times 10^{14}$ g cm^{-3} is the nuclear saturation density. Quark deconfinement is expected to occur at such ultra-high densities in the core region ([108, 109, 172]). Noting that the central density of a maximally massive neutron star is well above the nuclear saturation density, a deconfined quark core in the central region is motivated in this work.

These facts indicate that hadronic equations of state are not adequate representations for the ultra-high density core region. On the other hand, they are most suitable to repre-

sent the outer regions of lower densities (where they are causal).

We thus motivate the scenario of deconfined quark matter in the core region and hadronic matter in the region outside the core. For a simplistic analysis of this scenario, we employ the MIT bag model ([110, 174]) to represent the deconfined quark matter in the core region and one of the unified equations of state (SLy4, FPS and BSk $19-21$ [91, 157]) for the hadronic matter in the outer region. With this construction, we find that the hadronic equations of state remain causal because of crossover to the MIT bag model equation of state, so that causality is maintained throughout the star.

The Einstein field equation

$$G_{\mu\nu} = R_{\mu\nu} - \frac{1}{2} g_{\mu\nu} R = \kappa T_{\mu\nu}, \tag{1}$$

with the energy-momentum tensor

$$T_{\mu\nu} = \frac{(\varepsilon + P)}{c^2} u_\mu u_\nu + g_{\mu\nu} P, \tag{2}$$

where $\varepsilon = \rho c^2$ is the energy density, P is the pressure, and u^μ is the four-velocity with $u^\mu u_\mu = -c^2$, lead to the TOV equations

$$\frac{dP}{dr} = \frac{-\left[P(r) + \varepsilon(r)\right]}{r\left[c^2 r - 2Gm(r)\right]} \left[Gm(r) + \frac{4\pi G}{c^2} r^3 P(r)\right], \tag{3}$$

and

$$\frac{dm(r)}{dr} = \frac{4\pi r^2 \varepsilon(r)}{c^2}. \tag{4}$$

We integrate the above equations simultaneously for the interior as well as the exterior of the neutron star employing different equations of state (see Table 2.1).

As shown in Table 2.1, these combined equations of state yield maximal masses slightly less than $2\ M_\odot$, whereas, the MIT-BSk21 combination almost touches this value. In addition, we find that the causality condition ($c_s \leq c$) is well-respected for all these combined equations of state. Figure 2.8 displays the mass versus central density curves for different combinations of the MIT bag model with the unified equations of state. In each case, the maximum stable mass $M_{\max}$ corresponds to the maxima of the curve, where $\frac{\partial M}{\partial \rho_c} = 0$.

Equation 2.6 clearly shows that the integrand determining the total mass of the star is weighted by r^2 and the peak in ρr^2 occurs far from the center in Figure 2.6. Thus the dominant contribution to the total mass comes from the region around the peak. The regions near the center as well as the surface give small contributions to the total mass.

The combination MIT-BSk21 yields the highest maximal mass as its peak in ρr^2 occurs at the highest radial coordinate r (among the combinations considered). It may also be important to note that the deconfined quark core for MIT-BSk21 extends to a higher radial coordinate than the other combinations. The peak in ρr^2 occurs in the outer hadonic matter region and it is moved to a higher radial coordinate for MIT-BSk21 than in the other combinations. The positions of the peaks in ρr^2 are well-correlated with the maximal mass as displayed in Table 2.1.

As shown earlier by [170] and [83], a rapidly rotating neutron star can support $20-25$ $\%$ more mass than the gravitational threshold of the non-rotating neutron star. Our gravitational threshold being 1.98 $M_\odot$ for a non-rotating neutron star, the increased threshold due to rotation would be $2.38 - 2.48$ $M_\odot$. This is consistent with the new benchmark of 2.35 $M_\odot$ [164] that may explain the existance of massive pulsars.

Neutron star in $f(R)$ Gravity

One of the simplest extensions of general relativity is the $f(R)$ gravity theory, where the function $f(R)$ denotes an arbitrary function of the Ricci scalar R [28], replacing R in the Einstein-Hilbert action. In 1980, A.A. Starobinsky proposed a specific form of $f(R)$ given by $f(R) = R + \alpha R^2$ [179]. This model is considered a viable alternative to scalar field models of inflation.

However, relativistic stars in the Starobinsky $f(R)$ model were found to be problematic due to the appearance of singularities in the strong gravity regime [85, 117, 118]. Through numerical analysis using a polytropic equation of state, Babichev and Langlois [17] demonstrated the existence of singularity-free neutron stars in $f(R)$ gravity, provided the equation of state satisfies the condition $-\rho + 3P < 0$. This condition imposes a limit on the central density of stable relativistic stars, thereby preventing the formation of stars with densities beyond a critical threshold. Nonetheless, $f(R)$ gravity allows for a higher stable maximum mass $M_{\rm max}$ than general relativity, for a given equation of state.

As discussed in previous work, explaining the existence of massive neutron stars typically requires hadronic equations of state with high stiffness. Such equations often violate the condition $-\rho + 3P < 0$, thereby limiting the possibility of forming superdense stars in $f(R)$ gravity.

In this study, we analyze the structure of relativistic stars using the combined equations of state introduced previously. Employing the hybrid equations of state—MIT-SLy, MIT-BSk20, and MIT-BSk21—we determine the maximal stable mass $M_{\rm max}$ for various values of the parameter $\alpha = (1, 3, 5, 10)$, while ensuring that the condition $-\rho + 3P < 0$. Our

results show that the maximal stable mass, as observed from infinity, is larger in $f(R)$ gravity than in general relativity, as reported in the earlier work. However, the mass at the stellar surface, M_s, is smaller compared to general relativity. This discrepancy arises due to an additional contribution to the mass at infinity, attributed to the presence of a gravitational halo surrounding the star, since the Ricci scalar remains non-zero outside the surface.

Table 3.1 presents the maximal stable mass $M_{\max}$ as measured by a distant observer, the corresponding central density ρ_c, stellar radius r_s, surface mass M_s, and central Ricci scalar value R_c for different values of the parameter α, for each combination of equations of state.

Charged black holes in Eddington-inspired Born-Infeld gravity

In this work, we investigate the spacetime structure of charged black holes within the framework of Eddington-inspired Born-Infeld (EiBI) gravity. This theory represents a modification of the original Eddington action, formulated in analogy with the Born-Infeld model of electrodynamics [34]. The EiBI action applicable to a general astrophysical system [16] is expressed as

$$S(g,\tilde{\Gamma},\Psi)=\frac{1}{\kappa}\int d^4x\left(\sqrt{-|g_{\mu\nu}+\kappa\tilde{R}_{\mu\nu}(\tilde{\Gamma})|}-\lambda\sqrt{-g}\right)+\int d^4x\sqrt{-g}\mathcal{L}_m(g,\Psi). \quad (5)$$

Here, $\lambda = 1+\kappa\Lambda$, $g_{\mu\nu}$ denotes the metric tensor, and $\mathcal{L}m(g,\Psi)$ is the matter Lagrangian, which depends on both the metric $g_{\mu\nu}$ and the matter field Ψ. EiBI gravity is a Palatini-type theory [145], setting itself apart from general relativity by treating the affine connection $\Gamma^{\mu}_{\nu\rho}$ and the metric tensor $g_{\mu\nu}$ as independent geometrical entities.

We consider a charged black hole within the EiBI framework. Starting with a static, spherically symmetric metric $ds^2=-f(r)h^2(r)dt^2+\frac{1}{f(r)}dr^2+r^2\left(d\theta^2+\sin^2\theta d\varphi^2\right)$, we derive the field equations. This results in a differential equation for the metric coefficient, which depends on the electric charge Q and the EiBI coupling parameter κ, leading to a complex structure. Using this setup, we analytically examine the behaviour of the metric function in various regions of the black hole spacetime. Specifically, we explore the analytical forms of the metric coefficients and the Kretschmann scalar in the vicinity of the center, in intermediate regions, and near the event horizon, for both positive and negative EiBI couplings ($\kappa > 0$ and $\kappa < 0$). This analysis provides a comprehensive understanding of the spacetime properties of EiBI-Maxwell black holes.

Our findings indicate that, at large distances, the EiBI charged black hole space-

time asymptotically approaches that of the Reissner-Nordström solution, with a vanishing Kretschmann scalar. For positive coupling ($\kappa > 0$), the metric coefficient $f(r)$ diverges as r^{-2} near the center, while $h(r)$ vanishes as r^2. However, the Kretschmann scalar diverges as r^{-8} in this case. In contrast, for negative coupling ($\kappa < 0$), the spacetime becomes undefined in the central region due to the emergence of imaginary components in the metric function.

In the case $\kappa > 0$, the metric coefficients $f(r)$ and $f(r)h^2(r)$ both diverge as $(r-a)^{-1}$, where $a = (\kappa Q^2)^{1/4}$, and the Kretschmann scalar $\mathcal{K}(r)$ diverges as $(r-a)^{-6}$ as $r \to a$. For $\kappa < 0$, the metric coefficient $f(r)$ tends to zero like $(r-b)^{1/2}$, while $h(r)$ and $f(r)h^2(r)$ diverge as $(r-b)^{-1/2}$, where $b = (|\kappa|Q^2)^{1/4}$. In this scenario as well, the Kretschmann scalar $\mathcal{K}(r)$ diverges as $(r-b)^{-6}$ as $r \to b$.

$$ds^2 = -f(r)h^2(r)dt^2 + \frac{1}{f(r)}dr^2 + r^2\left(d\theta^2 + \sin^2\theta d\varphi^2\right), \tag{6}$$

By numerically integrating the field equations derived from the EiBI action, we determine the behavior of the metric coefficients $f(r)$, $h(r)$, $f(r)h^2(r)$, and the Kretschmann invariant $\mathcal{K}(r)$ for different values of the black hole charge Q and the EiBI coupling parameter κ. The numerical results closely match the analytical behavior obtained earlier from the EiBI-Maxwell field equations.

Figure 4.1 shows the radial profiles of the metric potential $f(r)$ and the Kretschmann scalar $\mathcal{K}(r)$ for the case $\kappa > 0$. Figure 4.1a illustrates the behavior of $f(r)$ for $\kappa/M^2 = 3$ and various values of electric charge Q. It is observed that in EiBI gravity, black holes can possess an additional singularity at $r = a = (\kappa Q^2)^{1/4}$, which marks a significant departure from general relativity. This singularity appears consistently for all values where $\kappa > 0$.

In the absence of matter, EiBI gravity reduces to general relativity. As the value of Q increases, the event horizon is seen to shift inward, as shown in Figure 4.1a for $Q/M = 0.5$ and 0.7. For sufficiently large Q, such as $Q = 1.5M$, the event horizon disappears, making the singularity at $r = a = (\kappa Q^2)^{1/4}$ a naked singularity. Thus, in contrast to the Reissner-Nordström case, EiBI gravity permits unphysical solutions without an event horizon.

By setting $\kappa = 0$, the metric coefficients reduce to those of the Reissner-Nordström solution. Our numerical results support this fact, as shown by the dotted line in Figure 4.1b. This figure also presents the radial profiles of $f(r)$ for different values of the coupling parameter $\kappa/M^2 > 0$, with the electric charge fixed at $Q = 0.5M$. As seen in Figure 4.1b, for $\kappa/M^2 = 3$ and 10, the event horizon shifts inward with increasing κ/M^2.

For large values such as $\kappa/M^2 = 16$, the event horizon vanishes, and the singularity becomes naked, again yielding an unphysical black hole. Figures 4.1c and 4.1d show the divergence of the Kretschmann scalar $\mathcal{K}(r)$ at $r = a = (\kappa Q^2)^{1/4}$.

We further analyze the geodesic motion of a test particle in the EiBI-Maxwell black hole spacetime. By computing the effective potential, we derive the conditions required for the existence of stable orbits around the black hole. Additionally, we evaluate the precession of the perihelion of the particle's orbit and find that it exhibits significant deviations from the predictions of general relativity.

Stability of charged scalar hair on Reissner-Nordström black holes

The Israel-Carter theorem, commonly referred to as the "no-hair theorem," restricts the permissible parameters characterizing a black hole to mass, electric charge, and angular momentum. In this context, Bekenstein formulated a set of no-hair theorems for various black hole configurations involving both neutral and electrically charged scalar fields.

In this work, we consider the Einstein-Maxwell-charged scalar field model,

$$S = \int d^4x\sqrt{-g}\left[\frac{R}{2} - (D_\mu\phi)^* D^\mu\phi - \mu^2\phi^*\phi - \frac{1}{4}F_{\mu\nu}F^{\mu\nu}\right], \tag{7}$$

where an electrically charged scalar field is gauge-coupled to the Maxwell field in the background of a charged black hole described by a static, spherically symmetric metric. Specifically, we focus on a quadratic scalar potential without including higher-order terms and do not impose any constraints on the relative magnitudes of the scalar charge and the black hole charge.

We begin by verifying that all relevant energy conditions, along with the causality condition, are satisfied within the Einstein-Maxwell-charged scalar field framework. This involves examining the energy conditions derived from the mixed components of the energy-momentum tensor, as well as enforcing causality. By expressing these mixed components in terms of the scalar field and other physical quantities, we find that all the energy and causality conditions hold. This result supports the possibility of the existence of charged hairy black hole solutions.

Contents

List of Figures

List of Tables

Chapter 1

Introduction

1.1 Prelude

Albert Einstein's theory of General Relativity has revolutionized our understanding of gravity, transforming it from the Newtonian concept of a force acting between masses into a manifestation of spacetime curvature. In this framework, gravity is no longer a force in the traditional sense, but a geometric property of a dynamic spacetime that interacts with matter and light. The mathematical formulation of General Relativity is grounded in four-dimensional Riemannian geometry, where the metric tensor $g_{\mu\nu}$ encodes all the information about the geometry of spacetime. A fundamental principle of the theory is *general covariance*, which asserts that the laws of physics retain their form under arbitrary coordinate transformation.

Solutions to the Einstein field equations—both in vacuum and in the presence of matter fields—have uncovered a wide array of physical phenomena, particularly involving compact, strongly gravitating objects such as black holes and neutron stars. These solutions provide insight into the structure of spacetime and the nature of singularities associated with such objects. The characteristics of spacetime vary depending on the type of solution: in vacuum, where no matter is present; in *electrovacuum*, where the central object is electrically charged; and in rotating scenarios. The simplest spherically symmetric vacuum solution to Einstein's equations is the Schwarzschild metric, which describes a non-rotating, uncharged black hole. When the spherically symmetric object carries an electric charge, the appropriate solution is the Reissner-Nordström metric, representing a charged, static black hole. In cases where the black hole is rotating, the solution is given by the Kerr metric, accounting for the angular momentum.

To date, General Relativity remains the most successful and extensively tested theory of gravitation. Its predictions have been confirmed across a wide range of scenar-

ios, particularly in weak gravitational fields, such as those found within the solar system [6, 72, 169, 190]. One of the earliest and most significant confirmations came from its ability to accurately account for the anomalous precession of Mercury's perihelion. In 1915, Einstein applied General Relativity to this problem and calculated an advance of approximately 43 arcseconds per century [73], closely matching the observed discrepancy that Newtonian gravity could not explain. This success provided a compelling early validation of the theory in regimes where gravitational effects are stronger than those captured by Newtonian mechanics.

A second major confirmation came through the deflection of light by gravity, experimentally verified during the total solar eclipse of 1919. General Relativity predicts that light rays passing near a massive object like the Sun should be deflected by approximately 1.75 arcseconds. This prediction was famously confirmed by an expedition led by Arthur Eddington, who measured the bending of starlight around the Sun during the eclipse [71], providing one of the earliest and most widely publicized pieces of evidence in support of the theory.

Additional tests of General Relativity include the *Shapiro time delay*, discovered in the 1970s, which involves the increased travel time of radar signals as they pass near massive objects [169]. Another milestone was the observation of the Hulse-Taylor binary pulsar PSR B1913+16 [105], which provided indirect evidence for the existence of gravitational waves. The observed orbital decay of the binary system matched the prediction of General Relativity for energy loss due to gravitational radiation to within 0.3%, marking a significant triumph for the theory.

With technological advancements, even more profound predictions of General Relativity have been confirmed. The direct detection of gravitational waves—ripples in the fabric of spacetime—by LIGO and Virgo [1, 2], and the imaging of black holes at the centers of galaxies by the Event Horizon Telescope [58–61], have further reinforced the theory's robustness. These observations not only validate General Relativity under extreme conditions but also open new windows into the nature of spacetime and compact astrophysical objects.

Beyond its successes in describing local gravitational phenomena, General Relativity also provides the mathematical foundation for modern cosmology, offering a framework to understand the large-scale structure and evolution of the universe. In 1917, Einstein applied his field equations to the cosmos in his seminal paper "*Kosmologische Betrachtungen zur allgemeinen Relativitätstheorie*" ("*Cosmological Considerations in the General Theory of Relativity*") [74]. His equations originally predicted a dynamic universe—either expanding or contracting, which conflicted with the then-prevailing belief in a static

cosmos. To reconcile his theory with this belief, Einstein introduced the cosmological constant, a term intended to counterbalance gravitational attraction to yield a static universe. However, this modification was later rendered unnecessary by Edwin Hubble's 1929 observation of the redshift of distant galaxies, which provided compelling evidence for an expanding universe, just as General Relativity had initially predicted.

A major turning point in cosmology came in 1998 with a discovery that profoundly reshaped our understanding of the universe. Two independent research collaborations—the Supernova Cosmology Project and the High-Z Supernova Search Team—observed distant Type Ia supernovae and found that the expansion of the universe is not slowing down, as previously assumed, but is instead accelerating. This unexpected result suggested the presence of a mysterious, repulsive component of the energy budget in the universe, now referred to as *dark energy*. The re-emergence of the cosmological constant, interpreted in this modern context, highlights the continuing relevance and adaptability of Einstein's theory in explaining phenomena on cosmic scales.

While General Relativity (GR) has proven to be an extraordinarily successful framework for explaining gravitational phenomena across a vast range of scales—from the motion of planets to the expansion of the universe—it is widely regarded as incomplete. One of the most fundamental theoretical limitations of GR lies in its prediction of singularities under quite general conditions. The seminal singularity theorems developed by Penrose and Hawking demonstrate that, under reasonable physical assumptions, regions of infinite spacetime curvature—so-called *singularities*—are inevitable within the classical theory [94, 153, 155]. These include the central singularity inside black holes and the initial singularity at the origin of the universe, commonly associated with the Big Bang.

At the singularity, the curvature of spacetime diverges, and the predictive power of the theory breaks down, indicating a fundamental incompleteness in classical GR. This failure becomes particularly acute in strong-field regimes, where quantum effects are expected to play a significant role. Consequently, the presence of singularities suggests that General Relativity, while robust in many domains, cannot fully describe the physics of extreme gravitational situations [95, 135, 154, 178, 180, 181, 189]. Although this realization has motivated the search for a more fundamental theory of gravity—one that can seamlessly incorporate quantum principles—such motivation has remained mostly elusive, and no generally accepted quantum theory of gravity exists to date.

However, to circumvent the theoretical limitations of General Relativity, numerous modifications to the theory have been proposed over the decades [28, 36, 47, 63, 67, 93, 140, 179]. These approaches seek to extend or revise General Relativity in a manner that remains consistent with its well-tested predictions, while offering improved behavior in

regimes of high curvature.

Among the most extensively studied of such modifications is $f(R)$ gravity, in which the Einstein-Hilbert action is generalized by replacing the Ricci scalar R with a more general function $f(R)$. Although this modification appears minimal, it introduces a new dynamical degree of freedom into the gravitational sector, enabling a more general set of gravitational dynamics without the need to invoke additional assumptions. Importantly, when $f(R) = R$, standard General Relativity is recovered, making this approach a natural extension rather than a radical departure.

The $f(R)$ gravity theory has attracted significant interest in cosmology, especially for its potential to account for the observed late-time acceleration of the universe without requiring a cosmological constant or traditional dark energy. By choosing suitable forms of $f(R)$, one can derive effective field equations that mimic dark energy behavior, thus offering a geometric resolution to the cosmological constant problem. Moreover, certain models, such as the Starobinsky model, also provide a compelling mechanism for early-universe inflation, suggesting that both early- and late-time cosmic acceleration might be explained within a single unified framework.

From a theoretical standpoint, $f(R)$ models often exhibit improved ultraviolet behavior. The additional scalar degree of freedom emerging from the modified action—commonly referred to as the *scalaron*—acts like a dynamical field that mediates new gravitational effects across both astrophysical and cosmological scales. In high-curvature regions where GR would predict singularities, this scalar field can moderate the divergence, potentially yielding a more complete description of gravity.

However, any viable $f(R)$ theory must also withstand experimental and observational scrutiny. Consistency with Solar System tests, gravitational wave propagation, and large-scale structure formation imposes tight constraints on the functional form of $f(R)$. While many proposed models are ruled out under these requirements, others remain consistent with current data, keeping $f(R)$ gravity as a promising candidate for extending our understanding of gravitation and the geometric structure of spacetime.

Another compelling avenue for extending General Relativity is found in *Eddington-inspired Born-Infeld (EiBI) gravity*, a theory motivated by both the affine formulation of gravity proposed by Eddington and the nonlinear structure of Born-Infeld electrodynamics. EiBI gravity modifies the gravitational action in such a way that it remains equivalent to GR in vacuum, but exhibits significant deviations in the presence of matter—particularly under high-density conditions. This distinctive feature makes the theory especially attractive for addressing singularities in gravitational collapse and early-universe cosmology.

The action in EiBI gravity is formulated using the Palatini approach, in which the metric and affine connection are treated as independent variables. This formalism allows the theory to preserve second-order field equations while avoiding ghost degrees of freedom—an issue that often plagues higher-derivative extensions of GR. The Born-Infeld-type structure of the action introduces a natural high-energy cutoff scale, analogous to the string scale in Born-Infeld electrodynamics, which serves to regularize divergences in the gravitational sector.

Beyond its theoretical appeal, EiBI gravity has shown considerable promise in resolving the cosmological singularity problem. It has been demonstrated that in a universe filled with ordinary matter, the theory naturally introduces an upper bound on the energy density, effectively preventing the formation of a singularity at the beginning of cosmic evolution [14]. Depending on the choice of model parameters, the universe can undergo a nonsingular bounce—transitioning smoothly from a contracting phase to an expanding one—or exhibit oscillatory behavior between two finite density limits before eventually settling into a GR-like expansion phase [165]. Within the cosmological context, EiBI gravity has been widely studied in connection with inflationary dynamics [56], the behavior of linear and scalar perturbations [57, 126, 194], and the evolution of large-scale structure [70], further highlighting its viability as an alternative cosmological framework.

The resolution of singularities in cosmology has naturally led to investigations of gravitational collapse within the EiBI framework. Studies of both non-relativistic [147] and relativistic [147, 148] dust collapse have shown that, under suitable circumstances, the theory avoids the formation of singularities. In particular, a positive value of the EiBI coupling parameter κ plays a critical role in regulating high-curvature behavior. However, in relativistic collapse scenarios, certain constraints on κ emerge under which the formation of black holes remains possible [148]. Further analysis in lower-dimensional spacetimes has revealed additional subtleties: for instance, in $2+1$ dimensions, singularities that do form are typically naked unless the parameters lie within specific bounded ranges [167]. Moreover, in the context of recent observations of massive neutron stars, EiBI has been found to support supermassive stars, with maximal mass significantly larger compared to that of general relativity [92, 158, 168].

These results underscore the richness and flexibility of EiBI gravity in describing high-energy gravitational phenomena, particularly in regimes where General Relativity loses predictability.

1.2 Field equations in general relativity

The action in general relativity is given by

$$\mathcal{S} = \frac{c^3}{16\pi G}\int d^4x\,\sqrt{-g}\,\mathcal{L}_g + \int d^4x\,\sqrt{-g}\,\mathcal{L}_m \tag{1.1}$$

where $\mathcal{L}_g$ is the gravity Lagrangian, $\mathcal{L}_m$ is the matter Lagrangian, g is the determinant of the metric tensor $g_{\mu\nu}$, c is the velocity of light, and G is the universal gravitational constant.

Since gravity and the geometry are mutually correlated, the gravity Lagrangian must contain the metric tensor $g_{\mu\nu}$ and its first derivative. The most suitable choice for the gravity Lagrangian is $\mathcal{L}_g = R$, where R is the Ricci scalar. Ricci scalar has the advantage that it depends on $g_{\mu\nu}$, its first derivative $\partial_\alpha\, g_{\mu\nu}$, and the second derivative $\partial_\alpha\partial_\beta\, g_{\mu\nu}$, and it is linear in second derivative. Consequently, the second derivative does not contribute upon varying the action with respect to $g_{\mu\nu}$ and by integrating the total derivative term.

The choice of the matter Lagrangian $\mathcal{L}_m$ depends on the matter field present. For example, in the presence of a scalar field ϕ,

$$\mathcal{L}_m = -\frac{1}{2}\partial_\mu\phi\partial^\mu\phi - V(\phi), \tag{1.2}$$

where $V(\phi)$ is the scalar field potential. On the other hand, in the presence of an electromagnetic field,

$$\mathcal{L}_m = -\frac{1}{16\pi}F_{\mu\nu}F^{\mu\nu}, \tag{1.3}$$

where $F_{\mu\nu} = \partial_\mu\, A_\nu - \partial_\nu\, A_\mu$ is the electromagnetic tensor and A_μ is the electromagnetic vector potential.

1.2.1 Field equations and Einstein tensor

In the presence of any general matter field Ψ, the Einstein-Hilbert action is written as

$$\mathcal{S} = \frac{c^3}{16\pi G}\int d^4x\,\sqrt{-g}\,R + \int d^4x\,\sqrt{-g}\,\mathcal{L}_m(\Psi, g). \tag{1.4}$$

The corresponding field equations can be obtained following two distinct formalisms, namely, the metric formalism and the Palatini formalism.

1.2.1.1 Metric formalism

In the metric formalism, the field equations corresponding to the action (1.4) are obtained by varying the action with respect to the metric $g_{\mu\nu}$, leading to

$$\delta\mathcal{S} = \frac{c^3}{16\pi G}\int d^4x\,\delta\left(\sqrt{-g}\,R\right) + \int d^4x\,\delta\left(\sqrt{-g}\,\mathcal{L}_m\right), \tag{1.5}$$

where the symbol δX represents an infinitesimal variation of X. The variation in the first integral in (1.5) is expressed as

$$\delta\left(\sqrt{-g}\,R\right) = \delta\left(\sqrt{-g}\right)\,R + \sqrt{-g}\,\delta R. \tag{1.6}$$

Using property of a determinant $\frac{\delta|M|}{|M|} = \mathrm{tr}\,(\mathbf{M}\delta\mathbf{M})$ for a second rank tensor $\mathbf{M}$, we have

$$\delta\sqrt{-g} = -\frac{1}{2}\sqrt{-g}\,g_{\mu\nu}\,\delta g^{\mu\nu}, \tag{1.7}$$

where $\delta g_{\mu\nu}$ represents an infinitesimal change in the metric tensor $g_{\mu\nu}$.

From Riemann curvature tensor $R^{\lambda}_{\ \mu\beta\nu}$, the Ricci scalar is defined as $R = g^{\alpha\beta}g^{\mu\nu}R_{\alpha\mu\beta\nu}$, so that

$$\delta R = 2R_{\mu\nu}\,\delta g^{\mu\nu} + g^{\alpha\beta}g^{\mu\nu}\,\delta R_{\alpha\mu\beta\nu}. \tag{1.8}$$

Using the definition for the Riemann curvature tensor $R^{\lambda}_{\ \mu\beta\nu} = \partial_\beta\Gamma^{\lambda}_{\mu\nu} - \partial_\nu\Gamma^{\lambda}_{\mu\beta} + \Gamma^{\lambda}_{\beta\rho}\Gamma^{\rho}_{\mu\nu} - \Gamma^{\lambda}_{\nu\rho}\Gamma^{\rho}_{\mu\beta}$, we have

$$\delta R^{\lambda}_{\ \mu\beta\nu} = \nabla_\beta\,\delta\Gamma^{\lambda}_{\mu\nu} - \nabla_\nu\,\delta\Gamma^{\lambda}_{\mu\beta}, \tag{1.9}$$

where $\Gamma^{\alpha}_{\mu\nu}$ is the Christoffel symbol, an affine connection with respect to the metric $g_{\mu\nu}$, defined as

$$\Gamma^{\alpha}_{\mu\nu} = \frac{g^{\alpha\rho}}{2}\left(-\partial_\rho g_{\mu\nu} + \partial_\nu g_{\mu\rho} + \partial_\mu g_{\rho\nu}\right), \tag{1.10}$$

and ∇_μ is the covariant derivative defined with respect to the affine connection $\Gamma^{\lambda}_{\mu\nu}$. Substituting (1.9) in (1.8) gives

$$\delta R = R_{\mu\nu}\,\delta g^{\mu\nu} + \nabla_\beta\left(g^{\nu\lambda}\,\delta\Gamma^{\beta}_{\nu\lambda} - g^{\nu\beta}\,\delta\Gamma^{\lambda}_{\nu\lambda}\right). \tag{1.11}$$

Consequently,the variation in the first term of the Einstein-Hilbert action (1.4) is obtained by inserting (1.11) and (1.7) in (1.6), leads to

$$\delta\left(\sqrt{-g}\,R\right) = \sqrt{-g}\,R_{\mu\nu}\,\delta g^{\mu\nu} + \partial_\beta\left(\sqrt{-g}\,\mathcal{B}^{\beta}\right) - \frac{1}{2}\sqrt{-g}\,g_{\mu\nu}\,R\,\delta g^{\mu\nu}, \tag{1.12}$$

where $\mathcal{B}^\beta = g^{\nu\lambda}\,\delta\Gamma^\beta_{\nu\lambda} - g^{\nu\beta}\,\delta\Gamma^\lambda_{\nu\lambda}$.

On the other hand, the variation of the second integrand in the Einstein-Hilbert action (1.4) is obtained as

$$\delta\left(\sqrt{-g}\mathcal{L}_m\right) = -\frac{1}{2c}\sqrt{-g}T_{\mu\nu}\delta g^{\mu\nu}, \tag{1.13}$$

where $T_{\mu\nu}$ is the energy-momentum tensor, defined as

$$T_{\mu\nu} = cg_{\mu\nu}\mathcal{L}_m - 2c\frac{\delta\mathcal{L}_m}{\delta g^{\mu\nu}}. \tag{1.14}$$

Using the expressions (1.12) and (1.13), the variation (1.5) in the total action is finally obtained as

$$\begin{aligned}\delta\mathcal{S} =& \frac{c^3}{16\pi G}\int d^4x\,\sqrt{-g}\,\left(R_{\mu\nu} - \frac{1}{2}\,g_{\mu\nu}\,R\right)\,\delta g^{\mu\nu} \\ &+ \frac{c^3}{16\pi G}\int d^4x\,\partial_\beta\,\left(\sqrt{-g}\,\mathcal{B}^\beta\right) - \int d^4x\,\frac{1}{2c}\sqrt{-g}T_{\mu\nu}\delta g^{\mu\nu}.\end{aligned} \tag{1.15}$$

The second integrand in the above equation, $\partial_\beta\,\left(\sqrt{-g}\,\mathcal{B}^\beta\right)$, is the Gibbons-Hawking-York term, which is a total derivative. Using Gauss' theorem, the integral can be converted to an integral over a hypersurface surrounding the four volume. In the limits of integration, the fields do not vary, and hence the term vanishes to zero.

From Hamilton's principle of least action, condition for extremum is $\delta\mathcal{S} = 0$. Thus, (1.15) leads to the Einstein field equations

$$G_{\mu\nu} = R_{\mu\nu} - \frac{1}{2}\,g_{\mu\nu}\,R = \frac{8\pi G}{c^4}T_{\mu\nu}. \tag{1.16}$$

where $G_{\mu\nu}$ is the Einstein tensor. Using the Bianchi identity

$$\nabla_\mu R_{\alpha\beta\rho\nu} + \nabla_\nu R_{\alpha\beta\mu\rho} + \nabla_\rho R_{\alpha\beta\nu\mu} = 0, \tag{1.17}$$

and properties of the Riemann curvature tensor, in addition to contracting appropriate indices, it can be shown that

$$\nabla_\mu G^\mu_{\ \nu} = 0. \tag{1.18}$$

1.2.1.2 Tensor density

Under a general coordinate transformation $x^\mu \to x'^\mu$, a tensor quantity transform following the law

$$T'^{\mu_1\mu_2\ldots\mu_n}{}_{\nu_1\nu_2\ldots\nu_m} = \frac{\partial x'^{\mu_1}}{\partial x^{\rho_1}}\frac{\partial x'^{\mu_2}}{\partial x^{\rho_2}}\cdots\frac{\partial x'^{\mu_n}}{\partial x^{\rho_n}}\cdot\frac{\partial x^{\sigma_1}}{\partial x'^{\nu_1}}\frac{\partial x^{\sigma_2}}{\partial x'^{\nu_2}}\cdots\frac{\partial x^{\sigma_3}}{\partial x'^{\nu_m}}\,T^{\rho_1\rho_2\ldots\rho_n}{}_{\sigma_1\sigma_2\ldots\sigma_m} \tag{1.19}$$

The covariant derivative of any tensor is defined as

$$\begin{aligned}\nabla_\alpha T^{\rho_1\rho_2\ldots\rho_n}{}_{\sigma_1\sigma_2\ldots\sigma_m} &= \partial_\alpha T^{\rho_1\rho_2\ldots\rho_n}{}_{\sigma_1\sigma_2\ldots\sigma_m} + \Gamma^{\rho_1}_{\alpha\beta}T^{\beta\rho_2\ldots\rho_n}{}_{\sigma_1\sigma_2\ldots\sigma_m} + \Gamma^{\rho_2}_{\alpha\beta}T^{\rho_1\beta\ldots\rho_n}{}_{\sigma_1\sigma_2\ldots\sigma_m} + \ldots \\ &\quad + \Gamma^{\rho_n}_{\alpha\beta}T^{\rho_1\rho_2\ldots\beta}{}_{\sigma_1\sigma_2\ldots\sigma_m} - \Gamma^{\beta}_{\alpha\sigma_1}T^{\rho_1\rho_2\ldots\rho_n}{}_{\beta\sigma_2\ldots\sigma_m} \\ &\quad - \Gamma^{\beta}_{\alpha\sigma_2}T^{\rho_1\rho_2\ldots\rho_n}{}_{\sigma_1\beta\ldots\sigma_m} + \cdots - \Gamma^{\beta}_{\alpha\sigma_m}T^{\rho_1\rho_2\ldots\rho_n}{}_{\sigma_1\sigma_2\ldots\beta},\end{aligned} \tag{1.20}$$

which is also a tensor.

There are some other quantities that transform differently under coordinate transformation compared to a tensor or scalar. Such quantities are called tensor densities. One such example is $\sqrt{-g}$, where g is the usual determinant of the metric tensor $g_{\mu\nu}$. Under coordinate transformation, $\sqrt{-g}$ transform as

$$\sqrt{-g'} = \sqrt{-\left|g'_{\mu\nu}\right|} = \sqrt{-\left|g_{\alpha\beta}\left(\frac{\partial x^\alpha}{\partial x'^\mu}\frac{\partial x^\beta}{\partial x'^\nu}\right)\right|} = \sqrt{-g}\left|\frac{\partial x}{\partial x'}\right|. \tag{1.21}$$

A more generalised form of the tensor density is defined as the product of a tensor with any tensor density. A general tensor density with arbitrary rank ω transforms as

$$\mathfrak{T}'^{\mu_1\mu_2\ldots\mu_n}{}_{\nu_1\nu_2\ldots\nu_m} = \left|\frac{\partial x}{\partial x'}\right|^\omega \frac{\partial x'^{\mu_1}}{\partial x^{\rho_1}}\frac{\partial x'^{\mu_2}}{\partial x^{\rho_2}}\cdots\frac{\partial x'^{\mu_n}}{\partial x^{\rho_n}}\cdot\frac{\partial x^{\sigma_1}}{\partial x'^{\nu_1}}\frac{\partial x^{\sigma_2}}{\partial x'^{\nu_2}}\cdots\frac{\partial x^{\sigma_3}}{\partial x'^{\nu_m}}\,\mathfrak{T}^{\rho_1\rho_2\ldots\rho_n}{}_{\sigma_1\sigma_2\ldots\sigma_m}, \tag{1.22}$$

where ω is the weight of the tensor density. Thus, the tensor density $\sqrt{-g}$ has the weight $\omega = 1$.

The covariant derivative of a general tensor density is defined as [135]

$$\begin{aligned}\nabla_\alpha \mathfrak{T}^{\rho_1\rho_2\ldots\rho_n}{}_{\sigma_1\sigma_2\ldots\sigma_m} &= \partial_\alpha \mathfrak{T}^{\rho_1\rho_2\ldots\rho_n}{}_{\sigma_1\sigma_2\ldots\sigma_m} - \omega\Gamma^{\beta}_{\beta\alpha}\mathfrak{T}^{\rho_1\rho_2\ldots\rho_n}{}_{\sigma_1\sigma_2\ldots\sigma_m} \\ &\quad + \Gamma^{\rho_1}_{\alpha\beta}\mathfrak{T}^{\beta\rho_2\ldots\rho_n}{}_{\sigma_1\sigma_2\ldots\sigma_m} + \Gamma^{\rho_2}_{\alpha\beta}\mathfrak{T}^{\rho_1\beta\ldots\rho_n}{}_{\sigma_1\sigma_2\ldots\sigma_m} + \cdots + \Gamma^{\rho_n}_{\alpha\beta}\mathfrak{T}^{\rho_1\rho_2\ldots\beta}{}_{\sigma_1\sigma_2\ldots\sigma_m} \\ &\quad - \Gamma^{\beta}_{\alpha\sigma_1}\mathfrak{T}^{\rho_1\rho_2\ldots\rho_n}{}_{\beta\sigma_2\ldots\sigma_m} - \Gamma^{\beta}_{\alpha\sigma_2}\mathfrak{T}^{\rho_1\rho_2\ldots\rho_n}{}_{\sigma_1\beta\ldots\sigma_m} + \cdots - \Gamma^{\beta}_{\alpha\sigma_m}\mathfrak{T}^{\rho_1\rho_2\ldots\rho_n}{}_{\sigma_1\sigma_2\ldots\beta},\end{aligned} \tag{1.23}$$

which is true for any connection. Consequently, for the tensor density $\mathfrak{g}^{\lambda\beta} = \sqrt{-g}g^{\lambda\beta}$,

the covariant derivative is expressed as

$$\nabla_\mu \mathfrak{g}^{\lambda\beta} = \partial_\mu \mathfrak{g}^{\lambda\beta} - \Gamma^\sigma_{\sigma\mu}\mathfrak{g}^{\lambda\beta} + \Gamma^\lambda_{\mu\rho}\mathfrak{g}^{\rho\beta} + \Gamma^\beta_{\mu\rho}\mathfrak{g}^{\lambda\rho}. \tag{1.24}$$

1.2.1.3 Palatini formalism of general relativity

In Palatini formalism [145], the affine connection $\Gamma^\alpha_{\mu\nu}$ and the metric tensor $g_{\mu\nu}$ are taken to be independent of each other, and their relation is obtained only through the variation of action. Consequently, the action (1.4) is varied with respect to both $g_{\mu\nu}$ and $\Gamma^\alpha_{\mu\nu}$ independently.

With respect to the variation $\delta g^{\mu\nu}$ in the metric, the action (1.4) varies as

$$\delta_g \mathcal{S} = \frac{c^3}{16\pi G}\int d^4x\, \left(\delta\sqrt{-g}\, R + \sqrt{-g}\, R_{\mu\nu}\delta g^{\mu\nu}\right) + \int d^4x\, \delta\left(\sqrt{-g}\,\mathcal{L}_m\right), \tag{1.25}$$

which, upon using the relations (1.7) and (1.13), leads to

$$\delta_g \mathcal{S} = \frac{c^3}{16\pi G}\int d^4x\,\sqrt{-g}\,\left(R_{\mu\nu} - \frac{1}{2}g_{\mu\nu}R\right)\delta g^{\mu\nu} - \int d^4x\,\frac{1}{2c}\sqrt{-g}T_{\mu\nu}\delta g^{\mu\nu}. \tag{1.26}$$

With the extremality condition $\delta_g \mathcal{S} = 0$, equation (1.26) gives the Einstein field equations (1.16).

$$G_{\mu\nu} = R_{\mu\nu} - \frac{1}{2}\, g_{\mu\nu}\, R = \frac{8\pi G}{c^4}T_{\mu\nu}. \tag{1.27}$$

Although this equation has the same structure as (1.27) obtained earlier, the affine connections occurring in R and $R_{\mu\nu}$ must be regarded as independent of the metric $g_{\mu\nu}$.

In order to obtain a relation between the metric tensor $g_{\mu\nu}$ and the affine connection $\Gamma^\alpha_{\mu\nu}$, action (1.4) is varied with respect to the affine connection $\Gamma^\alpha_{\mu\nu}$, giving

$$\delta_\Gamma \mathcal{S} = \frac{c^3}{16\pi G}\int d^4x\, \left(\sqrt{-g}g^{\mu\nu}\,\delta R_{\mu\nu}\right). \tag{1.28}$$

Defining the tensor density as $\mathfrak{g}^{\mu\nu} = \sqrt{-g}g^{\mu\nu}$, and using the relation (1.11), the variation (1.28) takes the form

$$\delta_\Gamma \mathcal{S} = \frac{c^3}{16\pi G}\int d^4x\, \mathfrak{g}^{\mu\nu}\, \left(\nabla_\lambda\, \delta\Gamma^\lambda_{\mu\nu} - \nabla_\nu\, \delta\Gamma^\lambda_{\mu\lambda}\right). \tag{1.29}$$

Applying Leibniz rule, equation (1.28) is re-expressed as

$$\begin{aligned}\delta_\Gamma \mathcal{S}(g,\Gamma,\Psi) =& \frac{c^3}{16\pi G}\int d^4x \left\{\nabla_\lambda\left(\mathfrak{g}^{\mu\nu}\,\delta\Gamma^\lambda_{\mu\nu}\right) - \nabla_\nu\left(\mathfrak{g}^{\mu\nu}\,\delta\Gamma^\lambda_{\mu\lambda}\right)\right. \\ & \left. -\nabla_\lambda\mathfrak{g}^{\mu\nu}\,\delta\Gamma^\lambda_{\mu\nu} + \nabla_\nu\mathfrak{g}^{\mu\nu}\,\delta\Gamma^\lambda_{\mu\lambda}\right\}.\end{aligned} \tag{1.30}$$

The first two terms in the above integrand form the covariant derivative of a tensor density,

$$\nabla_\lambda\mathfrak{A}^\lambda = \nabla_\lambda\left(\mathfrak{g}^{\mu\nu}\,\delta\Gamma^\lambda_{\mu\nu} - \mathfrak{g}^{\mu\lambda}\,\delta\Gamma^\nu_{\mu\nu}\right), \tag{1.31}$$

leading to the simplification

$$\delta_\Gamma\mathcal{S} = \frac{c^3}{16\pi G}\int d^4x\,\left(\nabla_\lambda\mathfrak{A}^\lambda - \nabla_\lambda\mathfrak{g}^{\mu\nu}\,\delta\Gamma^\lambda_{\mu\nu} + \nabla_\nu\mathfrak{g}^{\mu\nu}\,\delta\Gamma^\lambda_{\mu\lambda}\right). \tag{1.32}$$

From the definition of covariant derivative of a tensor density (1.23), the equation (1.31) takes the form

$$\nabla_\lambda\mathfrak{A}^\lambda = \partial_\lambda\mathfrak{A}^\lambda - \Gamma^\sigma_{\sigma\lambda}\mathfrak{A}^\lambda + \Gamma^\lambda_{\lambda\sigma}\mathfrak{A}^\sigma = \partial_\lambda\mathfrak{A}^\lambda, \tag{1.33}$$

which is a total derivative. Using Gauss' law, the corresponding integration can be transformed to a surface integral, with the variation of the connection vanishing at the boundary. Thus, the variation (1.32) reduces to

$$\delta_\Gamma\mathcal{S} = \frac{c^3}{16\pi G}\int d^4x\,\left(\nabla_\nu\mathfrak{g}^{\mu\nu}\,\delta\Gamma^\lambda_{\mu\lambda} - \nabla_\lambda\mathfrak{g}^{\mu\nu}\,\delta\Gamma^\lambda_{\mu\nu}\right). \tag{1.34}$$

Upon further simplification, we get

$$\delta_\Gamma\mathcal{S} = \frac{c^3}{16\pi G}\int d^4x\,\left(\nabla_\alpha\mathfrak{g}^{\mu\alpha}\delta^\nu_\lambda - \nabla_\lambda\mathfrak{g}^{\mu\nu}\right)\delta\Gamma^\lambda_{\mu\nu}. \tag{1.35}$$

The extremality condition $\delta_\Gamma\mathcal{S} = 0$ therefore requires vanishing of the symmetrised coefficient of $\delta\Gamma^\lambda_{\mu\nu}$,

$$\frac{1}{2}\nabla_\alpha\mathfrak{g}^{\mu\alpha}\delta^\nu_\lambda + \frac{1}{2}\nabla_\alpha\mathfrak{g}^{\nu\alpha}\delta^\mu_\lambda - \nabla_\lambda\mathfrak{g}^{\mu\nu} = 0, \tag{1.36}$$

giving the null solution [135]

$$\nabla_\lambda\mathfrak{g}^{\mu\nu} = 0. \tag{1.37}$$

The covariant derivative of any tensor density defined by (1.23) leads to

$$\nabla_\mu\sqrt{-g} = \partial_\mu\sqrt{-g} - \Gamma^\sigma_{\sigma\mu}\sqrt{-g}. \tag{1.38}$$

In addition, the covariant derivative of the tensor density $\sqrt{-g}g^{\lambda\beta}$ turns out to be

$$\nabla_\mu\left(\sqrt{-g}g^{\lambda\beta}\right) = \partial_\mu\left(\sqrt{-g}g^{\lambda\beta}\right) - \Gamma^\sigma_{\sigma\mu}\sqrt{-g}g^{\lambda\beta} + \sqrt{-g}\Gamma^\lambda_{\mu\rho}g^{\rho\beta} + \sqrt{-g}\Gamma^\beta_{\mu\rho}g^{\lambda\rho} = 0, \quad (1.39)$$

which vanishes due to the equation (1.37). Rearranging (1.39) gives

$$\partial_\mu\left(\sqrt{-g}g^{\lambda\beta}\right) = \Gamma^\sigma_{\sigma\mu}\sqrt{-g}g^{\lambda\beta} - \sqrt{-g}\Gamma^\lambda_{\mu\rho}g^{\rho\beta} - \sqrt{-g}\Gamma^\beta_{\mu\rho}g^{\lambda\rho}. \quad (1.40)$$

The identity $\partial_\mu\left(\sqrt{-g}g^{\lambda\beta}\right) = g^{\lambda\beta}\partial_\mu\sqrt{-g} + \sqrt{-g}\partial_\mu g^{\lambda\beta}$ can be re-expressed as

$$\partial_\mu\sqrt{-g} = g_{\lambda\beta}\partial_\mu\left(\sqrt{-g}g^{\lambda\beta}\right) + \sqrt{-g}g^{\lambda\beta}\partial_\mu g_{\lambda\beta}. \quad (1.41)$$

Inserting (1.40) in (1.41) leads to

$$\partial_\mu\sqrt{-g} = \Gamma^\sigma_{\sigma\mu}\sqrt{-g} - \sqrt{-g}\Gamma^\lambda_{\mu\rho}\delta^\rho_\lambda - \sqrt{-g}\Gamma^\beta_{\mu\rho}\delta^\beta_\rho + \sqrt{-g}g^{\lambda\beta}\partial_\mu g_{\lambda\beta}, \quad (1.42)$$

which can be substituted in (1.38) to get

$$\nabla_\mu\sqrt{-g} = -2\sqrt{-g}\Gamma^\rho_{\mu\rho} + \sqrt{-g}g^{\lambda\beta}\partial_\mu g_{\lambda\beta}. \quad (1.43)$$

Comparing (1.43) with (1.38), and using the identity $\partial_\mu\sqrt{-g} = \frac{1}{2}\sqrt{-g}g^{\rho\sigma}\partial_\mu g_{\rho\sigma}$, gives the relation

$$\Gamma^\rho_{\mu\rho} = \frac{1}{2}g^{\rho\sigma}\partial_\mu g_{\rho\sigma}, \quad (1.44)$$

so that (1.38) leads to

$$\nabla_\mu\sqrt{-g} = 0. \quad (1.45)$$

Finally, applying the Leibnitz rule in the equation of motion (1.37) gives

$$\nabla_\mu\left(\sqrt{-g}g^{\lambda\beta}\right) = \sqrt{-g}\nabla_\mu g^{\lambda\beta} + g^{\lambda\beta}\nabla_\mu\sqrt{-g} = 0. \quad (1.46)$$

Using (1.45) in (1.46), thus leads to the metricity condition

$$\nabla_\mu g^{\lambda\beta} = 0. \quad (1.47)$$

Employing the definition of covariant derivative $\nabla_\alpha g^{\mu\nu} = \partial_\alpha g^{\mu\nu} + \Gamma^\mu_{\alpha\beta}g^{\beta\nu} + \Gamma^\nu_{\alpha\beta}g^{\mu\beta}$ in (1.47), the relation between the affine connection and the metric tensor $g_{\mu\nu}$ is obtained as

$$\Gamma^\mu_{\alpha\beta} = \frac{g^{\mu\nu}}{2}\left(-\partial_\nu g_{\alpha\beta} + \partial_\beta g_{\alpha\nu} + \partial_\alpha g_{\nu\beta}\right). \quad (1.48)$$

1.2.2 Energy-momentum tensor and its conservation

The matter action in (1.4), in its general form, is defined with respect to the metric $g_{\mu\nu}$ as

$$S_m(\Psi, g) = \int d^4x \sqrt{-g}\mathcal{L}_m(\Psi, g), \tag{1.49}$$

where $\mathcal{L}_m$ is the matter Lagrangian and Ψ is the matter field.

Varying the general matter action (1.49) with respect to the metric tensor $g_{\mu\nu}$ leads to [121]

$$\delta S_m(\Psi, g) = \int d^4x \left\{ \frac{\partial\left(\sqrt{-g}\mathcal{L}_m\right)}{\partial g^{\mu\nu}}\delta g^{\mu\nu} + \frac{\partial\left(\sqrt{-g}\mathcal{L}_m\right)}{\partial\left(\partial_\rho g^{\mu\nu}\right)}\delta\left(\partial_\rho g^{\mu\nu}\right)\right\}. \tag{1.50}$$

The second term gives rise to a vanishing surface term. Consequently,

$$\delta S_m(\Psi, g) = \int d^4x \left\{ \frac{\partial\left(\sqrt{-g}\mathcal{L}_m\right)}{\partial g^{\mu\nu}} - \partial_\rho\left(\frac{\partial\left(\sqrt{-g}\mathcal{L}_m\right)}{\partial\left(\partial_\rho g^{\mu\nu}\right)}\right)\right\}\delta g^{\mu\nu}. \tag{1.51}$$

The integrand in (1.51) defines the energy-momentum tensor $T_{\mu\nu}$ as [121]

$$T_{\mu\nu} = \frac{2}{\sqrt{-g}}\left\{ \frac{\partial\left(\sqrt{-g}\mathcal{L}_m\right)}{\partial g^{\mu\nu}} - \partial_\rho\left(\frac{\partial\left(\sqrt{-g}\mathcal{L}_m\right)}{\partial\left(\partial_\rho g^{\mu\nu}\right)}\right)\right\}. \tag{1.52}$$

For example, the matter Lagrangian of a scalar field is given by

$$\mathcal{L}_m = -\frac{1}{2}g^{\mu\nu}\partial_\mu\phi\,\partial_\nu\phi - V(\phi), \tag{1.53}$$

where $V(\phi)$ is the potential of the scalar field. Using (1.53) in (1.52), the energy-momentum tensor for the scalar field is obtained as

$$T_{\mu\nu} = \partial_\mu\phi\,\partial_\nu\phi - \frac{g_{\mu\nu}}{2}\left\{g^{\rho\sigma}\partial_\rho\phi\,\partial_\sigma\phi + V(\phi)\right\}. \tag{1.54}$$

As for another example, the Lagrangian of an electromagnetic field is given by

$$\mathcal{L}_m = -\frac{1}{16\pi}F_{\mu\nu}F^{\mu\nu}, \tag{1.55}$$

where $F_{\mu\nu} = \partial_\mu A_\nu - \partial_\nu A_\mu$ is the electromagnetic tensor and A_μ is the electromagnetic vector potential. Consequently, the energy-momentum tensor for an electromagnetic field is given by

$$T_{\mu\nu} = \frac{1}{4\pi}\left(g^{\rho\sigma}F_{\mu\rho}F_{\nu\sigma} - \frac{g_{\mu\nu}}{4}F_{\rho\sigma}F^{\rho\sigma}\right). \tag{1.56}$$

The matter Lagrangian of a perfect fluid is given by [122]

$$T_{\mu\nu} = \frac{(\rho c^2 + P)}{c^2} u_\mu u_\nu + g_{\mu\nu} P, \tag{1.57}$$

where ρ is the density and P is the pressure, and u^μ is the four velocity.

1.2.2.1 Conservation of energy-momentum tensor

Conservation of energy-momentum tensor must be valid regardless of the detailed form of the action [121]. Consequently, a general matter action can be used to prove the conservation of energy-momentum tensor.

The general definition (1.52) of the energy-momentum tensor gives the variation (1.51) as

$$\delta S_m(\Psi, g) = \frac{1}{2} \int d^4x \sqrt{-g} T_{\mu\nu} \delta g^{\mu\nu}. \tag{1.58}$$

Under an infinitesimal coordinate transformation $x'^\mu = x^\mu + \delta x^\mu$, the metric transforms as $g'_{\mu\nu} = g_{\mu\nu} + \delta g_{\mu\nu}$. Thus the variation $\delta g_{\mu\nu}$ can be defined in terms of a Killing vector ξ^μ as

$$\delta g^{\mu\nu} = \nabla^\mu \xi^\nu + \nabla^\nu \xi^\mu, \tag{1.59}$$

so that the variation δS_m becomes

$$\delta S_m(\Psi, g) = \frac{1}{2} \int d^4x \sqrt{-g} T_{\mu\nu} \left(\nabla^\mu \xi^\nu + \nabla^\nu \xi^\mu \right). \tag{1.60}$$

Since $T_{\mu\nu}$ is a symmetric tensor, this variation reduces to

$$\delta S_m(\Psi, g) = \int d^4x \sqrt{-g} T^\mu_{\ \nu} \nabla_\mu \xi^\nu. \tag{1.61}$$

Using the identity $\nabla_\mu \left(T^\mu_{\ \nu} \xi^\nu \right) = T^\mu_{\ \nu} \nabla_\mu \xi^\nu + \left(\nabla_\mu T^\mu_{\ \nu} \right) \xi^\nu$, and noting that $\nabla_\mu A^\mu = \frac{1}{\sqrt{-g}} \partial_\mu \left(\sqrt{-g} A^\mu \right)$, we finally have

$$\delta S_m(\Psi, g) = - \int d^4x \sqrt{-g} \left(\nabla_\mu T^\mu_{\ \nu} \right) \xi^\nu, \tag{1.62}$$

upon dropping the surface term.

For the extremum condition, we require $\delta S_m = 0$. Since the Killing vector is arbitrary, 1.62 gives the condition

$$\nabla_\mu T^\mu_{\ \nu} = 0, \tag{1.63}$$

which is the conservation of the energy-momentum tensor.

1.3 Black holes

Consider a system where the matter distribution is spherically symmetric. Correspondingly, the most general spacetime metric reads

$$ds^2 = -A(r,t)\,c^2dt^2 + B(r,t)\,c\,dt\,dr + H(r,t)\,dr^2 + D(r,t)\left(d\theta^2 + \sin^2\theta\,d\varphi^2\right), \quad (1.64)$$

exhibiting in variance with respect to rotation. Furthermore, due to the arbitrariness of the choice of reference frame, one can diagonalise the metric with appropriate coordinate transformation. Consequently, it is possible to obtain the metric as

$$ds^2 = -F(r,t)\,c^2dt^2 + G(r,t)\,dr^2 + r^2\left(d\theta^2 + \sin^2\theta\,d\varphi^2\right), \quad (1.65)$$

where $F(r,t)$ and $G(r,t)$ are the new metric potentials after the coordinate transformations. It will be mathematically convenient to write $F(r,t) = e^{\nu(r,t)}$, and $G(r,t) = e^{\lambda(r,t)}$.

1.3.1 The Schwarzschild solution

Consider a spherically symmetric matter distribution. Outside the surface of the matter distribution, there is no matter field, and hence we assume the energy-momentum tensor to be zero. The spacetime metric given by (1.65) can be written as

$$ds^2 = -e^{\nu(r,t)}\,c^2dt^2 + e^{\lambda(r,t)}\,dr^2 + r^2\left(d\theta^2 + \sin^2\theta\,d\varphi^2\right). \quad (1.66)$$

Consequently, using the definition of affine connection, $\Gamma^\alpha_{\mu\nu} = \frac{g^{\alpha\rho}}{2}\left(-\partial_\rho g_{\mu\nu} + \partial_\mu g_{\rho\nu} + \partial_\nu g_{\mu\rho}\right)$, its nonzero connections are given by

$$\begin{array}{llll} \Gamma^t_{tt} = \frac{\dot\nu}{2}, & \Gamma^t_{tr} = \frac{\nu'}{2}, & \Gamma^t_{rr} = \frac{\dot\lambda}{2}e^{\lambda-\nu}, & \Gamma^r_{tr} = \frac{\dot\lambda}{2}, \\ \Gamma^r_{tt} = \frac{\nu'}{2}e^{\nu-\lambda}, & \Gamma^r_{rr} = \frac{\lambda'}{2}, & \Gamma^r_{\theta\theta} = -re^{-\lambda}, & \Gamma^r_{\varphi\varphi} = -r\sin^2\varphi e^{-\lambda}, \\ \Gamma^\theta_{r\theta} = \Gamma^\varphi_{r\varphi} = \frac{1}{r}, & \Gamma^\theta_{\varphi\varphi} = -\sin\varphi\cos\varphi, & \Gamma^\varphi_{\theta\varphi} = \cot\varphi, & \end{array} \quad (1.67)$$

where a prime denotes differentiation with respect to r, and $\dot x$ represents differentiation with respect to time.

Using (1.67), the Ricci tensor $R_{\mu\nu} = \partial_\beta\Gamma^\beta_{\mu\nu} - \partial_\nu\Gamma^\beta_{\mu\beta} + \Gamma^\beta_{\beta\rho}\Gamma^\rho_{\mu\nu} - \Gamma^\beta_{\nu\rho}\Gamma^\rho_{\mu\beta}$, and Ricci scalar $R = g^{\mu\nu}R_{\mu\nu}$, are computed.The ensuing tt, rt, and rr components of the Einstein

tensor $G_{\mu\nu} = R_{\mu\nu} - \frac{g_{\mu\nu}}{2}R$ are given by

$$\begin{aligned} G_{tt} =& e^{\nu-\lambda}\left(\frac{\lambda'}{r} - \frac{1}{r^2}\right) + \frac{e^{\nu}}{r^2}, \\ G_{rr} =& \left(\frac{\nu'}{r} + \frac{1}{r^2}\right) - \frac{e^{\lambda}}{r^2}, \\ G_{rt} =& \frac{\dot{\lambda}}{r}. \end{aligned} \tag{1.68}$$

Outside the matter distribution the energy-momentum tensor is zero. The Einstein equation $G_{\mu\nu} = 0$ in the exterior region yield the following set of equations

$$\nu' = -\frac{1 - e^{\lambda}}{r}, \tag{1.69}$$

$$\lambda' = \frac{1 - e^{\lambda}}{r}. \tag{1.70}$$

and

$$\dot{\lambda} = 0. \tag{1.71}$$

Equation (1.71) implies that λ is time independent. Adding (1.69) and (1.70), yields

$$\lambda' + \nu' = 0, \tag{1.72}$$

which upon integration gives $\lambda+\nu = f(t)$, where $f(t)$ is integration "constant". However, with appropriate transformation of the time coordinate in (1.66), it is possible to make $f(t)$ vanish. Moreover, the requirement that metric should be asymptotically flat require $\nu, \mu \to 0$ as $r \to \infty$. Hence

$$e^{\lambda} = e^{-\nu}. \tag{1.73}$$

Using (1.73) in (1.69)leads to the solution

$$e^{\nu} = 1 + \frac{k}{r}. \tag{1.74}$$

where k is a constant. In the weak gravity limit, as $r \to \infty$, the metric potential e^{ν} should approach the Newtonian limit, $e^{\nu} \sim 1 + \frac{2\phi_g}{c^2}$, where ϕ_g is the Newtonian potential, $\phi_g = -\frac{G\,M}{r}$, with M the mass of the matter distribution. Consequently, the integration constant in (1.74) is identified as $k = \frac{G\,M}{c^2}$, giving

$$e^{\nu} = e^{-\lambda} = 1 - \frac{2GM}{c^2\,r}. \tag{1.75}$$

Thus the metric (1.66) takes the form

$$ds^2 = -\left(1 - \frac{2GM}{c^2 r}\right) c^2 dt^2 + \frac{1}{1 - \frac{2GM}{c^2 r}}\, dr^2 + r^2 \left(d\theta^2 + \sin^2\theta\, d\varphi^2\right), \tag{1.76}$$

which is the well known Schwarzschild metric, first derived by Karl Schwarzschild in 1916 [166]. In this solution, there is only one constant of integration; the ADM mass M. This is significant because the external metric is independent of the internal matter composition.

Moreover, in the above described calculation we assumed metric to be time-dependent. However, the vacuum solution of the Einstein equation is time-independent. This result is known as the Birkhoff's theorem, which states that the vacuum solution of Einstein equation for a spherically symmetric matter distribution is static, and hence it is described by the Schwarzschild metric.

The Schwarzschild metric in (1.76) can be written as

$$ds^2 = -f(r)\, c^2 dt^2 + \frac{1}{f(r)}\, dr^2 + r^2 \left(d\theta^2 + \sin^2\theta\, d\varphi^2\right), \tag{1.77}$$

where $f(r) = 1 - \frac{2GM}{c^2 r}$. The metric coefficients diverge as $r \to r_{\rm s} = \frac{2GM}{c^2}$ and $r \to 0$. The radial distance $r_{\rm s}$ is known as Schwarzschild radius.

However, the divergence in the metric coefficients at $r = 0$ in the spacetime metric (1.76) is a curvature singularity. The divergence present at $r = r_{\rm s}$ is only a coordinate singularity. This is verifiable by calculating the Kretschmann scalar, which is an invariant quantity of the curvature tensor $R_{\mu\nu\alpha\beta}$, given by $\mathcal{K} = R_{\mu\nu\alpha\beta} R^{\mu\nu\alpha\beta}$. For Schwarzschild metric, the Kretschmann scalar is given by

$$\mathcal{K} = \frac{48\, G^2 M^2}{c^4 r^6}, \tag{1.78}$$

which is finite for $r = r_{\rm s}$, and diverging for $r = 0$. As a consequence, the singularity at $r = r_{\rm s}$ can be removed by an appropriate coordinate transformation. However, the singularity at $r = 0$, which is a curvature singularity, cannot be removed by employing any coordinate transformation.

For most astrophysical objects, the Schwarzschild radius $r_{\rm s}$ is smaller than their actual radius. For example, the Schwarzschild radius of a planet is $r_{\rm s} \sim 10^{-2}$ km, while the radius of a planet is $\sim 10^3$ km. Similarly, the Schwarzschild radius of the Sun is $r_{\rm s} \sim 3$ km, while its radius is 6.95×10^5 km. However, for massive astrophysical objects such as neutron stars, the Schwarzschild radius $r_{\rm s} \sim 4$ km is comparable to their stellar radius

$R \sim 10$ km..

When the physical conditions are such that a spherically symmetric star is compressed below its Schwarzschild radius r_s, it collapses indefinitely and a black hole is formed. In that case, the spherical surface of radius r_s is called the event horizon of the black hole.

With the metric potential $f(r) = 1 - \frac{r_s}{r}$, we have $f(r) > 0$ for $r > r_s$, and $f(r) < 0$ when $r < r_s$. Therefore, in the interior region $r < r_s$, the radial term dr^2 in (1.77) becomes time-like, and the dt^2 term becomes space-like. Consequently, the metric potentials are now explicitly time dependent, and hence the metric is not static inside the Schwarzschild radius. Due to this property of the spacetime in the interior region, any infalling matter through the event horizon cannot escape the black hole and must end up at the singularity at $r = 0$.

1.3.2 Reissner-Nordström solution

When the spherically symmetric matter distribution is electrically charged, the Einstein field equations (1.16) yield the Reissner-Nordström solution. Consider a charged and spherically symmetric matter distribution. Since the system is charged, the electric field and hence the energy-momentum tensor does not vanish outside the system.

Assuming the system to be non-rotating and the total charge in the system to be Q, we take the ansatz $A_\mu = (V(r), 0, 0, 0)$, where A_μ is the electromagnetic vector potential, and $V(r)$ is the electrostatic potential. The corresponding Maxwell tensor $F_{\mu\nu} = \partial_\mu A_\nu - \partial_\nu A_\mu$ is given by

$$F_{\mu\nu} = \begin{pmatrix} 0 & -V'(r) & 0 & 0 \\ V'(r) & 0 & 0 & 0 \\ 0 & 0 & 0 & 0 \\ 0 & 0 & 0 & 0 \end{pmatrix}. \tag{1.79}$$

With the matter Lagrangian $\mathcal{L}_m = -\frac{1}{16\pi} F_{\mu\nu} F^{\mu\nu}$, the Maxwell equations read

$$\nabla_\mu F^{\mu\nu} = 0 \tag{1.80}$$

in the exterior region, where there is no electric charge.

As discussed earlier, the most general metric for the spacetime in the exterior region is given by

$$ds^2 = -e^{\nu(r,t)}\, c^2 dt^2 + e^{\lambda(r,t)}\, dr^2 + r^2 \left(d\theta^2 + \sin^2\theta\, d\varphi^2\right). \tag{1.81}$$

Using this metric in (1.80) yields

$$V''(r) = \left(\frac{\lambda' + \nu'}{2} - \frac{2}{r}\right) V'(r). \tag{1.82}$$

Equation (1.82) is solvable upon direct integration, leading to

$$V' = \frac{k\, e^{\frac{\lambda+\nu}{2}}}{r^2}. \tag{1.83}$$

The integration constant k can be fixed by demanding $V' = \frac{Q}{r^2}$ as $r \to \infty$. This condition fixes the constant as $k = Q$, so that

$$V' = \frac{Q\, e^{\frac{\lambda+\nu}{2}}}{r^2}. \tag{1.84}$$

Using the metric as defined in (1.81) in the Einstein field equations (1.16) yields the following set of equations

$$e^{\nu-\lambda}\left(\frac{\lambda'}{r} - \frac{1}{r^2}\right) + \frac{e^{\nu}}{r^2} = \frac{G\, e^{-\lambda} V'^2}{c^4}, \tag{1.85}$$

$$\left(\frac{\nu'}{r} + \frac{1}{r^2}\right) - \frac{e^{\lambda}}{r^2} = -\frac{G\, e^{-\nu} V'^2}{c^4}, \tag{1.86}$$

and

$$\frac{\dot{\lambda}}{r} = 0. \tag{1.87}$$

Similar to what we saw in the case of Schwarzschild solution, we see from equation (1.87) that the Birkhoff's theorem is valid in this case as well.

Equations (1.85) and (1.86) together imply $e^{\lambda} = e^{-\nu}$. Substituting this result in (1.86), and using (1.84), one obtains

$$\nu' = \frac{e^{-\nu} - 1}{r} - \frac{G\, e^{-\nu} Q^2}{c^4\, r^3}. \tag{1.88}$$

Upon integration, this equation yields

$$e^{\nu} = 1 - \frac{k'}{r} + \frac{G\, Q^2}{c^4\, r^2}. \tag{1.89}$$

The integration constant k' is fixed by demanding the Newtonian limit as $r \to \infty$, leading to

$$e^{\nu} = 1 - \frac{2GM}{c^2\, r} + \frac{G\, Q^2}{c^2\, r^2}. \tag{1.90}$$

Consequently, the spacetime metric (1.81) exterior to a spherically symmetric charged matter distribution takes the form

$$ds^2 = -\left(1 - \frac{2GM}{c^2\,r} + \frac{G\,Q^2}{c^2\,r^2}\right) c^2 dt^2 + \frac{dr^2}{1 - \frac{2GM}{c^2\,r} + \frac{G\,Q^2}{c^2\,r^2}} + r^2\left(d\theta^2 + \sin^2\theta\, d\varphi^2\right), \tag{1.91}$$

which is the Reissner-Nordström solution, first obtained by Reissner [162] and Nordström [139].

Similarly to the Schwarzschild metric, the Reissner-Nordström metric can be written as

$$ds^2 = -f_{\rm RN}(r)\, c^2 dt^2 + \frac{1}{f_{\rm RN}(r)}\, dr^2 + r^2\left(d\theta^2 + \sin^2\theta\, d\varphi^2\right), \tag{1.92}$$

where

$$f_{\rm RN}(r) = 1 - \frac{2GM}{c^4\,r} + \frac{G\,Q^2}{c^4\,r^2} = 1 - \frac{2m}{r} + \frac{q^2}{r^2}, \tag{1.93}$$

with $m = \frac{G\,M}{c^2}$, and $q = \frac{\sqrt{G}Q}{c}$

The Reissner-Nordström metric (1.92) has singularities at $r = r_\pm$ and $r = 0$, where

$$r_\pm = m \pm \sqrt{m^2 - q^2}. \tag{1.94}$$

The Kretschmann scalar $\mathcal{K} = R_{\alpha\beta\mu\nu}R^{\alpha\beta\mu\nu}$ for the metric (1.91) turns out to be

$$\mathcal{K} = \frac{8G^2}{c^8 r^8}\left(7Q^4 - 12MQ^2 r + 6M^2 r^2\right), \tag{1.95}$$

which diverges only at $r = 0$. Hence, the singularities at $r = r_\pm$ are only coordinate singularities that can be removed upon appropriate coordinate transformation.

Consequently, r_+ and r_- represents two horizons of the Reissner-Nordstöm black hole, implying a significant difference from the Schwarzschild solution. Since $r_+ > r_-$, the horizon at r_+ is the outer horizon, whereas r_- is the radius of the inner horizon.

The behavior of the horizons, and the spacetime inside the outer horizon depends significantly on the magnitude of the charge Q enclosed within the black hole. As the charge q increases, the gap between r_+ and r_- decreases, and the two horizons coincide when $m = q$, which is the extremality condition.

For the case $q > m$, there exist no real roots for $f_{\rm RN} = 0$. In this case, the coordinate system stays valid in all regions. Consequently, the singularity at $r = 0$ is naked for $q > m$. However, the well-known cosmic censorship conjecture [153] bars the existence of naked singularities and hence the $q > m$ Reissner-Nordstöm solution is unphysical.

For the case $m = q$, the two horizons coincide $r = r_+ = r_-$. This is however not

equivalent to the Schwarzschild solution since the metric takes the form

$$ds^2 = -\left(1-\frac{m}{r}\right)^2 c^2dt^2 + \left(1-\frac{m}{r}\right)^{-2} dr^2 + r^2\left(d\theta^2 + \sin^2\theta\, d\varphi^2\right), \tag{1.96}$$

so that the metric potential is $f_{\rm RN}(r) = \left(1-\frac{m}{r}\right)^2$, which is quiet different from the Schwarzschild metric potential $f_{\rm Sch}(r) = 1-\frac{2m}{r}$. Consequently, unlike the Schwarzschild case, $f_{\rm RN}(r) \geq 0$ everywhere. Thus, the spacetime remains the same everywhere, and the singularity is time-like. Therefore, any infalling particle crossing the horizon can avoid the singularity.

For the non-extremal case, $m > q$, the metric potential $f_{\rm RN}(r) > 0$ in the range $0 \leq r < r_-$ and $r > r_+$, and $f_{\rm RN}(r) < 0$ in the range $r_- < r < r_+$. For an infalling particle crossing the outer horizon at r_+, its radial coordinate becomes timelike so that it can reach the inner horizon at r_-. Upon crossing the inner horizon at r_-, radial coordinate becomes spacelike again, and hence the singularity at $r = 0$ becomes spacelike. In this case, the particle can avoid hitting the singularity and exit into a different universe, as argued by Novikov [141]. However, Penrose and Simpson [175] objected to this idea of multiverse travel and proposed the phenomenon of mass inflation due to the development of a singularity at the inner horizon at r_- occurring from any infalling matter into the black hole [86].

The phenomenon of mass inflation has been extensively studied by Poisson, Israel and others. Infalling matter or radiation into a Reissner-Nordström black hole can make m much larger than q. Consequently, as m increases, r_- decreases, and the inner horizon r_- moves inwards while the outer horizon r_+ moves outward.

1.3.3 Rotating black holes

Apart from mass M and charge Q, rotation can also dictate the spacetime around a black hole. A rotating black hole with mass M and angular momentum J is known as Kerr black hole [54, 113]. The spacetime metric around a Kerr black hole in Boyer-Lindquist coordinate [35] is given by

$$\begin{aligned} ds^2 = -\left(1-\frac{2mr}{\rho^2}\right)c^2dt^2 - \frac{4mar\sin^2\theta}{\rho^2}c\,dt\,d\varphi + \frac{\rho^2}{\Delta}dr^2 + \rho^2 d\theta^2 \\ + \left(r^2 + a^2 + \frac{2mra^2\sin^2\theta}{\rho^2}\right)\sin^2\theta d\varphi^2 \end{aligned} \tag{1.97}$$

where

$$\rho^2 = r^2 + a^2\cos^2\theta, \tag{1.98}$$

$$\Delta = r^2 - 2mr + a^2, \tag{1.99}$$

$$m = \frac{G\,M}{c^2}, \tag{1.100}$$

and

$$a = \frac{J}{Mc}. \tag{1.101}$$

In the limit $a \to 0$, the Kerr metric (1.97) reduces to the Schwarzschild metric. Writing

$$\Sigma^2 = \left(r^2 + a^2\right)^2 - a^2\Delta \sin^2\theta, \tag{1.102}$$

the metric (1.97) can be transformed to

$$ds^2 = -\frac{\Delta - a^2\sin^2\theta}{\rho^2}c^2dt^2 - \frac{4mar\sin^2\theta}{\rho^2}c\,dt\,d\varphi + \frac{\rho^2}{\Delta}dr^2 + \rho^2 d\theta^2 + \frac{\Sigma^2\sin^2\theta}{\rho^2}d\varphi^2. \tag{1.103}$$

From this metric (1.103), the metric potentials and their inverse are given by

$$g_{tt} = -\frac{\Delta - a^2\sin^2\theta}{\rho^2}, \quad g_{rr} = \frac{\rho^2}{\Delta}, \quad g_{t\varphi} = -\frac{2mar\sin^2\theta}{\rho^2}, \quad g_{\theta\theta} = \rho^2, \quad g_{\varphi\varphi} = \frac{\Sigma^2\sin^2\theta}{\rho^2},$$

$$g^{tt} = -\frac{\Sigma^2}{\rho^2\Delta}, \qquad g^{rr} = \frac{\Delta}{\rho^2}, \quad g^{t\varphi} = -\frac{2mar}{\rho^2\Delta}, \qquad g^{\theta\theta} = \frac{1}{\rho^2}, \quad g^{\varphi\varphi} = \frac{a^2\sin^2\theta - \Delta}{\rho^2\Delta\sin^2\theta}. \tag{1.104}$$

From (1.104) we see that Kerr metric also posses singularities in the metric potentials. The potential $g_{rr} \to \infty$ when $\Delta \to 0$, and $g_{tt} \to \infty$ when $\rho \to 0$. However, the Kretschmann scalar $\mathcal{K} \to \infty$ only at $\rho = 0$, which is the physical singularity. Since $\rho^2 = r^2 + a^2\cos^2\theta$, for the existence of singularity at $\rho = 0$, we require both $r = 0$ and $\theta = \frac{\pi}{2}$. Such singularities are known as ring singularity. Consequently, a Kerr black hole posses ring singularity unlike Schwarzschild black hole which has a point singularity.

The Kretschmann scalar $\mathcal{K}$ is finite for the singularities at $\Delta = 0$. Consequently, $\Delta = 0$ is a coordinate singularity which gives the horizon structure of a Kerr black hole. From $\Delta = r^2 - 2mr + a^2 = 0$, we obtain the horizon radii

$$r_\pm = m \pm \sqrt{m^2 - a^2}. \tag{1.105}$$

For $m^2 < a^2$, horizons $r_\pm$ is unphysical, and hence singularity becomes naked. However, the existence naked singularities are deemed to be unphysical thanks to cosmic censorship theorem. For $m^2 > a^2$, there exist surface coordinate singularities at r_+ and r_-. These

horizons are null surfaces. The horizon at r_+ is the outer horizon, and r_- is the inner horizon.

Unlike in the case of non-rotating black holes, $g_{tt} = 0$ and $g^{rr} = 0$ coordinates do not coincide in the case of Kerr metric. In Kerr spacetime, $g_{tt} = 0$ gives rise to different surface known as ergosphere. For $g_{tt} = 0$, ergosphere is defined by

$$r_{s\pm} = m \pm \sqrt{m^2 - a^2 \cos^2 \theta}. \tag{1.106}$$

Consequently, the horizon positions are $r_- < r_{s-} < r_+ < r_{s+}$. With this, any mass that falls into a Kerr black hole encounters first with ergosphere r_{s+}, then the horizon at r_+. It further encounters with two more surfaces before reaching the ring singularity at $r = 0$.

A charged rotating black hole is known as Kerr-Newman black hole. The spacetime metric of Kerr-Newman black hole is parametrized by mass M, charge Q, and angular momentum J.

1.4 The no-hair theorem

Solutions of the Einstein field equations yield different spacetime metrics under different physical conditions as discussed in Sec. 1.3. Thus distinct solutions for the spacetime metric are obtained, such as the Schwarzschild metric (1.76) , the Reissner-Nordström metric (1.91) and the Kerr metric (1.103). The Schwarzschild metric is parametrized by the ADM mass of the black hole, the Reissner-Nordström solution is parametrized by the ADM mass and the electric charge of the black hole, and the Kerr solution is parametrized by the ADM mass and the angular momentum of the black hole.

The Israel-Carter conjecture states that, for all solutions with closed simply-connected equipotential surface $g_{tt} = \text{const.}$, the only one which have regular event horizons are Schwarzschild metric for asymptotically flat vacuum [106], Reissner-Nordström for asymptotically flat electrovacuum [107], and Kerr metric for rotating black holes with asymptotically flat vacuum [49]. As a consequence, mass M, electric charge Q, and angular momentum J are the only quantities that parametrize the spacetime of a black hole. This conjecture is known as the celebrated “no-hair theorem”.

It was Bekenstein who made the foremost study in search of other quantities that can parametrize the spacetime a black hole [25, 26]. Bekenstein considered an electrically charged black hole where a massless conformal scalar field is non-minimally coupled to gravity via a conformal coupling, $\xi R\phi^2$. The corresponding Einstein-Maxwell conformal

scalar field model is given by the action

$$\mathcal{S} = \frac{c^3}{16\pi G}\int d^4x\sqrt{-g}R - \int d^4x\sqrt{-g}\left(\frac{1}{2}\partial_\mu\phi\partial^\mu\phi + \frac{\xi}{12}R\phi^2 + \frac{1}{16\pi}F_{\mu\nu}F^{\mu\nu}\right). \tag{1.107}$$

Bekenstein could successfully show that apart from mass M, charge Q, and angular momentum J, the scalar charge q_s is also an admissible quantity in parametrizing the spacetime of the black hole. The corresponding field equations coming from the action give rise to solutions, where the line element is given by

$$ds^2 = -\left(1-\frac{m}{r}\right)^2 c^2dt^2 + \left(1-\frac{m}{r}\right)^{-2} dr^2 + r^2\left(d\theta^2 + \sin^2\theta\, d\varphi^2\right), \tag{1.108}$$

with the electromagnetic field tensor

$$F_{\mu\nu} = \frac{Q}{r^2}\left(\delta^r_\mu\delta^t_\nu - \delta^t_\mu\delta^r_\nu\right), \tag{1.109}$$

and the scalar field

$$\phi = \frac{q_s}{r-m} \tag{1.110}$$

where

$$m = \left(\frac{GQ^2}{c^2} + \frac{4\pi G}{3c^2}q_s^2\right)^{\frac{1}{2}}. \tag{1.111}$$

In this result the scalar field diverges at the horizon $r = m$. However, the infinity occurring in the scalar field ϕ does not serve as a barrier for an infalling test scalar particle. Moreover, tidal accelerations of this model remain bounded at the $r = m$ horizon, which is expected to diverge at the physical singularity.

Bekenstein's black hole models [25, 26] with conformal scalar hair gave rise to a spate of research studies with modifications. Models with conformally coupled scalar fields that are massless [133, 160], massive [191, 192], and self-interacting [130–132], and with a cosmological constant, were considered to obtain hairy solutions.

For a system to be physically acceptable, there are two conditions the total energy-momentum tensor must satisfy. The mixed components of the energy-momentum tensor $T^\mu_{\ \nu}$ must be bounded and it should remain causal at the horizon and exterior to the black hole.

In order to have no divergences in the curvature invariant $G_{\mu\nu}G^{\mu\nu}$, the energy-momentum invariant $T_{\mu\nu}T^{\mu\nu}$ must be bounded everywhere in the exterior including the horizon. In

the static and spherically symmetric geometry,

$$T_{\mu\nu}T^{\mu\nu} = (T^t_{\ t})^2 + (T^r_{\ r})^2 + (T^\theta_{\ \theta})^2 + (T^\varphi_{\ \varphi})^2. \tag{1.112}$$

Thus the components $T^t_{\ t}$, $T^r_{\ r}$, and $T^\theta_{\ \theta} = T^\varphi_{\ \varphi}$ should be finite and well-behaved everywhere including the horizon.

In addition, the Poynting vector

$$j^\mu = -T^\mu_{\ \nu}u^\nu \tag{1.113}$$

gives the causality condition

$$T^\mu_{\ \nu}u^\nu T^\rho_{\ \mu}u_\rho \leq 0 \tag{1.114}$$

with respect to a distant observer with the four-velocity u^ν. This condition can be simplified using $u^\mu u_\mu = -c^2$ along with the fact that $u^r u_r$ and $u^\varphi u_\varphi$ are always positive for any observer moving in the equatorial plane, yielding the the condition

$$|T^\theta_{\ \theta}| = |T^\varphi_{\ \varphi}| \leq |T^t_{\ t}| \geq |T^r_{\ r}|. \tag{1.115}$$

These energy conditions were discussed by Hawking and Ellis [96] and Mayo and Bekenstein [134].

1.5 Neutron stars

One other significant astrophysical compact object, where the gravitational effects are strong are neutron stars. The gravitational strength of a neutron star heavily departs from the Newtonian limit. They are the compact stellar remnants of massive stars, born from catastrophic supernova events. Surpassed only by black holes in their density and gravitational pull, a typical neutron star compresses a mass greater than that of the Sun (approximately 1.4 to 2.5 times the solar mass) into a sphere with a radius of only 10 to 13 kilometers [163]. These extreme conditions cannot be replicated in any terrestrial laboratory, making neutron stars unique cosmic laboratories for studying matter at supranuclear densities.

Soon after the emergence of general relativity and its promising astrophysical predictions, Landau [123] proposed the possible existence of a dense star, such as a neutron star. The earliest study of stellar structure of a neutron star was by Tolman[183] and Oppenheimer and Volkoff [143], employing the celebrated Tolman-Oppenheimer-Volkoff

(TOV) equations using general relativity. However, neutron stars became a topic of interest only after the discovery of X-ray sources by [87] and the discovery of pulsar in 1967 by [99], which were then identified as rotating neutron stars by Gold in 1968 [88, 89].

1.5.1 Tolman-Oppenheimer-Volkoff equation

In order to find out the stellar structure of a neutron star, we consider the matter composition to be a perfect fluid. The energy-momentum tensor of a perfect fluid (1.57 is given by

$$T_{\alpha\beta} = \frac{(\varepsilon + P)}{c^2} u_\alpha u_\beta + g_{\alpha\beta} P, \tag{1.116}$$

where $\varepsilon = \rho c^2$ is the energy density, P is the pressure, and u^a is the four-velocity with $u^\alpha u_\alpha = -c^2$. Assuming the neutron star to be static and the matter is distributed spherically, we take the metric to be $ds^2 = -e^{\nu(r)}\, c^2\, dt^2 + e^{\lambda(r)}\, dr^2 + r^2 d\theta^2 + r^2 \sin^2\theta\, d\varphi^2$. The corresponding field equations from the Einstein equation (1.16) are given by

$$\begin{aligned} \frac{d\lambda}{dr} &= \frac{1 - e^\lambda}{r} + \kappa r e^\lambda \varepsilon(r), \\ \frac{d\nu}{dr} &= \frac{e^\lambda - 1}{r} + \kappa r e^\lambda P(r), \end{aligned} \tag{1.117}$$

where $\lambda(r)$ and $\nu(r)$ are the undetermined metric potentials. The radial profile of the cumulative mass function $m(r)$ is defined as

$$m(r) = \frac{c^2}{2G} r\{1 - e^{-\lambda(r)}\}. \tag{1.118}$$

From equations (2.3), (2.4), and the conservation law, $\nabla_a T^{\alpha\beta} = 0$, the TOV equations are obtained as

$$\frac{dP}{dr} = \frac{-\left[P(r) + \varepsilon(r)\right]}{r\left[c^2 r - 2Gm(r)\right]} \left[Gm(r) + \frac{4\pi G}{c^2} r^3 P(r)\right], \tag{1.119}$$

and

$$\frac{dm(r)}{dr} = \frac{4\pi r^2 \varepsilon(r)}{c^2}. \tag{1.120}$$

Employing appropriate equation of state that relates pressure $P(r)$ and density $\rho(r)$, one ca obtain the stellar structure the neutron star.

1.5.2 Equation of state of a neutron star

Neutron stars are natural laboratories to test strongly interacting nuclear matter. Even though the lattice quantum chromodynamics and heavy ion collision experiments provide crucial understanding of the properties of nuclear matter, neutron stars are the most reliable testing grounds with advancement in the observational astronomy.

he internal structure of a neutron star is best understood as a series of concentric shells, each defined by a specific density and a corresponding phase of matter. This layered structure is a physical manifestation of a continuous phase diagram, where matter undergoes dramatic transformations in response to the relentless increase in gravitational pressure.[10] The composition progresses from conventional atomic nuclei on the surface to a theoretical sea of quarks in the core.

The macroscopic properties of a neutron star, such as its mass and radius, are critically determined by a fundamental physical relationship known as the Equation of State. The equation of state describes how pressure inside the star responds to changes in density. The nuclear matter in a neutron star is subjected to extreme conditions as it is under tremendous pressure with the central density $\rho_c \sim 10^{15}$ g cm^{-3} for maximal mass configurations. This makes the nuclear matter highly degenerate and the equation of state is independent of temperature [91], except for a thin outer layer.

There have been attempts to formulate the equation of state of neutron matter considering multi-body interactions employing various phenomenologies such as Skyrme-type forces [50, 51, 82, 146, 173, 185], relativistic mean field [33, 138, 187], chiral effective field theory [69], the Urbana model [7], relativistic Fermi liquid ([84]), etc.

Moreover, there exist formulations, usually referred to as unified equations of state, such as SLy4, FPS and BSk $19-21$ [91, 157]. These unified equations of state are based on Skyrme type nucleon-nucleon interactions. SLy4 was constructed from SLy (Skyrme Lyone) type interactions [50, 51] and FPS was from generalized Skyrme model [146] by fitting to the estimates of Ref. [82]. BSk$19-21$ were based on the corresponding energy density functionals (EDF), developed from generalized Skyrme force using the Hartee-Fock-Bogoliubov method by the Brussels-Montreal group [90, 151, 152]. BSk19 EDF was fitted with constraints from the equation of state in Ref. [82]. BSk20 EDF was fitted with constraints from APR equation of state [7], whereas BSk21 EDF was fitted with constraints from LS2 equation of state [127]. It may be noted that these hadronnic equations of state are fitted with constraints coming from standard equations of state which have been very successful in modelling neutron stars.

The parameterized form in the SLy and FPS unified equations of state is expressed as

[91],

$$\zeta = \frac{a_1 + a_2\xi + a_3\xi^3}{(a_4\xi + 1)\left(e^{a_5(\xi - a_6)} + 1\right)} + \frac{a_7 + a_8\xi}{e^{a_9(a_{10} - \xi)} + 1} + \frac{a_{11} + a_{12}\xi}{e^{a_{13}(a_{14} - \xi)} + 1} + \frac{a_{15} + a_{16}\xi}{e^{a_{17}(a_{18} - \xi)} + 1}, \tag{1.121}$$

where $\zeta = \log\left(P/P_{\rm ref}\right)$ with $P_{\rm ref} = 1.0$ dyne cm^{-2}, and $\xi = \log\left(\rho/\rho_{\rm ref}\right)$ with $\rho_{\rm ref} = 1.0$ g cm^{-3}. The eighteen parameters a_i are given in Ref. [91].

Additionally, the parameterized form of the pressure P as a function of density ρ for BSk19, BSk20, and BSk21 unified equations of state is given by the expression [157]

$$\begin{aligned}\zeta =& \frac{a_1 + a_2\xi + a_3\xi^3}{(a_4\xi + 1)\left(e^{a_5(\xi - a_6)} + 1\right)} + \frac{a_7 + a_8\xi}{e^{a_9(a_6 - \xi)} + 1} + \frac{a_{10} + a_1\xi}{e^{a_{12}(a_{13} - \xi)} + 1} \\ &+ \frac{a_{14} + a_{15}\xi}{e^{a_{16}(a_{17} - \xi)} + 1} + \frac{a_{18}}{\left[a_{19}(\xi - a_{20})\right]^2 + 1} + \frac{a_{21}}{\left[a_{22}(\xi - a_{23})\right]^2 + 1},\end{aligned} \tag{1.122}$$

with $\zeta = \log\left(P/P_{\rm ref}\right)$ and $\xi = \log\left(\rho/\rho_{\rm ref}\right)$, as before. The twenty-three parameters a_i are given in Ref. [157].

While there is no concrete result for the hadron-to-quark transition in the literature, [119] suggested that typical models predict the phase transition to occur between $2 - 10$ $\rho_{\rm nuc}$. On the other hand, [21] suggests that quark matter equation of state should be applied for densities higher than $\sim 4 - 7$ $\rho_{\rm nuc}$.

For the deconfined quark core, we employ the equation of state given by the MIT bag model [110, 174],

$$P = k(\rho c^2 - 4B), \tag{1.123}$$

where B is the bag constant. The parameter k depends on the mass of strange quark m_s and the QCD coupling α_s. For $m_s = 0$, $k = 1/3$, and for $m_s = 250$ MeV/c^2, $k = 0.28$. The bag constant B takes a value $0.982B_0 < B < 1.525B_0$ for $m_s = 0$, with $B_0 = 60$ MeV fm^{-3} ([150]).

1.6 $f(R)$ gravity

Among the theories of modified gravity, $f(R)$ gravity is one of the most extensively studied formalism. In this theory, the Lagrangian in the Einstein-Hilbert action (1.4) $\mathcal{L}_{\rm GR} = R$ is replaced with a new Lagrangian $\mathcal{L}_g = f(R)$ [44], which is an arbitrary function of the Ricci scalar R. General relativity, while being successful in explaining various aspects of the strong gravity regime, it showed incompliance in explaining other strong gravity aspects such as the big bang singularity, and inflationary cosmology. Moreover, existence of

singularities in black holes motivated in the quantization of general relativity, that turned out to be non-renormalizable.

In this context, Utiyama and Dewitt [184] proposed that the divergence appearing in the expectation value of the energy-momentum tensor can be removed by adding higher order curvature terms into the Einstein-Hilbert action. Moreover, when the quantum correction and results from the string theory are taken into consideration, higher order curvature invariants are found to be admissible in the gravitational action [30, 43].

The suitable higher-order curvature terms coming from quantum fluctuations in the vacuum are R^2, $R_{\mu\nu}R^{\mu\nu}$, and $R^{\mu\nu\alpha\beta}R_{\mu\nu\alpha\beta}$. Among these, one term can be disregarded due to the Gauss-Bonnet combination, $R^2-4R_{\mu\nu}R^{\mu\nu}+R^{\mu\nu\alpha\beta}R_{\mu\nu\alpha\beta}$, which corresponds to the Euler characteristic—a topological invariant of four-dimensional manifolds. For the sake of tractability, an additional term is often neglected, simplifying the effective gravitational action to the form $R+\alpha R^2$, where α is a coupling parameter with the dimension of $[L]^2$.

At a deeper theoretical level, Shore [171] demonstrated that quantum fluctuations of scalar fields in a de Sitter background could generate an effective potential in the gravitational Lagrangian, arising from the vacuum expectation value $\langle T^{\rm QM}_{\mu\nu}\rangle$ in Einstein's equations. Further, Birrell and Davies [30] computed the one-loop quantum corrections to $\langle T^{\rm QM}_{\mu\nu}\rangle$ resulting from vacuum fluctuations of scalar fields in a Robertson–Walker universe. This method of deducing the functional form of $f(R)$ is considered more fundamental, given that it accounts for the unavoidable vacuum effects from standard model particles.

The most general form of the action for $f(R)$ gravity is given by

$$\mathcal{S}=\int d^4x\,\sqrt{-g}\left\{\frac{c^3}{16\pi G}f\left(R\right)+\mathcal{L}_m(g_{\mu\nu},\Psi)\right\}, \tag{1.124}$$

where the terms has usual meaning as described earlier. The field equations can be obtained using both metric as well as Palatini formalism. In this discussion we follow metric formalism. Varying the action (1.124) with respect to the metric $g^{\mu\nu}$ yields

$$\delta\mathcal{S}=\frac{c^3}{16\pi G}\int d^4x\left(\delta\sqrt{-g}f(R)+\sqrt{-g}f_R\delta R\right)+\int d^4x\delta\left(\sqrt{-g}\mathcal{L}_m\right), \tag{1.125}$$

where we used $\delta f=f_R\delta R$ with $f_R=\frac{\partial f}{\partial R}$. Applying the metricity condition $\nabla_\alpha g_{\mu\nu}=0$, and using the definition of covariant differentiation in equation (1.11) leads to

$$\delta R=\delta g^{\mu\nu}R_{\mu\nu}+g_{\mu\nu}\Box\delta g^{\mu\nu}-\nabla_\mu\nabla_\nu\delta g^{\mu\nu}. \tag{1.126}$$

Substituting (1.126) in (1.125), results in

$$\delta\mathcal{S} = \frac{c^3}{16\pi G}\int d^4x\sqrt{-g}\left\{f_R R_{\mu\nu}\delta g^{\mu\nu} - \frac{1}{2}g_{\mu\nu}f\delta g^{\mu\nu} + f_R\left(g_{\mu\nu}\Box\delta g^{\mu\nu} - \nabla_\mu\nabla_\nu\delta g^{\mu\nu}\right)\right\} - \frac{1}{2c}\int d^4x\sqrt{-g}T_{\mu\nu}\delta g^{\mu\nu}, \tag{1.127}$$

upon using the definition of energy-momentum tensor in the matter sector (1.13).

By applying Leibniz rule and integrating out the total derivative term, that vanishes when Gauss' law is applied to transform it into a surface integral, gives

$$\int d^4x\sqrt{-g}f_R\left(g_{\mu\nu}\Box\delta g^{\mu\nu} - \nabla_\mu\nabla_\nu\delta g^{\mu\nu}\right) = \int d^4x\sqrt{-g}\delta g^{\mu\nu}\left(g_{\mu\nu}\Box - \nabla_\mu\nabla_\nu\right)f_R. \tag{1.128}$$

Substituting this result in (1.127), the field equation in $f(R)$ gravity is obtained as

$$f_R R_{\mu\nu} - \frac{1}{2}g_{\mu\nu}f + \left(g_{\mu\nu}\Box - \nabla_\mu\nabla_\nu\right)f_R = \frac{8\pi G}{c^4}T_{\mu\nu}, \tag{1.129}$$

that reduces to the Einstein equation when $f(R) = R$.

Taking trace on both sides of the modified field equation (1.129), one obtains

$$\Box f_R = \frac{1}{3}\left(2f - f_R R + \frac{8\pi G}{c^4}T\right), \tag{1.130}$$

which is a clear departure from the trace of Einstein equation, $R = -\frac{8\pi G}{c^4}T$, following from equation (1.16). As a result, the Ricci scalar does not vanish in the exterior region of a spherically symmetric matter distribution, unlike in the case of general relativity. This result has a significant impact in the effective mass profiles of compact objects.

The covariant differentiation of the left hand side of (1.129) yields

$$\nabla_\mu\left[f_R R^\mu_{\ \nu} - \frac{1}{2}\delta^\mu_{\ \nu}f + \left(\delta^\mu_{\ \nu}\Box - \nabla^\mu\nabla_\nu\right)f_R\right] = f_R\nabla_\mu R^\mu_{\ \nu} + R^\mu_{\ \nu}\nabla_\mu f_R - \frac{1}{2}\delta^\mu_{\ \nu}\nabla_\mu f + \nabla_\mu\left(\delta^\mu_{\ \nu}\Box - \nabla^\mu\nabla_\nu\right)f_R. \tag{1.131}$$

Upon re-arranging terms, one can write the first three terms of the above equation in terms of the Einstein tensor as

$$f_R\nabla_\mu R^\mu_{\ \nu} + R^\mu_{\ \nu}\nabla_\mu f_R - \frac{1}{2}\delta^\mu_{\ \nu}\nabla_\mu f = f_R\nabla_\mu G^\mu_{\ \nu} + R^\mu_{\ \nu}\nabla_\mu f_R. \tag{1.132}$$

Further, using $\nabla_\mu G^\mu_{\ \nu} = 0$ given by equation (1.18) following from the Bianchi identity,

and noting the simplification $\nabla_\mu \left(\delta^\mu_{\ \nu}\Box - \nabla^\mu\nabla_\nu\right) f_R = -R^\mu_\nu \nabla_\mu f_R$, equation (1.131) leads to

$$\nabla_\mu \left[f_R R^\mu_\nu - \frac{1}{2}\delta^\mu_{\ \nu} f + \left(\delta^\mu_{\ \nu}\Box - \nabla^\mu\nabla_\nu\right) f_R \right] = 0. \tag{1.133}$$

This result is in complete agreement with the energy-momentum conservation $\nabla_\mu T^\mu_{\ \nu} = 0$, as implied by the modified field equation (1.129).

One of the significant $f(R)$ models that has received wide attention is the Starobinsky model. In his work on cosmological inflation, Starobinsky [179] showed that quadratic curvature can lead to an early de Sitter phase, explaining the inflationary regime [179]. The Starobinsky $f(R)$ Lagrangian has the form

$$f(R) = R + \alpha R^2, \tag{1.134}$$

where α is a coupling parameter. This model incorporates an extra scalar degree of freedom, which emerges naturally from the correction term αR^2. The R^2 term is equivalent to single-field slow-roll inflation. This is due to the extra degree of freedom coming from the αR^2 term. Moreover, this model is well consistent with the temperature anisotropies observed in the CMB. One other aspect of the Starobinsky-type $f(R)$ gravity is that it naturally accommodates quantum vacuum fluctuations of matter fields through its modified Friedmann equations.

Using this form of $f(R)$ in the modified field equation (1.129) yields

$$G_{\mu\nu} + 2\alpha R\left(R_{\mu\nu} - \frac{1}{4}g_{\mu\nu}R\right) + 2\alpha\left(g_{\mu\nu}\Box - \nabla_\mu\nabla_\nu\right)R = \frac{8\pi G}{c^4}T_{\mu\nu}, \tag{1.135}$$

and the trace equation in $f(R)$ gravity (1.130) is

$$6\alpha\Box R = R + \frac{8\pi G}{c^4}T, \tag{1.136}$$

in the Starobinsky $f(R)$ model, significantly deviating from general relativity, where $R = -\frac{8\pi G}{c^4}T$. Due to this, the Ricci scalar R does not drop to zero in the absence of matter fields, similar to that in general relativity. As a consequence, a gravitational halo is formed outside the stellar surface, and it contributes to the ADM mass, supporting supermassive neutron stars.

The viability of the $f(R)$ gravity in solar system tests can be understood by using following Chameleon mechanism. The $f(R)$ gravity action (1.124), defined in the Jordan

frame, can be transformed into the Einstein frame by means of a conformal transformation

$$\tilde{g}_{\mu\nu} = \Omega^2 g_{\mu\nu}, \tag{1.137}$$

where Ω^2 is the conformal factor. The Ricci scalar R in the Jordan frame is related to the Ricci scalar $\tilde{R}$ in the Einstein frame by

$$R = \Omega^2 \left(\tilde{R} + 6\tilde{\Box}\phi - 6\tilde{g}^{\mu\nu}\partial_\mu\phi\partial_\nu\phi \right), \tag{1.138}$$

where $\phi = \ln \Omega$. The corresponding gravitational action in (1.124) is obtained as

$$S_{\text{grav}} = \int d^4x\sqrt{-g} \left(\frac{1}{2\kappa^2} f_R R - V(R) \right), \tag{1.139}$$

where $V(R)$ is the potential is defined as

$$V(R) = \frac{1}{2\kappa^2} \left(f_R R - f(R) \right), \tag{1.140}$$

and $\kappa^2 = \frac{8\pi G}{c^3}$. Using the equation (1.138) and the relation

$$\sqrt{-g} = \Omega^{-4}\sqrt{-\tilde{g}}, \tag{1.141}$$

in the action (1.139), we get

$$S_{\text{grav}} = \int d^4x\sqrt{-\tilde{g}} \left[\frac{1}{2\kappa^2} f_R \Omega^{-2} \left(\tilde{R} + 6\tilde{\Box}\phi - 6\tilde{g}^{\mu\nu}\partial_\mu\phi\partial_\nu\phi \right) - \Omega^{-4} V \right]. \tag{1.142}$$

The corresponding matter action in (1.124) is transformed as

$$S_m = \int d^4x\, \mathcal{L}_m \left(\Omega^{-2}\tilde{g}_{\mu\nu}, \Psi_m \right). \tag{1.143}$$

Choosing the conformal factor

$$\Omega^2 = f_R, \tag{1.144}$$

and using Gauss's theorem, the total action in the Einstein frame becomes

$$S_E = \int d^4x\sqrt{-\tilde{g}} \left[\frac{1}{2\kappa^2}\tilde{R} - \frac{1}{2}\tilde{g}^{\mu\nu}\partial_\mu\Phi\partial_\nu\Phi - U(\Phi) \right] + \int d^4x\, \mathcal{L}_m \left(f_R^{-1}(\Phi)\tilde{g}_{\mu\nu}, \Psi_m \right), \tag{1.145}$$

where $\Phi = \frac{\sqrt{6}}{\kappa}\phi$, and the scalar potential $U(\Phi)$ is given by

$$U(\Phi) = \frac{V}{f_R^2} = \frac{f_R R - f(R)}{2\kappa^2 f_R^2}. \tag{1.146}$$

The choice $\Omega^2 = f_R$ requires $f_R > 0$. Since the matter in Einstein frame is directly coupled with the scalar field Φ, variation of action in Einstein-frame (1.145cc) with respect to Φ yields

$$\tilde{\Box}\Phi - \frac{dU}{d\Phi} + \frac{1}{\sqrt{-\tilde{g}}}\frac{\partial \mathcal{L}_m}{\partial \Phi} = 0. \tag{1.147}$$

The functional derivative of the matter Lagrangian with respect to Φ gives

$$\frac{\partial \mathcal{L}_m}{\partial \Phi} = -\frac{\sqrt{-\tilde{g}}}{2f_R}\frac{df_R}{d\Phi}\tilde{T}^{\mu\nu}_{(m)}\tilde{g}_{\mu\nu}, \tag{1.148}$$

so that the scalar field equation becomes

$$\tilde{\Box}\Phi - \frac{dU}{d\Phi} - \frac{f_{R,\Phi}}{2f_R}\tilde{T} = 0. \tag{1.149}$$

From the above equation, the coupling strength between the scalar field and matter is defined as

$$q = -\frac{f_{R,\Phi}}{2\kappa f_R} = -\frac{1}{\sqrt{6}}, \tag{1.150}$$

which is constant in $f(R)$ gravity. The scalar field equation can therefore be written as

$$\tilde{\Box}\Phi - \frac{dU}{d\Phi} + \kappa q\tilde{T} = 0, \tag{1.151}$$

showing that the scalar field Φ is directly coupled to matter.

If the scalar field is massless, $U(\Phi) = 0$, this leads to a long-range force with large coupling, which is incompatible with solar-system experiments. However, in viable $f(R)$ gravity models, $U(\Phi) \neq 0$, allowing consistency with local gravity tests [37, 114, 115].

1.7 Eddington inspired Born-Infeld gravity

Einstein's formulation of general relativity inspired physicists in searching for new theories of gravity. While there have been attempts to modify general relativity in different regimes where general relativity fails, alternate theories are also gaining attention in the present era.

One such alternate theory, proposed by Eddington [72], is the inspiration behind this

new theory. Eddington considered the affine connection $\Gamma^{\mu}_{\nu\rho}$ to be more fundamental in free (de Sitter) space than the metric $g_{\mu\nu}$ as in Einstein-Hilbert action (1.4). Eddington's action for gravitation is given by

$$\mathcal{S}_{\rm Edd} = 2\kappa \int d^4x \sqrt{|R(\Gamma)|}, \tag{1.152}$$

where $R(\Gamma)$ is the Ricci scalar, which is a function of the affine connection $\Gamma^{\mu}_{\nu\rho}$. Since $\Gamma^{\mu}_{\nu\rho}$ is the fundamental field in this frame work, the Eddington action (1.152) is varied with respect to the affine connection, leading to

$$\delta_{\Gamma}\mathcal{S}_{\rm Edd} = 2\kappa \int d^4x \delta \sqrt{|R|}. \tag{1.153}$$

Using the identity $\frac{\delta|M|}{|M|} = \mathrm{tr}\,(\mathbf{M}\delta\mathbf{M})$ in the above equation gives

$$\delta_{\Gamma}\mathcal{S}_{\rm Edd} = \kappa \int d^4x \sqrt{|R|} R^{\mu\nu} \delta R_{\mu\nu}. \tag{1.154}$$

With the identity (1.9), the above variation can be expressed as

$$\delta_{\Gamma}\mathcal{S}_{\rm Edd} = \kappa \int d^4x \sqrt{|R|} R^{\mu\nu} \left(\nabla_{\lambda}\, \delta\Gamma^{\lambda}_{\mu\nu} - \nabla_{\nu}\, \delta\Gamma^{\lambda}_{\mu\lambda}\right). \tag{1.155}$$

Employing Leibniz rule, the above integrand gives rise to a total derivative term that vanishes upon using Gauss' law to transform it into a surface term. The non-vanishing terms in the variation of the action are given by

$$\delta_{\Gamma}\mathcal{S}_{\rm Edd} = \int d^4x \left\{\nabla_{\alpha}\left(\kappa\sqrt{|R|}R^{\mu\alpha}\right)\delta^{\nu}_{\lambda} - \nabla_{\lambda}\left(\kappa\sqrt{|R|}R^{\mu\nu}\right)\right\}\delta\Gamma^{\lambda}_{\mu\nu}. \tag{1.156}$$

Demanding $\delta\mathcal{S}_{\rm Edd} = 0$ for the extremal condition to be satisfied leads to

$$\nabla_{\alpha}\left(\kappa\sqrt{|R|}R^{\mu\nu}\right) = 0, \tag{1.157}$$

where ∇_{α} is the covariant derivative defined in terms of the affine connection $\Gamma^{\mu}_{\nu\rho}$ and $R^{\mu\nu}$ is the inverse of $R_{\mu\nu}$.

In order to solve the equation (1.157), it is convenient to define a new tensor $h^{\mu\nu}$ and demand $\nabla_{\alpha}\left(\sqrt{|h|}h^{\mu\nu}\right) = 0$. Combining with (1.157), the field equation in Eddington gravity is obtained as

$$\kappa\sqrt{|R|}R^{\mu\nu} = \sqrt{|h|}h^{\mu\nu}, \tag{1.158}$$

which is equivalent to Einstein equation (1.16) in vacuum upon identifying $h_{\mu\nu}$ with $g_{\mu\nu}$ and κ with Λ^{-1}.

A major shortcoming of Eddington's theory is the non-existence of coupling between gravity and matter. A recent development in this direction, by coupling matter field with gravity, is a modification of Eddington's theory, known as Eddington inspired Born-Infeld (EiBI) gravity [16]. This theory integrates Eddington's original idea with that of Born-Infeld electrodynamics [34] into a unified theory. The Born-Infeld action for electrodynamics is given by

$$\mathcal{S}_{\rm BI} = -\frac{1}{b^2}\left[\int d^4x\sqrt{-|\eta_{\mu\nu}+bF_{\mu\nu}|}-1\right], \tag{1.159}$$

where $\eta_{\mu\nu}$ is the Minkowsky metric and b is a free parameter.

Similar to the Born-Infeld action, the Eddington action (1.152) is modified to

$$\begin{aligned}\mathcal{S}_{\rm EiBI}(g,\tilde{\Gamma},\Psi) =& \frac{c^3}{8\pi\kappa G}\int d^4x\left(\sqrt{-|g_{\mu\nu}+\kappa R_{\mu\nu}(\tilde{\Gamma})|}-\lambda\sqrt{-g}\right)\\ &+\int d^4x\sqrt{-g}\mathcal{L}_m(\Psi,g),\end{aligned} \tag{1.160}$$

where $\lambda = 1+\kappa\Lambda$, $g_{\mu\nu}$ is the metric tensor that defines the physical spacetime, $\mathcal{L}_m(\Psi,g)$ is the matter Lagrangian, κ is a coupling parameter, Λ is the cosmological constant, and the symbol "|.|"implies the the determinant of the tensor.

The EiBI is a Palatini type theory [145] where the affine connection $\tilde{\Gamma}^{\alpha}_{\mu\nu}$ is not related to the metric tensor $g_{\mu\nu}$. As a consequence, the Ricci tensor $R_{\mu\nu}(\tilde{\Gamma})$ is a function of the affine connection $\tilde{\Gamma}^{\alpha}_{\mu\nu}$ alone and it is independent of the physical metric $g_{\mu\nu}$. On the other hand, the matter Lagrangian $\mathcal{L}_m(\Psi,g)$ is a function of the physical metric $g_{\mu\nu}$.

Defining an auxiliary metric $q_{\mu\nu}$ as

$$q_{\mu\nu} = g_{\mu\nu}+\kappa R_{\mu\nu}(\tilde{\Gamma}), \tag{1.161}$$

we first vary the action (1.160) with respect to the metric tensor $\delta g_{\mu\nu}$, and obtain

$$\begin{aligned}\delta_g\mathcal{S}_{\rm EiBI}(g,\tilde{\Gamma},\Psi) =& \frac{c^3}{8\pi\kappa G}\int d^4x\left(\delta\sqrt{-|g_{\mu\nu}+\kappa R_{\mu\nu}(\tilde{\Gamma})|}-\lambda\delta\sqrt{-g}\right)\\ &+\int d^4x\delta\left(\sqrt{-g}\mathcal{L}_m(\Psi,g)\right).\end{aligned} \tag{1.162}$$

Using the relation (1.7), and the definition of energy-momentum tensor $T_{\mu\nu}$ (1.13), we get

$$\begin{aligned}\delta_g \mathcal{S}_{\rm EiBI}(g,\tilde{\Gamma},\Psi) =& \frac{c^3}{8\pi\kappa G}\int d^4x \left(\frac{\delta|g_{\mu\nu}+\kappa R_{\mu\nu}(\tilde{\Gamma})|}{2\sqrt{-q}} - \frac{\lambda\delta g}{2\sqrt{-g}}\right) \\ & - \frac{1}{2c}\int d^4x \delta\left(\sqrt{-g}T^{\mu\nu}\delta g_{\mu\nu}\right),\end{aligned} \tag{1.163}$$

where $q = |g_{\mu\nu}+\kappa R_{\mu\nu}(\tilde{\Gamma})|$ and $g = |g_{\mu\nu}|$. Using the relation $\frac{\delta|M|}{|M|} = \mathrm{tr}\,(\mathbf{M}\delta\mathbf{M})$, we obtain

$$\begin{aligned}\delta_g \mathcal{S}_{\rm EiBI}(g,\tilde{\Gamma},\Psi) =& \frac{c^3}{8\pi\kappa G}\int d^4x \left(\frac{\sqrt{-q}q^{\mu\nu}\delta g_{\mu\nu}}{2} - \frac{\lambda\sqrt{-g}g^{\mu\nu}\delta g_{\mu\nu}}{2}\right) \\ & - \frac{1}{2c}\int d^4x \delta\left(\sqrt{-g}T^{\mu\nu}\delta g_{\mu\nu}\right).\end{aligned} \tag{1.164}$$

With the extremal condition $\delta_g \mathcal{S} = 0$, we get the first set of field equations

$$\sqrt{-q}q^{\mu\nu} = \lambda\sqrt{-g}g^{\mu\nu} - \frac{8\pi\kappa G}{c^4}\sqrt{-g}T^{\mu\nu}. \tag{1.165}$$

In vacuum, where $T_{\mu\nu} = 0$, and for the cosmological constant $\Lambda = 0$ (or $\lambda = 1$), EiBI is equivalent to general relativity. This can be seen from equation (1.165), which reduces to $\sqrt{-q}q^{\mu\nu} = \sqrt{-g}g^{\mu\nu}$, implying $q_{\mu\nu} = g_{\mu\nu}$. Consequently, from equation (1.161), we see that $\tilde{R}_{\mu\nu} = 0$, recovering general relativity in vacuum in the absence of cosmological constant [16].

Furthermore, varying the action (1.160) with respect to the affine connection $\tilde{\Gamma}^{\alpha}_{\mu\nu}$, we get

$$\delta_{\tilde{\Gamma}} \mathcal{S}_{\rm EiBI}(g,\tilde{\Gamma},\Psi) = \frac{c^3}{8\pi\kappa G}\int d^4x \left(\delta\sqrt{-|g_{\mu\nu}+\kappa R_{\mu\nu}(\tilde{\Gamma})|}\right) \tag{1.166}$$

We simplify the above equation using the relation $\frac{\delta|M|}{|M|} = \mathrm{tr}\,(\mathbf{M}\delta\mathbf{M})$, and obtain

$$\delta_{\tilde{\Gamma}} \mathcal{S}_{\rm EiBI}(g,\tilde{\Gamma},\Psi) = \frac{c^3}{16\pi\kappa G}\int d^4x\sqrt{-q}q^{\mu\nu}\delta R_{\mu\nu}. \tag{1.167}$$

In this framework, we have equation (1.9) in the form

$$\delta R_{\ \mu\nu} = \tilde{\nabla}_\lambda\, \delta\tilde{\Gamma}^{\lambda}_{\mu\nu} - \tilde{\nabla}_\nu\, \delta\tilde{\Gamma}^{\lambda}_{\mu\lambda}, \tag{1.168}$$

where $\tilde{\nabla}_\alpha$ is the covariant derivative defined in terms of the affine connection $\tilde{\Gamma}^{\beta}_{\mu\nu}$ as

$$\tilde{\nabla}_\alpha B^{\mu\nu} = \partial_\alpha B^{\mu\nu} + \tilde{\Gamma}^{\mu}_{\alpha\beta}B^{\beta\nu} + \tilde{\Gamma}^{\nu}_{\alpha\beta}B^{\mu\beta}. \tag{1.169}$$

Upon substituting (1.168) in (1.167) , we thus obtain

$$\delta_{\tilde{\Gamma}}\mathcal{S}_{\rm EiBI}(g,\tilde{\Gamma},\Psi)=\frac{c^3}{16\pi\kappa G}\int d^4x\sqrt{-q}q^{\mu\nu}\left(\tilde{\nabla}_\lambda\,\delta\tilde{\Gamma}^\lambda_{\mu\nu}-\tilde{\nabla}_\nu\,\delta\tilde{\Gamma}^\lambda_{\mu\lambda}\right), \tag{1.170}$$

where the quantity $\sqrt{-q}q^{\mu\nu}$ is a tensor density, which may be redefined as

$$\mathfrak{q}^{\mu\nu}=\sqrt{-q}q^{\mu\nu}. \tag{1.171}$$

Using this redefinition in the equation (1.170), and applying Leibniz rule, we obtain

$$\begin{aligned}\delta_g\mathcal{S}_{\rm EiBI}(g,\tilde{\Gamma},\Psi)=&\frac{c^3}{16\pi\kappa G}\int d^4x\left\{\tilde{\nabla}_\lambda\left(\mathfrak{q}^{\mu\nu}\,\delta\tilde{\Gamma}^\lambda_{\mu\nu}\right)-\tilde{\nabla}_\nu\left(\mathfrak{q}^{\mu\nu}\,\delta\tilde{\Gamma}^\lambda_{\mu\lambda}\right)\right.\\&\left.-\tilde{\nabla}_\lambda\mathfrak{q}^{\mu\nu}\,\delta\tilde{\Gamma}^\lambda_{\mu\nu}+\tilde{\nabla}_\nu\mathfrak{q}^{\mu\nu}\,\delta\tilde{\Gamma}^\lambda_{\mu\lambda}\right\}.\end{aligned} \tag{1.172}$$

We note that the first term in the above equation is a total derivative term. Therefore, we define $\tilde{\nabla}_\lambda\mathfrak{A}^\lambda=\tilde{\nabla}_\lambda\left(\mathfrak{q}^{\mu\nu}\,\delta\tilde{\Gamma}^\lambda_{\mu\nu}\right)-\tilde{\nabla}_\lambda\left(\mathfrak{q}^{\mu\lambda}\,\delta\tilde{\Gamma}^\nu_{\mu\nu}\right)$ and substitute in the above equation, giving

$$\delta_{\tilde{\Gamma}}\mathcal{S}_{\rm EiBI}(g,\tilde{\Gamma},\Psi)=\frac{c^3}{16\pi\kappa G}\int d^4x\left\{\tilde{\nabla}_\lambda\mathfrak{A}^\lambda-\tilde{\nabla}_\lambda\mathfrak{q}^{\mu\nu}\,\delta\tilde{\Gamma}^\lambda_{\mu\nu}+\tilde{\nabla}_\nu\mathfrak{q}^{\mu\nu}\,\delta\tilde{\Gamma}^\lambda_{\mu\lambda}\right\}. \tag{1.173}$$

Since the total derivative term vanishes upon using Gauss' theorem and integrating over a hypersurface, we obtain

$$\delta_{\tilde{\Gamma}}\mathcal{S}_{\rm EiBI}(g,\tilde{\Gamma},\Psi)=\frac{c^3}{16\pi\kappa G}\int d^4x\left\{\tilde{\nabla}_\nu\mathfrak{q}^{\mu\nu}\,\delta\tilde{\Gamma}^\lambda_{\mu\lambda}-\tilde{\nabla}_\lambda\mathfrak{q}^{\mu\nu}\,\delta\tilde{\Gamma}^\lambda_{\mu\nu}\right\}. \tag{1.174}$$

Upon further simplifying the above equation, we get

$$\delta_{\tilde{\Gamma}}\mathcal{S}_{\rm EiBI}(g,\tilde{\Gamma},\Psi)=\frac{c^3}{16\pi\kappa G}\int d^4x\left\{\tilde{\nabla}_\alpha\mathfrak{q}^{\mu\alpha}\delta^\nu_\alpha-\tilde{\nabla}_\lambda\mathfrak{q}^{\mu\nu}\right\}\delta\tilde{\Gamma}^\lambda_{\mu\nu}. \tag{1.175}$$

For the extremal condition $\delta_{\tilde{\Gamma}}\mathcal{S}_{\rm EiBI}=0$ to satisfy, we thus obtain the second set of field equations

$$\tilde{\nabla}_\lambda\mathfrak{q}^{\mu\nu}=0, \tag{1.176}$$

in EiBI gravity.

We had shown earlier that the metricity condition (1.47) follows from the equation of motion (1.37) in the Palatini formalism in Sec. 1.2.1.3. In a similar manner, the field

equation (1.176) gives the metricity relation for the auxiliary metric, $q_{\mu\nu}$, given by

$$\tilde{\nabla}_\lambda q^{\mu\nu} = 0, \tag{1.177}$$

with the covariant derivative $\tilde{\nabla}_\lambda$ defined as in equation (1.169). Using this definition, we obtain the affine connection in terms of the auxiliary metric $q_{\mu\nu}$ as

$$\tilde{\Gamma}^\mu_{\alpha\beta} = \frac{q^{\mu\nu}}{2}\left(-\partial_\nu q_{\alpha\beta} + \partial_\beta q_{\alpha\nu} + \partial_\alpha q_{\nu\beta}\right). \tag{1.178}$$

In the gravity sector, all tensor quantities raise and lower their indices using the auxiliary metric $q_{\mu\nu}$. In the EiBI formalism, the Riemann tensor is defined with respect to $\tilde{\Gamma}_{\beta,\mu\nu}$ as

$$R_{\alpha\beta\gamma\delta}(\tilde{\Gamma}) = \partial_\gamma \tilde{\Gamma}_{\alpha,\beta\delta} - \partial_\delta \tilde{\Gamma}_{\alpha,\beta\gamma} + \tilde{\Gamma}_{\alpha,\gamma\sigma}\tilde{\Gamma}^\sigma_{\beta\delta} - \tilde{\Gamma}_{\alpha,\delta\sigma}\tilde{\Gamma}^\sigma_{\beta\gamma}. \tag{1.179}$$

Thus, the Riemann tensor, Ricci tensor, and Ricci scalar are defined in terms of the auxiliary metric $q_{\mu\nu}$ and the affine connection $\tilde{\Gamma}^\mu_{\alpha\beta}$,

$$R_{\beta\delta}(\tilde{\Gamma}) = q^{\alpha\gamma} R_{\alpha\beta\gamma\delta}(\tilde{\Gamma}), \tag{1.180}$$

$$R(\tilde{\Gamma}) = q^{\beta\delta} R_{\beta\delta}(\tilde{\Gamma}), \tag{1.181}$$

$$\tilde{\Gamma}_{\beta,\mu\nu} = q_{\alpha\beta}\tilde{\Gamma}^\alpha_{\mu\nu}. \tag{1.182}$$

It is evident from the above discussion that, there are two metric tensors in this theory; the physical metric $g_{\mu\nu}$ and the auxiliary metric $q_{\mu\nu}$. Since the matter field in this theory is dependent of the metric $g_{\mu\nu}$, raising and lowering of indices in the matter sector is by the physical metric $g_{\mu\nu}$. Moreover, the covariant derivative in the matter sector is defined in terms of the affine connection $\Gamma^\mu_{\alpha\beta}$, which is in turn defined in terms of the physical metric $g_{\mu\nu}$ as

$$\Gamma^\mu_{\alpha\beta} = \frac{g^{\mu\nu}}{2}\left(-\partial_\nu g_{\alpha\beta} + \partial_\beta g_{\alpha\nu} + \partial_\alpha g_{\nu\beta}\right). \tag{1.183}$$

Moreover, the covariant derivative ∇_α in the matter sector is defined in terms of the affine connection $\Gamma^\mu_{\alpha\beta}$ as $\nabla_\alpha B^{\mu\nu} = \partial_\alpha B^{\mu\nu} + \Gamma^\mu_{\alpha\beta}B^{\beta\nu} + \Gamma^\nu_{\alpha\beta}B^{\mu\beta}$.

We can obtain a mathematical relation between the two affine connections $\Gamma_{\beta,\mu\nu}$ and $\tilde{\Gamma}_{\beta,\mu\nu}$, defined with respect to $g_{\mu\nu}$ and $q_{\mu\nu}$, respectively. Equation (1.161) relates $g_{\mu\nu}$ with $q_{\mu\nu}$ and $\tilde{\Gamma}_{\beta,\mu\nu}$ as

$$g_{\mu\nu} = q_{\mu\nu} - \kappa R_{\mu\nu}(\tilde{\Gamma}). \tag{1.184}$$

From relation (1.183), the affine connection $\Gamma_{\beta,\mu\nu}$ is given by

$$\Gamma_{\beta,\mu\nu} = \frac{1}{2}\left(-\partial_\beta g_{\mu\nu} + \partial_\mu g_{\beta\nu} + \partial_\nu g_{\mu\beta}\right). \tag{1.185}$$

Using (1.184), equation (1.185) can be written in terms of $q_{\mu\nu}$ and $\tilde{\Gamma}_{\beta,\mu\nu}$ as

$$\Gamma_{\beta,\mu\nu} = \frac{1}{2}\left\{-\partial_\beta q_{\mu\nu} + \partial_\mu q_{\beta\nu} + \partial_\nu q_{\mu\beta} - \kappa\left(-\partial_\beta R_{\mu\nu}(\tilde{\Gamma}) + \partial_\mu R_{\beta\nu}(\tilde{\Gamma}) + \partial_\nu R_{\mu\beta}(\tilde{\Gamma})\right)\right\}. \tag{1.186}$$

From equation (1.178), the affine connection $\tilde{\Gamma}_{\beta,\mu\nu}$is defined with respect to the metric $q_{\mu\nu}$ as

$$\tilde{\Gamma}_{\beta,\mu\nu} = \frac{1}{2}\left(-\partial_\beta q_{\mu\nu} + \partial_\mu q_{\beta\nu} + \partial_\nu q_{\mu\beta}\right). \tag{1.187}$$

Using (1.187) in (1.186), we get the relation between the affine connections $\Gamma_{\beta,\mu\nu}$ and $\tilde{\Gamma}_{\beta,\mu\nu}$ as

$$\Gamma_{\beta,\mu\nu} = \frac{1}{2}\left[\tilde{\Gamma}_{\beta,\mu\nu} - \kappa\left\{-\partial_\beta R_{\mu\nu}(\tilde{\Gamma}) + \partial_\mu R_{\beta\nu}(\tilde{\Gamma}) + \partial_\nu R_{\mu\beta}(\tilde{\Gamma})\right\}\right]. \tag{1.188}$$

1.8 Layout of the Thesis

This thesis is structured into six chapters, each contributing to a comprehensive study of compact astrophysical objects—ranging from neutron stars to black holes—under various extensions of the gravitational theory and matter content. The research aims to explore how modified gravity frameworks and exotic states of matter influence the internal structure, stability, and spacetime geometry of these objects.

Chapter 2 investigates the structure of neutron stars featuring a deconfined quark core. It begins with an overview of neutron star modeling and the relevance of quark matter at high densities. The chapter then derives the field equations and introduces various equations of state to represent both hadronic and quark matter phases. Numerical integration techniques are employed to solve the coupled equations under appropriate boundary conditions. The resulting hybrid star models are analyzed, and their macroscopic properties, such as mass-radius relations and core composition, are discussed. The chapter concludes by summarizing the implications of these findings for the existence of quark cores in neutron stars.

Chapter 3 extends the analysis to neutron stars within the framework of $f(R)$ gravity, a modified theory of gravity motivated by the Starobinsky model. The chapter outlines the theoretical background and derives the modified field equations for spherically sym-

metric configurations. Using the same equations of state as in Chapter 2 allows for direct comparison between models in general relativity and those in $f(R)$ gravity. Numerical methods are again employed to analyze the resulting stellar structures, highlighting the impact of gravitational modifications on observable parameters such as maximum mass and radius. The chapter ends with a discussion on the astrophysical viability of such models in light of observational constraints.

Chapter 4 shifts focus to black hole physics, specifically exploring the spacetime structure of charged black holes in Eddington-inspired Born-Infeld (EiBI) gravity. Starting with the EiBI-Maxwell action, the chapter derives the field equations and analyzes the resulting black hole solutions across different regimes: asymptotic (long-distance), near the central region, intermediate zones, and near the event horizon. Special attention is given to the role of the EiBI coupling parameter, with separate analyses for positive and negative values. Numerical integration of the field equations is performed to confirm the analytical findings, and also discussed in terms of deviations from the classical Reissner-Nordström solution.

Chapter 5 examines the stability of charged scalar hair on Reissner-Nordström black holes. The chapter introduces the Einstein-Maxwell-charged scalar field model and investigates the conditions under which non-trivial scalar hair can exist. It examines both analytic and numerical solutions to the field equations, applying appropriate boundary conditions at the black hole horizon. Energy conditions are studied to ensure physical viability. A detailed dynamical stability analysis is performed using both Sturm-Liouville and Schrödinger-like equations to assess the stability of the scalar hair configuration.

Chapter 6 provides a summary of the key results obtained across the thesis. It reflects on the implications of the findings for our understanding of compact objects and gravity under extreme conditions. Potential avenues for future research are also outlined.

Collectively, these chapters provide a comprehensive investigation into the structural and stability properties of compact objects within both conventional and modified gravitational frameworks.

Chapter 2

Neutron star with deconfined quark core

The nature of equation of state for the matter in the neutron star plays an important role in determining its maximal mass. In addition, it must comply with the condition of causality. Noting that the central density of a maximally massive neutron star is well above the nuclear saturation density, a deconfined quark core in the central region is motivated in this chapter. We analyze this scenario by employing the MIT bag model to represent the core region and one of the unified equations of state for the region outside the core. Such combination is found to solve the problem of causality violation. In each case of the combined equations of state, the radial profile of ρr^2 displays a peak and dominant contribution to the total mass of the star comes from the region around the peak value of ρr^2, whereas the contribution is small from the regions near the center and the surface. This peak occurs in the region of hadronic matter for the combinations considered in this chapter. Importantly, we find that the position of the peak in ρr^2 is well-correlated with the maximal mass— the highest value of $1.98\ M_\odot$ obtains for the case with the peak occurring farthest from the center. This gravitational threshold being obtained for a non-rotating neutron star, we expect the threshold to lie well above $2\ M_\odot$ for a rapidly rotating neutron star, that may explain the existance of massive pulsars from recent astronomical observations.

2.1 Introduction

The earliest proposal for possible existence of a dense star, such as a neutron star, was made by Landau [123] in 1932. Later, Tolman (1939) [183] and Oppenheimer and Volkoff (1939) [143], employing the celebrated Tolman-Oppenheimer-Volkoff (TOV)

equations, obtained the stellar structure of neutron stars in general relativity (GR). Neutron stars became a topic of interest after the discovery of X-ray sources by Giacconi et al. [87] in 1962 and the discovery of pulsar in 1967 by Hewish et al. [99]. Pulsars were then identified as rotating neutron stars by Gold [88, 89]. Binary neutron star was first discovered in 1975 by Hulse and Taylor [105], and the millisecond pulsar (MSP) by Baker et al. [18] in 1982. In all subsequent observations until before 2010, the pulsars were found to have masses well below $2\ M_{\odot}$.

However, the scenario underwent a remarkable change since 2010 when pulsars of stellar mass $\sim 2\ M_{\odot}$ were observed to exist in the Universe. For instance, Demorest et al. [66] discovered MSP J1614-2230 in 2010 having a pulsar mass of $1.928 \pm 0.017\ M_{\odot}$ (as re-estimated by Fonseca et al. [76]). Similarly, Antoniadis et al. [9] discovered MSP J0348+0432 in 2013 with a pulsar mass of $2.01 \pm 0.04\ M_{\odot}$. In recent years, massive pulsars have been detected such as PSR J2215+5135 by Linares et al. in 2018 with a pulsar mass of $2.27 \pm^{0.15}_{0.17}\ M_{\odot}$ [128], MSP J0740+6620 by Cromartie et al. in 2019 with a pulsar mass of $2.14 \pm^{0.10}_{0.09}\ M_{\odot}$ [62], and PSR J0952-0607 by Bassa et al. [75] with a pulsar mass of 2.35 ± 0.17 $M_{\odot}$ [164].

Recent gravitational wave detections also indicated the existence of massive neutron stars. The gravitational wave event GW170817 ([2]), the first observed binary neutron star merger by the LIGO, reported component masses in the range $1.0 - 1.89\ M_{\odot}$ with a total mass of $2.73^{+0.04}_{-0.01}\ M_{\odot}$ ([3]). The next observed binary neutron star merger event GW190425 ([4]) reported component masses between $1.15 - 2.52\ M_{\odot}$ with a total mass of $3.4^{+0.3}_{-0.1}\ M_{\odot}$. Moreover, the GW190814 event was predicted to be the merger of a massive compact object of $2.50 - 2.67\ M_{\odot}$ with a black hole of $22.2 - 24.3\ M_{\odot}$ ([5]). The compact object, although too massive to be a neutron star and too light to be a black hole, might as well be a candidate for a massive neutron star.

The observational evidences for massive neutron stars naturally require a theoretical explanation including their stellar structure and composition of matter interior to such massive objects. However, such evidences bring about constraints on the equation of state, so that a stellar mass of $\sim 2\ M_{\odot}$ could be obtained ([197]). Consequently, efforts have been made to obtain an equation of state with a high degree of stiffness. In fact, high stiffness was incorporated for the high density regions of the star by removing the hyperons from the nuclear matter ([78, 84, 104]). However, it was argued that hyperons would emerge in the high density nuclear matter leading to softening of the equation of state ([64, 129]).

There have been attempts to formulate the equation of state of neutron matter considering multi-body interactions employing various phenomenologies such as Skyrme-type

forces ([50, 51, 82, 146, 173, 185]), relativistic mean field ([33, 138, 187]), chiral effective field theory ([69]), the Urbana model ([7]), relativistic Fermi liquid ([84]), etc. Some of these equations of state are stiff enough to yield the maximum stable mass $M_{\rm max} \sim 2\ M_\odot$ or even higher. However, some of these equations of state violate the condition of causality in the high density region of the star.

Moreover, there exist formulations, usually referred to as unified equations of state, such as SLy4, FPS and BSk $19-21$ ([91, 157]). These unified equations of state are based on Skyrme type nucleon-nucleon interactions. SLy4 was constructed from SLy (Skyrme Lyone) type interactions ([50, 51]) and FPS was from generalized Skyrme model ([146]) by fitting to the estimates of Ref. ([82]). BSk$19-21$ were based on the corresponding energy density functionals (EDF), developed from generalized Skyrme force using the Hartee-Fock-Bogoliubov method by the Brussels-Montreal group ([90, 151, 152]). BSk19 EDF was fitted with constraints from the equation of state in Ref. ([82]). BSk20 EDF was fitted with constraints from APR equation of state ([7]), whereas BSk21 EDF was fitted with constraints from LS2 equation of state ([127]). It may be noted that these hadronnic equations of state are fitted with constraints coming from standard equations of state which have been very successful in modelling neutron stars.

These hadronic equations of state (SLy, FPS, and BSk19–21) have certain advantageous features. Each of these equations of state is formulated using the same many-body interaction so that transitions between different hadronic regions of the star are continuous. They also remain causal up to reasonably high densities.

Among the five unified equations of state, SLy, BSk20 and BSk21 satisfy the 2 $M_\odot$ constraint coming from observations of massive pulsars ([9, 62, 66, 76, 128]), as they are capable of yielding maximal stable mass $M_{\rm max} \sim 2\ M_\odot$ or greater, BSk21 giving the highest ([91, 157]).

As we shall see in Section 2.4 below, when some of these hadronic equations of state (BSk19 and BSk20) are employed throughout the star, they violate the condition of causality ($c_s \leq c$) just before the gravitational instability sets in, so that, at ultra-high densities in the core region, the speed of sound c_s exceeds the speed of light c. The remaining hadronic equations of state (Sly, FPS, BSk21) remain causal within their regions of gravitational stability.

It is also important to note that, when these hadronic equations of state (SLy, FPS, and BSk19–21) are employed throughout the star, in order to attain the maximal mass configurations ($M_{\rm max} \sim 2\ M_\odot$), the central densities turn out to be $\rho_c \sim 10\ \rho_{\rm nuc}$, where $\rho_{\rm nuc} = 2.67 \times 10^{14}$ g cm^{-3} is the nuclear saturation density. Quark deconfinement is expected to occur at such ultra-high densities in the core region ([108, 109, 172]).

The above facts indicate that hadronic equations of state are not adequate representations for the ultra-high density core region. On the other hand, they are most suitable to represent the outer regions of lower densities (where they are causal).

In this chapter, we thus motivate the scenario of deconfined quark matter in the core region and hadronic matter in the region outside the core. For a simplistic analysis of this scenario, we employ the MIT bag model ([110, 174]) to represent the deconfined quark matter in the core region and one of the unified equations of state (SLy4, FPS and BSk $19-21$ [91, 157]) for the hadronic matter in the outer region. With this construction, we find that the hadronic equations of state remain causal because of crossover to the MIT bag model equation of state, so that causality is maintained throughout the star.

While there is no concrete result for the hadron-to-quark transition in the literature, [119] suggested that typical models predict the phase transition to occur between $2-10$ $\rho_{\rm nuc}$. On the other hand, [21] suggests that quark matter equation of state should be applied for densities higher than $\sim 4-7\ \rho_{\rm nuc}$.

We find that these bounds are satisfied when we take the first crossover between the MIT bag model and the unified equations of state to determine the transition from the quark region to the hadronic region. Namely, the transition points occur at 2.92 $\rho_{\rm nuc}$, 4.10 $\rho_{\rm nuc}$, 4.72 $\rho_{\rm nuc}$, 6.33 $\rho_{\rm nuc}$ and 6.78 $\rho_{\rm nuc}$ for transition from the MIT bag model to BSk21, BSk20, SLy, BSk19 and FPS, respectively. Such piece-wise continuous crossover happens in a small region so that we do not expect a significant change in the *total* mass if this cross-over is made smooth by interpolation. With this scheme, we study the stellar structure and obtain the maximal stable mass $M_{\rm max}$ for central densities $\rho_c \sim 10\ \rho_{\rm nuc}$. Our analysis reveals interesting features in relation to the maximal mass within this framework.

The remainder of the chapter is organized as follows. Section 2.2 briefly outlines the field equations. Section 2.3 presents the analytical representations of the unified equations of state and the MIT bag model. In Section 2.4, we give an outline of the methodology adopted in numerical integration of the field equations together with the boundary conditions. Section 2.5 embodies the main motivation of this chapter, with details of the stellar structure predicted by different combinations of the MIT bag model with the unified equations of state. Finally, the chapter is concluded in Section 2.6 with a discussion of the results.

2.2 Field Equations

In general relativity, the Einstein-Hilbert action is expressed as

$$\mathcal{S} = \frac{1}{2c\kappa}\int d^4x\,\sqrt{-g}\,R + \int d^4x\,\sqrt{-g}\,\mathcal{L}_m, \tag{2.1}$$

where $\kappa = \frac{8\pi G}{c^4}$, with G the Newton's constant, R the scalar curvature, and $\mathcal{L}_m$ is the matter Lagrangian. Varying the action with respect to the metric g^{ab}, and applying Hamilton's principle, the Einstein field equations are obtained as

$$G_{ab} = R_{ab} - \frac{1}{2}g_{ab}R = \kappa T_{ab}, \tag{2.2}$$

where R_{ab} is the Ricci tensor, and $T_{ab} = cg_{ab}\mathcal{L}_m - 2c\frac{\delta\mathcal{L}_m}{\delta g^{ab}}$ is the energy-momentum tensor.

For a perfect fluid, $T_{ab} = \frac{(\varepsilon+P)}{c^2}u_a u_b + g_{ab}P$, where $\varepsilon = \rho c^2$ is the energy density, P is the pressure, and u^a is the four-velocity with $u^a u_a = -c^2$.

Using the spherically symmetric static metric, $ds^2 = -e^{\nu(r)}\,c^2\,dt^2 + e^{\lambda(r)}\,dr^2 + r^2 d\theta^2 + r^2\sin^2\theta\,d\varphi^2$, leads to the field equations

$$\begin{aligned}\frac{d\lambda}{dr} &= \frac{1-e^{\lambda}}{r} + \kappa r e^{\lambda}\varepsilon(r),\\ \frac{d\nu}{dr} &= \frac{e^{\lambda}-1}{r} + \kappa r e^{\lambda}P(r),\end{aligned} \tag{2.3}$$

where $\lambda(r)$ and $\nu(r)$ are the undetermined metric potentials. The radial profile of mass can be obtained from

$$m(r) = \frac{c^2}{2G}r\{1 - e^{-\lambda(r)}\}. \tag{2.4}$$

From equations (2.3), (2.4), and the conservation law, $\nabla_a T^{ab} = 0$, TOV equations are obtained as

$$\frac{dP}{dr} = \frac{-\left[P(r)+\varepsilon(r)\right]}{r\left[c^2 r - 2Gm(r)\right]}\left[Gm(r) + \frac{4\pi G}{c^2}r^3 P(r)\right], \tag{2.5}$$

$$\frac{dm(r)}{dr} = \frac{4\pi r^2\varepsilon(r)}{c^2}, \tag{2.6}$$

We integrate the above equations simultaneously for the interior as well as the exterior of the neutron star with appropriate boundary conditions (as discussed in Section 2.4) employing different equations of state (as given in Section 2.3).

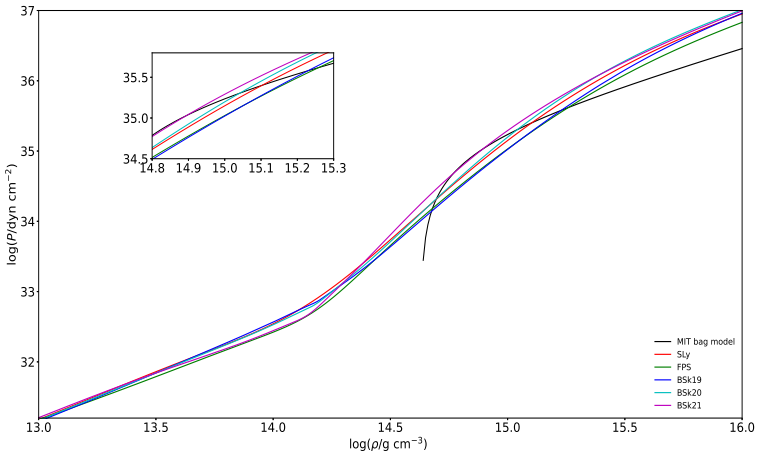

Figure 2.1: Plots for different unified equations of state expressed by equations 3.19 and 3.20, and the MIT bag model given by equation 3.21. The inset shows the crossover points between the MIT bag model and the unified equations of state.

2.3 Equations of State

The nuclear matter in a neutron star is subjected to extreme conditions as it is under tremendous pressure with the central density $\rho_c \sim 10^{15}$ g cm^{-3} for maximal mass configurations. This makes the nuclear matter highly degenerate and the equation of state is independent of temperature ([91]), except for a thin outer layer. The core is expected to consist of deconfined quark matter which we shall represent by the MIT-bag model ([110, 174]). The hadronic matter in the outer region will be represented by a unified equation of state such as, SLy, FPS ([91]), BSk19, BSk20 and BSk21 ([157].)

In order to have continuous representations for these equations of state, we employ the parameterized forms of the pressure P as a function of density ρ. The parameterized form in the SLy and FPS unified equations of state is expressed as ([91]),

$$\begin{aligned}\zeta = & \frac{a_1 + a_2\xi + a_3\xi^3}{(a_4\xi + 1)\left(e^{a_5(\xi - a_6)} + 1\right)} \\ & + \frac{a_7 + a_8\xi}{e^{a_9(a_{10} - \xi)} + 1} + \frac{a_{11} + a_{12}\xi}{e^{a_{13}(a_{14} - \xi)} + 1} \\ & + \frac{a_{15} + a_{16}\xi}{e^{a_{17}(a_{18} - \xi)} + 1},\end{aligned} \tag{2.7}$$

where $\zeta = \log\left(P/P_{\rm ref}\right)$ with $P_{\rm ref} = 1.0$ dyne cm^{-2}, and $\xi = \log\left(\rho/\rho_{\rm ref}\right)$ with $\rho_{\rm ref} = 1.0$ g cm^{-3}. The eighteen parameters a_i are given in Ref. ([91]).

Additionally, the parameterized form of the pressure P as a function of density ρ for

BSk19, BSk20, and BSk21 unified equations of state is given by the expression ([157])

$$\begin{aligned}\zeta = & \frac{a_1 + a_2\xi + a_3\xi^3}{(a_4\xi + 1)\left(e^{a_5(\xi - a_6)} + 1\right)} + \frac{a_7 + a_8\xi}{e^{a_9(a_6 - \xi)} + 1} \\ & + \frac{a_{10} + a_1\xi}{e^{a_{12}(a_{13} - \xi)} + 1} + \frac{a_{14} + a_{15}\xi}{e^{a_{16}(a_{17} - \xi)} + 1} \\ & + \frac{a_{18}}{\left[a_{19}(\xi - a_{20})\right]^2 + 1} + \frac{a_{21}}{\left[a_{22}(\xi - a_{23})\right]^2 + 1},\end{aligned} \tag{2.8}$$

with $\zeta = \log\left(P/P_{\rm ref}\right)$ and $\xi = \log\left(\rho/\rho_{\rm ref}\right)$, as before. The twenty-three parameters a_i are given in Ref. ([157]).

For the deconfined quark core, we employ the MIT bag model ([110, 174]), where quarks are treated as a non-interacting Fermi gas confined to a "bag". This allows the pressure–density relation in the MIT bag model to take the analytic form given by

$$P = k(\rho c^2 - 4B), \tag{2.9}$$

where B is the bag constant, which encapsulates quark confinement. The parameter k depends on the mass of the strange quark m_s and the QCD coupling α_s. For $m_s = 0$, $k = 1/3$, and for $m_s = 250$ MeV/c^2, $k = 0.28$. The bag constant B takes values $0.982B_0 < B < 1.525B_0$ for $m_s = 0$, with $B_0 = 60$ MeV fm^{-3} ([150]). In this chapter, we take $B = 60$ MeV fm^{-3} (that is, $B^{1/4} \sim 147$ MeV, corresponding to $\alpha_s = 0$, as in Figure 1 of Ref. [77]). Moreover, in the ultra-relativistic approximation, we take $m_s = 0$, so that $k = 1/3$.

The above equations of state are displayed in Fig. 3.1. The crossover between the MIT bag model and the unified equations of state are shown in the inset.

2.4 Initial Conditions and Numerical Integration

To obtain the stellar structure of neutron stars and the metric potentials, we need to solve the TOV equations (2.3), (2.5) and (2.6) by numerical integration. We re-scale these equations by defining dimensionless quantities, $\eta = r/r_g$, $\tilde{P} = P/P_0$, and $\tilde{\rho} = \rho/\rho_0$, where $P_0 = 4B$, $\rho_0 = P_0/c^2$ and $r_g = GM_\odot/c^2 = 1.4766 \times 10^5$ cm, the half of Schwarzchild radius of the Sun.

We set the initial conditions in carrying out the numerical integrations as follows. Initially, we supply a value for the central density $\rho(0) = \rho_c$. We note that $\lambda \to 0$ and $\nu \to \nu_c$ as $r \to 0$. Although it is straightforward to set the initial value $\lambda(0) = 0$, it is not so straightforward to set the initial value $\nu(0) = \nu_c$ consistent with the initial

choice $\rho(0) = \rho_c$. Since there is no direct dependence on ν in any of the equations, the central value ν_c is undetermined at this stage. However, it can be fixed so as to obtain an asymptotically flat solution at infinity. Consequently, the central value ν_c is fixed by looking at the exterior far-field solution, requiring it to be asymptotically flat so that $\lambda \to 0$ and $\nu \to 0$ as $r \to \infty$.

To validate this procedure, we solve equations (2.3), (2.5) and (2.6) employing the above initial conditions using different unified equations of state individually throughout the star, standard results for which are already available ([50, 157]). For each of these equations of state, we obtained the radial profiles of $\lambda(r)$ and $\nu(r)$ for the maximal central density corresponding to the maximal stable mass $M_{\rm max}$. We have confirmed that both $\lambda(r)$ and $\nu(r)$ asymptotically approach zero at infinity so that the space-time approaches the Minkowski flat geometry asymptotically.

The stellar mass of the star is obtained from

$$M = \frac{c^2}{2G} r_s \{1 - e^{-\lambda(r_s)}\} \tag{2.10}$$

where r_s is the stellar radius, determined from the condition of pressure approaching zero.

Our calculation with the purely hadronic equations of state yield the maximal stable mass $M_{\rm max}$ to be 2.05, 1.81,01.86, 2.16 and 2.27 $M_\odot$ with SLy, FPS, BSk19. BSk20 and BSk21, respectively. Thses values agree well with previous calculations by [50] and [157] validating our numerical procedure. We also note that the maximal stellar mass $M_{\rm max}$ is obtained for central densities between 2×10^{15} and 3.5×10^{15} g cm^{-3} across these hadronic equations of state.

However, just prior to attaining the maximal stable mass $M_{\rm max}$, BSk19 and BSk20 violate the condition of causality so that the velocity of sound given by $c_s = \sqrt{\frac{\partial P}{\partial \rho}}$ exceeds the velocity of light c. On the other hand, $M_{\rm max}$ given by SLy, FPS and BSk21 remain causal within the gravitational threshold of steability.

2.5 Stellar Structure with Combined Equations of State

As we have seen in the preceding section, some of the unified equations of state (BSk19 and BSk20) yield maximal masses by violating the condition of causality, occurring in the high density central region of the star. Moreover, the maximal mass was obtained for central densities between 2×10^{15} and 3.5×10^{15} g cm^{-3}. At such high densities, we expect that the core region to be composed of deconfined quark matter rather than

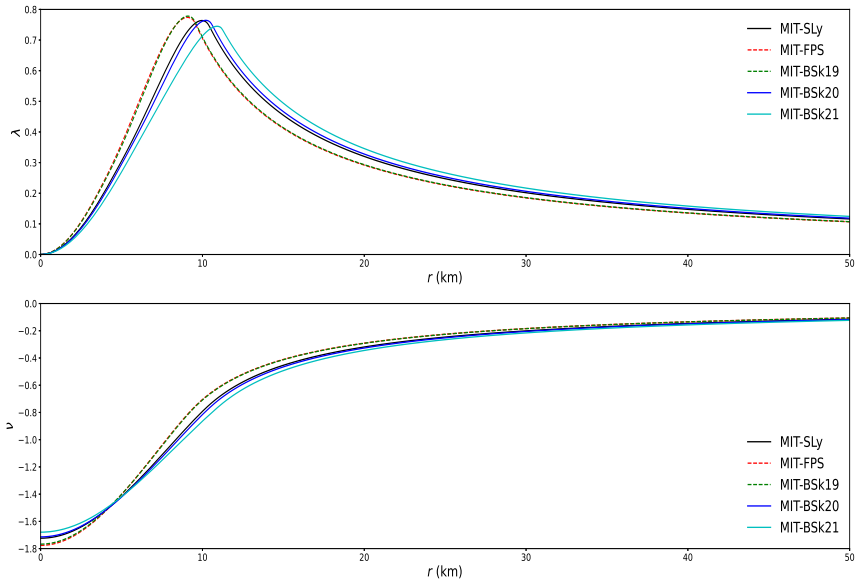

Figure 2.2: Radial profiles of the metric potentials $\lambda(r)$ [top] and $\nu(r)$ [bottom] for central densities corresponding to the maximal mass $M_{\rm max}$ using different combined equations of state.

hadronic matter. We thus take the MIT bag model to represent the deconfined quark matter in the core region. The region away from the core, on the other hand, is expected to be made up of predominantly hadronic matter that can be represented by one of the unified equations of state. This gives five combined equations of state, which we shall represent as MIT-SLy, MIT-FPS, MIT-BSk19, MIT-BSk20 and MIT-BSk21.

We take the crossover between the regions of deconfined quark matter and hadronic matter as the first intersection point between the two curves where both MIT bag model and the unified equation of state have the same pressure and the same density (shown in the inset of Fig. 3.1). This gives piece-wise continuous curves for each combination of

Table 2.1: Maximal stable mass $M_{\rm max}$, the corresponding central density ρ_c, and stellar radius r_s for different equations of state. The table also shows the speed of sound $c_{\rm s,c}$ at the center and $r_{\rm peak}$ is the radial position of the peak in ρr^2.

Equation of state	ρ_c (10^{15} g cm^{-3})	r_s (km)	$M_{\rm max}$ ($M_\odot$)	$r_{\rm peak}$ (km)	$c_{s,c}$ (10^{10} cm s^{-1})
MIT-SLy	2.39	10.75	1.85	7.89	1.73
MIT-FPS	2.94	9.86	1.71	6.98	1.73
MIT-BSk19	2.87	9.87	1.72	7.10	1.73
MIT-BSk20	2.28	10.93	1.89	8.23	1.73
MIT-BSk21	2.03	11.60	1.98	8.79	1.73

equations of state. With these models, we numerically integrate the TOV equations given by (2.3), (2.5) and (2.6), employing the boundary conditions as described in Section 2.4. This yields the interior and exterior solutions for the metric potentials $\lambda(r)$ and $\nu(r)$, and the radial profiles of density $\rho(r)$, pressure $P(r)$ and mass $m(r)$ for different combinations of the equations of state.

We display in Fig. 2.2 the radial profiles of the metric potentials $\lambda(r)$ and $\nu(r)$ for different combinations of the MIT bag model with the unified equations of state corresponding to the maximal stable mass $M_{\rm max}$ (shown in Table 2.1). These metric potentials display different behaviors up to 40 km from the center and thereafter they vary in similar ways with respect to different equations of state. Moreover, we have confirmed that both $\lambda(r)$ and $\nu(r)$ approach zero at large values of r signifying asymptotic approach to a flat Minkowski space-time at infinity.

Fig. 2.3 shows the density profiles corresponding to the maximum stable mass $M_{\rm max}$ for different combined equations of state. Although the MIT bag model represents the core in all cases, there are significant differences among the maximal central densities leading to different density profiles in all cases. Moreover, the density profiles show significant variation in the region near the surface where different unified equations of state describe the hadronic matter.

Table 2.1 summarizes the results for the maximum stable mass $M_{\rm max}$ obtained with different combinations of equations of state. It is evident that, although the central region is governed by the MIT bag model, the maximum central density $\rho_{c,\rm max}$, the maximal mass $M_{\rm max}$ and the stellar radius r_s differ for different combinations of equations of state. It is important to note that all these maximal central densities are consistent with the causality condition on the speed of sound, $c_s \leq c$.

Fig. 2.4 displays the pressure profiles for the maximum stable masses with the five combinations of equations of state. These profiles exhibit significant variation in the core region described by the MIT bag model, whereas there are small variations in the region near the surface described by different unified equations of state.

Fig. 2.5 displays the mass profile $m(r)$ given by equation (2.4) for the maximum stable masses $M_{\rm max}$ for different combinations of equations of state. The flattening of the curves near the surface occur due to negligible contribution to the total mass from near the surface.

Unlike the cases with the individual equations of state, the maximum stable mass in the present combined cases are below 2 $M_\odot$ as shown in Table 2.1. For example, BSk21 alone gave a maximum stable mass of 2.27 $M_\odot$ with a central density of 2.30×10^{15} g cm^{-3}, whereas the combination MIT-BSk21 yields 1.98 $M_\odot$ with a central density of

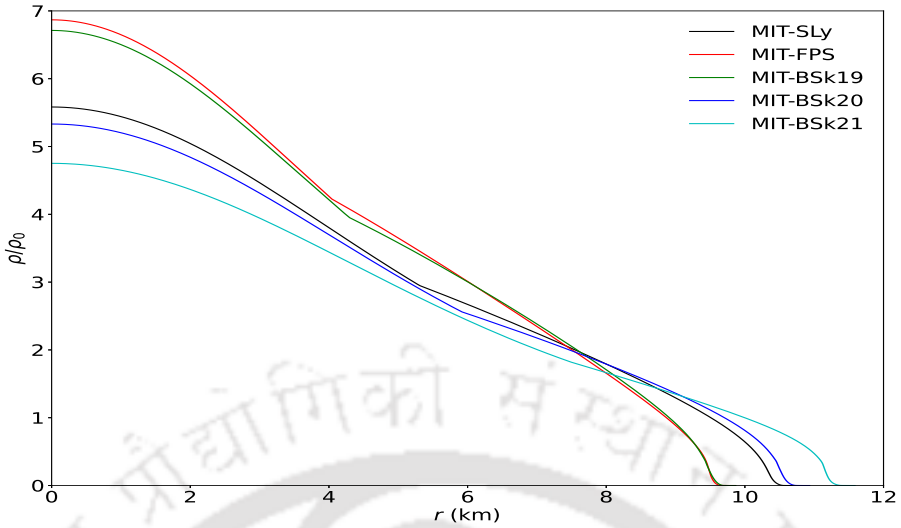

Figure 2.3: Density profiles $\rho(r)$ for central densities corresponding to the maximal mass $M_{\rm max}$ using different combined equations of state.

2.03×10^{15} g cm^{-3}. Although the value $1.98\ M_\odot$ is obtained with a deconfined quark core, it is the closest to the value of 2 $M_\odot$ among the combinations considered herein.

We further see from Table 2.1 that the maximal masses correlate well with the stellar radii. To understand this correlation, we plot in Fig. 2.6 the profile of ρr^2 for each of the combined equations of state. We note from Fig. 2.6 that the peaks in the radial profiles of ρr^2, and hence the mass distribution, continues farther outwards for the combination MIT-BSk21 compared to the rest of the combinations, giving the highest maximal mass. The positions of these peaks are given in Table 2.1. As the peaks shift to higher values of r, the mass distribution also shifts to higher values of r so that the contribution to the total mass increases. This clearly indicates that the position of the peak is correlated with the maximal mass.

The contribution to mass ΔM_{12} contained between the radial coordinates r_1 and r_2, given by

$$\Delta M_{12} = 4\pi \int_{r_1}^{r_2} \rho\, r^2\, dr, \tag{2.11}$$

is determined by the area under the curve between r_1 and r_2 in Fig. 2.6. Thus the contribution to ΔM_{12} from the central region (between 0 and 2 km, say) is much smaller compared to the total mass in all cases. Moreover, contribution from near the surface is negligible as the curves fall almost vertically near the surface in all cases. Thus the dominant contribution to the total mass comes from the intermediate region surrounding the peak value of ρr^2.

We further see from Fig. 2.6 that the MIT-BSk21 peak (as well as its profile) extend

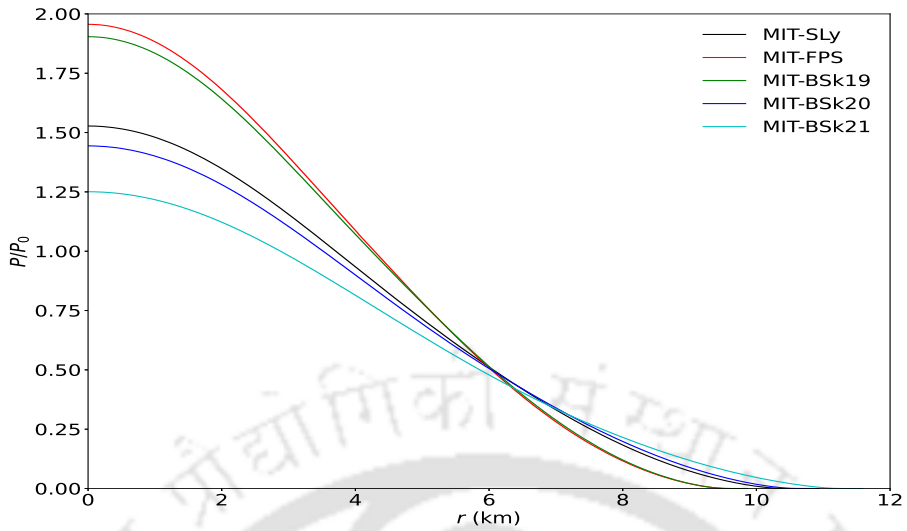

Figure 2.4: Pressure profiles $P(r)$ for central densities corresponding to the maximal mass $M_{\max}$ using different combined equations of state.

up to a higher radial coordinate compared to the other four combinations. This is correlated well with the fact that MIT-BSk21 yields the highest maximal mass. In addition, we observe that MIT-FPS and MIT-BSk19 have nearly the same peak positions (and profiles), explaining nearly equal masses for them. Moreover, MIT-SLy and MIT-BSk20 have similar peak positions (and profiles), giving similar masses.

The above behaviors of increasing mass are correlated well with the shift in the position of the peaks towards higher radial coordinates (as shown in Table 2.1). Since the integrand for ΔM_{12} given by equation (2.11) is weighted by the factor r^2, it is the extent

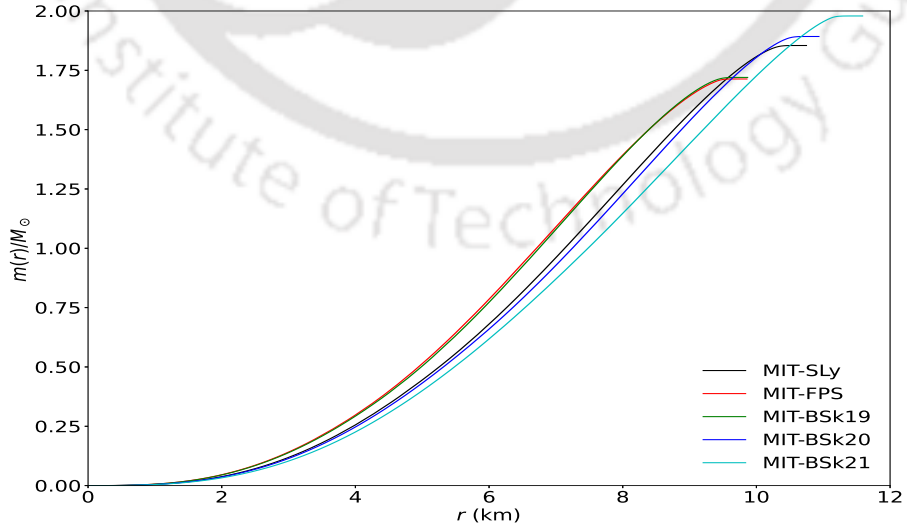

Figure 2.5: Radial profiles of the mass $m(r)$ corresponding to the maximal mass $M_{\max}$ with different combinations of equations of state.

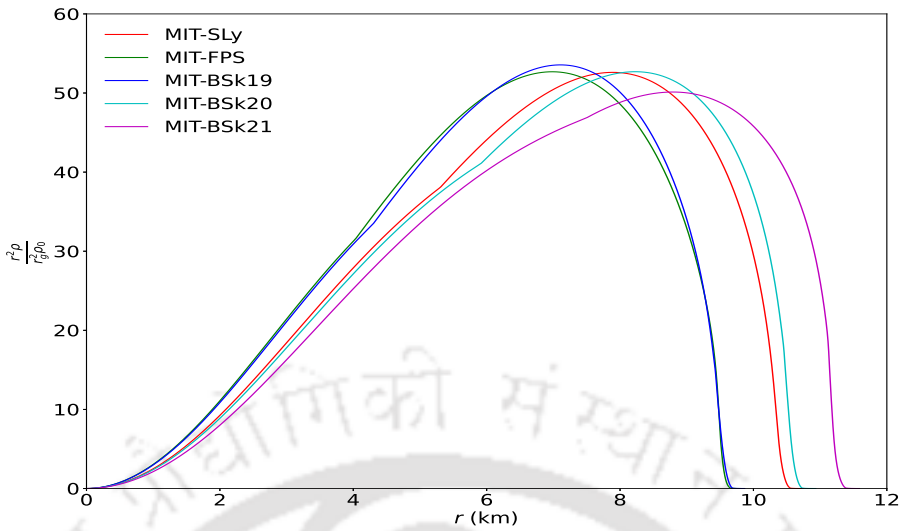

Figure 2.6: Radial profiles of ρr^2 corresponding to the maximal mass $M_{\max}$ with different combinations of equations of state. These radial profiles illustrate the fact that the mass distribution moves to higher radial values as the peak value of ρr^2 moves to the right, giving the highest total mass for the combination MIT-BSk21.

of the mass distribution that determines the maximal mass. Thus, it is the matter far from the center that gives dominant contribution to the total mass.

In the MIT-BSk21 combination, transition from the MIT bag model to BSk21 takes place at a lower density (higher radius) as compared to other combined cases. As a consequence, the MIT bag model dictates the stellar structure by forming a larger quark core region compared to the other combinations. In comparison, in the combinations MIT-

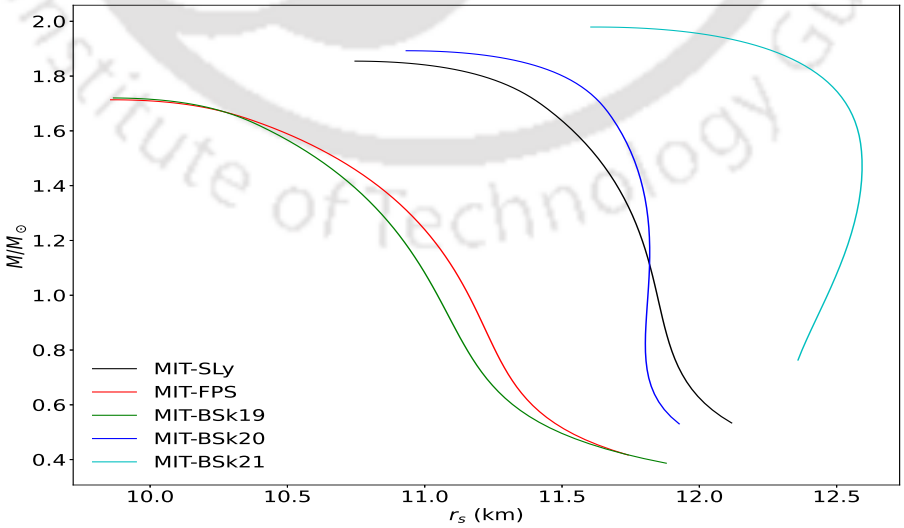

Figure 2.7: Mass-radius relations with different combinations of equations of state. Each curve is shown up to the corresponding $M_{\max}$ value.

BSk20 and MIT-SLy, the quark core is smaller, whereas in MIT-FPS and MIT-BSk19, the quark core is the smallest. In each combined case, a wide region around the peak is governed by the unified equation of state.

Fig. 2.7 displays the mass-radius curves obtained for different combined equations of state. The maximum mass value in each of these curves corresponds to the maximal stable mass $M_{\max}$. The figure shows only the stable branches so that the curves stop at the $M_{\max}$ values. It is clearly seen that the combination MIT-BSk21 yields the highest maximal mass, and the MIT-FPS combination yields the lowest. The combinations MIT-FPS and MIT-BSk19 give nearly coincident mass-radius curves and maximal masses. The maximal masses are summarized in Table 2.1.

Fig. 2.8 displays the mass versus central density curves for different combinations of the MIT bag model with the unified equations of state. In each case, the maximum stable mass $M_{\max}$ corresponds to the maxima of the curve, where $\frac{\partial M}{\partial \rho_c} = 0$. The region with the higher density segment beyond the maxima corresponds to the unstable regime, where $\frac{\partial M}{\partial \rho_c} < 0$. The stable regime corresponds to the segment where the mass increases with increase in central density, that is, for $\frac{\partial M}{\partial \rho_c} > 0$.

It is important to note that the maximum stable mass in each of these combined cases does not violate the causality condition ($c_s \leq c$), as shown in Table 2.1. Fig. 2.9 displays the radial profile of the speed of sound inside a neutron star for different combinations of equations of state. As can be seen, the causality condition is not violated in any case. Due to the piecewise continuous formulation of the equations of state considered in this chapter, the pressure–density relation is not differentiable at the point of cross-over between the two equations of state.

However, the existence of a discontinuity in the radial profile of the sound velocity does not affect observables such as stellar mass and stellar radius [136, 186]. As shown in [186] by comparing a piecewise-polytropic equation of state with a thermodynamically consistent construction of the equation of state, the mass–radius relation and the pressure–density relation are insensitive to the thermodynamic consistency check. However, the total baryon number and the chemical potential were found to have a jump across the phase transition. Moreover, Mroczek et al. [136] show that equations of state with non-trivial features such as bumps in the speed of sound are compatible with current constraints and found that mass, radius, and tidal deformability are insensitive to such micro-structures.

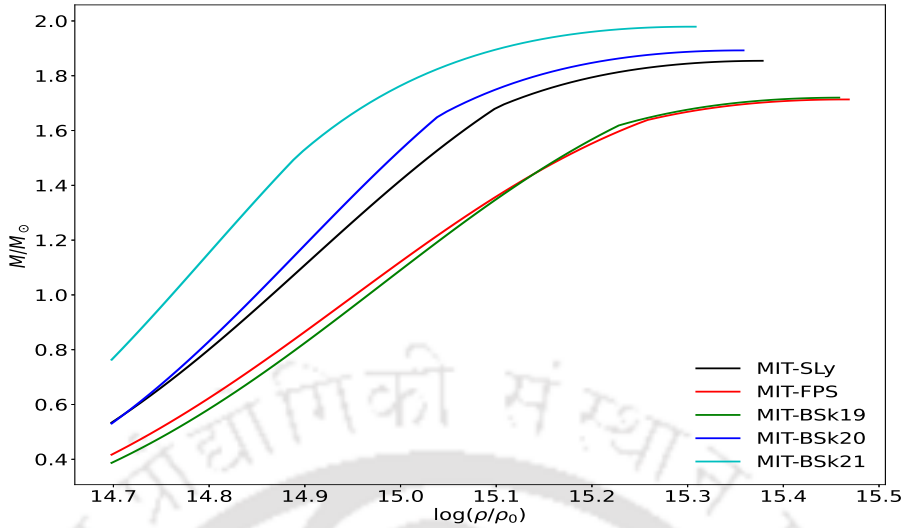

Figure 2.8: Mass versus central density for different combinations of equations of state.

2.6 Conclusions

In this work we studied the stellar structure and maximal mass of neutron stars using different combinations of equations of state. As we have discussed earlier, the relativistic equations of state, without involving quark deconfinement in the central region, have been employed throughout the star, yielding maximal mass $\sim 2\ M_\odot$ or even higher (Cf. Table III in Ref. [161]). However, as shown by [161] some of the relativistic equations of state violate the condition of causality upon piecewise polytropic fits to the tabulated equations of state in the high density region.

When a unified equation of state is used throughout the star, we have seen in Section 2.4 that some of them yield the maximal mass $M_{\rm max} \sim 2\ M_\odot$ or higher. However, BSk19 and BSk20 violate the causality condition ($c_s \leq c$) in the high density central region for the maximal mass.

We also found that the central density corresponding to the maximal mass $M_{\rm max}$ is $\rho_c \sim 10\,\rho_{\rm nuc}$ or even higher, where $\rho_{\rm nuc} = 2.67 \times 10^{14}$ g cm^{-3} is the nuclear saturation density. This indicates that the matter is mainly deconfined quark matter in the central region. The MIT bag model is therefore a more suitable choice than the the unified equations of state in the central region. The outer region, on the other hand, may be assumed to be composed of mainly hadronic matter where one of the unified equations of state can be employed. The crossover between these two regions is determined by the matching point between the two equations of state. Since the crossover between the two phases happens in a small region, an accurate interpolation is not expected to make a significant difference in the *total* mass and a piece-wise continuous representation is expected to be

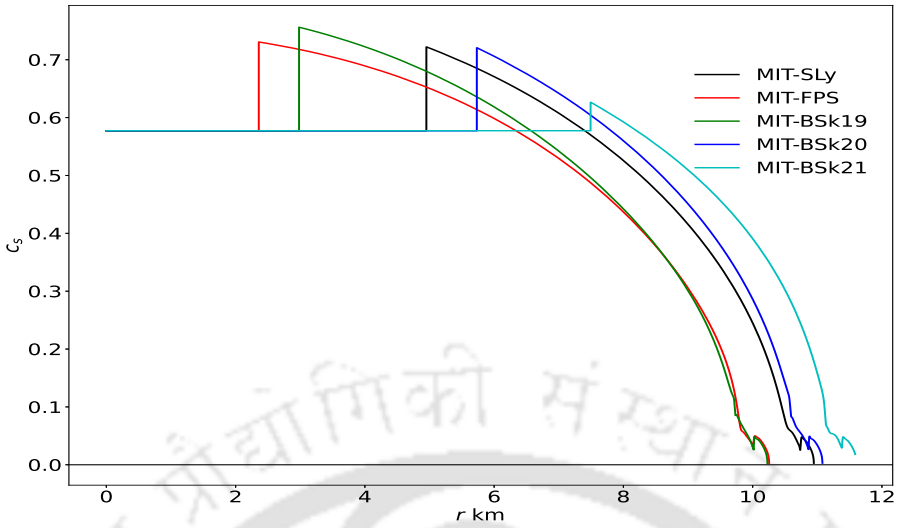

Figure 2.9: Radial profiles of the speed of sound c_s inside the neutron star, corresponding to the maximal mass $M_{\rm max}$ with different combinations of equations of state.

reliable.

As shown in Table 2.1, these combined equations of state yield maximal masses slightly less than 2 $M_\odot$, whereas, the MIT-BSk21 combination almost touches this value. In addition, we find that the causality condition ($c_s \leq c$) is well-respected for all these combined equations of state.

Our calculations illustrate another important feature determining the maximal mass. The integrand determining the total mass of the star is weighted by r^2 and the peak in ρr^2 occurs far from the center. Thus the dominant contribution to the total mass comes from the region around the peak. The regions near the center as well as the surface give small contributions to the total mass. The combination MIT-BSk21 yields the highest maximal mass as its peak in ρr^2 occurs at the highest radial coordinate r (among the combinations considered). It may also be important to note that the deconfined quark core for MIT-BSk21 extends to a higher radial coordinate than the other combinations. The peak in ρr^2 occurs in the outer hadonic matter region and it is moved to a higher radial coordinate for MIT-BSk21 than in the other combinations. The positions of the peaks in ρr^2 are well-correlated with the maximal mass as displayed in Table 2.1.

Recently, [164] estimated a pulsar mass of 2.35 ± 0.17 $M_\odot$ for PSR J0952-0607 observed by [75], which is a rapidly rotating neutron star with a pulsar frequency of 707 Hz. As shown earlier by [170] and [83], a rapidly rotating neutron star ($\sim$ 1 kHz) can support 20–25 % more mass than the gravitational threshold of a non-rotating neutron star. Our gravitational threshold being 1.98 $M_\odot$ for a non-rotating neutron star, the increased threshold due to maximal rotation would be 2.38–2.48 $M_\odot$. A stiffer choice of equation

of state to represent the outer shell of the star can further increase the maximal mass of neutron stars rotating at angular frequencies ~ 700 Hz.

Our study thus illustrates that it is possible to approach the desired value of $2\,M_{\odot}$ for a non-rotating neutron star with a proper combination of equations of state for deconfined quark matter and hadronic matter so that the peak in ρr^2 occurs at a sufficiently high value of the radial coordinate. As the total mass is significantly dependent on the outer region where the peak in ρr^2 occurs, an adequate formulation of the equation of state for hadronic matter is also important. Consequently, a different choice of equation of state that can represent both the deconfined core and the hadronic outer region, satisfying this condition, can achieve a similar (or even a better) result.

In the realistic scenario, we expect a continuous phase transition from the deconfined quark matter in the core region to the hadronic matter in the outer region. This phase transition, which is not yet well-understood, needs an adequate formulation on the basis of quantum chromodynamics. This is however a formidable task and improvements in the neutron star models would require well-formulated phenomenological models accounting for the necessary features of such continuous phase transition.

Chapter 3

Stellar structure of neutron stars in $f(R)$ gravity

This chapter investigates the stellar structure of neutron stars within the framework of the Starobinsky $f(R)$ gravity model, focusing on the impact of causal constraints on the equation of state. We consider hybrid models in which the stellar core consists of deconfined quark matter, described by the MIT bag model, while the outer layers are composed of hadronic matter represented by unified equations of state such as SLy4, BSk20 and BSk21. This two-phase construction maintains causality throughout the star, and within $f(R) = R + \alpha R^2$ gravity, the tunable parameter α provides flexibility to accommodate higher stable masses. We derive the modified field equations for this model, specialize to static spherical symmetry, and integrate them numerically for the chosen hybrid equation of state. The results include radial profiles of pressure, Ricci scalar, and mass function, as well as the variation of the ADM mass with central density and stellar radius radius. Our findings highlight the potential of $f(R)$ gravity to support massive neutron stars beyond the general relativistic limit while preserving causality.

3.1 Introduction

One of the notable predictions of general relativity (GR) is the existence of neutron stars [123, 143, 183], where gravitational effects are extreme. The discovery of pulsars [87, 99], later identified by Gold [88, 89] as rapidly rotating neutron stars, confirmed this prediction. Additional support came in 1975 with the discovery of the first binary neutron star system by Hulse and Taylor [105], which also provided indirect observational evidence for gravitational waves. For decades following these discoveries, all measured

pulsar masses remained well below $2\ \mathrm{M}_\odot$, consistent with GR-based expectations.

A major shift occurred after 2010 with the detection of pulsars whose masses approached or exceeded $2\ \mathrm{M}_\odot$. In 2010, Demorest et al. [66] reported MSP J1614–2230, with an updated mass measurement by Fonseca et al. [76] of $1.928 \pm 0.017\ \mathrm{M}_\odot$. In 2013, Antoniadis et al. [9] measured MSP J0348+0432 to be $2.01 \pm 0.04\ \mathrm{M}_\odot$. Subsequent observations have revealed even more massive pulsars, including PSR J2215+5135 with $2.27^{+0.15}_{-0.17}\ \mathrm{M}_\odot$ [128], MSP J0740+6620 with $2.14^{+0.10}_{-0.09}\ \mathrm{M}_\odot$ [62], and PSR J0952–0607, whose mass was determined by Bassa et al. [75, 164] to be $2.35 \pm 0.17\ \mathrm{M}_\odot$.

Gravitational wave astronomy has provided further evidence for high-mass neutron stars. The binary neutron star merger GW170817 [2], detected by LIGO, involved component masses between 1.0 and $1.89\ \mathrm{M}_\odot$, with a total system mass of $2.73^{+0.04}_{-0.01}\ \mathrm{M}_\odot$ [3]. GW190425 [4] indicated component masses in the range 1.15–$2.52\ \mathrm{M}_\odot$, with a combined mass of $3.4^{+0.3}_{-0.1}\ \mathrm{M}_\odot$. Another remarkable event, GW190814 [5], was interpreted as a merger between a 2.50–$2.67\ \mathrm{M}_\odot$ compact object and a black hole of 22.2–$24.3\ \mathrm{M}_\odot$. The nature of the lighter object remains uncertain, lying in the so-called mass gap—too massive to be a standard neutron star yet too light to be a typical black hole—making it a strong candidate for an ultra-massive neutron star.

The existence of such massive neutron stars poses significant theoretical challenges, particularly concerning their internal composition and the properties of matter at supranuclear densities. These observations place stringent constraints on the equation of state, which must be sufficiently stiff to support stars of $\sim 2\ \mathrm{M}_\odot$ [197]. One strategy to achieve the necessary stiffness is to suppress the presence of hyperons in dense nuclear matter [78, 84, 104]. However, theoretical models suggest that hyperons are likely to form under extreme densities, softening the equation of state and reducing the maximum stable mass [64, 129].

Numerous equation of state models for neutron-rich matter have been proposed, incorporating multi-body interactions and different phenomenological approaches [7, 33, 50, 51, 69, 82, 84, 138, 146, 173, 185, 187]. While some of these are stiff enough to yield $M_{\max} \sim 2\ \mathrm{M}_\odot$ or higher, certain models violate causality at high densities. Achieving maximal masses around $2\ \mathrm{M}_\odot$ often requires central densities on the order of $\rho_c \sim 10\rho_{\mathrm{nuc}}$, where $\rho_{\mathrm{nuc}} = 2.67 \times 10^{14}\ \mathrm{g\ cm^{-3}}$ is the nuclear saturation density. At such extreme densities, quark deconfinement is expected to occur in the stellar core [108, 109, 172].

Extended theories of gravity have also been explored as a means to achieve neutron star masses above $2\ \mathrm{M}_\odot$ [65, 142]. In this chapter, we focus on the Starobinsky $f(R)$ gravity model [179], given by $f(R) = R + \alpha R^2$. Treating the αR^2 term as a perturbation, Arapoğlu et al. [10] found that, for certain equations of state, the maximum mass

could approach $\sim 2\ \mathrm{M}_\odot$ only for negative α. By contrast, Yazadjiev et al. [195] solved for stellar equilibrium configurations non-perturbatively using an equivalent scalar–tensor formulation, avoiding the unphysical behaviour seen in perturbative treatments, such as a decrease in enclosed mass within the stellar interior [144].

Astashenok et al. [11] extended the non-perturbative analysis of $R + \alpha R^2$ gravity to both neutron and quark stars. For positive α, they found that the Ricci scalar remains finite at the surface and decays exponentially outside the star, adding an external gravitational mass component to the total observed mass. This feature influences observable effects such as gravitational redshift.

The viability of $f(R)$ gravity in high-curvature regimes has been debated, with some works [85, 117, 118] reporting the formation of curvature singularities inside highly compact stars. However, Babichev and Langlois [17] demonstrated that stable, relativistic stars can be obtained numerically in $f(R)$ gravity using polytropic equations of state, provided the condition $\rho c^2 - 3P > 0$ is satisfied throughout the stellar interior. This result was later confirmed in [48] using unified equations of state. Nonetheless, the same condition restricts the stiffness of the equation of state, thereby limiting the maximum stable mass achievable in $f(R)$ gravity.

From the above discussion, it follows that the condition $\rho c^2 - 3P > 0$ constrains the equation of state in such a way that it remains causal, avoiding superluminal sound speeds. Under this restriction, an appropriately chosen $f(R)$ gravity model may still accommodate neutron stars with maximum stable masses exceeding $2\ \mathrm{M}_\odot$. This is plausible since certain $f(R)$ forms, such as $R + \alpha R^2$ gravity, possess a tunable parameter α. Motivated by this, in the present chapter we explore hybrid equations of state in which the stellar core is composed of deconfined quark matter, while the outer layers are formed of hadronic matter. The presence of the quark core is expected to maintain the equation of state within the causal limit at high densities.

In the present analysis, the quark phase is modeled using the MIT bag model [110, 174], while the hadronic phase is described by unified equations of state such as SLy4, FPS, and BSk19–21 [91, 157]. This two-phase construction ensures that the transition from hadronic matter to quark matter preserves causality throughout the stellar interior. As summarized earlier in Table 2.1, these hybrid equations of state yield maximum masses marginally below $2\ \mathrm{M}_\odot$ based on GR, with the MIT–BSk21 combination coming closest to this threshold.

The remainder of this chapter is structured as follows. Section 3.2 introduces the action for $f(R)$ gravity, supplemented by a general matter action, and derives the corresponding modified field equations for the Starobinsky $f(R)$ model. In Section 3.3, we

specialize to a static, spherically symmetric spacetime and extract the differential equations governing the metric potentials and the Ricci scalar from the modified field equations. Section 3.4 presents the complete set of equations of state employed in this analysis, while Section 3.5 outlines the initial conditions used for the numerical integration. The results of these integrations, including the radial profiles of pressure, Ricci scalar, and mass function, as well as the dependence of the ADM mass on central density and stellar radius, are discussed in Section 3.6. Finally, Section 3.7 provides concluding remarks.

3.2 Action and field equations

The most general form of the action for $f(R)$ gravity is given by

$$\mathcal{S}(\Psi, g) = \int d^4x \sqrt{-g} \left\{ \frac{c^3}{16\pi G} f\left(R\right) + \mathcal{L}_m(\Psi, g) \right\}, \tag{3.1}$$

where R is the Ricci scalar, g is the determinant of the metric tensor $g_{\mu\nu}$, G is the gravitational constant, c is the velocity of light in the vacuum, and $\mathcal{L}_m(\Psi, g)$ is the matter Lagrangian with Ψ being the matter field. The energy-momentum tensor is obtained from the matter Lagrangian using

$$T_{\mu\nu} = c g_{\mu\nu} \mathcal{L}_m - 2c \frac{\delta \mathcal{L}_m}{\delta g^{\mu\nu}}. \tag{3.2}$$

Field equations corresponding to the action (3.1) is obtained using the metric formalism, where the action is varied with respect to the metric tensor $g_{\mu\nu}$. Demanding the extremality condition $\delta\mathcal{S} = 0$ gives the modified field equations

$$f_R R_{\mu\nu} - \frac{1}{2} g_{\mu\nu} f + \left(g_{\mu\nu}\Box - \nabla_\mu \nabla_\nu\right) f_R = \kappa\, T_{\mu\nu}, \tag{3.3}$$

where $\kappa = \frac{8\pi G}{c^4}$, and $f_R = \frac{\partial f}{\partial R}$.

The energy-momentum conservation $\nabla_\mu T^\mu_{\ \nu} = 0$ is satisfied in $f(R)$ gravity. Using Bianchi identity and tensor properties, we obtain the covariant derivative of the L.H.S. of the modified field equations (3.3)

$$\nabla_\mu \left[f_R R^\mu_{\ \nu} - \frac{1}{2} \delta^\mu_{\ \nu} f + \left(\delta^\mu_{\ \nu}\Box - \nabla^\mu \nabla_\nu\right) f_R \right] = 0, \tag{3.4}$$

satisfiying the conservation of energy-momentum tensor.

In the present work, we use the Starobinky $f(R)$ model [179], with

$$f(R) = R + \alpha R^2, \tag{3.5}$$

where α is a coupling parameter with the dimension of $[L^2]$. Using the above form of $f(R)$ in (3.3), the modified field equations in the Starobinky $f(R)$ model is given by

$$G_{\mu\nu} + 2\alpha R\left(R_{\mu\nu} - \frac{1}{4}g_{\mu\nu}R\right) + 2\alpha\left(g_{\mu\nu}\Box - \nabla_\mu\nabla_\nu\right)R = \kappa\, T_{\mu\nu}, \tag{3.6}$$

where $G_{\mu\nu}$ is the Einstein tensor defined as $G_{\mu\nu} = R_{\mu\nu} - \frac{1}{2}g_{\mu\nu}R$. Taking the trace of equation (3.6) gives

$$6\alpha\Box R = R + \kappa\, T, \tag{3.7}$$

which is a clear departure from the trace of Einstein equation, $R = -\kappa\, T$. This result has significant impact in the stellar structure of a neutron, which is discussed in details in the following sections.

3.3 Spherically symmetric solution

We assume the star to be static, spherically symmetric and non-rotating. Therefore, the most general metric that describes the spacetime is given by

$$ds^2 = -e^{\nu(r)}\, c^2\, dt^2 + e^{\lambda(r)}\, dr^2 + r^2 d\theta^2 + r^2 \sin^2\theta\, d\varphi^2, \tag{3.8}$$

where $\lambda(r)$ and $\nu(r)$ ate the metric potentials. The matter present inside a neutron star is a perfect fluid. The energy-momentum tensor of a perfect fluid is given by

$$T_{\mu\nu} = \frac{(\varepsilon + P)}{c^2}u_\mu u_\nu + g_{\mu\nu}P, \tag{3.9}$$

where $\varepsilon = \rho c^2$ is the energy density, P is the pressure, and u^μ is the four-velocity with $u^\mu u_\nu = -c^2$.

Using the metric (3.8) and the trace of the energy-momentum tensor (3.9) in (3.7), we get

$$R'' = \left(\frac{\lambda' - \nu'}{2} - \frac{2}{r}\right)R' + \frac{\kappa}{6\alpha}e^{\lambda}T + \frac{e^{\lambda}R}{6\alpha}, \tag{3.10}$$

where $T = 3P - \varepsilon$. Using the modified field equations from (3.6), the tt and rr compo-

nents give

$$\lambda' = \frac{1-e^{\lambda}}{r} + \frac{re^{\lambda}}{6}\left(\frac{2R+3\alpha R^2}{1+2\alpha R}\right) - \left(\frac{\alpha r R'}{1+2\alpha R}\right)\nu' + \frac{\kappa r e^{\lambda}}{3}\left(\frac{T+3\varepsilon}{1+2\alpha R}\right), \quad (3.11)$$

and

$$\gamma\nu' = \frac{e^{\lambda}-1}{r} + \frac{\kappa r e^{\lambda} P}{1+2\alpha R} - \frac{r\alpha e^{\lambda} R^2}{2\left(1+2\alpha R\right)} - \frac{4}{r}\left(\frac{\alpha r R'}{1+2\alpha R}\right), \quad (3.12)$$

where $\gamma = 1 + \frac{\alpha r R'}{1+2\alpha R}$.

Using the energy-momentum tensor of a perfect fluid in the conservation of energy-momentum tensor equation, $\nabla_{\mu} T^{\mu}_{\nu} = 0$, we get

$$P' = -\frac{\nu'}{2}\left(P+\varepsilon\right), \quad (3.13)$$

which is the well-known Tolman-Oppenheimer-Volkoff equation. The cumulative mass $m(r)$ is obtained from the metric potential $\lambda(r)$ as

$$m(r) = \frac{c^2}{2G} r\left(1 - e^{-\lambda(r)}\right). \quad (3.14)$$

In the exterior of a star, the energy-momentum tensor vanishes. We expect the pressure $P = 0$ at the surface of a star as there are no matter beyond the surface. Thus, the trace of the energy -momentum tensor $T = 0$ in the exterior of the star. Consequently, from equation (3.10), we have

$$R'' = \left(\frac{\lambda' - \nu'}{2} - \frac{2}{r}\right) R' + \frac{e^{\lambda} R}{6\alpha}. \quad (3.15)$$

Note that, as the coupling parameter $\alpha \to 0$, the last term in the above equation dominates, and we obtain the $R = 0$ solution, which is equivalent to the general relativity. It is therefore evident that, in the weak gravity limit we recover the general relativistic solution.

It is therefore safe to demand $\mu(r), \nu(r) \to 0$ and $\mu'(r), \nu'(r) \to 0$ as $r \to \infty$, in order to obtain an asymptotically flat spacetime. Consequently, equation (3.16) in the asymptotic limit $r \to \infty$ takes the form

$$R'' + \frac{2}{r} R' - \frac{R}{6\alpha} = 0, \quad (3.16)$$

which has a solution

$$R(r) = \frac{c_1}{r} e^{-\frac{r}{\sqrt{6\alpha}}} + \frac{c_2}{2r}\sqrt{6\alpha} e^{\frac{r}{\sqrt{6\alpha}}}. \quad (3.17)$$

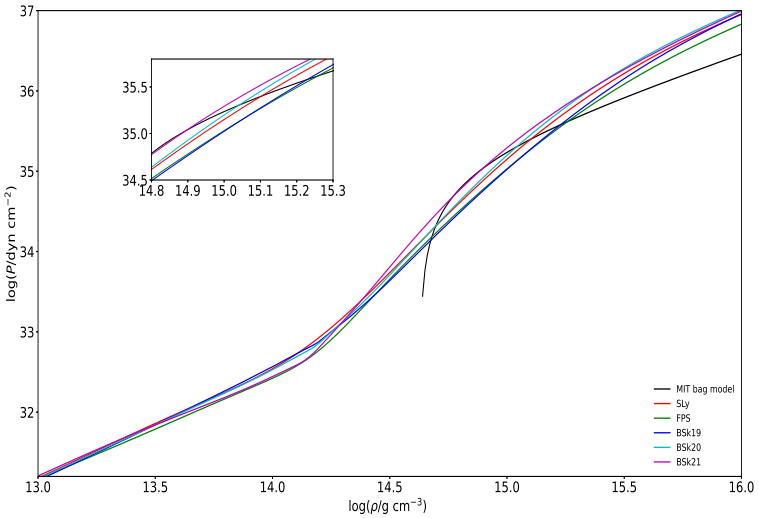

Figure 3.1: Plots for different unified equations of state expressed by equations 3.19 and 3.20, and the MIT bag model given by equation 3.21. The inset shows the crossover points between the MIT bag model and the unified equations of state.

The constant of integration c_2 must vanish since $R \to 0$ in the asymptotic limit $r \to \infty$, giving

$$R(r) = \frac{c_1}{r} e^{-\frac{r}{\sqrt{6\alpha}}}. \tag{3.18}$$

which approaches zero exponentially for values of $\alpha > 0$, faster than $\frac{1}{r}$ as $r \to \infty$. However, when $\alpha < 0$, the solution is oscillatory in nature, which is unphysical.

3.4 Equations of State

The nuclear matter inside a neutron star gives the pressure-density relation in the TOV equation. The nuclear matter in a neutron star is subjected to extreme conditions as it is under tremendous pressure with the central density $\rho_c \sim 10^{15}$ g cm^{-3} for maximal mass configurations. This makes the nuclear matter highly degenerate and the equation of state is independent of temperature [91], except for a thin outer layer. We use the combined equations of state in Chapter 2.

The core is expected to consist of deconfined quark matter which we shall represent by the MIT-bag model ([110, 174]). The hadronic matter in the outer region will be represented by a unified equation of state such as, SLy, [91], BSk20 and BSk21 [157].

In order to have continuous representations for these equations of state, we employ the parameterized forms of the pressure P as a function of density ρ. The parameterized

form in the SLy unified equations of state is expressed as [91],

$$\zeta = \frac{a_1 + a_2\xi + a_3\xi^3}{(a_4\xi + 1)\left(e^{a_5(\xi - a_6)} + 1\right)} + \frac{a_7 + a_8\xi}{e^{a_9(a_{10} - \xi)} + 1} + \frac{a_{11} + a_{12}\xi}{e^{a_{13}(a_{14} - \xi)} + 1} + \frac{a_{15} + a_{16}\xi}{e^{a_{17}(a_{18} - \xi)} + 1}, \quad (3.19)$$

where $\zeta = \log\left(P/P_{\rm ref}\right)$ with $P_{\rm ref} = 1.0$ dyne cm^{-2}, and $\xi = \log\left(\rho/\rho_{\rm ref}\right)$ with $\rho_{\rm ref} = 1.0$ g cm^{-3}. The eighteen parameters a_i are given in Ref. [91].

Additionally, the parameterized form of the pressure P as a function of density ρ for BSk19, BSk20, and BSk21 unified equations of state is given by the expression [157]

$$\begin{aligned}\zeta =& \frac{a_1 + a_2\xi + a_3\xi^3}{(a_4\xi + 1)\left(e^{a_5(\xi - a_6)} + 1\right)} + \frac{a_7 + a_8\xi}{e^{a_9(a_6 - \xi)} + 1} + \frac{a_{10} + a_1\xi}{e^{a_{12}(a_{13} - \xi)} + 1} \\ &+ \frac{a_{14} + a_{15}\xi}{e^{a_{16}(a_{17} - \xi)} + 1} + \frac{a_{18}}{\left[a_{19}(\xi - a_{20})\right]^2 + 1} + \frac{a_{21}}{\left[a_{22}(\xi - a_{23})\right]^2 + 1},\end{aligned} \quad (3.20)$$

with $\zeta = \log\left(P/P_{\rm ref}\right)$ and $\xi = \log\left(\rho/\rho_{\rm ref}\right)$, as before. The twenty-three parameters a_i are given in Ref. [157].

For the deconfined quark core, we employ the equation of state given by the MIT bag model ([110, 174]),

$$P = k(\rho c^2 - 4B), \quad (3.21)$$

where B is the bag constant. The parameter k depends on the mass of strange quark m_s and the QCD coupling α_s. For $m_s = 0$, $k = 1/3$, and for $m_s = 250$ MeV/c^2, $k = 0.28$. The bag constant B takes a value $0.982B_0 < B < 1.525B_0$ for $m_s = 0$, with $B_0 = 60$ MeV fm^{-3} [150]. In this chapter, we take $B = 60$ MeV fm^{-3} (that is, $B^{1/4} \sim 147$ MeV, corresponding to $\alpha_s = 0$, as in Figure 1 of Ref. [77]). Moreover, in the ultra-relativistic approximation, we take $m_s = 0$, so that $k = 1/3$.

The above equations of state are displayed in Fig. 3.1. The crossover between the MIT bag model and the unified equations of state are shown in the inset.

3.5 Initial Conditions and Numerical Integration

The modified field equations (3.10), (3.11), and (3.12), and the TOV equation (3.13) are coupled differential equations. These equations are solved numerically using appropriate initial conditions followed from the asymptotic requirements.

In order to numerically integrate the differential equations (3.10), (3.11), (3.12), and (3.13), we first make them dimensionless by defining the quantities $\eta = r/r_g$, $\tilde{P} = P/P_0$, $\tilde{\rho} = \rho/\rho_0$, $\chi = Rr_g^2$, $\tilde{T} = T/O_0$ and $\Omega = d\chi/d\eta$, where $P_0 = 4B$, $\rho_0 = P_0/c^2$ and

$r_g = GM_\odot/c^2 = 1.4766 \times 10^5$ cm, the half of Schwarzchild radius of the Sun.

In order to carry out the numerical integration, initial conditions has to be set properly. At $r = 0$, the cumulative mass $m(r) = 0$. From the definition of the cumulative mass given by (3.14), we expect $\lambda(0) = 0$. Moreover, since $\nu(r)$ does not appear explicitly in any of the field equations above and they depend only on ν', we take $\nu(0) = \nu_c$, where ν_c is any value that give asymptotically Minkowsky solution $\nu(\infty) = 0$.

In order to obtain the initial value of the Ricci scalar R, we use an initial guess for the central value of the Ricci scalar. Making the initial guess between $R_c = 0$ and $R_c = (3P_c - \rho_c c^2)$, where P_c and ρ_c are central values of pressure P and density ρ, we check whether the subsequent numerical values of R diverges or decays. Adjusting the initial guess in this manner, we require steady numerical values in the subsequent iterations.

In general relativity, the Ricci scalar R is given by $R = -\kappa T$. Since $T = 0$ outside the stellar surface, Ricci scalar vanishes outside the surface. However, as we have seen in equation (3.18), the Ricci scalar does not vanish outside the surface of the star, and it decays exponentially as $r \to \infty$. As a consequence, the mass of the star measured by an observer at infinity,

$$M = \frac{c^2}{2G} r_\infty \left(1 - e^{-\lambda(r_\infty)}\right), \tag{3.22}$$

is greater than the stellar mass calculated at the surface of the star,

$$M_s = m(r_s) = \frac{c^2}{2G} r_s \left(1 - e^{-\lambda(r_s)}\right), \tag{3.23}$$

where r_s and r_∞ denote the stellar surface and the asymptotic infinity. The stellar radius r_s is determined by the condition $P = 0$. On the other hand, r_∞ is the radial distance obtained when $R \sim 0$.

This difference in the measured value occurs due to the gravitational energy from the Ricci scalar in the exterior of the star. It contributes to the cumulative mass $m(r)$ from (3.14) and (3.11).

3.6 Stellar structure

Table 3.1 shows the maximum stable mass $M_{\max}$ for different values of the Starobinky parameter α. Beyond this maximal mass, the neutron star would undergo gravitational collapse. The corresponding values surface mass $m(r_s)$, stellar radius r_s, central value of the curvature scalar R_c, and central density ρ_c are also displayed.

It is clear from the table that the combined equation of state MIT-BSk21 can support

maximal mass up to 2.07 $M_\odot$ with $\alpha = 10\, r_g^2$. It is also obvious from the table that, by increasing the α value, the maximal mass can be made compatible with the recent observation of milli-second pulsar such as MSP J0740+6620 by Cromartie et al. in 2019 with a pulsar mass of $2.14 \pm^{0.10}_{0.09} M_\odot$ [62].

Corresponding to the maximal mass values shown in Table 3.1, Figure 3.2 shows the radial pressure profiles P(r) of the neutron star or different values of the Starobinky parameter α with the combined equations of state: MIT-SLy (Top left), MIT-BSk20 (top right), and MIT-BSk21 (bottom left). The bottom-right pannel compares the pressure profiles between the three combined equations of state for $\alpha = 5r_g^2$, showing that MIT-SLy can support the highest pressure at the centre. In all cases, the stellar radius is seen to lie between 10 km and 12 km, identified with the pressure dropping to zero value.

Figure 3.3 shows the radial profiles of the Ricci scalar $R(r)$ for the neutron star with maximal mass (as shown in Table 3.1) for different values of the Starobinky parameter α with the combined equations of state: MIT-SLy (Top left), MIT-BSk20 (top right), and MIT-BSk21 (bottom left). The bottom-right pannel compares the profiles between the three combined equations of state for $\alpha = 5r_g^2$, showing no remarkable difference in the value of the Ricci scalar at the centre. In all cases, the Ricci scalar does not fall to zero immediately outside the stellar radius; on the contrary, it falls gradually to zero extending

Table 3.1: The maximum stable mass $M_{\max}$ for different values of the parameter α. The corresponding values surface mass $m(r_s)$, stellar radius r_s, central value of the curvature scalar R_c, and central density ρ_c are also displayed. $M_\odot$ denotes one solar mass.

Equation of state	α r_g^2	$\rho_c \times 10^{15}$ $g.cm^{-3}$	R_c r_g^2	$m(r_s)$ $M_\odot$	r_s km	M_∞ $M_\odot$
MIT-SLy	GR	2.39	-	1.85	10.75	1.85
	1.0	2.45	0.016	1.78	10.81	1.88
	3.0	2.50	0.010	1.73	10.89	1.91
	5.0	2.55	0.008	1.71	10.92	1.92
	10.0	2.55	0.005	1.69	11.01	1.95
MIT-BSk20	GR	2.28	-	1.89	10.93	1.89
	1.0	2.35	0.015	1.81	10.98	1.92
	3.0	2.40	0.010	1.76	11.07	1.94
	5.0	2.40	0.008	1.74	11.13	1.96
	10.0	2.55	0.005	1.72	11.14	1.98
MIT-BSk21	GR	2.03	-	1.98	11.60	1.98
	1.0	2.10	0.015	1.90	11.65	2.00
	3.0	2.15	0.010	1.84	11.72	2.03
	5.0	2.20	0.008	1.82	11.75	2.04
	10.0	2.20	0.005	1.79	11.84	2.07

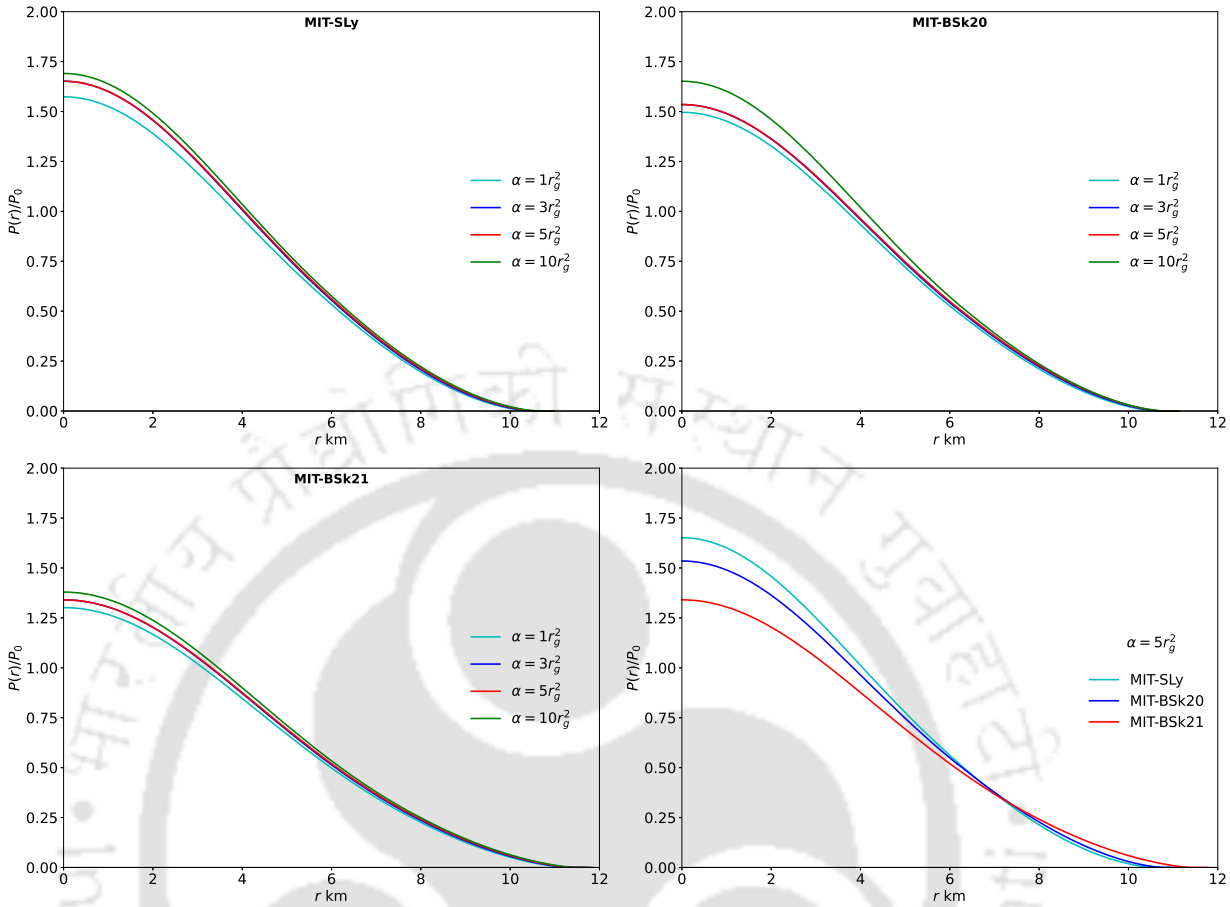

Figure 3.2: The radial pressure profiles of the neutron star with maximal mass (as shown in Table 3.1) for different values of the Starobinky parameter α with the combined equations of state: MIT-SLy (Top left), MIT-BSk20 (top right), and MIT-BSk21 (bottom left). The bottom-right pannel compares the pressure profiles between the three combined equations of state for $\alpha = 5r_g^2$, showing that MIT-SLy can support the highest pressure at the centre. In all cases, the stellar radius is seen to lie between 10 km and 12 km, identified with the pressure dropping to zero value.

beyond 50 kms. This is in contrast with general relativity, where the Ricci scalar falls to zero immediately outside the stellar surface. The non-zero value of the Ricci scalar outside the stellar surface in the case of $f(R)$ gravity indicates the contribution from the extra degree of freedom, known as the scalaron, in Starobinky gravity.

Figure 3.4 displays the radial profiles of the cumulative mass $m(r)$ for the neutron star with maximal mass (as shown in Table 3.1) for different values of the Starobinky parameter α with the combined equations of state: MIT-SLy (Top left), MIT-BSk20 (top right), and MIT-BSk21 (bottom left). The bottom-right pannel compares the profiles between the three combined equations of state for $\alpha = 5r_g^2$, showing that the ADM mass attains its maximum value for MIT-BSk21 equation of state. In all cases, the mass value gradually increases to the ADM mass beyond 50 kms. This gradual increase in mass beyond

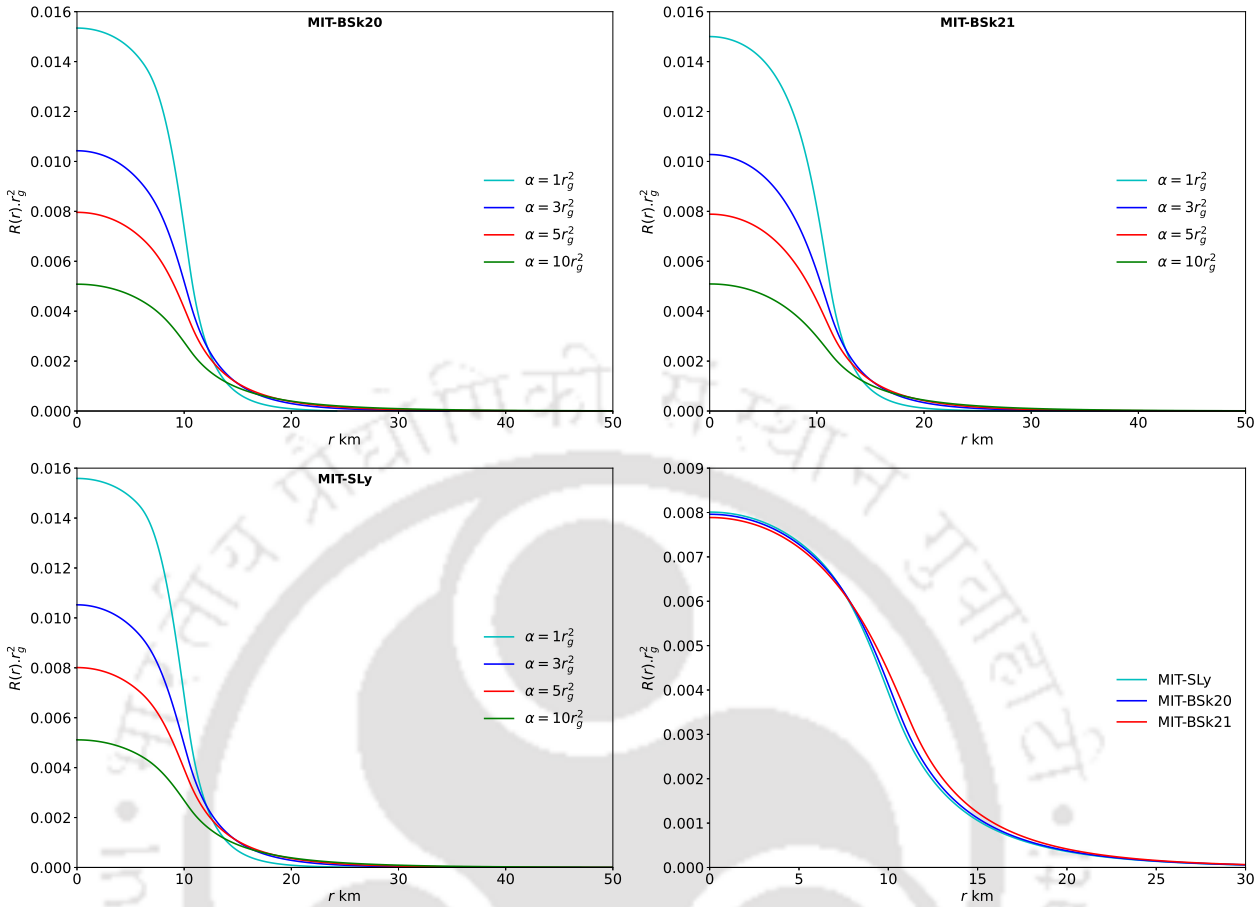

Figure 3.3: The radial profiles of the Ricci scalar $R(r)$ for the neutron star with maximal mass (as shown in Table 3.1) for different values of the Starobinky parameter α with the combined equations of state: MIT-SLy (Top left), MIT-BSk20 (top right), and MIT-BSk21 (bottom left). The bottom-right pannel compares the profiles between the three combined equations of state for $\alpha = 5r_g^2$, showing no remarkable difference in the value of the Ricci scalar at the centre. In all cases, the Ricci scalar does not fall to zero immediately outside the stellar radius; on the contrary, it falls gradually to zero extending beyond 50 kms.

the stellar surface indicates the contribution from the extra degree of freedom, called the dilaton (scalaron), in $f(R)$ gravity.

Figure 3.5 illustrates how the ADM mass M_∞ changes with respect to the central density ρ_c of the neutron star for different values of the Starobinky parameter α with the combined equations of state: MIT-SLy (Top left), MIT-BSk20 (top right), and MIT-BSk21 (bottom left). For comparison, the corresponding graphs with general relativity (GR) are also shown. The bottom-right pannel compares the curves between the three combined equations of state for $\alpha = 5r_g^2$. In all cases, the ADM mass M_∞ exhibit a monotonic increase with respect to increase in the central density ρ_c. Thus the chosen $f(R)$ gravity model, namely the Starobinky gravity, gives the expected behaviour of the ADM mass.

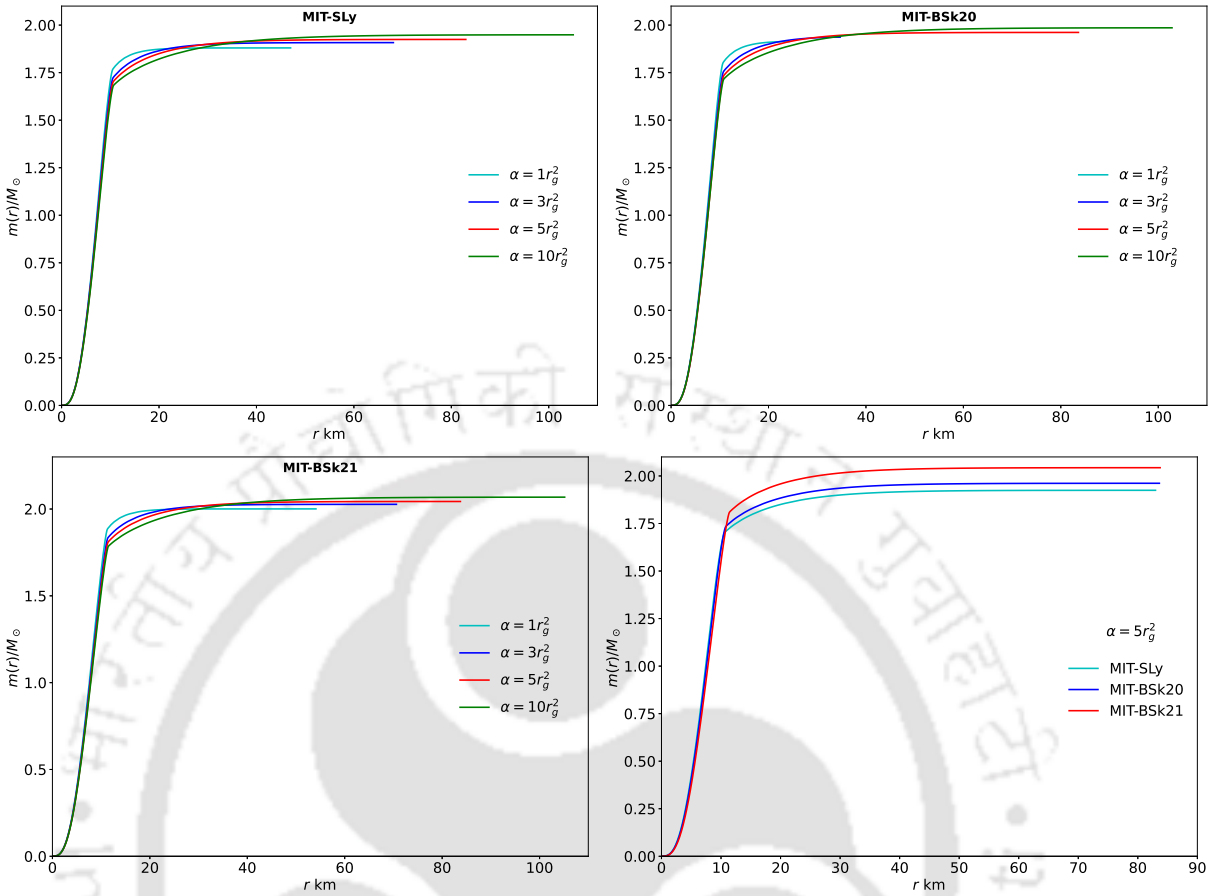

Figure 3.4: The radial profiles of the cumulative mass $m(r)$ for the neutron star with maximal mass (as shown in Table 3.1) for different values of the Starobinky parameter α with the combined equations of state: MIT-SLy (Top left), MIT-BSk20 (top right), and MIT-BSk21 (bottom left). The bottom-right pannel compares the profiles between the three combined equations of state for $\alpha = 5r_g^2$, showing that the ADM mass attains its maximum value for MIT-BSk21 equation of state. In all cases, the mass value gradually increases to the ADM mass beyond 50 kms.

Figure 3.6 illustrates the ADM mass M_∞ versus stellar radius r_s of the neutron star for different values of the Starobinky parameter α with the combined equations of state: MIT-SLy (Top left), MIT-BSk20 (top right), and MIT-BSk21 (bottom left). For comparison, the corresponding graphs with general relativity (GR) are also shown. The bottom-right pannel compares the curves between the three combined equations of state for $\alpha = 5r_g^2$. In all cases, we see that the stellar radius r_s decreases monotonically as the ADM mass M_∞ increases. This is a quite expected behaviour because the higher gravitational pull in a neutron star of higher mass will make its radius smaller.

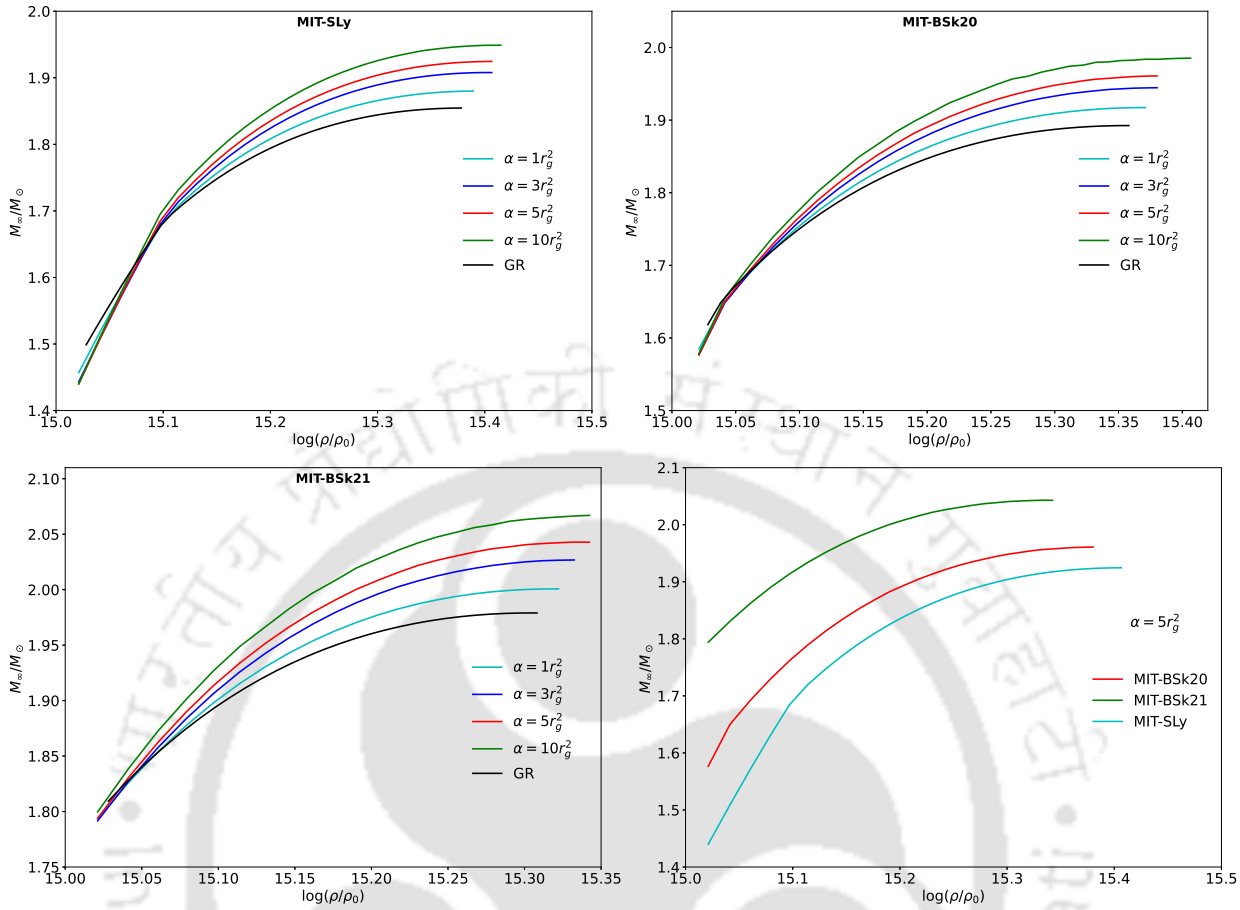

Figure 3.5: ADM mass M_∞ versus central density ρ_c for the neutron star for different values of the Starobinky parameter α with the combined equations of state: MIT-SLy (Top left), MIT-BSk20 (top right), and MIT-BSk21 (bottom left). For comparison, the corresponding graphs with general relativity (GR) are also shown. The bottom-right pannel compares the curves between the three combined equations of state for $\alpha = 5r_g^2$.

3.7 Conclusions

In this work, we investigated the structure of neutron stars within the framework of Starobinsky gravity, characterized by the modified gravitational action $f(R) = R + \alpha R^2$. By deriving the corresponding Tolman–Oppenheimer–Volkoff (TOV) equations and solving them numerically for a range of values of the Starobinsky parameter α, we analyzed the impact of higher-order curvature corrections on neutron star properties.

Our numerical results, summarized in Table 3.1, show that the maximum stable mass $M_{\max}$ of neutron stars increases with increasing α, indicating that the quadratic curvature term effectively enhances the gravitational support against collapse. For the combined MIT-BSk21 equation of state (EOS), a maximal mass of 2.07 $M_\odot$ is achieved for $\alpha = 10\, r_g^2$, bringing the theoretical prediction into agreement with the observed mass of the

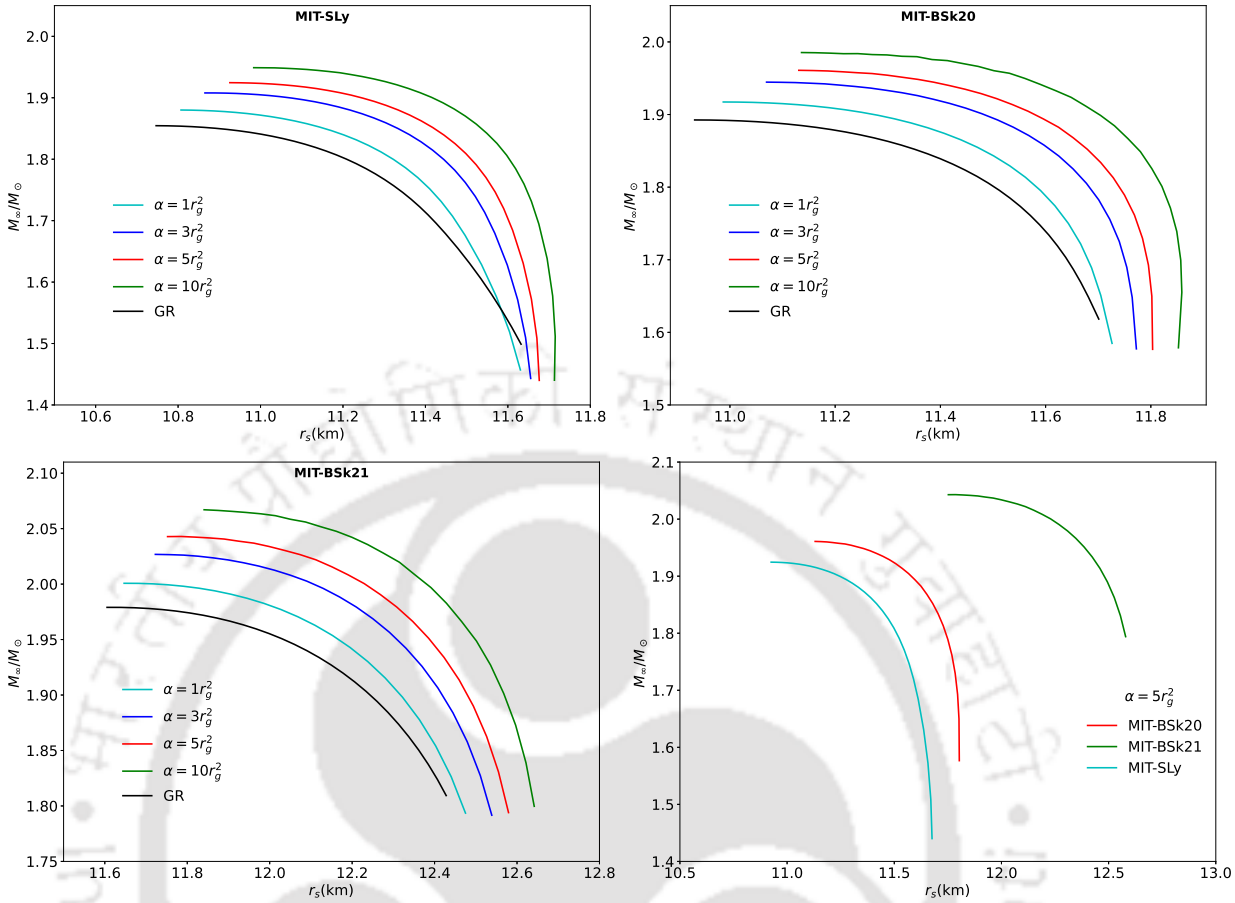

Figure 3.6: ADM mass M_∞ versus stellar radius r_s for the neutron star for different values of the Starobinky parameter α with the combined equations of state: MIT-SLy (Top left), MIT-BSk20 (top right), and MIT-BSk21 (bottom left). For comparison, the corresponding graphs with general relativity (GR) are also shown. The bottom-right pannel compares the curves between the three combined equations of state for $\alpha = 5r_g^2$.

heavy millisecond pulsar MSP J0740+6620 ($2.14^{+0.10}_{-0.09}$ $M_\odot$) reported by Cromartie et al. [62].

Additionally, Figure 3.2 presents the radial pressure profiles $P(r)$ for various EOSs and values of α. The profiles reveal that all modeled stars possess radii in the range of 10–12 km, consistent with current observational constraints. Among the EOSs considered, MIT-SLy supports the highest central pressure, highlighting the role of the nuclear matter model in determining the internal structure of compact stars.

Figure 3.3 further illustrates the radial profiles of the Ricci scalar $R(r)$ for neutron stars at their respective maximum mass configurations. Unlike in general relativity, where the Ricci scalar vanishes immediately outside the stellar surface, in Starobinsky gravity it exhibits a gradual decay and remains non-zero well beyond the stellar radius, extending past 50 km. This behavior is a clear signature of the additional scalar degree of freedom—

commonly referred to as the scalaron—present in $f(R)$ theories. The extended non-zero curvature outside the star reflects the influence of modified gravity in the star's exterior region. Interestingly, for fixed α, the central values of the Ricci scalar remain similar across different EOSs, suggesting a degree of universality in the core curvature behavior under this modified theory.

Figure 3.4 shows the cumulative mass profiles $m(r)$, highlighting how the total gravitational mass builds up with radius for different values of α and EOSs. In all cases, the mass function does not plateau at the stellar surface but instead continues to increase gradually beyond it, reaching the ADM mass only past 50 km. This extended mass profile again reflects the contribution from the scalaron field outside the star, a feature absent in general relativity. Among the EOSs considered, the MIT-BSk21 model yields the highest ADM mass for a fixed $\alpha = 5r_g^2$, as seen in the bottom-right panel of the figure. These results underscore the nontrivial role of the extra scalar degree of freedom in modifying both the interior and exterior gravitational structure of neutron stars.

Figure 3.5 explores the dependence of the ADM mass M_∞ on the central density ρ_c of the neutron star for different EOSs and values of the Starobinsky parameter α, along with corresponding results from general relativity. In all cases, a monotonic increase in M_∞ with respect to ρ_c is observed, as expected for a physically viable stellar model. This confirms that Starobinsky gravity preserves the essential thermodynamic behavior of compact stars while introducing meaningful deviations in mass distribution and exterior structure through the scalaron contribution.

Lastly, Figure 3.6 presents the relationship between ADM mass M_∞ and stellar radius r_s for different values of α and equations of state, again compared to the general relativistic predictions. As expected, a monotonic decrease in radius is observed with increasing mass, indicating that more massive neutron stars are more compact due to stronger gravitational binding. This behavior confirms that the inclusion of the R^2 term in the gravitational action does not disrupt the physically intuitive mass–radius relation, further reinforcing the viability of Starobinsky gravity as a consistent extension of general relativity in the high-density regime. One may also note that the mass–radius relation is sensitive to both the choice of the equation of state and the strength of the gravitational interaction (through α). The degeneracy between modified gravity effects and the equation of state uncertainty in this context is worth exploring further.

The results presented in this study thus demonstrate that Starobinsky gravity can accommodate neutron stars with properties consistent with recent astrophysical observations, while also introducing distinctive signatures—such as extended scalar curvature and mass profiles—arising from the scalar degree of freedom. These features offer poten-

tial avenues for distinguishing $f(R)$ gravity from general relativity through observations of neutron stars and gravitational wave signals from neutron star mergers. For inspiraling stars, since the effective mass felt by the companion reduces in the later stages, a slow down is expected. However, an in-depth numerical relativity calculation is required for a detailed understanding of the possible detection in advanced gravitational wave detectors. At present, no such studies are found in the literature in the context of the Starobinsky $f(R)$ gravity considered. Other observational consequences due to the gravitational halo include gravitational redshift and bending of light, since the spacetime geometry is no longer Schwarzschild.

Chapter 4

Structure of spacetime of charged black holes in EiBI gravity

In this chapter, we focus upon the behaviour of spacetime of charged black holes described by Eddington-inspired Born-Infeld (EiBI) gravity. With a static and spherically symmetric metric, we solve the ensuing field equations obtained from the EiBI-Maxwell action in the Palatini formalism. Consequently we carry out, for the first time, an in-depth analysis of the structure of spacetime geometry in several regions of the charged EiBI black hole. In particular, we consider the analytical behaviours of the metric coefficients and the Kretschmann scalar by probing their asymptotic nature analytically *in different regions of the black hole spacetime, such as, near the center, in the intermediate region, and near the horizon, for both positive and negative EiBI coupling. These analyses give a thorough understanding of the nature of spacetime of EiBI-Maxwell black holes. In order to aide our understanding further, we solve the EiBI-Maxwell field equation numerically with different values of the parameters involved. We find close agreement between the analytical behaviours and those obtained from numerical integration of the EiBI-Maxwell field equation.*

4.1 Introduction

Einstein's pioneering formulation of general relativity (GR) is the most successful theory of gravity, having passed various tests in weak gravitational scenarios of the solar system [6, 72, 169, 190]. With the advancement of technology, various other predictions of GR, such as production of gravitational waves in binary collapse [2], and the existence of black hole at the centre of the galaxy[58–61], have also been confirmed. However, GR predicts the existence of an essential singularity in the black hole and in the big-bang

cosmology of the universe [94, 95, 135, 153–155, 178, 180, 181, 189]. This shows that GR is incapable of explaining the physics in strong gravitational situations. This dilemma warrants the search for a new theory of gravity which has been a major goal in research in modern times. There have been various modifications proposed [28, 36, 47, 63, 67, 93, 140, 179] in order to explain the strong gravity regime.

Ever since the formulation of Einstein's general relativity, physicists have continually sought alternative theories of gravity. One such theory, proposed by Eddington at the dawn of the last century [72], has recently gained renewed attention. Eddington's theory is incomplete since matter was not coupled to the gravity in that framework. A modification of Eddington's theory, accommodating matter field has been coined as Eddington-inspired Born-Infeld (EiBI) gravity [16]. This theory integrates Eddington's original idea with that of Born-Infeld electrodynamics [34] into a unified theory.

The EiBI gravity is a Palatini-type theory [145], distinguishing itself from general relativity by treating the affine connection $\Gamma^{\mu}_{\nu\rho}$ and metric tensor $g_{\mu\nu}$ as independent geometric entities. Consequently, the EiBI action is varied with respect to both $\Gamma^{\mu}_{\nu\rho}$ and $g_{\mu\nu}$ independently, resulting in two equations of motion that couple matter with gravity.

EiBI gravity differs from general relativity in the presence of matter. In the absence of matter, EiBI reduces to general relativity. The strength of gravity in the EiBI theory is determined by a coupling parameter κ. For small values of $\kappa R_{\mu\nu}$, EiBI gravity reduces general relativity, while for large values of $\kappa R_{\mu\nu}$, it approaches Eddington gravity. When the matter field vanishes, the EiBI action reduces to the Eddington action, which is equivalent to the Einstein-Hilbert action, yielding general relativity [16].

The EiBI theory of gravity offers a promising avenue for further exploration. The distinction from general relativity becomes particularly relevant in the strong gravity regime, especially in the presence of matter, as discusse above. Under such conditions, the Poisson equation is modified in EiBI for strong gravitational fields or dense matter[147]. This characteristic is of paramount importance for studying compact objects like black holes [13, 16, 55, 111, 176, 177, 188] and neutron stars [92, 116, 147, 149], exhibiting deviations from general relativity when interacting with dense matter.

The EiBI gravity further offers a promising avenue for addressing the cosmological singularity problem. Research has shown that a universe filled with regular matter in EiBI has a maximum finite density (or minimum length) limit, preventing the formation of the cosmological singularity [14]. Additionally, depending on the specific parameter values, EiBI can exhibit a regular bounce from contraction to expansion, oscillating between two finite density values before transitioning to a GR-like expansion phase [165]. Within the cosmological framework, EiBI has been extensively studied in relation to inflation

[56], linear perturbations [194], scalar perturbations [57, 126], and large-scale structure formation [70].

Resolution of the cosmological singularity has prompted investigations into the collapse of matter. Studies of non-relativistic [147] and relativistic [147, 148] dust collapse in EiBI have revealed that singularities do not form in EiBI. While the positive coupling parameter κ occurring in the EiBI theory prevents singularities in general, in the case of relativistic collapse, a constraint on the parameter (κ) emerges, making the formation of black holes still possible [148]. Additionally, analysis of $2+1$ dimensional collapse in EiBI [167] has shown that singularities, when they do form, are typically naked except within a specific range of parameter values.

In the case of compact objects such as neutron stars, κ modifies the gravitational field (and hence the TOV equations). For $\kappa > 0$, stellar masses are found to be larger than those in general relativity [92, 158, 168]. Moreover, the mass is found to depend on the value of κ. This is because $\kappa > 0$ introduces an effective pressure that can support more mass. Unlike in general relativity, EiBI can support stable pressureless stars, as reported by Pani et al. [148]. However, there are no realistic stars when $\kappa < 0$ [116].

On the other hand, singularities on the stellar surface have been reported in the context of neutron stars by Pani and Sotiriou [149]. However, Kim (2014) [116] reconsidered the neutron star solution and found that the singularities can be resolved when the gravitational back-reaction is considered in the matter dynamics. The effect of the back-reaction is captured by the geodesic deviation equation, which is similar to Hooke's law. For $\kappa > 0$, the geodesic deviation equation modifies the equation of state, making the surface singularity vanish. However, for $\kappa < 0$, they did not report any stable stellar solutions.

Vacuum solution of general relativity give Schwarzchild solution, whereas eletrovacuum solution gives Reissner-Nordström solution. EiBI deviates from general relativity primarily in the presence of matter, and the simplest matter configuration within a black hole is an electric charge [176, 177, 188]. Analysis of charged black hole solutions in EiBI showed an asymptotically flat solution that will approaches the de Sitter form as $r \to \infty$. For the coupling parameter $\kappa > 0$ as well as $\kappa < 0$, there exist an event horizon with singularities in a certain parameter range. Moreover, for certain parameter ranges, there is no bound on the black hole charge in contrast with Reissner-Nordström solution in general relativity. In comparison with general relativity, the horizon radius is smaller (larger) for the coupling parameter $\kappa > 0$ ($\kappa < 0$) [176].

The charged black hole solutions in EiBI [176] clearly demonstrate deviations from GR, especially in the vicinity of the black hole. Extending the solutions interior to the event horizon reveals two singularities: at $r = 0$ and at $r = \sqrt{\sqrt{\kappa} Q}$, for a black hole with

charge Q. This behavior differs significantly from that of general relativity.

Although charged black holes in the EiBI framework have been extensively studied, for a deeper understanding of the nature of spacetime of the black hole requires further studies by means of analytical considerations.

In this work, we therefore consider a charged black hole in the EiBI framework. With a static spherically symmetric metric, we first obtain the field equations from the EiBI action minimally coupled to the Maxwell action. This leads to a differential equation for the metric coefficient that contains the charge Q and the EiBI coupling κ giving it a very intricate form. With this, we probe the nature of the metric coefficient by *analytically* studying its behaviour in different regions of the black hole spacetime. Consequently, we obtain the analytical nature of the metric coefficients and the Kretschmann scalar in the region near the center, in the intermediate region, in the region near the horizon, for both positive and negative EiBI coupling ($\kappa > 0$ and $\kappa < 0$). This analytical study gives a thorough understanding of the nature of spacetime of the EiBI-Maxwell black hole.

In order to aide our understanding further, we solve the EiBI-Maxwell field equation numerically with different values of the parameters involved. We find close agreement between the analytical behaviours and those obtained from numerical integration of the EiBI-Maxwell field equation.

The rest of the chapter is organised as follows. In Section 5.2, we consider the EiBI action with a minimally coupled Maxwell field and obtain the field equations in the Palatini formalism. In Section 4.3, we carry out an in-depth analysis of the nature of spacetime in several regions of the charged EiBI black hole. There, we obtain the analytical behaviours of the metric coefficients and the Kretschmann scalar by probing their asymptotic nature analytically in different regions of the black hole spacetime for both positive and negative EiBI coupling. In Section 4.4, we solve the EiBI-Maxwell field equation numerically, where we illustrate the radial profiles of the metric coefficients and the Kretschmann scalar for different values of the parameters involved. Finally, we conclude the chapter with a discussion in Section 4.5. Throughout this chapter, we use the convention $c = 1$ and $8\pi G = 1$.

4.2 EiBI-Maxwell action and field equations

Eddington proposed [72] that the relevant field in free (de Sitter) space is the affine connection $\Gamma^{\mu}_{\nu\rho}$ and that the correct action should be $S_{\rm Edd} = 2\kappa \int d^4x \sqrt{|R|}$, where κ is a constant having the dimension of Λ^{-1}, where Λ is the cosmological constant.

In the EiBI model, the Eddington action is modified in analogy with the Born-Infeld

model of electrodynamics [34]. The EiBI action for any general astrophysical system [16] is given by

$$S(g,\tilde{\Gamma},\Psi)=\frac{1}{\kappa}\int d^4x\left(\sqrt{-|g_{\mu\nu}+\kappa\tilde{R}_{\mu\nu}(\tilde{\Gamma})|}-\lambda\sqrt{-g}\right)+\int d^4x\sqrt{-g}\mathcal{L}_m(g,\Psi). \tag{4.1}$$

where $\lambda=1+\kappa\Lambda$, $g_{\mu\nu}$ is the metric tensor, $\mathcal{L}_m(g,\Psi)$ is the matter Lagrangian (a function of the metric tensor $g_{\mu\nu}$ and the matter field Ψ), and the symbol "$|.|$"implies the the determinant of the tensor. It is important to note that the affine connection $\tilde{\Gamma}^{\mu}_{\nu\rho}$ and Ricci tensor $\tilde{R}_{\mu\nu}(\tilde{\Gamma})$ are independent of the physical metric $g_{\mu\nu}$ in Palatini formalism [145]. Consequently, there are two different affine connections in this theory. The first one is the usual Levi-Civita connection $\Gamma^{\mu}_{\nu\rho}$ defined with respect to the physical metric $g_{\mu\nu}$. The matter sector in the action follows this affine connection. However, the gravity sector follows the affine connection $\tilde{\Gamma}^{\mu}_{\nu\rho}$, which is different from $\Gamma^{\mu}_{\nu\rho}$.

In the Palatini formalism, $g_{\mu\nu}$ and $\tilde{\Gamma}^{\mu}_{\nu\rho}$ are treated as independent variables. Defining an auxiliary metric $q_{\mu\nu}$ as

$$q_{\mu\nu}=g_{\mu\nu}+\kappa\tilde{R}_{\mu\nu}(\tilde{\Gamma}), \tag{4.2}$$

Variation of the action (4.1) with respect to $g_{\mu\nu}$ yields

$$\sqrt{-q}q^{\mu\nu}=\lambda\sqrt{-g}g^{\mu\nu}-\kappa\sqrt{-g}T^{\mu\nu}, \tag{4.3}$$

whereas variation with respect to $\tilde{\Gamma}^{\mu}_{\nu\rho}$ leads to

$$\tilde{\nabla}_{\rho}\left(\sqrt{-q}q^{\mu\nu}\right)=0, \tag{4.4}$$

where q is the determinant of $q_{\mu\nu}$ and $\tilde{\nabla}_{\rho}$ is the covariant differentiation with respect to the affine connection $\tilde{\Gamma}^{\mu}_{\nu\rho}$.

Using the identities given in Ref. [135], equation (4.4) yields the affine connection in terms of $q_{\mu\nu}$, functioning as an auxiliary metric,

$$\tilde{\Gamma}^{\mu}_{\alpha\beta}=\frac{q^{\mu\nu}}{2}\left(-\partial_{\nu}q_{\alpha\beta}+\partial_{\beta}q_{\alpha\nu}+\partial_{\alpha}q_{\nu\beta}\right). \tag{4.5}$$

In the gravity sector, all tensor quantities raise and lower their indices using the auxiliary metric $q_{\mu\nu}$. Consequently, the Riemann tensor, Ricci tensor, and Ricci scalar are defined in terms of the auxiliary metric $q_{\mu\nu}$ and the affine connection $\tilde{\Gamma}^{\mu}_{\alpha\beta}$.

In vacuum, where $T_{\mu\nu}=0$, and for the cosmological constant $\Lambda=0$ (or $\lambda=1$), EiBI is equivalent to the general relativity. This can be seen from equation (4.3), which reduces

to $\sqrt{-q}q^{\mu\nu} = \sqrt{-g}g^{\mu\nu}$, implying $q_{\mu\nu} = g_{\mu\nu}$. Consequently, from equation (4.2), we see that $\tilde{R}_{\mu\nu} = 0$, recovering general relativity in vacuum in the absence of cosmological constant [16].

Unlike the gravity sector, the matter part of the action (4.1) is defined in terms of the physical metric $g_{\mu\nu}$. Consequently, for black holes having an electric charge Q, the Lagrangian of the electromagnetic field is

$$\mathcal{L}_m = -\frac{1}{2} g_{\mu\rho} g_{\nu\sigma} F^{\mu\nu} F^{\rho\sigma}, \tag{4.6}$$

where $F_{\mu\nu} = \partial_\mu A_\nu - \partial_\nu A_\mu$, with A_μ the electromagnetic vector potential. The corresponding Maxwell's equation and the energy-momentum tensor are given by

$$\nabla_\mu F^{\mu\nu} = 0 \tag{4.7}$$

and

$$T_{\mu\nu} = 2F_\mu{}^\sigma F_{\nu\sigma} - \frac{g_{\mu\nu}}{2} F_{\alpha\beta} F^{\alpha\beta}, \tag{4.8}$$

where ∇_μ represents covariant differentiation with respect to the affine connection $\Gamma^\mu_{\nu\rho}$ corresponding to the physical metric $g_{\mu\nu}$.

It is important to note that the equation of motion for the electromagnetic field (5.8) depends only on the physical metric $g_{\mu\nu}$. In addition the energy-momentum tensor given by equation (4.8) depends only on the physical metric $g_{\mu\nu}$ (and independent of the auxiliary metric $q_{\mu\nu}$). Consequently, energy-momentum conservation in EiBI is given by $\nabla_\mu T^{\mu\nu} = 0$, similar to that in general relativity [16, 111, 121].

Since the matter part of the action (4.1) is defined in terms of the physical metric $g_{\mu\nu}$, the conservation law can be proved using the matter action. For detailed proof, see Ref. [121]. On the other hand, the gravity sector is defined by the auxiliary metric $q_{\mu\nu}$ and the corresponding affine connection $\tilde{\Gamma}^\mu_{\nu\rho}$.

For a static and spherically symmetric spacetime around the black hole, we consider the metric $g_{\mu\nu}$ to be given by

$$ds^2 = -f(r)h^2(r)dt^2 + \frac{1}{f(r)}dr^2 + r^2\left(d\theta^2 + \sin^2\theta d\varphi^2\right), \tag{4.9}$$

and the auxiliary metric $q_{\mu\nu}$ as

$$ds_q^2 = -A(r)B^2(r)dt^2 + \frac{1}{A(r)}dr^2 + C^2(r)\left(d\theta^2 + \sin^2\theta d\varphi^2\right). \tag{4.10}$$

For the electromagnetic vector potential, we consider the ansatz $A_\mu = (V(r), 0, 0, 0)$,

where $V(r)$ is the electrostatic potential. Using Maxwell's equation (5.8), we get

$$V'(r) = \frac{\alpha_0 h}{r^2}. \tag{4.11}$$

Upon demanding $V' \to \frac{Q}{r^2}$ and $h \to 1$ as $r \to \infty$, we can fix the integration constant as $\alpha_0 = Q$.

Extracting the metric variables $g_{\mu\nu}$ and $q_{\mu\nu}$ from (4.9) and (4.10), and using them in the field equation (4.3), we obtain the equations of motion, with tt, rr, and $\theta\theta$ (or $\varphi\varphi$) components as

$$\frac{C^2}{AB} = \frac{1}{fhr^2}\left(\lambda r^4 + \kappa Q^2\right), \tag{4.12}$$

$$ABC^2 = \frac{fh}{r^2}\left(\lambda r^4 + \kappa Q^2\right), \tag{4.13}$$

and

$$B = \frac{h}{r^4}\left(\lambda r^4 - \kappa Q^2\right). \tag{4.14}$$

Eliminating B from the above equations leads to

$$A = fr^4\left(\lambda r^4 - \kappa Q^2\right)^{-1}, \tag{4.15}$$

and

$$C = \frac{1}{r}\sqrt{\lambda r^4 + \kappa Q^2}. \tag{4.16}$$

The Ricci tensor $\tilde{R}_{\mu\nu}(\tilde{\Gamma})$ depends on the affine connection $\tilde{\Gamma}^{\mu}_{\alpha\beta}$, which is defined in terms of the auxiliary metric $q_{\mu\nu}$ expressed by (4.5). Thus using (4.10), all components of the field equation (4.2) can be obtained, with the tt, rr, and $\theta\theta$ (or $\varphi\varphi$) components as

$$3\frac{A'}{A}\frac{B'}{B} + 2\frac{A'}{A}\frac{C'}{C} + 4\frac{B'}{B}\frac{C'}{C} + \frac{A''}{A} + 2\frac{B''}{B} = \frac{2}{\kappa A}\left(\frac{r^4}{\lambda r^4 - \kappa Q^2} - 1\right), \tag{4.17}$$

$$3\frac{A'}{A}\frac{B'}{B} + 2\frac{A'}{A}\frac{C'}{C} + \frac{A''}{A} + 2\frac{B''}{B} + 4\frac{C''}{C} = \frac{2}{\kappa A}\left(\frac{r^4}{\lambda r^4 - \kappa Q^2} - 1\right), \tag{4.18}$$

and

$$\frac{C''}{C}+\frac{A'}{A}\frac{C'}{C}+\frac{B'}{B}\frac{C'}{C}+\left(\frac{C'}{C}\right)^2-\frac{1}{AC^2}=\frac{1}{\kappa A}\left(\frac{r^4}{\lambda r^4+\kappa Q^2}-1\right). \tag{4.19}$$

From equations (4.17) and (4.18) we find

$$\frac{C''}{C'}=\frac{B'}{B}. \tag{4.20}$$

Integrating this equation, we get the relation $B=\alpha_1 C'$, which leads to $h=\frac{\alpha_1 r^2}{\sqrt{\lambda r^4+\kappa Q^2}}$, upon using (4.14) and (4.16). Demanding $h\to 1$ as $r\to\infty$, we fix the integration constant $\alpha_1=\sqrt{\lambda}$, giving

$$h=\frac{\sqrt{\lambda}r^2}{\sqrt{\lambda r^4+\kappa Q^2}}, \tag{4.21}$$

and substituting (4.21) in (4.11) with $\alpha_0=Q$, we get

$$V'(r)=\frac{\sqrt{\lambda}Q}{\sqrt{\lambda r^4+\kappa Q^2}}. \tag{4.22}$$

We obtain the differential equation for the metric coefficient $f(r)$ by employing (4.14), (4.15), (4.16), and (4.20) in (4.19), leading to

$$f'(r)+\frac{\{\kappa^2Q^4+6\lambda\kappa Q^2r^4+\lambda^2r^8\}}{r\{\lambda^2r^8-\kappa^2Q^4\}}f(r)+\frac{1}{r^3}\left(Q^2-r^2\right)+\Lambda r=0. \tag{4.23}$$

4.3 Nature of EiBI-Maxwell black hole spacetime: in-depth analyses

In this section, we shall discuss the asymptotic behaviours of the metric coefficients and the Kretschmann scalar near a few points of interest, such as, at long distances, near the center, in intermediate region and near the horizon. We shall also discuss the conditions for the existence of an event horizon.

Using (4.16) and (4.20) in equation (4.19) and rearranging, we obtain

$$\left(ACC'^2\right)'=C'+\frac{C'}{\kappa}\left(r^2-C^2\right). \tag{4.24}$$

This equation immediately leads to the integral form

$$A = \frac{1}{C'^2} + \frac{1}{CC'^2}\int \frac{C'}{\kappa}\left(r^2 - C^2\right)dr + \alpha_3, \tag{4.25}$$

where α_3 is the integration constant. Substituting for $A(r)$ and $C(r)$ from (4.15) and (4.16), we get

$$f(r) = \frac{\lambda r^4 + \kappa Q^2}{\lambda r^4 - \kappa Q^2} + \frac{r\sqrt{\lambda r^4 + \kappa Q^2}}{\lambda r^4 - \kappa Q^2}\left[\int \frac{\{Q^2 + \Lambda r^4\}\{\kappa Q^2 - \lambda r^4\}}{r^4\sqrt{\lambda r^4 + \kappa Q^2}}dr - 2\sqrt{\lambda}M\right], \tag{4.26}$$

where $-2\sqrt{\lambda}M$ is the integration constant α_3 fixed by taking the asymptotic limit $r \to \infty$ and demanding that $f(r)$ goes over to the de Sitter form $f(r) = 1 - \frac{2M}{r} + \frac{Q^2}{r^2} - \frac{1}{3}\Lambda r^2$.

In addition, the metric (4.9) gives the Kretschmann scalar $\mathcal{K} = R^{\alpha\beta\gamma\delta}R_{\alpha\beta\gamma\delta}$ in the form

$$\begin{aligned}\mathcal{K}(r) =& \frac{2f'(r)^2}{r^2} + \frac{4\left[f(r)-1\right]^2}{r^4} + \frac{2\left[h(r)f'(r) + 2f(r)h'(r)\right]^2}{r^2 h(r)^2} \\ &+ \frac{\left[h(r)f''(r) + 3f'(r)h'(r) + 2f(r)h''(r)\right]^2}{h(r)^2}.\end{aligned} \tag{4.27}$$

We shall consider the cosmological constant $\Lambda = 0$ in the rest of the discussion, so that $\lambda = 1$. Consequently, $f(r)$ would approach Reissner-Nordström spacetime as $r \to \infty$.

4.3.1 Long distance behaviour

In order to find the long distance behaviour of the metric coefficient $f(r)$, we expand (4.26) in the asymptotic limit $r \to \infty$, giving

$$f(r) \approx 1 + \frac{1}{r}\left\{-\int \frac{Q^2}{r^2}dr - 2M\right\}. \tag{4.28}$$

with $\Lambda = 0$ and $\lambda = 1$. This immediately yields the Reissner-Nordström metric

$$f(r) = 1 - \frac{2M}{r} + \frac{Q^2}{r^2}, \tag{4.29}$$

noting that $fh^2 = f$ since $h \to 1$ as $r \to \infty$ from equation (4.21).

The above asymptotic form (4.29) can also be obtained from equation (4.23) which has the asymptotic form

$$f'(r) + \frac{1}{r}f(r) - \frac{1}{r} + \frac{Q^2}{r^3} \approx 0, \tag{4.30}$$

whose solution is immediately obtained as (4.29) with integration constant $-2M$, by demanding that the spacetime goes over to the Reissner-Nordström form as $r \to \infty$. The constant M can be interpreted as the ADM mass of the black hole as measured by an observer at $r \to \infty$. It is evident that $f(r)$ approaches general relativistic solution.

Upon using (4.29) and the asymptotic form and $h \approx 1 - \frac{\kappa Q^2}{2r^4}$ in (4.27), the Kretschmann scalar is found to be

$$\mathcal{K} = \frac{48M^2}{r^6} \tag{4.31}$$

in the leading order, that approaches zero as $r \to \infty$.

4.3.2 Behaviour near the center

The behavior near the centre can be obtained by approximating equation (4.26) in the limit $r \to 0$, giving

$$f(r) = -1 + \frac{Q^2}{3r^2} + \frac{2Mr}{\sqrt{\kappa Q^2}}. \tag{4.32}$$

Thus the metric coefficient $f(r) \to \infty$ as $r \to 0$.

Moreover, we see from equation (4.21) that $h^2 \to \frac{r^4}{\kappa Q^2}$ as $r \to 0$. Consequently,

$$fh^2 = \frac{r^4}{\kappa Q^2}\left(\frac{2Mr}{\sqrt{\kappa Q^2}} + \frac{Q^2}{3r^2} - 1\right) \tag{4.33}$$

as $r \to 0$, irrespective of the value of $Q \neq 0$.

Upon using (4.32) and $h \approx \frac{r^2}{\sqrt{\kappa Q^2}}$ in (4.27), the Kretschmann scalar is found to be

$$\mathcal{K} = \frac{52Q^4}{9r^8} \tag{4.34}$$

in the leading order, which diverges strongly as $r \to 0$.

For the chargeless case $Q = 0$, equation (4.26) gives

$$f(r) = 1 - \frac{2M}{r}, \tag{4.35}$$

suggesting that $f(r) \to -\infty$ as $r \to 0$ in the Schwarzchild case. Moreover, we see from equation (4.21) that $h = 1$ for $Q = 0$. Consequently,

$$fh^2 = 1 - \frac{2M}{r} \tag{4.36}$$

as $r \to 0$ for the chargeless case $Q = 0$.

The above solution (4.35) can also be obtained from equation (4.23), which has the asymptotic behaviour

$$f'(r) + \frac{f(r)}{r} - \frac{1}{r} = 0 \tag{4.37}$$

near the center, $r \to 0$, immediately leading to the solution (4.35) with $2M$ as the integration constant.

Upon using (4.35) and $h = 1$ in (4.27), the Kretschmann scalar is found to be

$$\mathcal{K} = \frac{48M^2}{r^6}, \tag{4.38}$$

that diverges strongly as $r \to 0$.

4.3.3 Intermediate behaviour

4.3.3.1 The case of positive EiBI coupling

Equation (4.26) shows that the metric coefficient $f(r)$ diverges when $r^4 = \kappa Q^2$ with $\lambda = 1$. To find the singular behavior around this point, we substitute $r = a + x$, where $a = (\kappa Q^2)^{1/4}$, and expand about $x = 0$. In the leading order, equation (4.26) takes the form

$$f(x) = \frac{C_{-1}}{x} + C_0 + C_1 x + C_2 x^2 + \dots, \tag{4.39}$$

where

$$\begin{aligned} C_{-1} &= \frac{a}{2} - \frac{M}{\sqrt{2}}, \\ C_0 &= \frac{1}{4} - \frac{M}{2\sqrt{2}a}, \\ C_1 &= -\frac{M}{4\sqrt{2}a^2} - \frac{Q^2}{2a^3} + \frac{5}{8a}, \\ C_2 &= \frac{11Q^2}{12a^4} - \frac{5}{16a^2} + \frac{M}{8\sqrt{2}a^3}. \end{aligned} \tag{4.40}$$

This shows that $f(x) \to \infty$ upon approaching $x \to 0$, equivalently $r \to a = (\kappa Q^2)^{1/4}$.

Substituting $r = a + x$ in equation (4.21) with $\lambda = 1$, and expanding around $x = 0$, we have

$$h(x) = \frac{1}{\sqrt{2}}\left(1 + \frac{x}{a} - \frac{x^2}{a^2} + \dots\right). \tag{4.41}$$

Consequently, the behaviour of the metric coefficient $f(x)h^2(x)$ near $x = 0$, or equiv-

alently near $r = a$, is obtained as

$$f(x)h^2(x) = \frac{C_{-1}}{2x} + \left(\frac{C_{-1}}{a} + \frac{C_0}{2}\right) + \left(-\frac{C_{-1}}{2a^2} + \frac{C_0}{a} + \frac{C_1}{2}\right)x + \ldots, \tag{4.42}$$

implying that $f(x)h^2(x) \to \infty$ as $x \to 0$, or equivalently $r \to a = (\kappa Q^2)^{1/4}$.

Using (4.39) and (4.41) in (4.27), we obtain the Kretschmann scalar

$$\mathcal{K}(x) = \frac{\left(a - \sqrt{2}M\right)^2}{x^6} \tag{4.43}$$

in the leading order. This shows that the Kretschmann scalar $\mathcal{K} \to \infty$ upon approaching $x \to 0$, equivalently $r \to a = (\kappa Q^2)^{1/4}$.

4.3.3.2 The case of negative EiBI coupling

Equations (4.21) and (4.26) show that the metric coefficients $f(r)$ and $h(r)$ diverge when $r^4 = |\kappa|Q^2$ with $\lambda = 1$. To find the singular behavior around this point, we substitute $r = b + x$, where $b = (|\kappa|Q^2)^{1/4}$, and expand about $x = 0$. In the leading order, equation (4.26) takes the form

$$f(x) = -\alpha_{1/2}x^{1/2} + \alpha_1 x + \alpha_{3/2}x^{3/2} + \alpha_2 x^2 + \ldots, \tag{4.44}$$

where

$$\begin{aligned} \alpha_{1/2} &= \frac{2M}{b^{3/2}}, \\ \alpha_1 &= \frac{2}{b} - \frac{2Q^2}{b^3}, \\ \alpha_{3/2} &= \frac{M}{2b^{5/2}}, \\ \alpha_2 &= \frac{7Q^2}{3b^4} - \frac{1}{b^2}, \end{aligned} \tag{4.45}$$

which shows that $f(x) \to 0$ upon approaching $x \to 0$, equivalently $r \to b = (|\kappa|Q^2)^{1/4}$.

Substituting $r = b + x$ in equation (4.21) with $\lambda = 1$, and expanding around $x = 0$, we have

$$h(x) = \frac{\beta_{-1/2}}{x^{1/2}} + \beta_{1/2}x^{1/2} + \beta_{3/2}x^{3/2} + \ldots, \tag{4.46}$$

where

$$\begin{aligned}\beta_{-1/2} &= \frac{b^{1/2}}{2},\\ \beta_{1/2} &= \frac{5}{8b^{1/2}},\\ \beta_{3/2} &= -\frac{5}{64b^{3/2}},\end{aligned} \tag{4.47}$$

so that $h(x) \to \infty$ upon approaching $x \to 0$, or $r \to b = (|\kappa|Q^2)^{1/4}$.

Consequently, the behaviour of the metric coefficient $f(x)h^2(x)$ near $x = 0$, or equivalently near $r = b$, is obtained as

$$f(x)h^2(x) = -\frac{\gamma_{-1/2}}{x^{1/2}} + \gamma_0 + \gamma_{1/2}x^{1/2} + \gamma_1 x + \gamma_{3/2}x^{3/2} + \dots, \tag{4.48}$$

where

$$\begin{aligned}\gamma_{-1/2} &= \frac{M}{2b^{1/2}},\\ \gamma_0 &= \frac{b^2 - Q^2}{2b^2},\\ \gamma_{1/2} &= -\frac{9M}{8b^{3/2}},\\ \gamma_1 &= \frac{1}{b} - \frac{2Q^2}{3b^3},\\ \gamma_{3/2} &= -\frac{5M}{16b^{5/2}},\end{aligned} \tag{4.49}$$

implying that $f(x)h^2(x) \to \infty$ as $x \to 0$, or equivalently $r \to b = (|\kappa|Q^2)^{1/4}$.

Using (4.44) and (4.46) in (4.27), the Kretschmann scalar is found to be

$$\mathcal{K}(x) = \frac{\left(b - \sqrt{2}M\right)^2}{x^6} \tag{4.50}$$

in the leading order. This shows that the Kretschmann scalar $\mathcal{K} \to \infty$ upon approaching $x \to 0$, or equivalently $r \to b = (|\kappa|Q^2)^{1/4}$.

In summary, for the case $\kappa > 0$, $f(r)$ and $f(r)h^2(r)$ diverge at $r = (\kappa Q^2)^{1/4}$ with $h(r)$ approaching a constant. On the other hand, for the case $\kappa < 0$, $h(r)$ and $f(r)h^2(r)$ diverge at $r = (|\kappa|Q^2)^{1/4}$ with $f(r)$ approaching zero. However, the Kretschmann scalar $\mathcal{K}(r)$ diverges strongly in both cases, $\kappa > 0$ and $\kappa < 0$.

4.3.4 Near-horizon behaviour

We can find the behaviour around the event horizon at $r = R$, by writing $r = R + x$ in equation (4.23) and expanding about $x = 0$. This yields

$$f'(x) + \left(a_0 + a_1 x + a_2 x^2\right) f(x) + \left(b_0 + b_1 x + b_2 x^2\right) \approx 0, \tag{4.51}$$

where

$$\begin{aligned}
a_0 &= \frac{\kappa^2 Q^4 + 6\kappa Q^2 R^4 + R^8}{R\left(R^8 - \kappa^2 Q^4\right)}, \\
a_1 &= \frac{\kappa^4 Q^8 - 18\kappa^3 Q^6 R^4 - 16\kappa^2 Q^4 R^8 - 30\kappa Q^2 R^{12} - R^{16}}{R^2\left(R^8 - \kappa^2 Q^4\right)^2}, \\
a_2 &= \frac{1}{R^3\left(R^8 - \kappa^2 Q^4\right)^3}\left[\kappa^6 Q^{12} + 18\kappa^5 Q^{10} R^4 + 39\kappa^4 Q^8 R^8 + 276\kappa^3 Q^6 R^{12}\right. \\
&\qquad \left. + 87\kappa^2 Q^4 R^{16} + 90\kappa Q^2 R^{20} + R^{24}\right] \\
b_0 &= \frac{Q^2 - R^2}{R^3}, \\
b_1 &= \frac{R^2 - 3Q^2}{R^4}, \\
b_2 &= \frac{6Q^2 - R^2}{R^5}.
\end{aligned} \tag{4.52}$$

The solution of equation (4.51) is given by

$$f(x) = -\left(\frac{b_0}{a_0} - \frac{b_1}{a_0^2} + \frac{2b_2}{a_0^3}\right) - \left(\frac{b_1}{a_0} - \frac{2b_2}{a_0^2}\right) x - \frac{b_2}{a_0} x^2 + C\left(1 - a_0 x + \frac{a_0^2}{2} x^2\right) + \ldots, \tag{4.53}$$

where C is the integration constant.

It is well-known that EiBI gravity reduces to general relativity in the absence of matter. This fact is obvious from equation (4.23) by setting $Q = 0$, leading to

$$f'(r) + \frac{1}{r} f(r) - \frac{1}{r} = 0, \tag{4.54}$$

giving the solution

$$f(r) = 1 - \frac{2M}{r}, \tag{4.55}$$

where $-2M$ is the integration constant.

The above property should be recovered when we set $Q = 0$ in our solution given by equation (4.53).

Setting $Q \to 0$ in equation (4.52), we have $a_0 \to 1/R$, , $a_2 \to 1/R^3$, $b_0 \to -1/R$,

$b_1 \to 1/R^2$, and $b_2 \to -1/R^3$ so that the solution (4.53) reduces to

$$f(x) = (4+C) - (3+C)\,\frac{x}{R} + \frac{x^2}{R^2} + \dots . \tag{4.56}$$

Using $r = R + x$ in the Schwarzchild solution (4.55) and expanding about $x = 0$, we get

$$f(x) = 1 - \frac{2M}{R} + \frac{2M}{R^2}x + \frac{2M}{R^3}x^2 + \dots . \tag{4.57}$$

Demanding that EiBI black hole reduces to Schwarzchild black hole for $Q = 0$, we can therefore compare (4.56) with (4.57) and obtain the integration constant as

$$C = -3 - \frac{2M}{R}. \tag{4.58}$$

Using this value of the integration constant in (4.53), we obtain

$$f(x) = c_0 + c_1 x + c_2 x^2 + \dots \tag{4.59}$$

where

$$\begin{aligned} c_0 &= -3 - \frac{2M}{R} - \frac{b_0}{a_0} + \frac{b_1}{a_0^2} - \frac{2b_2}{a_0^3}, \\ c_1 &= a_0\left(3 + \frac{2M}{R} - \frac{b_1}{a_0^2} + \frac{2b_2}{a_0^3}\right), \\ c_2 &= -\frac{a_0^2}{2}\left(3 + \frac{2M}{R} + \frac{4b_2}{a_0^3}\right). \end{aligned} \tag{4.60}$$

Substituting $r = R + x$ in equation (4.21) with $\lambda = 1$, and expanding around $x = 0$, we have

$$h(x) = k_0 + k_1 x + k_2 x^2 + \dots , \tag{4.61}$$

where

$$\begin{aligned} k_0 &= \frac{R^2}{\sqrt{a^4 + R^4}}, \\ k_1 &= \frac{2a^4 R}{\left(a^4 + R^4\right)^{3/2}}, \\ k_2 &= \frac{\left(a^8 - 5a^4 R^4\right)}{\left(a^4 + R^4\right)^{5/2}}. \end{aligned} \tag{4.62}$$

Thus, the metric potential $f(r)h^2(r) \to 0$ as $r \to R$ (or $x \to 0$).

Using (4.59) and (4.61) in (4.27), we have the Kretschmann scalar

$$\mathcal{K}(x) = \mathcal{K}_0 + \mathcal{K}_1 x + \mathcal{K}_2 x^2 + \dots , \tag{4.63}$$

where

$$
\begin{aligned}
\mathcal{K}_0 &= \frac{(2c_2k_0+3c_1k_1)^{\,2}}{k_0^2}+\frac{4c_1^2}{R^2}+\frac{4}{R^4},\\
\mathcal{K}_1 &= \frac{2\,(2c_2k_0+3c_1k_1)\,(6c_2k_0k_1+10c_1k_0k_2-3c_1k_1^2)}{k_0^3}\\
&\quad+\frac{4\,(2c_2c_1k_0R+c_1^2(-k_0)+2c_1^2k_1R)}{k_0R^3}-\frac{8\,(c_1R+2)}{R^5}+\frac{4\,(2c_1c_2R-c_1^2)}{R^3},\\
\mathcal{K}_2 &= \frac{1}{k_0^4R^6}\,\big[16c_2^2k_0^4R^4-32c_1c_2k_0^4R^3+16c_1^2k_0^4R^2-8c_2k_0^4R^2\\
&\quad+32c_1k_0^4R+24c_1c_2k_0^3k_1R^4-16c_1^2k_0^3k_1R^3+64c_2^2k_0^3k_2R^6\\
&\quad+16c_1^2k_0^3k_2R^4+12c_2^2k_0^2k_1^2R^6+164c_1c_2k_0^2k_1k_2R^6+100c_1^2k_0^2k_2^2R^6\\
&\quad-60c_1c_2k_0k_1^3R^6-138c_1^2k_0k_1^2k_2R^6+27c_1^2k_1^4R^6+40k_0^4.
\end{aligned}
\tag{4.64}
$$

It is obvious from (4.63) and the first line in (4.64) that the Kretschmann scalar converges to the finite value $\mathcal{K}_0$ at the horizon $r = R$ (or $x = 0$).

4.4 Numerical integration of the field equation

In order to find the nature of spacetime more concretely for charged black holes in EiBI gravity, we shall obtain the radial profiles of the metric potential $f(r)$ and the Kretschmann scalar $\mathcal{K}(r)$ by solving the differential equation (4.23) numerically without any approximation for different values of the parameters κ/M^2 and Q/M.

Figure 4.1 displays the radial profiles of the metric potential $f(r)$ and the Kretschmann scalar $\mathcal{K}(r)$ for the case $\kappa > 0$. Figure 4.1a shows the behaviour of $f(r)$ for $\kappa/M^2 = 3$ and different values of electric charge Q. We note from equation (4.23) and (4.39) that black holes can exist with an additional singularity at $r = a = (\kappa Q^2)^{1/4}$ in EiBI gravity, which is clearly a departure from general relativity. This singularity is seen to occur for all cases of $\kappa > 0$.

Equations (4.21) and (4.23) indicate that the metric coefficients reduce to the Schwarzchild solution for the case $Q = 0$. Setting $Q = 0$, our numerical results are consistent with this fact as shown by the dotted line in Figure 4.1a. Thus in the absence of matter, EiBI gravity reduces to general relativity. On the other hand, as the value of Q is increased, the event horizon shifts inwards as evident from figure 4.1a for the cases $Q/M = 0.5$ and 0.7. For sufficiently large values of Q, for example $Q = 1.5M$, the event horizon disappears, so that the singularity at $r = a = (\kappa Q^2)^{1/4}$ given by equation (4.39) becomes naked. Thus, unlike the Reissner-Nordström case, unphysical solutions can exist in EiBI gravity

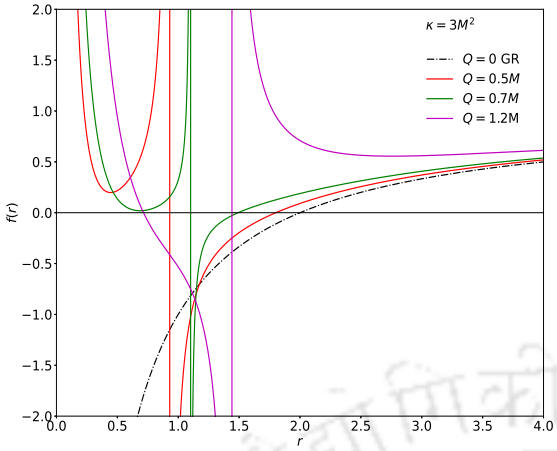

(a) Radial profiles of $f(r)$ with $\kappa/M^2 = 3$ for different values of Q/M.

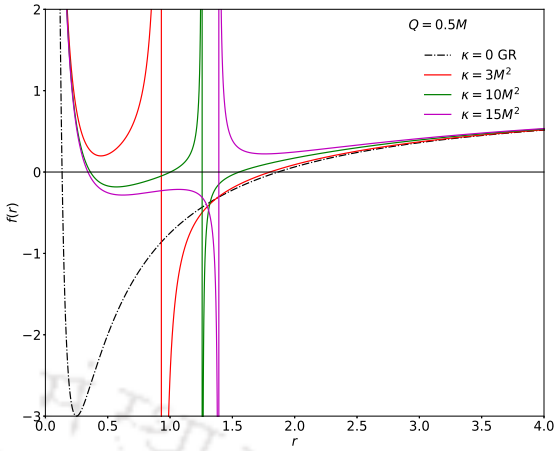

(b) Radial profiles of $f(r)$ with $Q/M = 0.5$ for different values of $\kappa/M^2 > 0$.

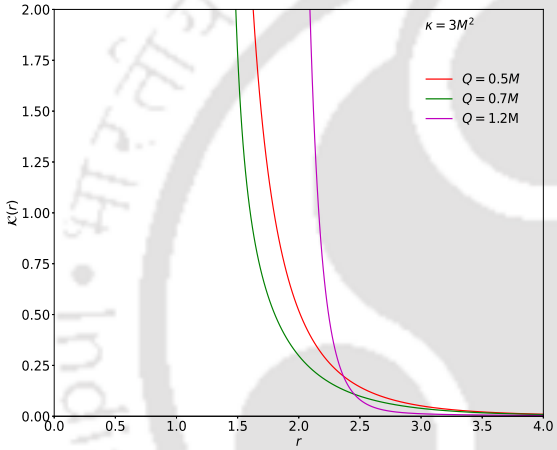

(c) Radial profiles of $\mathcal{K}(r)$ with $\kappa/M^2 = 3$ for different values of Q.

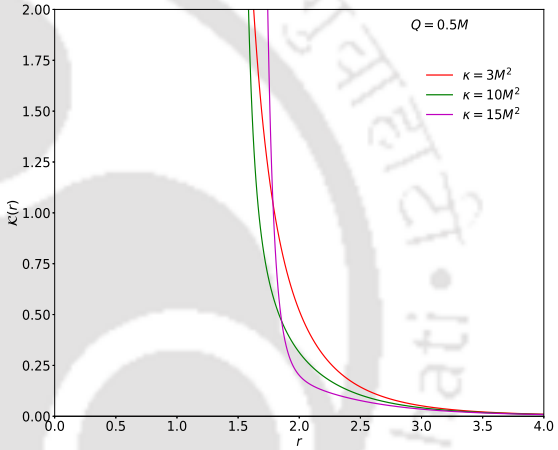

(d) Radial profiles of $\mathcal{K}(r)$ with $Q/M = 0.5$ for different values of $\kappa/M^2 > 0$.

Figure 4.1: Radial profiles of the metric potential $f(r)$ and the Kretschmann scalar $\mathcal{K}(r)$ for the EiBI coupling $\kappa > 0$.

without an event horizon.

Furthermore, Equations (4.21) and (4.23) indicate that the metric coefficients reduce to the Reissner-Nordström case for $\kappa = 0$. Setting $\kappa = 0$, our numerical results are consistent with this fact as shown by the dotted line in Figure 4.1b. Figure 4.1b also displays radial profiles of $f(r)$ with respect to different values of the coupling parameter $\kappa/M^2 > 0$ while the electric charge is fixed at $Q = 0.5M$. As shown in figure 4.1b, for $\kappa/M^2 = 3$ and 10, the event horizon shifts inwards with increase in the value of the parameter κ/M^2. For sufficiently high values of κ/M^2, for example $\kappa/M^2 = 16$, an event horizon ceases to exist and the singularity becomes naked. Such black hole solutions are unphysical.

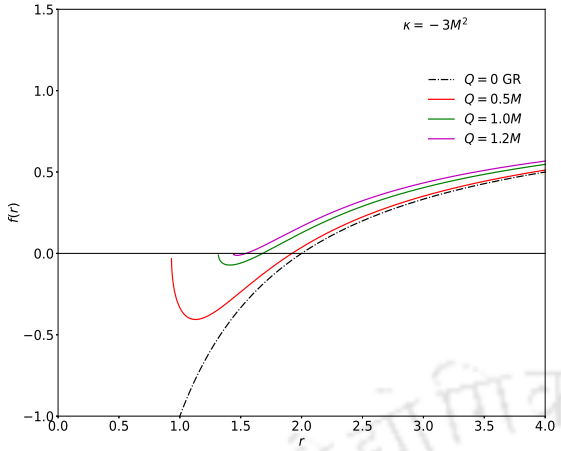

(a) Radial profiles of $f(r)$ with $\kappa/M^2 = -3$ for different values of Q/M.

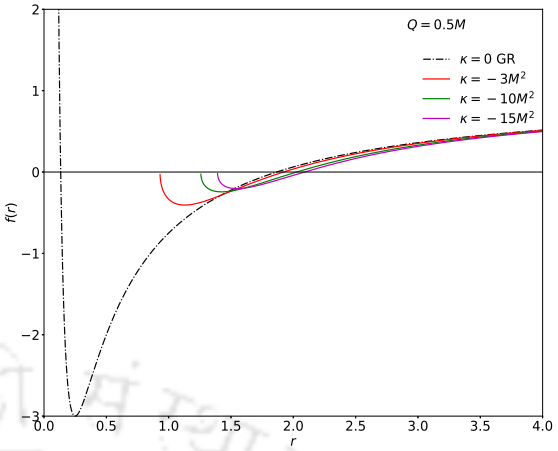

(b) Radial profiles of $f(r)$ with $Q/M = 0.5$ for different values of $\kappa/M^2 < 0$.

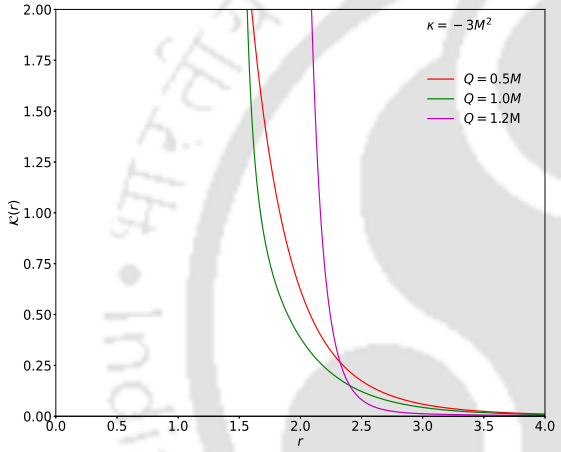

(c) Radial profiles of $\mathcal{K}(r)$ with $\kappa/M^2 = -3$ for different values of Q/M.

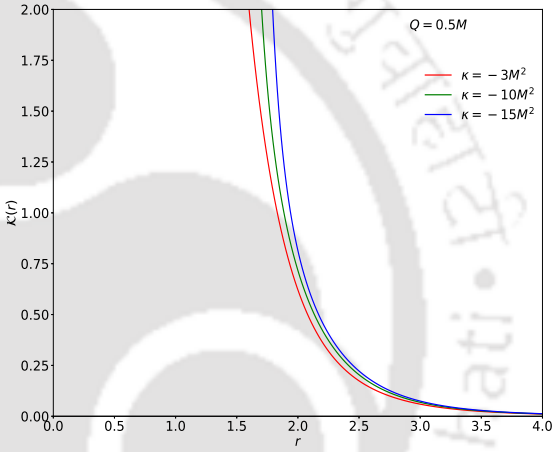

(d) Radial profiles of $\mathcal{K}(r)$ with $Q/M = 0.5$ for different values of $\kappa/M^2 < 0$.

Figure 4.2: Radial profiles of the metric potential $f(r)$ and the Kretschmann scalar $\mathcal{K}(r)$ for the EiBI coupling $\kappa < 0$.

Figures 4.1c and 4.1d show the divergence of the Kretschmann scalar $\mathcal{K}(r)$ at $r = a = (\kappa Q^2)^{1/4}$. As shown by equation (4.43), this strong divergence is also obvious from these plots.

Figure 4.2 displays radial profiles of the metric potential $f(r)$ and the Kretschmann scalar $\mathcal{K}(r)$ when $\kappa < 0$. As seen from equation (4.21), the metric potential $h(r)$ becomes imaginary for $r^4 < |\kappa|Q^2$, so that the spacetime becomes unphysical. Consequently, we have not shown the profile for $f(r)$ in the region $0 \leq r \leq |\kappa|Q^2$ in figure 4.2. Figure 4.2a shows the profiles of $f(r)$ with different values of the electric charge Q while $\kappa = -3M^2$ is fixed. The dotted line shows radial profile of $f(r)$ for $Q = 0$, which is the same as the Schwarzchild solution as also obvious from equations (4.21) and (4.23) with $\lambda = 1$.

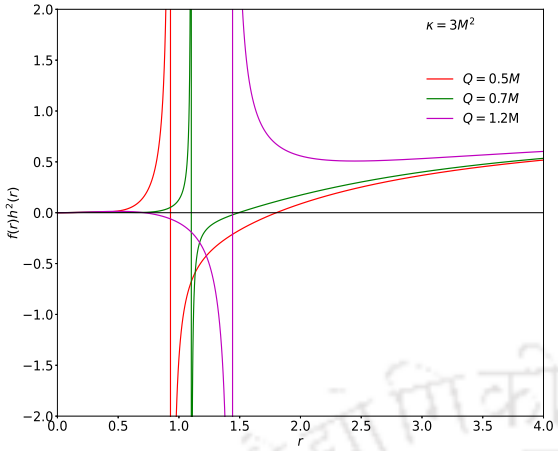

(a) Radial profiles of $f(r)h^2(r)$ with $\kappa/M^2 = 3$ for different values of Q/M.

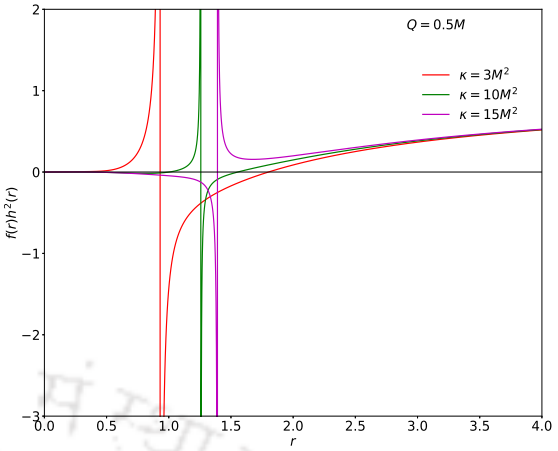

(b) Radial profiles of $f(r)h^2(r)$ with $Q/M = 0.5$ for different values of $\kappa/M^2 > 0$.

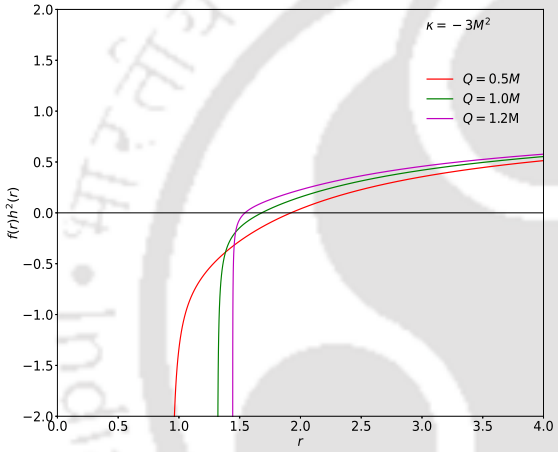

(c) Radial profiles of $f(r)h^2(r)$ with $\kappa/M^2 = -3$ for different values of Q/M.

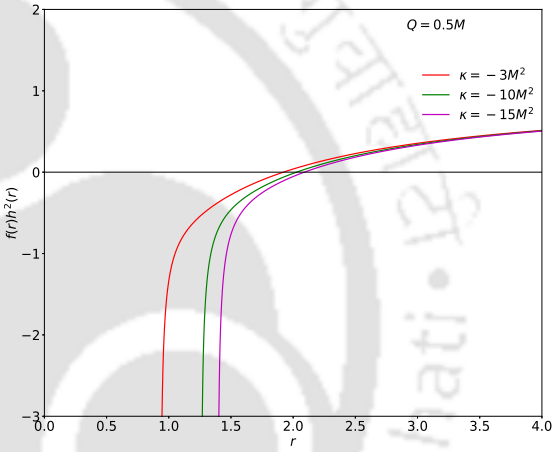

(d) Radial profiles of $f(r)h^2(r)$ with $Q/M = 0.5$ for different values of $\kappa/M^2 < 0$.

Figure 4.3: Radial profiles of the metric potential $f(r)h^2(r)$ for the cases $\kappa > 0$ and $\kappa < 0$.

We further note that, upon increasing the electric charge Q, the horizon shifts inward, as shown for the cases $Q/M = 0.5$ to 1.2 in figure 4.2a. Consequently, event horizon can exist for black holes carrying electric charge $Q > M$ in EiBI gravity, which is a clear departure from the Reissner-Nordström solution. However, for sufficiently high values of the charge Q, for example $Q/M = 1.5$, the horizon disappears and the singularity becomes naked.

Moreover, Figure 4.2b displays the profiles of $f(r)$ for different values of $\kappa < 0$ while the electric charge $Q = 0.5M$ is fixed. The general relativistic case is shown by the dotted line with $\kappa = 0$ which is equivalent to the Reissner-Nordström solution. As $|\kappa|$ is increased, for example for $\kappa/M^2 = -0.3, -10., -15$, we see that the horizon moves outward.

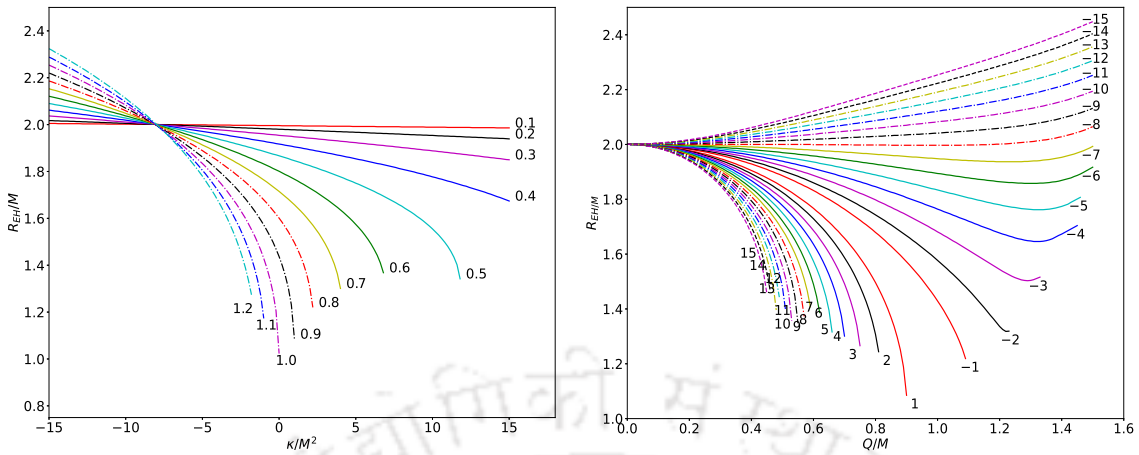

(a) Event horizon $R_{\rm EH}/M$ with respect to κ/M^2 for different values of the parameter Q/M.

(b) Event horizon $R_{\rm EH}/M$ with respect to Q/M for different values of the parameter κ/M^2.

Figure 4.4: Parametric plots for the event horizon $R_{\rm EH}/M$.

As shown by equation (4.50), the Kretschmann scalar diverges strongly at $r = (|\kappa|Q^2)^{1/4}$. This behaviour is displayed in figures 4.2c and 4.2d , showing the radial profiles of the Kretschmann scalar $\mathcal{K}(r)$.

Figure 4.3 displays the radial profiles of the metric potential $f(r)h^2(r)$ for the cases $\kappa > 0$ and $\kappa < 0$. As seen from figures 4.3a and 4.3b, $f(r)h^2(r) \to 0$ as $r \to 0$, in agreement with the asymptotic analysis giving equation (4.33) for $\kappa > 0$.

Figure 4.3a displays the profiles of $f(r)h^2(r)$ with $\kappa = 3M^2$ for different values of Q/M. Equation (4.42) indicates that $f(r)h^2(r)$ diverges as $r \to a$ (or $x \to 0$), where $a = (\kappa Q^2)^{1/4}$. This behaviour is evident in figure 4.3a for the cases $Q/M = 0.5, 0.7$ and 1.2. Likewise, figure 4.3b displays the profiles of $f(r)h^2(r)$ with $Q = 0.5M$ for different positive values of κ. The diverging nature of $f(r)h^2(r)$ as $r \to a$ is also evident from figure 4.3b for the cases $\kappa/M^2 = 3, 10$ and 15.

Equation (4.48) implies that $f(r)h^2(r) \to -\infty$ as $r \to b$ (or $x \to 0$), where $b = (|\kappa|Q^2)^{1/4}$. This nature of $f(r)h^2(r)$ is evident from figure 4.3c and 4.3d for all cases of $\kappa < 0$.

Figure 4.4 displays the dimensionalised event horizon $R_{\rm EH}/M$ for different values of the parameters κ/M^2 and Q/M for a few cases where covered black hole singularities exist.

Figure 4.4a displays the parametric plot for $R_{\rm EH}/M$ with respect to the coupling κ/M^2 for different values of the parameter Q/M. We see that, larger the value of the coupling κ/M^2, lesser is the amount of charge that the black hole can accommodate. When the EiBI coupling is negative, $\kappa < 0$, an EiBI black hole can accommodate charge

$Q > M$, unlike the Reissner-Nordström case.

Figure 4.4b displays the parametric plot for $R_{\rm EH}/M$ with respect to Q/M for different values of the parameter κ/M^2. We once again see that, when the coupling is negative, the black hole can accommodate charge $Q > M$, unlike the Reissner-Nordström case.

4.5 Discussion and conclusion

In this chapter, we considered the behaviour of the spacetime of charged black holes described by Eddington-inspired Born Infeld gravity, often abbreviated as EiBI gravity. We first obtained the field equations in the Palatini formalism from the EiBI action (4.1) with a Maxwell field minimally coupled to gravity. We solved the field equation with a static and spherically symmetric metric leading to a differential equation for the metric coefficient $f(r)$, given by equation (4.23).

In order to explore the behaviour of the spacetime of the charged EiBI black hole, we carried out an in-depth analysis for asymptotic nature of the spacetime, such as its behaviour at long distances, near the center, in the intermediate region, and near-horizon behaviour, as discussed in Section 4.3. In these regions of the spacetime, we analysed the behaviour of the metric coefficients $f(r)$, $h(r)$, $f(r)h^2(r)$, and the Kretschmann invariant $\mathcal{K}(r)$, that gave a thorough analytical understanding of the nature of spacetime.

We thus made, for the first time, a critical study of the behaviour of the geometry in several regions of the black hole spacetime in EiBI gravity by *analytical* means.

In order to aide our understanding further, we solved the differential equation (4.23) for the metric coefficient $f(r)$ numerically. In consequence, we obtained how the metric coefficients $f(r)$, $h(r)$, $f(r)h^2(r)$, and the Kretschmann invariant $\mathcal{K}(r)$ behave for different values of the black hole charge Q and the EiBI coupling κ.

The key points of the findings from our *analytical* study are the following:

- The long distance behaviour of the EiBI charged black hole approaches the Reissner-Nordström spacetime with vanishing Kretschmann curvature.

- With a positive EiBI coupling, $\kappa > 0$, the metric coefficient $f(r)$ diverges like r^{-2} at the center. Although the metric coefficient $h(r)$ vanishes like r^2, the Kretschmann scalar diverges like r^{-8} for $\kappa > 0$.

- For a negative EiBI coupling, $\kappa < 0$, the spacetime ceases to exist in the region at and around the center since the metric coefficient has imaginary parts.

- For the case $\kappa > 0$, the metric coefficients $f(r)$ and $f(r)h^2(r)$ both diverge like $(r-a)^{-1}$, where $a = (\kappa Q^2)^{1/4}$, whereas the Kretschmann scalar $\mathcal{K}(r)$ diverges like $(r-a)^{-6}$ as $r \to a$.

- For the case $\kappa < 0$, the metric coefficients $f(r)$ goes to zero like $(r-b)^{1/2}$, and $h(r)$ and $f(r)h^2(r)$ both diverge like $(r-b)^{-1/2}$, where $b = (|\kappa|Q^2)^{1/4}$. The Kretschmann scalar $\mathcal{K}(r)$ diverges like $(r-b)^{-6}$ as $r \to b$ in this case as well.

- Near the horizon, the metric coefficients and the Kretschmann scalar are finite.

We found close agreement between the above analytical behaviours and those obtained from numerical integration of the differential equation for $f(r)$ given by 4.23. For illustration, the numerical data are displayed by several plots in Section 4.4.

We may therefore conclude that a charged black hole in EiBI gravity, although having a intricate structure of the spacetime geometry, can lead to an in-depth understanding of the spacetime structure by means of probing the asymptotic behaviour in different regions of the spacetime by analytical means.

Chapter 5

Stability of charged scalar hair on Reissner-Nordström black holes

The Israel-Carter theorem (also known as the "no-hair theorem") puts a restriction on the existence of parameters other than mass, electric charge, and angular momentum of a black hole. In this context, Bekenstein proposed no-hair theorems in various black hole models with neutral and electrically charged scalar fields.

In this chapter, we take the Einstein-Maxwell-charged scalar model with an electrically charged scalar field gauge-coupled to the Maxwell field surrounding a charged black hole with a static spherically symmetric metric. In particular, we consider a quadratic scalar potential without any higher order terms and we do not impose any restriction on the magnitude of the scalar charge with respect to the black hole charge.

With this setting, we ascertain the validity of all energy conditions coupled with the causality condition, suggesting the possibility of existence of charged hairy solutions. Consequently, we obtain, by exact numerical integration, detailed solutions of the field equations that incorporate backreaction on the spacetime due to the presence of the charged scalar field. The solutions exhibit damped oscillatory behaviours for the charged scalar hair. We also find that the electric potential is a monotonic function of the radial coordinate, as required by electrodynamics.

In order to ascertain the existence of our charged hairy solutions, we carry out dynamic stability analyses against time-dependant perturbations about the static solutions. For a definite conclusion, we employ two different methodologies. The first methodology involves a Sturm-Liouville equation, whereas the second methodology employs a Schrödinger-like equation, for the dynamic perturbations. We find that our solutions are stable against time-dependant perturbations by both methodologies, confirming the existence of the charged hairy solutions.

5.1 Introduction

The Israel-Carter conjecture, or the "no-hair theorem" [49, 106, 107], asserts the uniqueness of the Schwarzschild, Reissner-Nordström, and Kerr black hole solutions. As a consequence, a black hole can be parametrised only in terms of its mass, electric charge and angular momentum. Early studies in relation to the no-hair theorem in different contexts were made by Bekenstein in the early Seventies [22, 23].

Bekenstein showed in a later work [27] that a minimally coupled multi-component scalar field with positive energy density cannot exist as a hairy solution which follows from conservation of the energy-momentum tensor. He further argued that a Higgs field with a potential having two or more wells cannot exist as hairy solution for uncharged black holes.

Ever since the no-hair conjecture was made, there have been searches for other possible parameters apart from mass, electric charge and angular momentum in the black hole solution.

One of the foremost studies in this direction was made by Bekenstein in 1974 [25], which was further extended in Ref. [26]. Bekenstein considered an electrically charged black hole with a massless conformal scalar field non-minimally coupled to gravity via conformal coupling, $\xi R\phi^2$. This study established a scalar charge, like other parameters allowed by the no-hair theorem, may also be an admissible parameter in black hole solutions. Bekenstein's hairy solution [25, 26] was analysed for stability by Bronnikov and others [41, 42] and found that a spherically symmetric perturbation destabilizes the scalar hair. They concluded that the scalar hair decays by evaporation due to this instability, leaving no scalar hair around the black hole.

Bekenstein's black hole models [25, 26] with conformal scalar hair gave rise to a spate of research studies with modifications. Models with conformally coupled scalar fields that are massless [133, 160], massive [191, 192], and self-interacting [130–132], and with a cosmological constant, were considered to obtain hairy solutions.

Furthermore, Poisson [156] examined the black hole solution in Einstein-Gauss-Bonnet gravity in $4 + n$ dimensions. Assuming the n-dimensional internal space to be slightly perturbed from constant radius, it was found that the internal radius behaves like a scalar hair. Subsequent works on scalar hair in Einstein-Gauss-Bonnet gravity can be found in Refs. [8, 15, 29, 31, 38–40, 68, 112, 124, 182, 193]. Black hole solutions with axionic hair were studied by Campbell et al. [45, 46], Lee and Weinberg [125], and Bardoux et al. [20].

There also exists a new family of Einstein-Maxwell-scalar field models where an elec-

trically neutral scalar field φ is minimally coupled to gravity and non-minimally coupled to the Maxwell field via the interaction $f(\varphi)F^{\mu\nu}F_{\mu\nu}$ [98]. Such models undergo spontaneous scalarization when the effective mass-squared given by $f''(0)F^{\mu\nu}F_{\mu\nu}$ changes sign from positive to negative, creating (uncharged) hairy solutions by dynamical growth of the scalar field profile. A comparative study on the choice for $f(\varphi)$ is reported in Ref. [79] and its stability is analysed in Ref. [137]. Extension of such scalarised black hole models with massless [12, 32, 80, 120], massive [196], massive-self-interacting [81] scalar fields, and with negative cosmological constant [159] , have also been studied.

In an important work, Mayo and Bekenstein [134] considered different combinations of electrically neutral as well as charged black holes with self-interacting neutral and charged scalar fields conformally coupled with gravity via $\xi R|\phi|^2$. The charged scalar field was gauge coupled to the Maxwell field. In the case of electrically neutral scalar field, they established a no-hair theorem for the conformal parameter in the ranges $\xi < 0$ and $\xi \geq \frac{1}{2}$. They however indicated that the total *integrated* charge should be unbounded for any value of ξ in the case of charged scalar field. In order to circumvent this situation, they further made the choice of vanishing electric potential $V(r)$ at infinity. However, they found that this latter choice contradicts the fact that $V(r)$ must be a monotonic function of r.

The no scalar hair theorem by Mayo and Bekenstein [134] was further examined for charged scalar fields gauge coupled with Maxwell field by Hong et al. [102, 103]. It was pointed out that the contribution of the scalar mass in the asymptotic solution was not properly taken into consideration in the analysis of Mayo and Bekenstein. They considered a charged scalar field gauge coupled to the Maxwell field with polynomial interacting potential with scalar charge being very small compared to the charge of the black hole. Such a system with a charged scalar cloud around the black hole was studied without any backreaction to the Reissner-Nordström background in Ref. [102] and with backreaction in Ref. [103]. The latter model was further studied by Herdeiro and Radu [97] for Schwarzschild and Reissner-Nordström black holes with charged clouds as hair. They examined various conditions for the existence of charged scalar hair.

A common feature in these models was to take the scalar potential to be a polynomial of sixth degree and the scalar charge to be much smaller than the black hole charge. Consequently, we may ask the question whether a charged scalar hair would exist as a stable solution if the scalar field is taken to be a charged massive Klein-Gordon field (with quadratic potential) without any limitation to its charge compared to the black hole charge.

In this chapter, we therefore consider an Einstein–Maxwell charged scalar field model

where an electrically charged and massive Klein–Gordon field (with quadratic potential) is gauge-coupled to the Maxwell field, giving rise to an interaction of the electric charge q of the scalar field with the electromagnetic field surrounding a charged black hole. Importantly, we take account of the backreaction on the exterior spacetime due to the presence of the scalar field by considering all field equations without making any approximation. We solve this model in a static, spherically symmetric spacetime by numerical integration and obtain black hole solutions with electrically charged scalar hair. We also consider all energy conditions stemming from the energy–momentum tensor as well as the Poynting vector, giving the causality condition, and find that all these conditions are satisfied.

We further ascertain the stability of the charged hairy solutions by carrying out dynamical stability analyses employing two different methodologies. The first methodology [19, 52, 53] involves an analysis based on the Sturm–Liouville equation for sinusoidal perturbations about the static hairy solutions. The second methodology [41, 42] involves an analysis of a Schrödinger-like equation for the dynamical perturbations. We find that the charged hairy solutions are stable against dynamical, spherically symmetric radial perturbations of the charged scalar field in both methodologies.

The rest of the chapter is organized as follows. In Section 5.2, we define the Einstein-Maxwell-charged scalar field model and obtain the corresponding field equations using a static spherically symmetric metric. In Section 5.3, we ascertain the validity of all energy conditions coupled with causality condition. In Section 5.4, we describe the boundary conditions for the field equations and solve them exactly by numerical integration. There, we also describe the hairy solutions and illustrate them with several plots. Section 5.5 is devoted to detailed stability analyses of the hairy solutions obtained in the previous Section where we employ two different methodologies to ascrtain the stability of the solutions. Section 5.6 gives a discussion and conclusion of the chapter. Throughout this chapter, we use the convention $c = 1$ and $8\pi G = 1$.

5.2 Einstein-Maxwell-charged scalar field model

We consider the Einstein-Maxwell model gauge coupled to a charged scalar field described by the action,

$$S = \int d^4x\sqrt{-g}\left[\frac{R}{2} - (D_\mu\phi)^* D^\mu\phi - \mu^2\phi^*\phi - \frac{1}{4}F_{\mu\nu}F^{\mu\nu}\right], \tag{5.1}$$

where D_μ is the covariant derivative $D_\mu = \partial_\mu + iqA_\mu$, with A_μ the four-potential of the Maxwell field $F_{\mu\nu} = \partial_\mu A_\nu - \partial_\nu A_\mu$, and q and μ are the charge and mass of the scalar

field, respectively. The gauge coupling term generates an interaction between the scalar field and the electromagnetic field.

In the above Einstein-Maxwell-charged scalar field model, we shall explore the possibility of obtaining black hole solutions with charged scalar hair for various parameter values. We shall also perform stability analyses of such hairy solutions employing two different methodologies.

We first obtain the field equations from the extremum of the above action (5.1) with respect to the variations $\delta g_{\mu\nu}$, $\delta\phi^*$, and δA_μ. As a consequence, we obtain the modified Einstein field equation,

$$\begin{aligned} G_{\mu\nu} =& 2\left(\partial_\mu - iqA_\mu\right)\phi^*\left(\partial_\nu + iqA_\nu\right)\phi - g_{\mu\nu}\left\{\left(\partial_\rho - iqA_\rho\right)\phi^*\left(\partial^\rho + iqA^\rho\right)\phi + \mu^2\phi^*\phi\right\} \\ &+ F_\mu{}^\sigma F_{\nu\sigma} - \frac{g_{\mu\nu}}{4}F_{\rho\sigma}F^{\rho\sigma}, \end{aligned} \tag{5.2}$$

the modified Klein-Gorden equation,

$$\Box_g\phi + iq\phi\nabla_\mu A^\mu + 2iqA^\mu\nabla_\mu\phi - q^2A_\mu A^\mu\phi - \mu^2\phi = 0, \tag{5.3}$$

and the modified Maxwell equation,

$$\nabla_\mu F^{\mu\nu} - 2q^2A^\nu\phi^*\phi - iq\left(\phi\partial^\nu\phi^* - \phi^*\partial^\nu\phi\right) = 0. \tag{5.4}$$

Upon writing the complex scalar field as $\phi = \frac{1}{\sqrt{2}}\left(\psi + i\chi\right)$, the above field equations can be rewritten as

$$\begin{aligned} G_{\mu\nu} =& \partial_\mu\psi\partial_\nu\psi + \partial_\mu\chi\partial_\nu\chi + q^2A_\mu A_\nu\left(\psi^2+\chi^2\right) + q\psi\left(A_\mu\partial_\nu\chi + A_\nu\partial_\mu\chi\right) \\ &- q\chi\left(A_\mu\partial_\nu\psi + A_\nu\partial_\mu\psi\right) + F_\mu{}^\sigma F_{\nu\sigma} - \frac{g_{\mu\nu}}{4}F_{\rho\sigma}F^{\rho\sigma} \\ &- \frac{g_{\mu\nu}}{2}\left\{\partial_\rho\psi\partial^\rho\psi + \partial_\rho\chi\partial^\rho\chi + \left(\mu^2 + q^2A_\rho A^\rho\right)\left(\psi^2+\chi^2\right) + 2q\left(\psi A_\rho\partial^\rho\chi - \chi A_\rho\partial^\rho\psi\right)\right\}, \end{aligned} \tag{5.5}$$

$$\Box_g\psi - q\chi\nabla_\mu A^\mu - 2qA^\mu\nabla_\mu\chi - \left(\mu^2 + q^2A_\mu A^\mu\right)\psi = 0, \tag{5.6}$$

$$\Box_g\chi + q\psi\nabla_\mu A^\mu + 2qA^\mu\nabla_\mu\psi - \left(\mu^2 + q^2A_\mu A^\mu\right)\chi = 0, \tag{5.7}$$

and

$$\nabla_\mu F^{\mu\nu} - q^2A^\nu\left(\psi^2+\chi^2\right) - q\left(\psi\partial^\nu\chi - \chi\partial^\nu\psi\right) = 0 \tag{5.8}$$

We consider a static and spherically symmetric metric

$$ds^2 = -f(r)e^{-2\eta(r)}dt^2 + \frac{dr^2}{f(r)} + r^2\left(d\theta^2 + \sin^2\theta d\varphi^2\right), \tag{5.9}$$

and obtain the equations for the metric coefficients $f(r)$ and $\eta(r)$ employing equations 5.5, 5.6, 5.7 and (5.8).

For simplicity in obtaining the solutions, we consider the ansatz $A_\mu = (V(r), 0, 0, 0)$, where $V(r)$ is the electrostatic potential. Using this ansatz in (5.8), we have the four-current

$$\mathcal{J}^\nu = (\psi\partial^\nu\chi - \chi\partial^\nu\psi) = 0. \tag{5.10}$$

Thus, as a consequence of this simplifying ansartz, we see that ψ and χ are related as $\chi = \alpha\psi$. Substituting this in (5.6) and (5.7), we find that the proportionality constant can be fixed as $\alpha = 1$.

Employing this ansatz in the Maxwell equation (5.8) yields the differential equation for the electrostatic potential as

$$V'' + \left(\eta'(r) + \frac{2}{r}\right)V' - \frac{2q^2}{f}V\psi^2 = 0, \tag{5.11}$$

where a prime denotes differentiation with respect to r. Here $V'(r)$ is the magnitude of the electric field due to electric charges of both the black hole as well as the scalar field enclosed by a sphere of radius r. In addition, from the Einstein field equation (5.5), we obtain

$$f' = \frac{1-f}{r} - r\left\{f\left(\psi'\right)^2 + \frac{e^{2\eta(r)}}{2}\left(V'\right)^2 + \left(\mu^2 + q^2\frac{e^{2\eta(r)}}{f}V^2\right)\psi^2\right\} \tag{5.12}$$

and

$$\eta'(r) = -r\left[\left(\psi'\right)^2 + q^2\frac{e^{2\eta(r)}}{f^2}V^2\psi^2\right]. \tag{5.13}$$

Similarly, equation (5.6) leads to

$$\psi'' + \left(\frac{f'}{f} - \eta' + \frac{2}{r}\right)\psi' + \left(q^2\frac{e^{2\eta}}{f^2}V^2 - \frac{\mu^2}{f}\right)\psi = 0. \tag{5.14}$$

The above set of field equations (5.11), (5.12), (5.13) and (5.14) are nonlinear in addition to being coupled in a very complicated way. Consequently, in order to obtain exact solutions, we solve them numerically with appropriate boundary conditions at the horizon. We lay out the details of the numerical procedure in Section 5.4.

5.3 Energy conditions for charged scalar hair

Before obtaining the exact solutions, it is important to examine all relevant energy conditions supplemented with the causality conditions in the Einstein-Maxwell-charged scalar field model.

We thus require that the energy-momentum tensor with mixed components $T^{\mu}_{\ \nu}$ must be bounded and it should not violate causality conditions. In order to have no divergences in the curvature invariant $G_{\mu\nu}G^{\mu\nu}$, the energy-momentum invariant $T_{\mu\nu}T^{\mu\nu}$ must be bounded everywhere in the exterior including the horizon. In the static and spherically symmetric geometry, $T_{\mu\nu}T^{\mu\nu} = (T^{t}_{\ t})^2 + (T^{r}_{\ r})^2 + (T^{\theta}_{\ \theta})^2 + (T^{\varphi}_{\ \varphi})^2$. Thus the components $T^{t}_{\ t}$, $T^{r}_{\ r}$, and $T^{\theta}_{\ \theta} = T^{\varphi}_{\ \varphi}$ should be finite and well-behaved everywhere including the horizon.

In addition, the Poynting vector $j^{\mu} = -T^{\mu}_{\ \nu}u^{\nu}$ gives the causality condition $T^{\mu}_{\ \nu}u^{\nu}T^{\rho}_{\ \mu}u_{\rho} \leq 0$ with respect to a distant observer with the four-velocity u^{ν}. This condition can be simplified using $u^{\mu}u_{\mu} = -1$ along with the fact that $u^{r}u_{r}$ and $u^{\varphi}u_{\varphi}$ are always positive for any observer moving in the equatorial plane, yielding the the condition

$$|T^{\theta}_{\ \theta}| = |T^{\varphi}_{\ \varphi}| \leq |T^{t}_{\ t}| \geq |T^{r}_{\ r}|. \tag{5.15}$$

These energy condition were discussed by Hawking and Ellis [96] and Mayo and Bekenstein [134].

For the action given by Equation (5.1), the energy-momentum tensor can be obtained from the right-hand side of the Einstein equation (5.5) as

$$\begin{aligned} T_{\mu\nu} =& \partial_{\mu}\psi\partial_{\nu}\psi + \partial_{\mu}\chi\partial_{\nu}\chi + q^2A_{\mu}A_{\nu}\left(\psi^2+\chi^2\right) + q\psi\left(A_{\mu}\partial_{\nu}\chi + A_{\nu}\partial_{\mu}\chi\right) \\ & - q\chi\left(A_{\mu}\partial_{\nu}\psi + A_{\nu}\partial_{\mu}\psi\right) + F_{\mu}^{\ \sigma}F_{\nu\sigma} - \frac{g_{\mu\nu}}{4}F_{\rho\sigma}F^{\rho\sigma} \\ & - \frac{g_{\mu\nu}}{2}\left\{\partial_{\rho}\psi\partial^{\rho}\psi + \partial_{\rho}\chi\partial^{\rho}\chi + \left(\mu^2 + q^2A_{\rho}A^{\rho}\right)\left(\psi^2+\chi^2\right) + 2q\left(\psi A_{\rho}\partial^{\rho}\chi - \chi A_{\rho}\partial^{\rho}\psi\right)\right\}, \end{aligned} \tag{5.16}$$

Following the discussion in the previous Section 5.2 for a static and spherically symmetric geometry, we obtain the mixed components $T^{\mu}_{\ \nu}$ as

$$\begin{aligned} -T^{t}_{\ t} =& f\psi'^2 + \frac{e^{2\eta}V'^2}{2} + \frac{q^2V^2}{fe^{-2\eta}}\psi^2 + \mu^2\psi^2 \\ T^{r}_{\ r} =& f\psi'^2 - \frac{e^{2\eta}V'^2}{2} + \frac{q^2V^2}{fe^{-2\eta}}\psi^2 - \mu^2\psi^2 \\ T^{\theta}_{\ \theta} =& T^{\varphi}_{\ \varphi} = -f\psi'^2 + \frac{q^2V^2}{fe^{-2\eta}}\psi^2 - \mu^2\psi^2. \end{aligned} \tag{5.17}$$

As we shall see in Sec. 5.4, we must have the boundary condition $V(r = r_h) = 0$

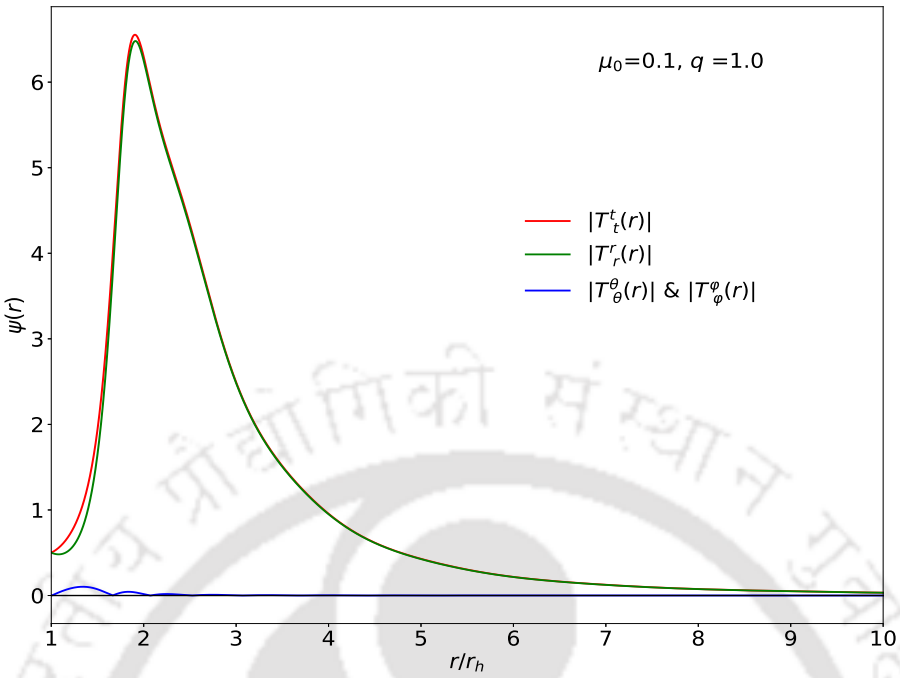

Figure 5.1: Radial profiles of the mixed components of energy-momentum tensor $|T^t_t(r)|$, $|T^r_r(r)|$, $|T^\theta_\theta(r)|$, and $|T^\varphi_\varphi(r)|$ with $q = 1.0$ and $\mu = 0.1$ in units of r_h. The boundary conditions chosen are $V'(r_h) = 1.0$ and $\psi(r_h) = 0.5$.

at the horizon for consistency with the field equations. To analyse the behaviours of the above mixed components at the horizon, we may assume the metric potential to have the Reissner-Nordström form, $f(r) = 1 - \frac{2M(r)}{r} + \frac{Q^2(r)}{r^2}$, and the electric potential $V(r) = \frac{Q(r)}{r} - \frac{Q_h}{r_h}$. Very close to the horizon, we may write $r = r_h + \epsilon$, so that $f(r) = f_1\epsilon + O(\epsilon^2)$ and $V(r) = V_1\epsilon + O(\epsilon^2)$, where $f_1 = \frac{2M_h}{r_h^2} - \frac{2M'_h}{r_h} - \frac{2Q_h^2}{r_h^3} + \frac{2Q_hQ'_h}{r_h^2}$ and $V_1 = \frac{Q'_h}{r_h} - \frac{Q_h}{r_h^2}$, giving $\frac{V^2(r)}{f(r)} = \frac{V_1^2}{f_1}\epsilon + O(\epsilon^2)$, which is zero at the horizon ($\epsilon \to 0$).

Thus all terms in each mixed component given by (5.17) are finite and well-behaved at the horizon for finite boundary conditions on $\psi(r = r_h)$, $\psi'(r = r_h)$, together with $\eta(r = r_h) = 0$. Consequently, all energy conditions, supplemented by the causality condition, given by the inequalities in (5.15) are readily satisfied. In order to illustrate the validity of these energy conditions, we show in Figure 5.1 the radial profiles of the mixed components of the energy momentum tensor.

In this context, we note that no violation of these energy conditions provide only a *necessary* criterion for the existence of scalar hair. The *sufficient* condition for the existence of scalar hair is provided by the stability of a hairy solution. (On the other hand, violation of any of the above energy conditions would be sufficient to prove a no-hair theorem.)

In the next Section 5.4, we shall solve the coupled field equations exactly by numerical

integration to obtain hairy solutions. In the subsequent Section 5.5, we shall analyse the stability of the hairy solutions employing two different methodologies.

5.4 Exact solutions of the field equations

We carry out numerical integrations for the coupled set of nonlinear differential equations (5.11), (5.12), (5.13) and (5.14) starting from the horizon.

5.4.1 Horizon boundary conditions

In order to set up the boundary conditions for the gradients of the fields, we expand them about the horizon, $r = r_h$, as

$$\begin{aligned} f(r) &= f_0 + (r - r_h) f_1 + \frac{1}{2}(r - r_h)^2 f_2 + \dots \\ \eta(r) &= \eta_0 + (r - r_h)\eta_1 + \frac{1}{2}(r - r_h)^2 \eta_2 + \dots \\ \psi(r) &= \psi_0 + (r - r_h)\psi_1 + \frac{1}{2}(r - r_h)^2 \psi_2 + \dots \\ V(r) &= V_0 + (r - r_h) V_1 + \frac{1}{2}(r - r_h)^2 V_2 + \dots \end{aligned} \tag{5.18}$$

where we have used the notation $Y_0 = Y(r_h)$, $Y_1 = Y'(r_h)$ and $Y_2 = Y''(r_h)$.

We note that $f_0 = 0$ and we take $\eta_0 = 0$ without any loss of generality since $e^{-2\eta(r)}$ corresponds to a gauge choice in the definition of the time coordinate.

Substituting the expansions given by (5.18) in the Maxwell equation (5.11), and equating powers of the same order in $r - r_h$, we find $V_0 \psi_0^2 = 0$. For a general boundary condition $\psi_0 \neq 0$, we therefore must choose the boundary condition $V_0 = 0$ at the horizon.

We further obtain the horizon conditions by expanding the field equations about the horizon. Upon substituting $r = r_h + \epsilon$ in equations (5.11), (5.12), (5.13) and (5.14), the radial derivatives at the horizon are obtained as

$$\begin{aligned} f_1 &= \frac{1}{r_h} - \mu^2 r_h \psi_0^2 - \frac{r_h V_1^2}{2} \\ \psi_1 &= \frac{\mu^2}{f_1}\psi_0 \\ \eta_1 &= -r_h \psi_1^2 - q^2 r_h \psi_0^2 \frac{V_1^2}{f_1^2}. \end{aligned} \tag{5.19}$$

The parameter ϵ is a very small radial displacement from the horizon, which will be controlled in the numerical algorithm.

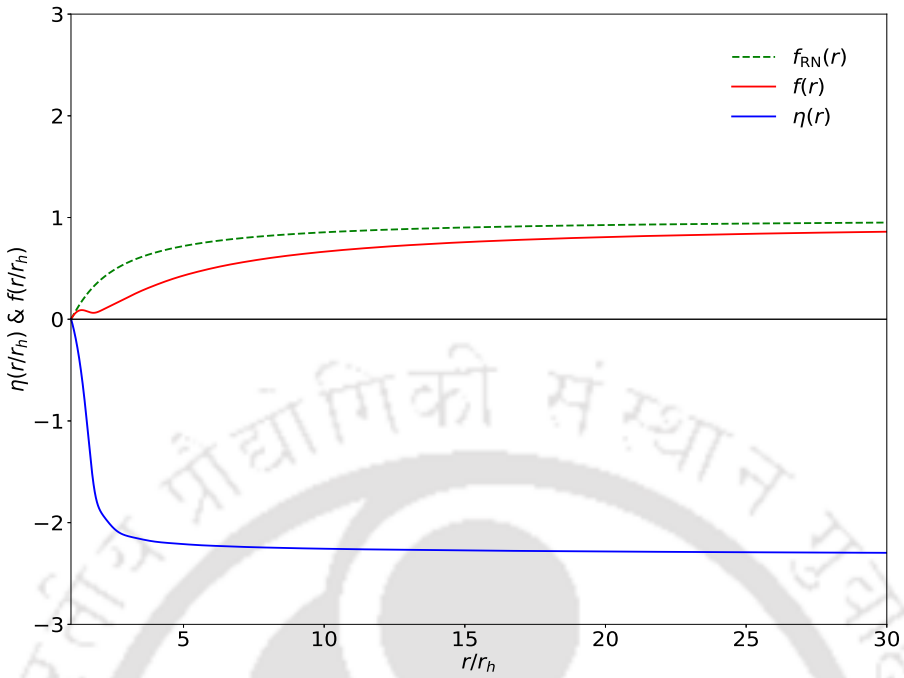

Figure 5.2: Radial profiles of metric potentials $f(r)$ and $\eta(r)$ with $q = 1.0$ and $\mu = 0.1$ in units of r_h. The boundary conditions chosen are $V'(r_h) = 1.0$ and $\psi(r_h) = 0.5$. For comparison, the radial profile of the Reissner-Nordström metric potential $f_{\rm RN}(r)$ is also shown.

On the other hand, we expect a Minkoskian spacetime as $r \to \infty$ so that $f \to 1$. Moreover, with the gauge choice of $V = 0$ at the horizon, $V(r)$ and $\eta(r)$ approach constant values as $r \to \infty$. With these asymptotic behaviours, equation (5.14) reduces to $\psi'' + \frac{2}{r}\psi' + \omega^2\psi = 0$ at infinity, where $\omega^2 = q^2 e^{2\eta_\infty} V_\infty^2 - \mu^2 =$ constant. The corresponding solutions that satisfy the above asymptotic requirements is $\psi \propto \frac{\cos(\omega r)}{r}$ for $\omega^2 > 0$ and $\psi \propto \frac{e^{-\omega r}}{r}$ for $\omega^2 < 0$. Both solutions vanish as $r \to \infty$. However, the latter solution is not possible in the present model with boundary conditions discussed above.

5.4.2 Numerical integration

Employing the boundary conditions at the horizon as discussed in the previous subsection, we carry out simultaneous numerical integrations of the coupled set of field equations (5.11), (5.12), (5.13) and (5.14) by choosing the parameters V_1, ψ_0, q and μ, so as to obtain exact solutions for the radial profiles of $\psi(r)$, $V(r)$, $f(r)$, and $\eta(r)$, until the radial distance from the black hole horizon is sufficiently high, where the scalar field approaches a vanishing value. The results of the numerical integration are presented below.

Figure 5.2 displays the radial profiles of the metric potentials $f(r)$ and $\eta_(r)$ with scalar charge $q = 1.0$ and mass $\mu = 0.1$, in units of r_h, with the horizon values taken as

$V'(r_h) = 1.0$, and $\psi_0 = \psi(r_h) = 0.5$. For comparison with the Reissner-Nordström solution, we have plotted the profile of $f_{\rm RN}(r)$ with the horizon condition $V'(r_h) = 1.0$.

Our numerical data indicates that $f_{\rm RN} = 0.95$ and $f = 0.86$ at $\frac{r}{r_{\rm h}} = 30$, $f_{\rm RN} = 0.98$ and $f = 0.94$ at $\frac{r}{r_{\rm h}} = 100$, and $f_{\rm RN} = 0.99$ and $f = 0.96$ at $\frac{r}{r_{\rm h}} = 200$. Thus the metric coefficient $f(r)$ approaches the limiting value of unity slowly (compared to the Reissner-Nordström case) due to backreaction of the charged scalar hair. It is however clear that the flat spacetime limit would be reached upon carrying out the numerical computation up to sufficiently high values of the radial coordinate r.

As we can see from Figure 5.2, the metric coefficient $f(r)$ is slightly non-monotonic near the horizon with a dip at about $r \sim 2r_h$, and it acquires a profile similar to $f_{\rm RN}(r)$ for large r. We also see a steep fall in the metric potential $\eta(r)$ until about $r \sim 2r_h$. This correlation originates from the coupled differential equations determining these metric coefficients. Afterwards, $\eta(r)$ appears to approach a constant negative value at infinity, indicating a re-parametrization of the time. These effects are solely due to the presence of the scalar hair. In the absence of scalar hair, $\eta(r)$ would remain zero everywhere.

Figure 5.3 shows the radial profiles of the scalar field $\psi(r)$ for different values of mass μ and charge q of the scalar field, with $V'(r_h) = 1.0$ and $\psi(r_h) = 0.5$ at the horizon. All these profiles show a damped oscillatory behaviour with respect to the radial distance r. The profile with $\mu = 0.1$ and $q = 1.0$ shows a steep fall until $r \sim 2r_h$. We note that this steep fall in $\psi(r)$ is correlated with the non-monotonic behaviour of $f(r)$ and a steep fall of $\eta(r)$ as noted previously in Figure 5.2.

It is clear from Figure 5.3 that the hairy solution $\psi(r)$ approaches zero at infinity while performing a damped oscillation with increasing radial coordinate r. This creates a halo of charged cloud surrounding the black hole, the charge density approaching zero at infinity.

Figure 5.4 shows radial profiles of the hairy solutions $\psi(r)$ with pair-wise positive and negative values of $\psi(r_h)$ at the horizon, with $V'(r_h) = 1.0$. Once again we can see damped oscillatory behaviours in all cases. An important observation here is that the solutions with pair-wise positive and negative values of $\psi(r_h)$ are exact mirror images of each other.

The results shown in Figures 5.3 and 5.4 suggest possible existence of charged and massive scalar hair surrounding the charged black hole. Stability of such hairy solutions is discussed in Section 5.5.

It is also important to find the behaviour of the scalar charge density $\rho(r) = 2q^2V\psi^2$ surrounding the black hole. In Figure 5.5, we display the radial profile of $\rho(r)$ in one of the cases of our solutions. It is evident from the figure that the charge density $\rho(r)$

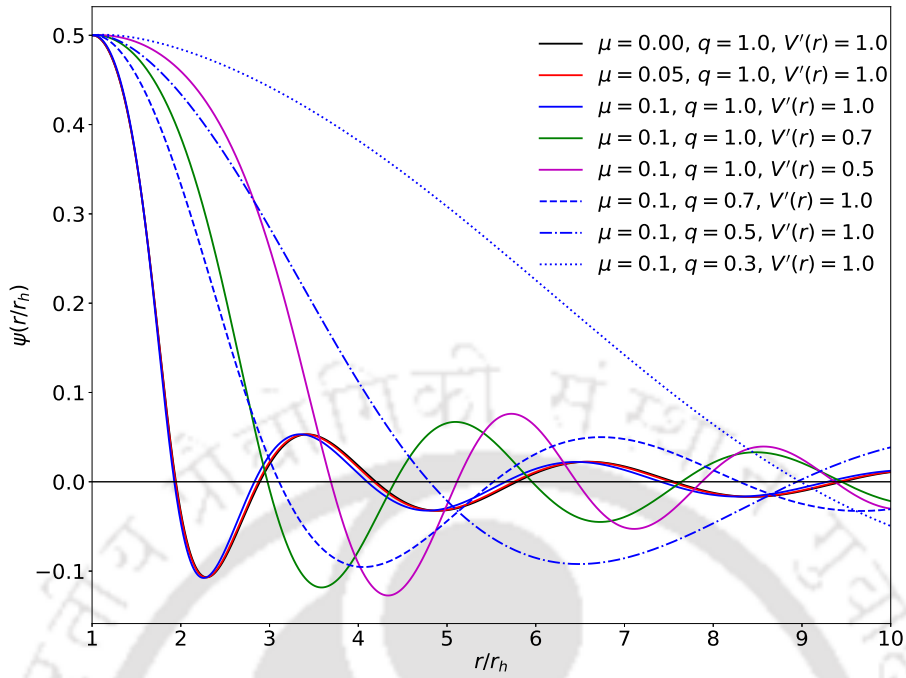

Figure 5.3: Radial profiles of hairy solutions $\psi(r)$ for different values of $V'(r_h)$, q and μ, with the horizon value $\psi(r_h) = 0.5$.

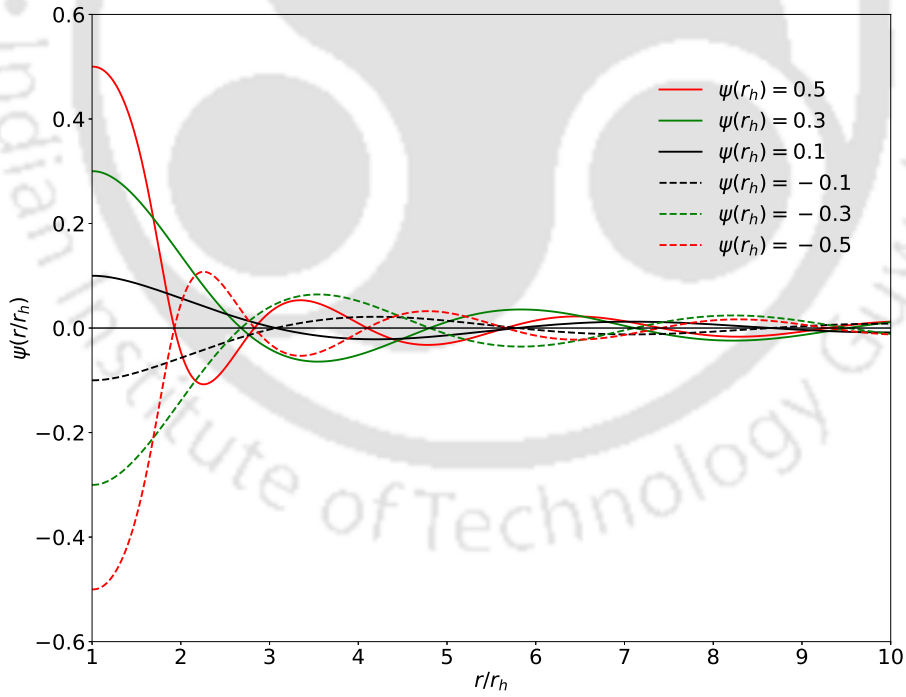

Figure 5.4: Radial profiles of $\psi(r)$ for different horizon values of $\psi(r_h)$, all having $V'(r_h) = 1.0$, with scalar hair parameters $q = 1.0$ and $\mu = 0.1$.

oscillates and falls off very rapidly with the radial coordinate r. We also note that there is a vanishing charge density at the horizon. The charge distribution appears to form

concentric shells with varying charge densities that approach zero quickly with the shell radius. Practically, there would be no measurable charge density far from the black hole.

Figure 5.6 shows the radial profiles of the electrostatic potential $V(r)$ with different values of the parameters q and μ of the scalar field, with horizon conditions $V'(r_h) = 1.0$, and $\psi(r_h) = 0.5$. All profiles of $V(r)$ show *monotonic* behaviours: the potential monotonically increases from zero at the horizon and appears to saturate to constant values at infinity. For the case μ fixed at 0.1, as q is increased, the profiles of $V(r)$ deviate further from the Reissner-Nordström profile; q changing from 0.7 to 1.0 shows a rapid deviation, reaching a value much higher the Reissner-Nordström value at infinity. On the other hand, for the case q fixed at 1.0, the profiles undergo slight deviation as μ is increased from zero to 0.1. It is obvious that the electrostatic potential $V(r)$ acquires additional contribution from the charged scalar hair so that it approaches a higher constant value at infinity. Moreover, the magnitude of the electric field $V'(r)$ vanishes as $r \to \infty$, as expected.

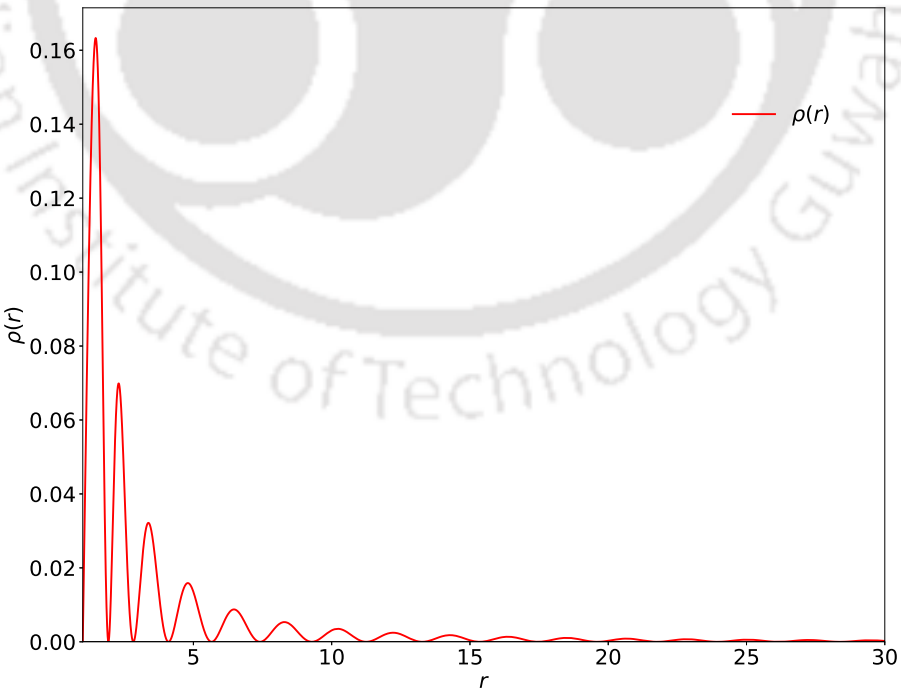

Figure 5.5: Radial profile of the charge density $\rho(r) = 2q^2V\psi^2$ of the scalar hair with the choices $q = 1.0$, $\mu = 0.1$, $\psi(r_h) = 0.5$ and $V'(r_h) = 1.0$.

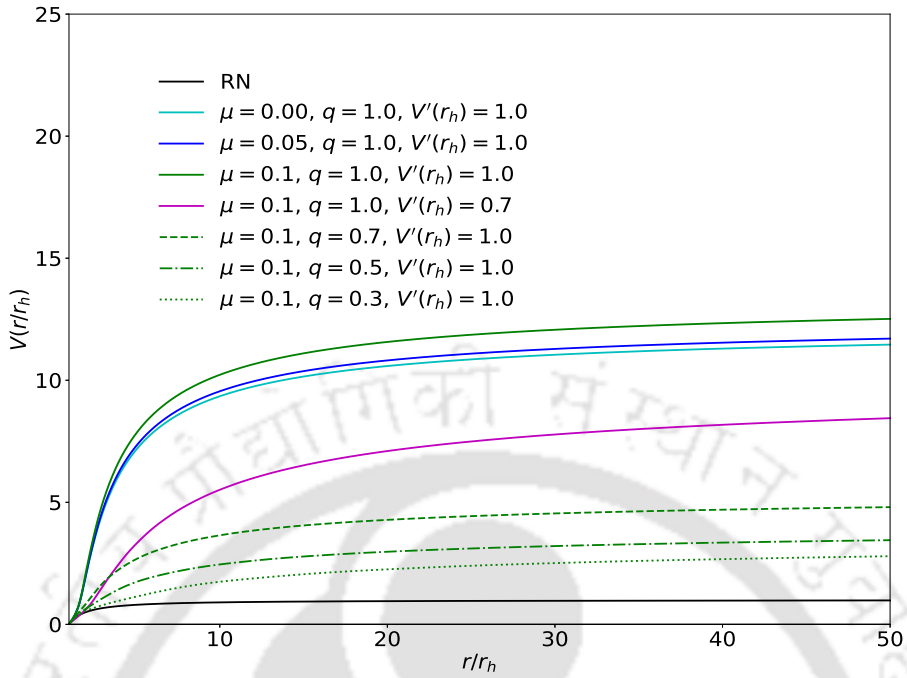

Figure 5.6: Radial profiles of the electrostatic potential $V(r)$ for different values of $V'(r_h)$ and scalar hair parameters q and μ, with the horizon condition $\psi(r_h) = 0.5$. For comparison, the profile of the Reissner-Nordström potential is also shown.

5.5 Dynamical stability analyses

In order for the existence of the charged scalar hair surrounding a charged black hole, the hairy solution must be stable under time-dependant perturbation of the scalar field.

Consequently, we shall analyse the stability of the hairy solutions obtained in the previous sections. For definiteness, we shall carry out the stability analysis in two different ways. The first is based on Sturm-Liouville equation [19, 52, 53] whereas the second is based on a Schrödinger-like equation [41, 42] for the dynamic perturbation.

To carry out a dynamic stability analysis, we introduce time-dependence into the original scalar field, $\phi(r) \to \tilde{\phi}(r,t)$. The effect of this time-dependant field will make all the rest of the quantities time-dependant. We therefore make the changes: $f(r) \to \tilde{f}(r,t)$, $\eta(r) \to \tilde{\eta}(r,t)$ and $V(r) \to \tilde{V}(r,t)$. Accordingly, we have the modified metric as

$$ds^2 = -\tilde{f}(r,t)e^{-2\tilde{\eta}(r,t)}dt^2 + \frac{dr^2}{\tilde{f}(r,t)} + r^2\left(d\theta^2 + \sin^2\theta d\varphi^2\right). \tag{5.20}$$

Employing the above metric in the field equations (5.5), (5.6), (5.7) and (5.8), we obtain time-dependant differential equations. The Einstein field equation (5.5) leads to

$$\tilde{f}' = \frac{\left(1-\tilde{f}\right)}{r} - \frac{r}{2}\left[\frac{\left(\dot{\tilde{\psi}}^2+\dot{\tilde{\chi}}^2\right)}{fe^{-2\eta}} + \tilde{f}\left(\tilde{\psi}'^2+\tilde{\chi}'^2\right) + \frac{2q\tilde{V}}{\tilde{f}e^{-2\tilde{\eta}}}\left(\tilde{\psi}\dot{\tilde{\chi}}-\tilde{\chi}\dot{\tilde{\psi}}\right) + e^{2\tilde{\eta}}\tilde{V}'^2 + \left\{\mu^2+\frac{q^2\tilde{V}^2}{\tilde{f}e^{-2\tilde{\eta}}}\right\}\left(\tilde{\psi}^2+\tilde{\chi}^2\right)\right], \tag{5.21}$$

$$\tilde{\eta}' = -\frac{r}{2}\left[\frac{\left(\dot{\tilde{\psi}}^2+\dot{\tilde{\chi}}^2\right)}{\tilde{f}^2e^{-2\tilde{\eta}}} + \left(\tilde{\psi}'^2+\tilde{\chi}'^2\right) + \frac{q^2\tilde{V}^2}{\tilde{f}^2e^{-2\tilde{\eta}}}\left(\tilde{\psi}^2+\tilde{\chi}^2\right) + \frac{2q\tilde{V}}{\tilde{f}^2e^{-2\tilde{\eta}}}\left(\tilde{\psi}\dot{\tilde{\chi}}-\tilde{\chi}\dot{\tilde{\psi}}\right)\right], \tag{5.22}$$

and

$$\dot{\tilde{f}} = -r\tilde{f}\left[\tilde{\psi}'\dot{\tilde{\psi}}+\tilde{\chi}'\dot{\tilde{\chi}}+q\tilde{V}\left(\tilde{\psi}\tilde{\chi}'-\tilde{\chi}\tilde{\psi}'\right)\right]. \tag{5.23}$$

Similarly, the Maxwell equation (5.8) yields

$$\tilde{V}'' + \left(\tilde{\eta}'+\frac{2}{r}\right)\tilde{V}' - \frac{q^2\tilde{V}}{\tilde{f}}\left(\tilde{\psi}^2+\tilde{\chi}^2\right) - \frac{q}{\tilde{f}}\left(\tilde{\psi}\dot{\tilde{\chi}}-\tilde{\chi}\dot{\tilde{\psi}}\right) = 0 \tag{5.24}$$

and

$$\dot{\tilde{V}}' + \tilde{V}'\dot{\tilde{\eta}} - q\tilde{f}e^{-2\tilde{\eta}}\left(\tilde{\psi}\tilde{\chi}'-\tilde{\chi}\tilde{\psi}'\right) = 0. \tag{5.25}$$

In addition, the Klein-Gorden equations (5.6) and (5.7) are now modified to

$$\ddot{\tilde{\psi}} - \tilde{f}^2e^{-2\tilde{\eta}}\tilde{\psi}'' - \dot{\tilde{\psi}}\left(\frac{\dot{\tilde{f}}}{\tilde{f}}-\dot{\tilde{\eta}}\right) - \left\{\frac{\tilde{f}'}{\tilde{f}}-\tilde{\eta}'+\frac{2}{r}\right\}\tilde{f}^2e^{-2\tilde{\eta}}\tilde{\psi}' - q\tilde{\chi}\dot{\tilde{V}} + q\tilde{\chi}\tilde{V}\left(\frac{\dot{\tilde{f}}}{\tilde{f}}-\dot{\tilde{\eta}}\right) - 2q\tilde{V}\dot{\tilde{\chi}} - q^2\tilde{V}^2\tilde{\psi} + \mu^2\tilde{f}e^{-2\tilde{\eta}}\tilde{\psi} = 0 \tag{5.26}$$

and

$$\ddot{\tilde{\chi}} - \tilde{f}^2e^{-2\tilde{\eta}}\tilde{\chi}'' - \dot{\tilde{\chi}}\left(\frac{\dot{\tilde{f}}}{\tilde{f}}-\dot{\tilde{\eta}}\right) - \left\{\frac{\tilde{f}'}{\tilde{f}}-\tilde{\eta}'+\frac{2}{r}\right\}\tilde{f}^2e^{-2\tilde{\eta}}\tilde{\chi}' + q\tilde{\psi}\dot{\tilde{V}} - q\tilde{\psi}\tilde{V}\left(\frac{\dot{\tilde{f}}}{\tilde{f}}-\dot{\tilde{\eta}}\right) + 2q\tilde{V}\dot{\tilde{\psi}} - q^2\tilde{V}^2\tilde{\chi} + \mu^2\tilde{f}e^{-2\tilde{\eta}}\tilde{\psi} = 0. \tag{5.27}$$

In order to carry out the stability analysis, we assume that the time-dependant perturbations are sinusoidal, and we perturb the time-dependant fields around the static solutions as

$$\begin{aligned}
\tilde{f}(r,t) &= f(r) + \varepsilon f_1(r) e^{-i\Omega t}, \\
\tilde{\eta}(r,t) &= \eta(r) + \varepsilon \eta_1(r) e^{-i\Omega t}, \\
\tilde{V}(r,t) &= V(r) + \varepsilon V_1(r) e^{-i\Omega t}, \\
\tilde{\psi}(r,t) &= \psi(r) + \varepsilon \psi_1(r) e^{-i\Omega t}, \\
\tilde{\chi}(r,t) &= \chi(r) + \varepsilon \chi_1(r) e^{-i\Omega t},
\end{aligned} \tag{5.28}$$

where ε is a very small quantity ($\varepsilon \ll 1$). In this Section, quantities carrying a subscript 1 indicates the perturbation field depending on the radial coordinate, and Ω is the eigen frequency to be determined from the stability analysis.

Substituting the above expressions (5.28) in (5.21), (5.22), (5.23), (5.24) and (5.26), we obtain the following set of equations:

$$f_1 = -2fr\psi'\psi_1, \tag{5.29}$$

$$\eta_1' = 2r\left[\frac{q^2V^2}{f^2e^{-2\eta}}\psi\psi_1 - \psi'\psi_1'\right], \tag{5.30}$$

$$V_1' = -V'\eta_1, \tag{5.31}$$

and

$$\begin{aligned}
&f^2e^{-2\eta}r\psi_1'' + f^2e^{-2\eta}\left\{\frac{f'}{f} - \eta' + \frac{2}{r}\right\}r\psi_1' + f^2e^{-2\eta}\left(\frac{f'}{f} - \eta'\right)\psi_1 \\
&- \left\{\frac{f^2e^{-2\eta}}{r}\left(\frac{f'}{f} - \eta'\right) + \mu^2 fe^{-2\eta} + 3q^2V^2 - 2rfe^{-2\eta}f'\psi'^2 - 2f^2e^{-2\eta}\psi'^2\right. \\
&\left. + 4\mu^2 rfe^{-2\eta}\psi'\psi - 2r^2f^2e^{-2\eta}\psi'^4 - 2r^2q^2V^2\psi^2\psi'^2\right\}r\psi_1 = -\Omega^2 r\psi_1.
\end{aligned} \tag{5.32}$$

To obtain the scalar perturbation equation in the Sturm-Liouville form, we define $\xi = r\psi_1$, leading to

$$\begin{aligned}
&\left(fe^{-\eta}\xi'\right)' - \left\{\frac{1}{r}\left(fe^{-\eta}\right)' + \mu^2e^{-\eta} + \frac{3q^2V^2}{fe^{-\eta}} - 2re^{-\eta}f'\psi'^2 - 2fe^{-\eta}\psi'^2\right. \\
&\left. + 4\mu^2re^{-\eta}\psi'\psi - 2r^2fe^{-\eta}\psi'^4 - 2r^2\frac{q^2V^2}{fe^{-\eta}}\psi^2\psi'^2\right\}\xi = -\frac{\Omega^2}{fe^{-\eta}}\xi.
\end{aligned} \tag{5.33}$$

Equation (5.33) is in the form of an eigenvalue equation. We notice from (5.28) that

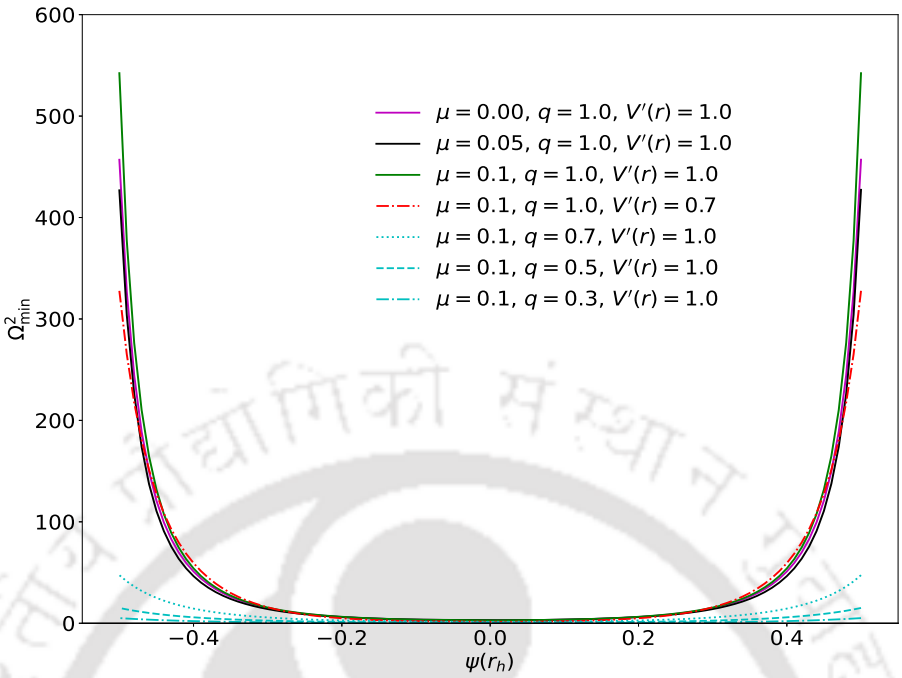

Figure 5.7: The minimum Sturm-Liouville eigenvalue $\Omega^2_{\rm min}$ with respect to horizon value $\psi(r_h)$ with the choice of trial function $\xi(x) = a\tanh(x)$.

the exponential terms will have a growing mode if $\Omega^2 < 0$. Writing $\Omega = \pm i\alpha$, with $\alpha > 0$, the eigen solutions will have an exponentially growing mode $e^{\alpha t}$ and a decaying mode $e^{-\alpha t}$. The exponentially growing mode $e^{\alpha t}$ makes the solution unstable. On the other hand, for the case $\Omega^2 > 0$, we may write $\Omega = \pm\omega$, so that both modes $e^{i\omega t}$ and $e^{-i\omega t}$ perform stable sinusoidal oscillations.

Thus the sign of the eigenvalue Ω^2 dictates the stability of the hairy solution. Solutions with $\Omega^2 > 0$ are stable, whereas $\Omega^2 < 0$ corresponds to instability, and $\Omega^2 = 0$ signifies onset of instability.

5.5.1 Analysis of Sturm-Liouville equation

As noted earlier, Equation (5.33) can be expressed in the Sturm-Liouville form,

$$\frac{d}{dr}\left(P(r)\frac{d\xi(r)}{dr}\right) + Q(r)\xi(r) + \Omega^2 R(r)\xi(r) = 0, \tag{5.34}$$

where

$$
\begin{aligned}
P(r) &= fe^{-\eta}, \\
Q(r) &= -\left[\frac{1}{r}\left(fe^{-\eta}\right)' + \mu^2 e^{-\eta} + \frac{3q^2V^2}{fe^{-\eta}} - 2re^{-\eta}f'\psi'^2 - 2fe^{-\eta}\psi'^2\right. \\
&\quad \left. +4\mu^2 re^{-\eta}\psi'\psi - 2r^2\left(fe^{-\eta}\psi'^4 + \frac{q^2V^2}{fe^{-\eta}}\psi^2\psi'^2\right)\right], \\
R(r) &= \frac{1}{fe^{-\eta}}.
\end{aligned}
\tag{5.35}
$$

The smallest eigenvalue Ω^2_{min} of the Sturm-Liouville equation (5.34) can be obtained by employing the variational principle, giving

$$
\Omega^2_{\text{min}} =^{\text{min}}_{\xi(r)} \frac{\int_{r_h}^{\infty} dr\ P(r)\xi'^2(r) - \int_{r_h}^{\infty} dr\ Q(r)\xi^2(r)}{\int_{r_h}^{\infty} dr\ R(r)\xi^2(r)}, \tag{5.36}
$$

which can be evaluated with a trial function for $\xi(r)$.

For definiteness, we choose two different trial functions, $\xi(x) = a\tanh x$ and $\xi(x) = bxe^{-x}$, where $x = \frac{r-r_h}{r_h}$ and a and b are disposable constants. With these trial functions, we carry out the integrations numerically in Equation (5.36) to obtain the minimum eigenvalue Ω^2_{min}.

Figure 5.7 shows the behaviours of Ω^2_{min} with respect to $\psi(r_h)$, with different values of the parameters q and μ, employing the trial function $\xi = a\tanh x$. It is clear from the figure that Ω^2_{min} is positive and non-zero over a continuous range of horizon conditions $\psi(r_h)$ involving both positive and negative values.

We confirm the above results with another choice of trial function for $\xi(r)$. Figure 5.8 shows the behaviours of Ω^2_{min} with respect to $\psi(r_h)$ for different values of the parameters q and μ, with the choice of trial function $\xi = bxe^{-x}$. We once again see that Ω^2_{min} turns out to be positive and non-zero over a continuous range of positive and negative horizon conditions for $\psi(r_h)$.

In order to analyse whether Ω^2_{min} can become negative, we see from Figures 5.7 and 5.8 that such possibility may exist for the initial condition $\psi(r_h) = 0$. We therefore have to analyse equation (5.33) at the horizon, $r = r_h$. Equation (5.19) indicates that $\psi'(r_h)$ is proportional to $\psi(r_h)$. The analysis in the paragraph after equation (5.17) shows that$V^2(r_h)/f(r_h) = 0$. Thus, at the horizon equation (5.33) reduces to $\left(fe^{-\eta}\xi'\right)' - \left\{\frac{1}{r}\left(fe^{-\eta}\right)' + \mu^2 e^{-\eta}\right\}\xi = -\frac{\Omega^2}{fe^{-\eta}}\xi$. Since $\eta(r_h) = 0$, this equation further reduces to $f^2\eta'\xi' - f^2\xi'' + f\left\{\frac{1}{r}f' - \frac{1}{r}f\eta' + \mu^2\right\} = \Omega^2$. Moreover, with the boundary condition $\xi(r_h) = 0$ as well as $\xi'(r_h) = 0$, this equation further reduces to $f\left\{-f\xi'' + \frac{1}{r}f' - \frac{1}{r}f\eta' + \mu^2\right\} =$

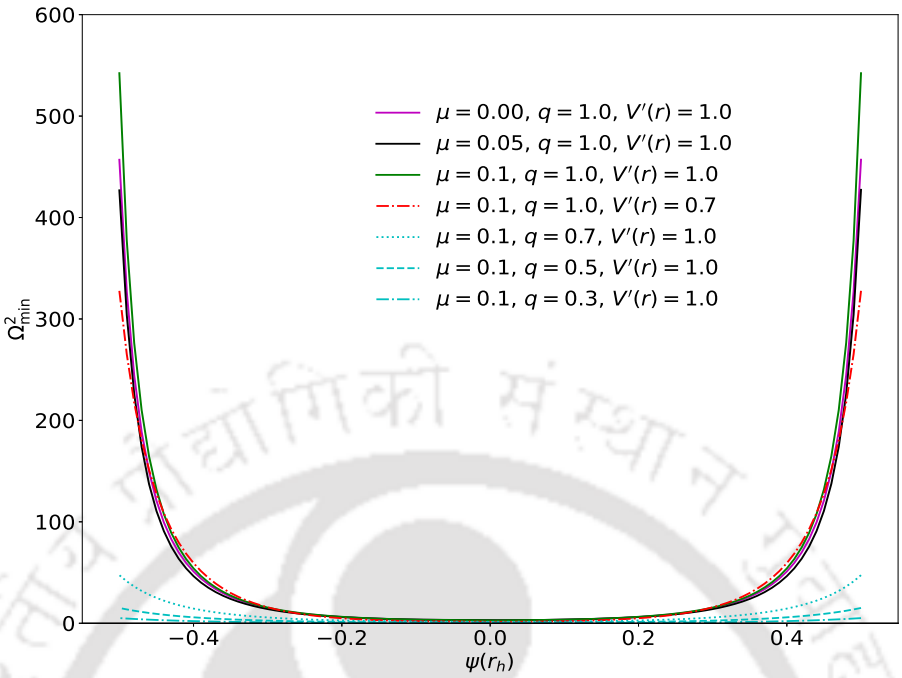

Figure 5.8: The minimum Sturm-Liouville eigenvalue $\Omega^2_{\min}$ with respect to horizon value $\psi(r_h)$ with the choice of trial function $\xi(x) = bxe^{-x}$.

Ω^2. This implies $\Omega^2_{\min} = 0$ since $f(r_h) = 0$. Thus, $\Omega^2_{\min}$ cannot become negative for the initial condition $\psi(r_h) = 0$. For other initial conditions with $\psi(r_h) \neq 0$ we can infer from Figures 5.7 and 5.8 that $\Omega^2_{\min} > 0$.

The above results indicate that $\Omega^2_{\min} > 0$ over a continuous range of horizon values $\psi(r_h)$, both positive and negative. It may therefore be concluded that the scalar hair solutions remain stable with respect to sinusoidal perturbations.

We further confirm this conclusion employing another method for stability analysis in the next Subsection.

5.5.2 Analysis of Schrödinger-like equation

Transforming to the tortoise coordinate r^*, defined by $dr^* = \frac{e^\eta}{f} dr$, Equation (5.33) can be reduced to a Schrödinger-like equation,

$$-\frac{d^2\xi}{dr^{*2}} + V_{\text{eff}}\xi = \Omega^2\xi, \tag{5.37}$$

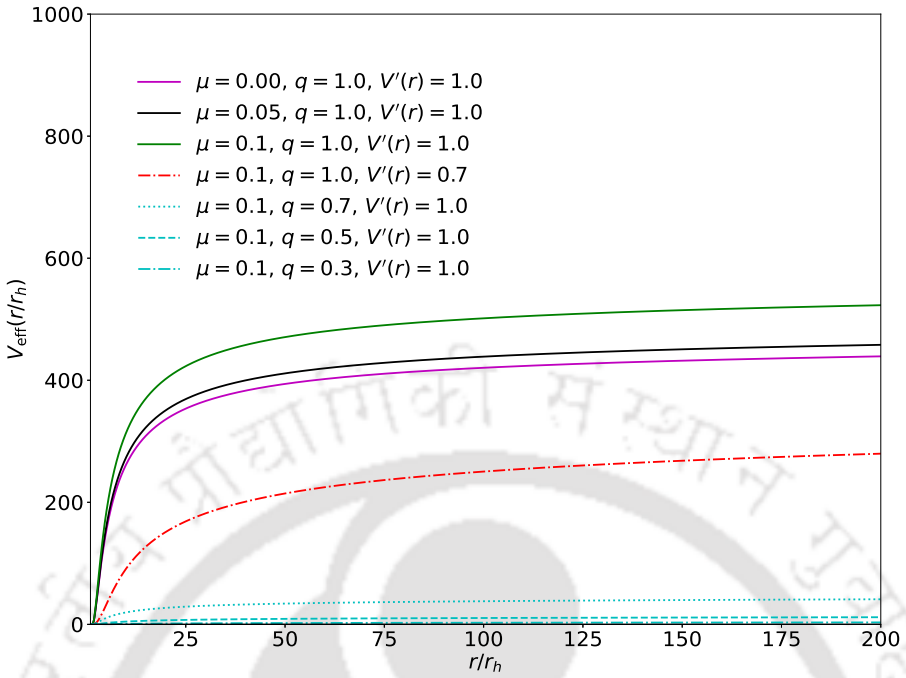

Figure 5.9: Radial profiles of the effective potential $V_{\rm eff}(r)$ with horizon values $\psi(r_h) = 0.5$ and $V'(r_h) = 1.0$, making different choices for the scalar hair parameters q and μ.

where the effective potential $V_{\rm eff}$ is defined as

$$V_{\rm eff} = \frac{fe^{-\eta}}{r}\left(fe^{-\eta}\right)' + \mu^2 fe^{-2\eta} + 3q^2V^2 - 2rfe^{-2\eta}f'\psi'^2 - 2f^2e^{-2\eta}\psi'^2 + 4\mu^2 rfe^{-2\eta}\psi'\psi - 2r^2f^2e^{-2\eta}\psi'^4 - 2r^2q^2V^2\psi^2\psi'^2. \tag{5.38}$$

Left-multiplying Equation (5.37) with the conjugate $\bar{\xi}$ and integrating from the horizon ($-\infty$ in the tortoise coordinate) to infinity, we obtain

$$-\left[\bar{\xi}\frac{d\xi}{dr^*}\right]_{-\infty}^{\infty} + \int_{-\infty}^{\infty} dr^* \left[\left|\frac{d\xi}{dr^*}\right|^2 + V_{\rm eff}\left|\xi\right|^2\right] = \Omega^2 \int_{-\infty}^{\infty} dr^* \left|\xi\right|^2. \tag{5.39}$$

The first term on the left hand side vanishes upon imposing the boundary conditions $\bar{\xi} \to 0$ as $r^* \to \pm\infty$. This leads to

$$\int_{-\infty}^{\infty} dr^* \left[\left|\frac{d\xi}{dr^*}\right|^2 + V_{\rm eff}\left|\xi\right|^2\right] = \Omega^2 \int_{-\infty}^{\infty} dr^* \left|\xi\right|^2. \tag{5.40}$$

It is evident from Equation (5.40) that if the profile of $V_{\rm eff}$ stays always positive, we

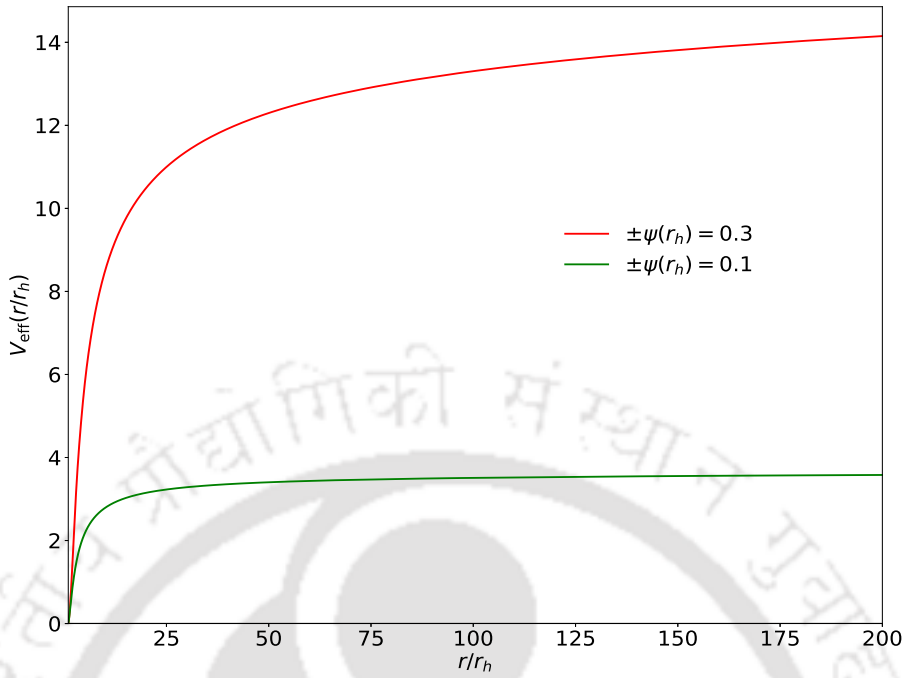

Figure 5.10: Radial profiles of the effective potential $V_{\text{eff}}(r)$ with pair-wise positive and negative horizon values of $\psi(r_h)$, all having $V'(r_h) = 1.0$, with scalar hair parameters, $q = 1.0$ and $\mu = 0.1$.

must have $\Omega^2 > 0$. This follows from the fact that all remaining quantities in (5.40) are positive. On the other hand, if V_{eff} is negative in some regions, Ω^2 can either be positive or negative depending upon whether the contributions from the negative regions are sufficiently small or sufficiently large, respectively.

We therefore plot $V_{\text{eff}}(r)$ with different values for the parameters q and μ. Figure 5.9 shows the profiles of $V_{\text{eff}}(r)$ with the horizon condition $\psi(r_h) = 0.5$. Moreover, Figure 5.10 shows the profiles of $V_{\text{eff}}(r)$ for pair-wise positive and negative values of $\psi(r_h)$, each with $q = 1.0$ and $\mu = 0.1$. Interestingly, the curves for every pair overlap exactly, implying that the stability of the solution is unaffected by flipping the phase of $\psi(r)$ at the horizon.

Remarkably, all these profiles of $V_{\text{eff}}(r)$ are positive everywhere, and therefore they imply that $\Omega^2 > 0$, so that the corresponding hairy solutions are stable. This is consistent with our previous stability analysis based on the Sturm-Liouville equation.

5.6 Discussion and conclusion

As we have noted, the no-hair theorem forbids any property other than mass, charge and angular momentum to parametrize a black hole. In this regard, investigations on the possibility of existence of a scalar hair surrounding the black hole was first considered by

Bekenstein [25, 26] with a scalar field conformally coupled to the geometry of a charged black hole. In addition, as discussed earlier, Mayo and Bekenstein [134] considered the possibility of having hairy solutions with both electrically neutral and charged scalar fields having conformal coupling with the gravitational field of a charged black hole.

Subsequently, although charged hairy solutions were obtained in Mayo and Bekenstein's model with polynomial scalar potential of sixth degree and the scalar charge much smaller than the black hole charge, a natural question arises as to whether a charged scalar hair would *exist* if the scalar field is taken to be a charged massive Klein-Gordon field (with quadratic potential) without any limitation on its charge.

We note that the *existence* of a hairy solution can be established if the following two conditions are satisfied: (i) the necessary condition of meeting all relevant energy conditions supplemented with the causality condition, and (ii) the sufficient condition that the hairy solution is *stable* against time dependant perturbations.

In this context, we considered in this chapter the Einstein-Maxwell-charged scalar field model with a spherically symmetric charged scalar field electromagnetically coupled to a charged black hole. The electromagnetic coupling naturally follows from gauge coupling (via covariant derivative) of the charged scalar field. We also considered both massless and massive cases of the charged scalar field.

In this Einstein-Maxwell-charged scalar framework, we found that the Einstein field equations, Maxwell's equations, and the Klein-Gorden equation are substantially modified by acquiring additional terms coming from the charged scalar field. These equations form a coupled set of nonlinear differential equations.

Before proceeding any further, it was important to ascertain whether the necessary condition (i) of all relevant energy conditions supplemented by the causality condition are obeyed by the Einstein-Maxwell-charged scalar field model. We therefore considered all energy conditions following from the mixed components of the energy-momentum tensor and the causality condition. Upon expressing the mixed components of the energy-momentum tensor in terms of the scalar field and other quantities, we found that all energy conditions coupled with the causality condition are satisfied. This suggests the possibility of existence of a charged hairy solution.

Thus our next task was to find charged hairy solutions from the field equations. Since the field equations consist of a set of *nonlinear* coupled differential equations, any analytical attempt to solve them was not possible. Consequently, we solved the field equations by exact numerical integration, with appropriate boundary conditions at the horizon, and with different values of the electric charge q and mass μ of the scalar field.

Our numerical integration showed oscillatory solutions for the scalar field which damps

out with the radial distance. We also studied the behaviour of the charge density $\rho(r)$ of the scalar hair. We found that its radial profile makes a series of bounces with heights falling off rapidly with the radial coordinate. This structure indicates that the scalar charge is distributed in concentric shells around the black hole. The rapid falloff of the charge density indicates that there would be practically no measurable charge at a large distance from the black hole.

Our solutions further indicate that the electric potential $V(r)$ surrounding the black hole is a monotonic function of the radial distance r. This behaviour is consistent with the requirement from the Maxwell's equation.

Furthermore, the electric potential can take highly enhanced values compared to the normal Reissner-Nordström case without a hair. This is due to additional contribution to the electric potential coming from the charged scalar hair in addition to that from the charged black hole.

Although we obtained the charged hairy solutions by exact numerical integration, their existence can be confirmed only by stability analysis with respect to time dependant perturbations about the static hairy solutions. Consequently, we carried out dynamical stability analyses by perturbing the static solution with a sinusoidal perturbation. For definiteness in the result, we employed two different methodologies of stability analyses.

In the first methodology, we obtained the minimum frequency of the eigenmodes of the Sturm-Liouville equation for the dynamics of the radial perturbation. We found that the minimum eigen frequency turns out to be real-valued for our solutions, indicating their stability.

In the second methodology, we confirmed the above stability analysis. We converted the dynamical equation of the perturbation into a Schrödinger-like equation with an effective potential determined by the static hairy solution. An analysis of this Schrödinger equation indicated that the eigen frequency will be real-valued, giving stability of the solution, provided the effective potential remains positive everywhere. Upon plotting the effective potential using our different static solutions, we found that the effective potential remains positive everywhere, indicating real valuedness of all eigen frequencies for the static solutions. This confirms our previous stability analysis based on the determination of minimum eigen frequency of the Sturm-Liouville equation.

We note in passing that in references [97, 102, 103] the potential of the scalar field was considered to be a polynomial of degree 6, with only even powers of ϕ, having the form $V(\phi) = a\phi^2 - b\phi^4 + c\phi^6$. On the other hand, the potential in the present work is only quadratic, that is $V(\phi) = a\phi^2$. This difference in the forms of the potentials makes a crucial change in the solutions. In references [97, 102, 103], a non-oscillatory decaying

solution was obtained in the polynomial model for the potential with specific choices for the parameters. On the other hand, we obtained a decaying oscillatory solution for the scalar hair with the quadratic potential. In addition, we confirmed the stability of our decaying oscillatory solutions.

The fact that all energy conditions coupled with the causality condition are satisfied, in addition to satisfying the condition of stability of the static hairy solutions with respect to dynamical perturbations, suggest that a Reissner-Nordström black hole can be surrounded by a stable and electrically charged scalar hair with quadratic scalar potential.

In this context, we note that our theory considers *static* hairy solutions and confirms their stability while it does not include the dynamics of how such hairy solutions form around the black hole. It is well-known that a Reissner-Nordström black hole may undergo the phenomenon of superradiance instability due to scattering of incident charged particles, giving rise to outgoing charges if the condition of superradiance is fulfilled [24]. However, for an asymptotically flat Reissner-Nordström spacetime, the necessary conditions required to trigger a possible superradiance instability cannot be satisfied [100, 101]. Thus the origin of charged scalar hair in our model does not lie in the phenomenon of superradiance instability and it remains a matter of exploration in the future.

Chapter 6

Conclusion

This thesis explored the structure and properties of compact objects in strong gravity regimes, focusing on neutron stars and black holes in both general relativity and two classes of modified gravity theories: Starobinsky gravity and Eddington-inspired Born-Infeld (EiBI) gravity. The investigations were based on numerical and analytical methods applied to physically motivated models, primarily involving realistic and hybrid equations of state (EOSs) for dense nuclear matter and scalar fields coupled to black hole spacetimes.

In Chapter 2, we studied the internal structure and maximum stable mass of neutron stars within the framework of general relativity, employing a range of unified and hybrid EOSs. It was shown that some unified EOSs, such as BSk21, can support neutron star masses up to or slightly below $2\,M_\odot$, but others like BSk19 and BSk20 violate causality at high densities. The analysis revealed that the central densities for maximal mass configurations often exceed $10\,\rho_{\rm nuc}$, where $\rho_{\rm nuc} = 2.67 \times 10^{14}$ g/cm^3, suggesting the presence of deconfined quark matter in the core. This motivated the construction of hybrid EOSs that combine the MIT bag model for the core with hadronic EOSs for the outer layers.

Among these combinations, the MIT-BSk21 model provided a maximal mass closest to $2\,M_\odot$ while satisfying the causality condition. It was also found that the contribution to the total mass of the star is largely determined by the radial location of the peak in ρr^2, with the MIT-BSk21 combination shifting this peak farther from the center—resulting in a higher total mass. These results are consistent with recent high-mass pulsar observations, including PSR J0952-0607 ($2.35 \pm 0.17\,M_\odot$), when rotational corrections are taken into account. The findings emphasize the importance of realistic modeling of both deconfined and hadronic matter, particularly in regions where the phase transition between the two is expected to occur. A robust understanding of this transition, likely governed by QCD, remains a crucial challenge for future work.

In Chapter 3, we extended our analysis of neutron stars to the context of Starobinsky gravity, characterized by a modified gravitational Lagrangian of the form $f(R) = R + \alpha R^2$. The inclusion of the quadratic curvature term introduces a scalar degree of freedom—known as the scalaron—that modifies the standard TOV equations and changes the internal and external structure of the neutron star. Numerical integration of the modified TOV equations showed that the maximum stable mass $M_{\max}$ increases with increasing α, thereby enhancing the gravitational support against collapse. For the MIT-BSk21 EOS, a mass of $2.07\,M_\odot$ was achieved for $\alpha = 10\,r_g^2$, consistent with the measured mass of MSP J0740+6620.

One of the key features distinguishing Starobinsky gravity from general relativity is the extended non-zero Ricci scalar profile outside the star, which decays slowly over tens of kilometers due to the influence of the scalaron field. Similarly, the mass profile continues to increase beyond the stellar surface, indicating that the ADM mass is only reached at large distances. Despite these modifications, fundamental properties such as the monotonic increase of mass with central density and the mass-radius relationship are preserved, demonstrating the physical viability of the model. These deviations from general relativity may lead to observational signatures, potentially detectable through gravitational waves of neutron star mergers, offering a means of testing such modified theories.

In Chapter 4, we investigated charged black hole spacetimes in EiBI gravity—a theory that modifies the Eddington's determinant-based action inspired by Born-Infeld electrodynamics. Working within the Palatini formalism, we derived the field equations for a charged black hole and analyzed their behavior in various asymptotic regimes. Through a combination of analytical and numerical methods, we examined the radial dependence of the metric functions and the Kretschmann curvature invariant.

Our results revealed a complex structure of spacetime near the center, highly sensitive to the sign and magnitude of the EiBI coupling parameter κ. For $\kappa > 0$, the geometry exhibits singular behavior at a critical radius $r = a = (\kappa Q^2)^{1/4}$, while for $\kappa < 0$, the spacetime metric develops imaginary parts, rendering it unphysical near the center. At large distances, the solutions asymptotically approach the familiar Reissner-Nordström form. Importantly, curvature invariants remain finite near the event horizon, suggesting regular horizon structure despite the presence of non-linear corrections. The analytical predictions matched closely with our numerical solutions, establishing the reliability of the asymptotic analysis. This study enhances our understanding of non-linear gravity effects in black hole spacetimes and provides a foundation for further exploration of EiBI gravity in astrophysical settings.

In Chapter 5, we turned our attention to the existence and stability of charged scalar

hair around Reissner-Nordström black holes. Motivated by earlier works by Bekenstein and Mayo, we extended the analysis to include a massive and electrically charged scalar field governed by the Klein-Gordon equation with a quadratic potential. The scalar field is minimally coupled to both gravity and electromagnetism, leading to a set of coupled, nonlinear field equations.

We established the necessary condition for the existence of scalar hair by verifying that the energy-momentum tensor satisfies all energy conditions and the causality condition. Numerical integration of the field equations, with appropriate boundary conditions, yielded damped oscillatory solutions for the scalar field, indicating that the scalar charge is distributed in concentric shells around the black hole. The associated charge density falls off rapidly with distance, and the electric potential is enhanced compared to the standard Reissner-Nordström solution—due to additional contributions from the charged scalar hair.

To further confirm the existence of the hairy solution, we performed a thorough dynamical stability analysis using two distinct methods. First, we solved the Sturm-Liouville eigenvalue problem and showed that the lowest eigenfrequency is real. Second, we cast the perturbation equation into a Schrödinger-like form and demonstrated that the effective potential remains positive for all radial coordinates, ensuring real eigenfrequencies and hence stability. These analyses conclusively demonstrated that the hairy solutions obtained are not only mathematically valid but also physically stable.

Unlike earlier models that relied on a sixth-degree scalar potential, our model uses only a quadratic potential. This leads to distinct qualitative differences in the solutions: whereas previous works obtained non-oscillatory decaying profiles, we observed decaying oscillatory behavior, which we confirmed to be stable. The existence of such charged scalar hair does not result from superradiant instabilities, which are absent in asymptotically flat Reissner-Nordström spacetimes. The origin of these configurations remains an open question for future investigation.

The wide variety of results obtained in this thesis demonstrate the richness and complexity of compact object physics when viewed through the lens of both general relativity and modified gravity theories. The study of neutron stars highlights the importance of accurate modeling of dense matter EOSs, particularly with respect to causality and phase transitions. The exploration of modified gravity theories like Starobinsky and EiBI gravity shows how theoretical extensions can accommodate observational constraints while introducing new, potentially observable phenomena.

The investigation of scalar hair in black holes contributes to the ongoing effort to test the limits of the no-hair theorem and expands our understanding of black hole structure

and stability. Altogether, the findings offer multiple pathways for connecting high-energy physics, astrophysics, and gravitation, and they open promising avenues for future work in gravitational theory and observational astrophysics.

Several promising avenues for future research arise naturally from the findings in this thesis:

- *Continuous Phase Transition Modeling*: Extend the hybrid neutron star models to include realistic, continuous quark-hadron phase transitions. Incorporating QCD-based or effective field theory models could improve the physical fidelity of the EOS.

- *Rotating Compact Objects*: Incorporate rotation into neutron star and black hole models, especially in modified gravity. Rapid rotation significantly affects the mass-radius relation and stability criteria, and is relevant for many observed pulsars.

- *Gravitational Wave Phenomenology*: Investigate how the presence of extended scalar curvature profiles in Starobinsky gravity, or non-trivial matter distributions in EiBI gravity, may leave observable imprints on gravitational wave signals from neutron star mergers or black hole ringdowns.

- *Dynamical Formation of Scalar Hair*: Explore time-dependent simulations of scalar field accretion or collapse in the Einstein-Maxwell-scalar system to understand how charged hairy black holes may dynamically form in astrophysical settings.

- *Scalarized Black Holes in EiBI Gravity*: A particularly intriguing direction is to study the spontaneous scalarization of black holes in EiBI gravity. Just as scalarized solutions have been found in scalar-Gauss-Bonnet and scalar-tensor theories, it is natural to ask whether EiBI gravity—due to its nonlinear curvature structure—admits dynamically stable scalarized black hole solutions, possibly even without requiring a scalar potential. This may lead to new classes of solutions and novel observational signatures.

- *Constraints from Observations*: Use observational data from missions like NICER, and gravitational wave detectors (LIGO/Virgo/KAGRA), to constrain the parameters α (in Starobinsky gravity), κ (in EiBI gravity), or the scalar field couplings in hairy black hole scenarios.

- *Extensions to Other Modified Theories*: Generalize the analysis to other modified gravity theories such as Horndeski, beyond Horndeski, or $f(R, T)$ theories, where additional scalar degrees of freedom may couple to matter or curvature in non-trivial ways.

Bibliography

[1] B. P. Abbott et al. Observation of gravitational waves from a binary black hole merger. *Phys. Rev. Lett.*, 116:061102, Feb 2016. URL: https://link.aps.org/doi/10.1103/PhysRevLett.116.061102, doi:10.1103/PhysRevLett.116.061102.

[2] B. P. Abbott et al. GW170817: Observation of gravitational waves from a binary neutron star inspiral. *Phys. Rev. Lett.*, 119:161101, Oct 2017. URL: https://link.aps.org/doi/10.1103/PhysRevLett.119.161101, doi:10.1103/PhysRevLett.119.161101.

[3] B. P. Abbott et al. Properties of the binary neutron star merger GW170817. *Phys. Rev. X*, 9:011001, Jan 2019. URL: https://link.aps.org/doi/10.1103/PhysRevX.9.011001, doi:10.1103/PhysRevX.9.011001.

[4] B. P. Abbott et al. GW190425: Observation of a compact binary coalescence with total mass $\sim$ 3.4 m$\odot$. *The Astrophysical Journal Letters*, 892(1):L3, mar 2020. doi:10.3847/2041-8213/ab75f5.

[5] B. P. Abbott et al. GW190814: Gravitational waves from the coalescence of a 23 solar mass black hole with a 2.6 solar mass compact object. *The Astrophysical Journal Letters*, 896(2):L44, jun 2020. doi:10.3847/2041-8213/ab960f.

[6] E.G. Adelberger, B.R. Heckel, and A.E. Nelson. Tests of the gravitational inverse-square law. *Annual Review of Nuclear and Particle Science*, 53(Volume 53, 2003):77–121, 2003. URL: https://www.annualreviews.org/content/journals/10.1146/annurev.nucl.53.041002.110503, doi:10.1146/annurev.nucl.53.041002.110503.

[7] A. Akmal, V. R. Pandharipande, and D. G. Ravenhall. Equation of state of nucleon matter and neutron star structure. *Phys. Rev. C*, 58:1804–1828, Sep 1998. URL: https://link.aps.org/doi/10.1103/PhysRevC.58.1804, doi:10.1103/PhysRevC.58.1804.

[8] S. Alexeyev, A. Barrau, and K. A. Rannu. Internal structure of a maxwell-gauss-bonnet black hole. *Phys. Rev. D*, 79:067503, Mar 2009. URL: https://link.aps.org/doi/10.1103/PhysRevD.79.067503, doi:10.1103/PhysRevD.79.067503.

[9] John Antoniadis et al. A massive pulsar in a compact relativistic binary. *Science*, 340:448, Apr 2013. eprint: arXiv:1304.6875. URL: https://ui.adsabs.harvard.edu/

abs/2013Sci...340..448A, doi:10.1126/science.1233232.

[10] Savaş Arapoğlu, Cemsinan Deliduman, and K. Yavuz Ekşi. Constraints on perturbativef(r) gravity via neutron stars. *Journal of Cosmology and Astroparticle Physics*, 2011(07):020–020, jul 2011. URL: https://doi.org/10.1088%2F1475-7516%2F2011%2F07%2F020, doi:10.1088/1475-7516/2011/07/020.

[11] Artyom V Astashenok, Sergei D Odintsov, and Álvaro de la Cruz-Dombriz. The realistic models of relativistic stars in $f(R) = R + \alpha R^2$ gravity. *Classical and Quantum Gravity*, 34(20):205008, sep 2017. URL: https://doi.org/10.1088%2F1361-6382%2Faa8971, doi:10.1088/1361-6382/aa8971.

[12] D. Astefanesei, C. Herdeiro, A. Pombo, and E. Radu. Einstein-maxwell-scalar black holes: classes of solutions, dyons and extremality. *Journal of High Energy Physics*, 2019(10):78, Oct 2019. doi:10.1007/JHEP10(2019)078.

[13] P. P. Avelino. Inner structure of black holes in eddington-inspired born-infeld gravity: The role of mass inflation. *Phys. Rev. D*, 93:044067, Feb 2016. URL: https://link.aps.org/doi/10.1103/PhysRevD.93.044067, doi:10.1103/PhysRevD.93.044067.

[14] P. P. Avelino and R. Z. Ferreira. Bouncing eddington-inspired born-infeld cosmologies: An alternative to inflation? *Phys. Rev. D*, 86:041501, Aug 2012. URL: https://link.aps.org/doi/10.1103/PhysRevD.86.041501, doi:10.1103/PhysRevD.86.041501.

[15] Dimitry Ayzenberg, Kent Yagi, and Nicolás Yunes. Linear stability analysis of dynamical quadratic gravity. *Phys. Rev. D*, 89:044023, Feb 2014. URL: https://link.aps.org/doi/10.1103/PhysRevD.89.044023, doi:10.1103/PhysRevD.89.044023.

[16] Máximo Bañados and Pedro G. Ferreira. Eddington's theory of gravity and its progeny. *Phys. Rev. Lett.*, 105:011101, Jul 2010. URL: https://link.aps.org/doi/10.1103/PhysRevLett.105.011101, doi:10.1103/PhysRevLett.105.011101.

[17] E. Babichev and D. Langlois. Relativistic stars in $f(r)$ gravity. *Phys. Rev. D*, 80:121501, Dec 2009. URL: https://link.aps.org/doi/10.1103/PhysRevD.80.121501, doi:10.1103/PhysRevD.80.121501.

[18] D. C. Backer, Shrinivas R. Kulkarni, Carl Heiles, M. M. Davis, and W. M. Goss. A millisecond pulsar. *Nature*, 300(5893):615–618, Dec 1982. doi:10.1038/300615a0.

[19] James M. Bardeen, Kip S. Thorne, and David W. Meltzer. A catalogue of methods for studying the normal modes of radial pulsation of general-relativistic stellar models. *Astrophysical Journal*, 145:505, Aug 1966. doi:10.1086/148791.

[20] Yannis Bardoux, Marco M. Caldarelli, and Christos Charmousis. Conformally coupled scalar black holes admit a flat horizon due to axionic charge. *Journal of High Energy Physics*, 2012(9):8, Sep 2012. doi:10.1007/JHEP09(2012)008.

[21] Gordon Baym, Tetsuo Hatsuda, Toru Kojo, Philip D Powell, Yifan Song, and Tat-

suyuki Takatsuka. From hadrons to quarks in neutron stars: a review. *Reports on Progress in Physics*, 81(5):056902, mar 2018. URL: https://dx.doi.org/10.1088/1361-6633/aaae14, doi:10.1088/1361-6633/aaae14.

[22] Jacob D. Bekenstein. Nonexistence of baryon number for static black holes. *Phys. Rev. D*, 5:1239–1246, Mar 1972. URL: https://link.aps.org/doi/10.1103/PhysRevD.5.1239, doi:10.1103/PhysRevD.5.1239.

[23] Jacob D. Bekenstein. Transcendence of the law of baryon-number conservation in black-hole physics. *Phys. Rev. Lett.*, 28:452–455, Feb 1972. URL: https://link.aps.org/doi/10.1103/PhysRevLett.28.452, doi:10.1103/PhysRevLett.28.452.

[24] Jacob D. Bekenstein. Extraction of energy and charge from a black hole. *Phys. Rev. D*, 7:949–953, Feb 1973. URL: https://link.aps.org/doi/10.1103/PhysRevD.7.949, doi:10.1103/PhysRevD.7.949.

[25] Jacob D. Bekenstein. Exact solutions of einstein-conformal scalar equations. *Annals of Physics*, 82(2):535–547, 1974. URL: https://www.sciencedirect.com/science/article/pii/0003491674901249, doi:10.1016/0003-4916(74)90124-9.

[26] Jacob D Bekenstein. Black holes with scalar charge. *Annals of Physics*, 91(1):75–82, 1975. URL: https://www.sciencedirect.com/science/article/pii/0003491675902791, doi:10.1016/0003-4916(75)90279-1.

[27] Jacob D. Bekenstein. Novel "no-scalar-hair" theorem for black holes. *Phys. Rev. D*, 51:R6608–R6611, Jun 1995. URL: https://link.aps.org/doi/10.1103/PhysRevD.51.R6608, doi:10.1103/PhysRevD.51.R6608.

[28] Peter G. Bergmann. Comments on the scalar-tensor theory. *International Journal of Theoretical Physics*, 1(1):25–36, May 1968. doi:10.1007/BF00668828.

[29] Sourav Bhattacharya and Sumanta Chakraborty. Constraining some horndeski gravity theories. *Phys. Rev. D*, 95:044037, Feb 2017. URL: https://link.aps.org/doi/10.1103/PhysRevD.95.044037, doi:10.1103/PhysRevD.95.044037.

[30] N. D. Birrell and P. C. W. Davies. *Quantum Fields in Curved Space*. Cambridge Monographs on Mathematical Physics. Cambridge University Press, Cambridge, UK, 1982. doi:10.1017/CBO9780511622632.

[31] Jose Luis Blázquez-Salcedo, Caio F. B. Macedo, Vitor Cardoso, Valeria Ferrari, Leonardo Gualtieri, Fech Scen Khoo, Jutta Kunz, and Paolo Pani. Perturbed black holes in einstein-dilaton-gauss-bonnet gravity: Stability, ringdown, and gravitational-wave emission. *Phys. Rev. D*, 94:104024, Nov 2016. URL: https://link.aps.org/doi/10.1103/PhysRevD.94.104024, doi:10.1103/PhysRevD.94.104024.

[32] Jose Luis Blázquez-Salcedo, Carlos A.R. Herdeiro, Jutta Kunz, Alexandre M. Pombo, and Eugen Radu. Einstein-maxwell-scalar black holes: The hot, the cold and the bald. *Physics Letters B*, 806:135493, 2020. URL: https://www.sciencedirect.com/science/article/pii/S0370269320302975, doi:

10.1016/j.physletb.2020.135493.

[33] J. Boguta and A.R. Bodmer. Relativistic calculation of nuclear matter and the nuclear surface. *Nuclear Physics A*, 292(3):413–428, 1977. URL: https://www.sciencedirect.com/science/article/pii/0375947477906261, doi:10.1016/0375-9474(77)90626-1.

[34] Max Born, L. Infeld, and Ralph Howard Fowler. Foundations of the new field theory. *Proceedings of the Royal Society of London. Series A, Containing Papers of a Mathematical and Physical Character*, 144(852):425–451, 1934. URL: https://royalsocietypublishing.org/doi/abs/10.1098/rspa.1934.0059, arXiv:https://royalsocietypublishing.org/doi/pdf/10.1098/rspa.1934.0059, doi:10.1098/rspa.1934.0059.

[35] Robert H. Boyer and Richard W. Lindquist. Maximal analytic extension of the kerr metric. *Journal of Mathematical Physics*, 8(2):265–281, 02 1967. doi:10.1063/1.1705193.

[36] C. Brans and R. H. Dicke. Mach's principle and a relativistic theory of gravitation. *Phys. Rev.*, 124:925–935, Nov 1961. URL: https://link.aps.org/doi/10.1103/PhysRev.124.925, doi:10.1103/PhysRev.124.925.

[37] Philippe Brax, Carsten van de Bruck, and Anne-Christine Davis. Swampland and screened modified gravity. *Phys. Rev. D*, 101:083514, Apr 2020. URL: https://link.aps.org/doi/10.1103/PhysRevD.101.083514, doi:10.1103/PhysRevD.101.083514.

[38] Yves Brihaye and Betti Hartmann. Critical phenomena of charged einstein–gauss–bonnet black holes with charged scalar hair. *Classical and Quantum Gravity*, 35(17):175008, jul 2018. URL: https://dx.doi.org/10.1088/1361-6382/aad389, doi:10.1088/1361-6382/aad389.

[39] Yves Brihaye and Betti Hartmann. Spontaneous scalarization of charged black holes at the approach to extremality. *Physics Letters B*, 792:244–250, 2019. URL: https://www.sciencedirect.com/science/article/pii/S0370269319302023, doi:10.1016/j.physletb.2019.03.043.

[40] Yves Brihaye, Carlos Herdeiro, and Eugen Radu. The scalarised schwarzschild-nut spacetime. *Physics Letters B*, 788:295–301, 2019. URL: https://www.sciencedirect.com/science/article/pii/S0370269318308621, doi:10.1016/j.physletb.2018.11.022.

[41] K. A. Bronnikov and A. V. Khodunov. Scalar field and gravitational instability. *General Relativity and Gravitation*, 11(1):13–18, Sep 1979. doi:10.1007/BF00756667.

[42] K.A. Bronnikov and Yu.N. Kireyev. Instability of black holes with scalar charge. *Physics Letters A*, 67(2):95–96, 1978. URL: https://www.sciencedirect.com/science/article/pii/0375960178900300, doi:10.1016/0375-9601(78)90030-0.

[43] I. L. Buchbinder, S. D. Odintsov, and I. L. Shapiro. *Effective Action in Quantum Gravity*. Routledge, 9 2017. doi:10.1201/9780203758922.

[44] H. A. Buchdahl. Non-linear lagrangians and cosmological theory. *Monthly Notices of the Royal Astronomical Society*, 150(1):1–8, 09 1970. arXiv:https://academic.oup.com/mnras/article-pdf/150/1/1/8075909/mnras150-0001.pdf, doi:10.1093/mnras/150.1.1.

[45] Bruce A. Campbell, M.J. Duncan, Nemanja Kaloper, and Keith A. Olive. Axion hair for kerr black holes. *Physics Letters B*, 251(1):34–38, 1990. URL: https://www.sciencedirect.com/science/article/pii/037026939090227W, doi:10.1016/0370-2693(90)90227-W.

[46] Bruce A. Campbell, Nemanja Kaloper, and Keith A. Olive. Axion hair for dyon black holes. *Physics Letters B*, 263(3):364–370, 1991. URL: https://www.sciencedirect.com/science/article/pii/0370269391904745, doi:10.1016/0370-2693(91)90474-5.

[47] SALVATORE CAPOZZIELLO. Curvature quintessence. *International Journal of Modern Physics D*, 11(04):483–491, 2002. arXiv:https://doi.org/10.1142/S0218271802002025, doi:10.1142/S0218271802002025.

[48] Salvatore Capozziello, Mariafelicia De Laurentis, Ruben Farinelli, and Sergei D. Odintsov. Mass-radius relation for neutron stars in $f(r)$ gravity. *Phys. Rev. D*, 93:023501, Jan 2016. URL: https://link.aps.org/doi/10.1103/PhysRevD.93.023501, doi:10.1103/PhysRevD.93.023501.

[49] B. Carter. Axisymmetric black hole has only two degrees of freedom. *Phys. Rev. Lett.*, 26:331–333, Feb 1971. URL: https://link.aps.org/doi/10.1103/PhysRevLett.26.331, doi:10.1103/PhysRevLett.26.331.

[50] E. Chabanat, P. Bonche, P. Haensel, J. Meyer, and R. Schaeffer. A skyrme parametrization from subnuclear to neutron star densities. *Nuclear Physics A*, 627(4):710–746, 1997. URL: https://www.sciencedirect.com/science/article/pii/S0375947497005964, doi:10.1016/S0375-9474(97)00596-4.

[51] E. Chabanat, P. Bonche, P. Haensel, J. Meyer, and R. Schaeffer. A skyrme parametrization from subnuclear to neutron star densities part ii. nuclei far from stabilities. *Nuclear Physics A*, 635(1):231–256, 1998. URL: https://www.sciencedirect.com/science/article/pii/S0375947498001808, doi:10.1016/S0375-9474(98)00180-8.

[52] S. Chandrasekhar. Dynamical instability of gaseous masses approaching the schwarzschild limit in general relativity. *Phys. Rev. Lett.*, 12:114–116, Jan 1964. URL: https://link.aps.org/doi/10.1103/PhysRevLett.12.114, doi:10.1103/PhysRevLett.12.114.

[53] S. Chandrasekhar and Robert F. Tooper. The dynamical instability of the white-dwarf configurations approaching the limiting mass. *Astrophysical Journal*, 139:1396, May 1964. doi:10.1086/147883.

[54] Subrahmanyan Chandrasekhar. *The mathematical theory of black holes*. Oxford, 1985.

[55] Che-Yu Chen and Pisin Chen. Quasinormal modes of massless scalar fields for

charged black holes in the palatini-type gravity. *Phys. Rev. D*, 98:044042, Aug 2018. URL: https://link.aps.org/doi/10.1103/PhysRevD.98.044042, doi:10.1103/PhysRevD.98.044042.

[56] Inyong Cho, Hyeong-Chan Kim, and Taeyoon Moon. Precursor of inflation. *Phys. Rev. Lett.*, 111:071301, Aug 2013. URL: https://link.aps.org/doi/10.1103/PhysRevLett.111.071301, doi:10.1103/PhysRevLett.111.071301.

[57] Inyong Cho and Naveen K. Singh. Scalar perturbation produced at the pre-inflationary stage in eddington-inspired born–infeld gravity. *The European Physical Journal C*, 75(6):240, Jun 2015. doi:10.1140/epjc/s10052-015-3458-x.

[58] Event Horizon Telescope Collaboration. First sagittarius a* event horizon telescope results. ii. eht and multiwavelength observations, data processing, and calibration. *The Astrophysical Journal Letters*, 930(2):L13, may 2022. URL: https://dx.doi.org/10.3847/2041-8213/ac6675, doi:10.3847/2041-8213/ac6675.

[59] Event Horizon Telescope Collaboration. First sagittarius a* event horizon telescope results. iii. imaging of the galactic center supermassive black hole. *The Astrophysical Journal Letters*, 930(2):L14, may 2022. URL: https://dx.doi.org/10.3847/2041-8213/ac6429, doi:10.3847/2041-8213/ac6429.

[60] Event Horizon Telescope Collaboration and Kazunori Akiyama et al. First sagittarius a* event horizon telescope results. i. the shadow of the supermassive black hole in the center of the milky way. *The Astrophysical Journal Letters*, 930(2):L12, may 2022. URL: https://dx.doi.org/10.3847/2041-8213/ac6674, doi:10.3847/2041-8213/ac6674.

[61] The Event Horizon Telescope Collaboration. First m87 event horizon telescope results. i. the shadow of the supermassive black hole. *The Astrophysical Journal Letters*, 875(1):L1, apr 2019. URL: https://dx.doi.org/10.3847/2041-8213/ab0ec7, doi:10.3847/2041-8213/ab0ec7.

[62] H. T. Cromartie, E. Fonseca, S. M. Ransom, P. B. Demorest, Z. Arzoumanian, H. Blumer, P. R. Brook, M. E. DeCesar, T. Dolch, J. A. Ellis, R. D. Ferdman, E. C. Ferrara, N. Garver-Daniels, P. A. Gentile, M. L. Jones, M. T. Lam, D. R. Lorimer, R. S. Lynch, M. A. McLaughlin, C. Ng, D. J. Nice, T. T. Pennucci, R. Spiewak, I. H. Stairs, K. Stovall, J. K. Swiggum, and W. W. Zhu. Relativistic shapiro delay measurements of an extremely massive millisecond pulsar. *Nature Astronomy*, 4(1):72–76, Jan 2020. doi:10.1038/s41550-019-0880-2.

[63] T. Damour and G. Esposito-Farese. Tensor-multi-scalar theories of gravitation. *Classical and Quantum Gravity*, 9(9):2093–2176, September 1992. doi:10.1088/0264-9381/9/9/015.

[64] H. Dapo, B.-J. Schaefer, and J. Wambach. Appearance of hyperons in neutron stars. *Phys. Rev. C*, 81:035803, Mar 2010. URL: https://link.aps.org/doi/10.1103/PhysRevC.81.035803, doi:10.1103/PhysRevC.81.035803.

[65] Antonio De Felice and Shinji Tsujikawa. f(r) theories. *Living Reviews in Relativity*, 13(1):3,

Jun 2010. doi:10.12942/lrr-2010-3.

[66] P. B. Demorest, T. Pennucci, S. M. Ransom, M. S. E. Roberts, and J. W. T. Hessels. A two-solar-mass neutron star measured using shapiro delay. *Nature*, 467:1081–1083, Oct 2010. eprint: arXiv:1010.5788. URL: https://ui.adsabs.harvard.edu/abs/2010Natur.467.1081D, doi:10.1038/nature09466.

[67] S Deser and G W Gibbons. Born - infeld - einstein actions? *Classical and Quantum Gravity*, 15(5):L35, may 1998. URL: https://dx.doi.org/10.1088/0264-9381/15/5/001, doi:10.1088/0264-9381/15/5/001.

[68] Daniela D. Doneva, Stella Kiorpelidi, Petya G. Nedkova, Eleftherios Papantonopoulos, and Stoytcho S. Yazadjiev. Charged gauss-bonnet black holes with curvature induced scalarization in the extended scalar-tensor theories. *Phys. Rev. D*, 98:104056, Nov 2018. URL: https://link.aps.org/doi/10.1103/PhysRevD.98.104056, doi:10.1103/PhysRevD.98.104056.

[69] C. Drischler, J.W. Holt, and C. Wellenhofer. Chiral effective field theory and the high-density nuclear equation of state. *Annual Review of Nuclear and Particle Science*, 71(1):null, 2021. arXiv:https://doi.org/10.1146/annurev-nucl-102419-041903, doi:10.1146/annurev-nucl-102419-041903.

[70] Xiao-Long Du, Ke Yang, Xin-He Meng, and Yu-Xiao Liu. Large scale structure formation in eddington-inspired born-infeld gravity. *Phys. Rev. D*, 90:044054, Aug 2014. URL: https://link.aps.org/doi/10.1103/PhysRevD.90.044054, doi:10.1103/PhysRevD.90.044054.

[71] F. W. Dyson, A. S. Eddington, and C. Davidson. A Determination of the Deflection of Light by the Sun's Gravitational Field, from Observations Made at the Total Eclipse of May 29, 1919. *Philosophical Transactions of the Royal Society of London Series A*, 220:291–333, January 1920. doi:10.1098/rsta.1920.0009.

[72] A.S. Eddington. *The Mathematical Theory of Relativity*. Cambridge University Press, 1923.

[73] A. Einstein. Erklarung der Perihelionbewegung der Merkur aus der allgemeinen Relativitatstheorie. *Sitzungsberichte der Königlich Preussischen Akademie der Wissenschaften*, 47:831–839, January 1915.

[74] Albert Einstein. Kosmologische Betrachtungen zur allgemeinen Relativitätstheorie. *Sitzungsberichte der Königlich Preussischen Akademie der Wissenschaften*, pages 142–152, January 1917.

[75] C. G. Bassa et al. Lofar discovery of the fastest-spinning millisecond pulsar in the galactic field. *The Astrophysical Journal Letters*, 846(2):L20, sep 2017. URL: https://dx.doi.org/10.3847/2041-8213/aa8400, doi:10.3847/2041-8213/aa8400.

[76] Emmanuel Fonseca et al. The NANOGrav nine-year data set: Mass and geometric measurements of binary millisecond pulsars. *The Astrophysical Journal*, 832(2):167, dec 2016. doi:10.3847/0004-637x/832/2/167.

[77] Edward Farhi and R. L. Jaffe. Strange matter. *Phys. Rev. D*, 30:2379–2390, Dec 1984. URL: https://link.aps.org/doi/10.1103/PhysRevD.30.2379, doi:10.1103/PhysRevD.30.2379.

[78] F. J. Fattoyev and J. Piekarewicz. Relativistic models of the neutron-star matter equation of state. *Phys. Rev. C*, 82:025805, Aug 2010. URL: https://link.aps.org/doi/10.1103/PhysRevC.82.025805, doi:10.1103/PhysRevC.82.025805.

[79] Pedro G S Fernandes, Carlos A R Herdeiro, Alexandre M Pombo, Eugen Radu, and Nicolas Sanchis-Gual. Spontaneous scalarisation of charged black holes: coupling dependence and dynamical features. *Classical and Quantum Gravity*, 36(13):134002, jun 2019. URL: https://dx.doi.org/10.1088/1361-6382/ab23a1, doi:10.1088/1361-6382/ab23a1.

[80] Pedro G S Fernandes, Carlos A R Herdeiro, Alexandre M Pombo, Eugen Radu, and Nicolas Sanchis-Gual. Spontaneous scalarisation of charged black holes: coupling dependence and dynamical features. *Classical and Quantum Gravity*, 36(13):134002, jun 2019. URL: https://dx.doi.org/10.1088/1361-6382/ab23a1, doi:10.1088/1361-6382/ab23a1.

[81] Pedro G.S. Fernandes. Einstein–maxwell-scalar black holes with massive and self-interacting scalar hair. *Physics of the Dark Universe*, 30:100716, 2020. URL: https://www.sciencedirect.com/science/article/pii/S2212686420304295, doi:10.1016/j.dark.2020.100716.

[82] B. Friedman and V.R. Pandharipande. Hot and cold, nuclear and neutron matter. *Nuclear Physics A*, 361(2):502–520, 1981. URL: https://www.sciencedirect.com/science/article/pii/0375947481906497, doi:10.1016/0375-9474(81)90649-7.

[83] John L. Friedman and James R. Ipser. On the Maximum Mass of a Uniformly Rotating Neutron Star. *Astrophysical Journal*, 314:594, March 1987. doi:10.1086/165088.

[84] Bengt Friman and Wolfram Weise. Neutron star matter as a relativistic fermi liquid. *Phys. Rev. C*, 100:065807, Dec 2019. URL: https://link.aps.org/doi/10.1103/PhysRevC.100.065807, doi:10.1103/PhysRevC.100.065807.

[85] Andrei V. Frolov. Singularity problem with $f(r)$ models for dark energy. *Phys. Rev. Lett.*, 101:061103, Aug 2008. URL: https://link.aps.org/doi/10.1103/PhysRevLett.101.061103, doi:10.1103/PhysRevLett.101.061103.

[86] Nihar Ranjan Ghosh and Malay K. Nandy. Nonlinear dynamics of the inner horizon in reissner-nordström black holes: insights into mass inflation. *The European Physical Journal Plus*, 140(7):680, Jul 2025. doi:10.1140/epjp/s13360-025-06620-6.

[87] Riccardo Giacconi, Herbert Gursky, Frank R. Paolini, and Bruno B. Rossi. Evidence for x rays from sources outside the solar system. *Phys. Rev. Lett.*, 9:439–443, Dec 1962. URL: https://link.aps.org/doi/10.1103/PhysRevLett.9.439, doi:10.1103/PhysRevLett.9.439.

[88] T. Gold. Rotating neutron stars as the origin of the pulsating radio sources. *Nature*,

218(5143):731–732, May 1968. doi:10.1038/218731a0.

[89] T Gold. Rotating neutron stars and the nature of pulsars. *Nature*, 221(5175):25–27, Jan 1969. doi:10.1038/221025a0.

[90] S. Goriely, N. Chamel, and J. M. Pearson. Further explorations of skyrme-hartree-fock-bogoliubov mass formulas. xii. stiffness and stability of neutron-star matter. *Phys. Rev. C*, 82:035804, Sep 2010. URL: https://link.aps.org/doi/10.1103/PhysRevC.82.035804, doi:10.1103/PhysRevC.82.035804.

[91] Haensel, P. and Potekhin, A. Y. Analytical representations of unified equations of state of neutron-star matter. *Astronomy and Astrophysics*, 428(1):191–197, 2004. doi:10.1051/0004-6361:20041722.

[92] Tiberiu Harko, Francisco S. N. Lobo, M. K. Mak, and Sergey V. Sushkov. Structure of neutron, quark, and exotic stars in eddington-inspired born-infeld gravity. *Phys. Rev. D*, 88:044032, Aug 2013. URL: https://link.aps.org/doi/10.1103/PhysRevD.88.044032, doi:10.1103/PhysRevD.88.044032.

[93] Tiberiu Harko, Francisco S. N. Lobo, Shin'ichi Nojiri, and Sergei D. Odintsov. $f(r,t)$ gravity. *Phys. Rev. D*, 84:024020, Jul 2011. URL: https://link.aps.org/doi/10.1103/PhysRevD.84.024020, doi:10.1103/PhysRevD.84.024020.

[94] S. W. Hawking. Black holes in general relativity. *Communications in Mathematical Physics*, 25(2):152–166, Jun 1972. doi:10.1007/BF01877517.

[95] S. W. Hawking. Breakdown of predictability in gravitational collapse. *Phys. Rev. D*, 14:2460–2473, Nov 1976. URL: https://link.aps.org/doi/10.1103/PhysRevD.14.2460, doi:10.1103/PhysRevD.14.2460.

[96] S. W. Hawking and G. F. R. Ellis. *The Large Scale Structure of Space-Time*. Cambridge Monographs on Mathematical Physics. Cambridge University Press, 1973.

[97] Carlos A. R. Herdeiro and Eugen Radu. Spherical electro-vacuum black holes with resonant, scalar q-hair. *The European Physical Journal C*, 80(5):390, May 2020. doi:10.1140/epjc/s10052-020-7976-9.

[98] Carlos A. R. Herdeiro, Eugen Radu, Nicolas Sanchis-Gual, and José A. Font. Spontaneous scalarization of charged black holes. *Phys. Rev. Lett.*, 121:101102, Sep 2018. URL: https://link.aps.org/doi/10.1103/PhysRevLett.121.101102, doi:10.1103/PhysRevLett.121.101102.

[99] A. Hewish, S. J. Bell, J. D. H. Pilkington, P. F. Scott, and R. A. Collins. Observation of a rapidly pulsating radio source. *Nature*, 217(5130):709–713, Feb 1968. doi:10.1038/217709a0.

[100] Shahar Hod. Stability of the extremal reissner–nordström black hole to charged scalar perturbations. *Physics Letters B*, 713(4):505–508, 2012. URL: https://www.sciencedirect.com/science/article/pii/S037026931200682X, doi:10.1016/j.physletb.2012.06.043.

[101] Shahar Hod. No-bomb theorem for charged reissner–nordström black holes. *Physics Letters B*, 718(4):1489–1492, 2013. URL: https://www.sciencedirect.

com/science/article/pii/S037026931201252X, doi:10.1016/j.physletb.2012.12.013.

[102] Jeong-Pyong Hong, Motoo Suzuki, and Masaki Yamada. Charged black holes in non-linear q-clouds with o(3) symmetry. *Physics Letters B*, 803:135324, 2020. URL: https://www.sciencedirect.com/science/article/pii/S0370269320301283, doi:10.1016/j.physletb.2020.135324.

[103] Jeong-Pyong Hong, Motoo Suzuki, and Masaki Yamada. Spherically symmetric scalar hair for charged black holes. *Phys. Rev. Lett.*, 125:111104, Sep 2020. URL: https://link.aps.org/doi/10.1103/PhysRevLett.125.111104, doi:10.1103/PhysRevLett.125.111104.

[104] Nadine Hornick, Laura Tolos, Andreas Zacchi, Jan-Erik Christian, and Jürgen Schaffner-Bielich. Relativistic parameterizations of neutron matter and implications for neutron stars. *Phys. Rev. C*, 98:065804, Dec 2018. URL: https://link.aps.org/doi/10.1103/PhysRevC.98.065804, doi:10.1103/PhysRevC.98.065804.

[105] R. A. Hulse and J. H. Taylor. Discovery of a pulsar in a binary system. *The Astrophysical Journal*, 195:L51–L53, Jan 1975. URL: https://ui.adsabs.harvard.edu/abs/1975ApJ...195L..51H, doi:10.1086/181708.

[106] Werner Israel. Event horizons in static vacuum space-times. *Phys. Rev.*, 164:1776–1779, Dec 1967. URL: https://link.aps.org/doi/10.1103/PhysRev.164.1776, doi:10.1103/PhysRev.164.1776.

[107] Werner Israel. Event horizons in static electrovac space-times. *Communications in Mathematical Physics*, 8(3):245–260, Sep 1968. doi:10.1007/BF01645859.

[108] Naoki Itoh. Hydrostatic Equilibrium of Hypothetical Quark Stars. *Progress of Theoretical Physics*, 44(1):291–292, 07 1970. arXiv:https://academic.oup.com/ptp/article-pdf/44/1/291/5357142/44-1-291.pdf, doi:10.1143/PTP.44.291.

[109] D. Ivanenko and D. F. Kurdgelaidze. Remarks on quark stars. *Lettere al Nuovo Cimento (1969-1970)*, 2(1):13–16, Jul 1969. doi:10.1007/BF02753988.

[110] R. L. Jaffe and F. E. Low. Connection between quark-model eigenstates and low-energy scattering. *Phys. Rev. D*, 19:2105–2118, Apr 1979. URL: https://link.aps.org/doi/10.1103/PhysRevD.19.2105, doi:10.1103/PhysRevD.19.2105.

[111] Soumya Jana, Rajibul Shaikh, and Sudipta Sarkar. Overcharging black holes and cosmic censorship in eddington-inspired born-infeld gravity. *Phys. Rev. D*, 98:124039, Dec 2018. URL: https://link.aps.org/doi/10.1103/PhysRevD.98.124039, doi:10.1103/PhysRevD.98.124039.

[112] P. Kanti, N. E. Mavromatos, J. Rizos, K. Tamvakis, and E. Winstanley. Dilatonic black holes in higher curvature string gravity. *Phys. Rev. D*, 54:5049–5058, Oct 1996. URL: https://link.aps.org/doi/10.1103/PhysRevD.54.5049, doi:10.1103/PhysRevD.54.5049.

[113] Roy P. Kerr. Gravitational field of a spinning mass as an example of alge-

braically special metrics. *Phys. Rev. Lett.*, 11:237–238, Sep 1963. URL: https://link.aps.org/doi/10.1103/PhysRevLett.11.237, doi:10.1103/PhysRevLett.11.237.

[114] Justin Khoury and Amanda Weltman. Chameleon cosmology. *Phys. Rev. D*, 69:044026, Feb 2004. URL: https://link.aps.org/doi/10.1103/PhysRevD.69.044026, doi:10.1103/PhysRevD.69.044026.

[115] Justin Khoury and Amanda Weltman. Chameleon fields: Awaiting surprises for tests of gravity in space. *Phys. Rev. Lett.*, 93:171104, Oct 2004. URL: https://link.aps.org/doi/10.1103/PhysRevLett.93.171104, doi:10.1103/PhysRevLett.93.171104.

[116] Hyeong-Chan Kim. Physics at the surface of a star in eddington-inspired born-infeld gravity. *Phys. Rev. D*, 89:064001, Mar 2014. URL: https://link.aps.org/doi/10.1103/PhysRevD.89.064001, doi:10.1103/PhysRevD.89.064001.

[117] Tsutomu Kobayashi and Kei-ichi Maeda. Relativistic stars in $f(r)$ gravity, and absence thereof. *Phys. Rev. D*, 78:064019, Sep 2008. URL: https://link.aps.org/doi/10.1103/PhysRevD.78.064019, doi:10.1103/PhysRevD.78.064019.

[118] Tsutomu Kobayashi and Kei-ichi Maeda. Can higher curvature corrections cure the singularity problem in $f(r)$ gravity? *Phys. Rev. D*, 79:024009, Jan 2009. URL: https://link.aps.org/doi/10.1103/PhysRevD.79.024009, doi:10.1103/PhysRevD.79.024009.

[119] Kojo, Toru. Phenomenological neutron star equations of state - 3-window modeling of qcd matter. *Eur. Phys. J. A*, 52(3):51, 2016. doi:10.1140/epja/i2016-16051-0.

[120] R. A. Konoplya and A. Zhidenko. Analytical representation for metrics of scalarized einstein-maxwell black holes and their shadows. *Phys. Rev. D*, 100:044015, Aug 2019. URL: https://link.aps.org/doi/10.1103/PhysRevD.100.044015, doi:10.1103/PhysRevD.100.044015.

[121] L.D. Landau and E.M. Lifshitz. Chapter 11 - the gravitational field equations. In *The Classical Theory of Fields (Fourth Edition)*, volume 2 of *Course of Theoretical Physics*, pages 259–294. Pergamon, Amsterdam, fourth edition edition, 1975. URL: https://www.sciencedirect.com/science/article/pii/B9780080250724500186, doi:10.1016/B978-0-08-025072-4.50018-6.

[122] L.D. Landau and E.M. Lifshitz. Chapter 4 - the electromagnetic field equations. In *The Classical Theory of Fields (Fourth Edition)*, volume 2 of *Course of Theoretical Physics*, pages 66–88. Pergamon, Amsterdam, fourth edition edition, 1975. URL: https://www.sciencedirect.com/science/article/pii/B9780080250724500113, doi:10.1016/B978-0-08-025072-4.50011-3.

[123] Lev Davidovich Landau. On the theory of stars. *Phys. Z. Sowjetunion*, 1(285):152, 1932.

[124] Bum-Hoon Lee, Wonwoo Lee, and Daeho Ro. Expanded evasion of the black hole no-hair theorem in dilatonic einstein-gauss-bonnet theory. *Phys. Rev. D*, 99:024002, Jan 2019. URL: https://link.aps.org/doi/10.1103/PhysRevD.99.024002, doi:

10.1103/PhysRevD.99.024002.

[125] Kimyeong Lee and Erick J. Weinberg. Charged black holes with scalar hair. *Phys. Rev. D*, 44:3159–3163, Nov 1991. URL: https://link.aps.org/doi/10.1103/PhysRevD.44.3159, doi:10.1103/PhysRevD.44.3159.

[126] Shou-Long Li and Hao Wei. Stability of the einstein static universe in eddington-inspired born-infeld theory. *Phys. Rev. D*, 96:023531, Jul 2017. URL: https://link.aps.org/doi/10.1103/PhysRevD.96.023531, doi:10.1103/PhysRevD.96.023531.

[127] Z. H. Li and H.-J. Schulze. Neutron star structure with modern nucleonic three-body forces. *Phys. Rev. C*, 78:028801, Aug 2008. URL: https://link.aps.org/doi/10.1103/PhysRevC.78.028801, doi:10.1103/PhysRevC.78.028801.

[128] M. Linares, T. Shahbaz, and J. Casares. Peering into the dark side: Magnesium lines establish a massive neutron star in PSR j2215+5135. *The Astrophysical Journal*, 859(1):54, may 2018. doi:10.3847/1538-4357/aabde6.

[129] Diego Lonardoni, Alessandro Lovato, Stefano Gandolfi, and Francesco Pederiva. Hyperon puzzle: Hints from quantum monte carlo calculations. *Phys. Rev. Lett.*, 114:092301, Mar 2015. URL: https://link.aps.org/doi/10.1103/PhysRevLett.114.092301, doi:10.1103/PhysRevLett.114.092301.

[130] Cristián Martínez and Ricardo Troncoso. Electrically charged black hole with scalar hair. *Phys. Rev. D*, 74:064007, Sep 2006. URL: https://link.aps.org/doi/10.1103/PhysRevD.74.064007, doi:10.1103/PhysRevD.74.064007.

[131] Cristián Martínez, Ricardo Troncoso, and Jorge Zanelli. de sitter black hole with a conformally coupled scalar field in four dimensions. *Phys. Rev. D*, 67:024008, Jan 2003. URL: https://link.aps.org/doi/10.1103/PhysRevD.67.024008, doi:10.1103/PhysRevD.67.024008.

[132] Cristián Martínez, Ricardo Troncoso, and Jorge Zanelli. Exact black hole solution with a minimally coupled scalar field. *Phys. Rev. D*, 70:084035, Oct 2004. URL: https://link.aps.org/doi/10.1103/PhysRevD.70.084035, doi:10.1103/PhysRevD.70.084035.

[133] Cristián Martínez and Jorge Zanelli. Conformally dressed black hole in 2 + 1 dimensions. *Phys. Rev. D*, 54:3830–3833, Sep 1996. URL: https://link.aps.org/doi/10.1103/PhysRevD.54.3830, doi:10.1103/PhysRevD.54.3830.

[134] Avraham E. Mayo and Jacob D. Bekenstein. No hair for spherical black holes: Charged and nonminimally coupled scalar field with self-interaction. *Phys. Rev. D*, 54:5059–5069, Oct 1996. URL: https://link.aps.org/doi/10.1103/PhysRevD.54.5059, doi:10.1103/PhysRevD.54.5059.

[135] Charles W. Misner, K. S. Thorne, and J. A. Wheeler. *Gravitation*. W. H. Freeman, San Francisco, 1973.

[136] D. Mroczek, M. C. Miller, J. Noronha-Hostler, and N. Yunes. Nontrivial features in the speed of sound inside neutron stars. *Phys. Rev. D*, 110:123009, Dec 2024. URL:

https://link.aps.org/doi/10.1103/PhysRevD.110.123009, doi:10.1103/PhysRevD.110.123009.

[137] Yun Soo Myung and De-Cheng Zou. Stability of scalarized charged black holes in the einstein–maxwell–scalar theory. *The European Physical Journal C*, 79(8):641, Aug 2019. doi:10.1140/epjc/s10052-019-7176-7.

[138] Horst Müller and Brian D. Serot. Relativistic mean-field theory and the high-density nuclear equation of state. *Nuclear Physics A*, 606(3):508–537, 1996. URL: https://www.sciencedirect.com/science/article/pii/037594749600187X, doi:10.1016/0375-9474(96)00187-X.

[139] G. Nordström. On the Energy of the Gravitation field in Einstein's Theory. *Koninklijke Nederlandse Akademie van Wetenschappen Proceedings Series B Physical Sciences*, 20:1238–1245, January 1918.

[140] Jr. Nordtvedt, Kenneth. Post-Newtonian Metric for a General Class of Scalar-Tensor Gravitational Theories and Observational Consequences. *The Astrophysical Journal*, 161:1059, September 1970. doi:10.1086/150607.

[141] ID Novikov. Change of relativistic collapse into anticollapse and kinematics of a charged sphere. *JETP Lett.(USSR)(Engl. Transl.)*, 3, 1966.

[142] Gonzalo J. Olmo, Diego Rubiera-Garcia, and Aneta Wojnar. Stellar structure models in modified theories of gravity: Lessons and challenges. *Physics Reports*, 876:1–75, 2020. Stellar structure models in modified theories of gravity: Lessons and challenges. URL: https://www.sciencedirect.com/science/article/pii/S0370157320302507, doi:10.1016/j.physrep.2020.07.001.

[143] J. R. Oppenheimer and G. M. Volkoff. On massive neutron cores. *Phys. Rev.*, 55:374–381, Feb 1939. URL: https://link.aps.org/doi/10.1103/PhysRev.55.374, doi:10.1103/PhysRev.55.374.

[144] M. Orellana, F. García, F. A. Teppa Pannia, and G. E. Romero. Structure of neutron stars in R-squared gravity. *General Relativity and Gravitation*, 45(4):771–783, Apr 2013. doi:10.1007/s10714-013-1501-5.

[145] Attilio Palatini. Deduzione invariantiva delle equazioni gravitazionali dal principio di hamilton. *Rendiconti del Circolo Matematico di Palermo (1884-1940)*, 43(1):203–212, Dec 1919. doi:10.1007/BF03014670.

[146] V. R. Pandharipande and D. G. Ravenhall. *Hot Nuclear Matter*, pages 103–132. Springer US, Boston, MA, 1989. doi:10.1007/978-1-4684-5715-5_4.

[147] Paolo Pani, Vitor Cardoso, and Térence Delsate. Compact stars in eddington inspired gravity. *Phys. Rev. Lett.*, 107:031101, Jul 2011. URL: https://link.aps.org/doi/10.1103/PhysRevLett.107.031101, doi:10.1103/PhysRevLett.107.031101.

[148] Paolo Pani, Térence Delsate, and Vitor Cardoso. Eddington-inspired born-infeld gravity: Phenomenology of nonlinear gravity-matter coupling. *Phys. Rev. D*, 85:084020, Apr 2012. URL: https://link.aps.org/doi/10.1103/PhysRevD.85.084020, doi:

10.1103/PhysRevD.85.084020.

[149] Paolo Pani and Thomas P. Sotiriou. Surface singularities in eddington-inspired born-infeld gravity. *Phys. Rev. Lett.*, 109:251102, Dec 2012. URL: https://link.aps.org/doi/10.1103/PhysRevLett.109.251102, doi:10.1103/PhysRevLett.109.251102.

[150] Vasileios Paschalidis and Nikolaos Stergioulas. Rotating stars in relativity. *Living Reviews in Relativity*, 20(1):7, Nov 2017. doi:10.1007/s41114-017-0008-x.

[151] J. M. Pearson, N. Chamel, S. Goriely, and C. Ducoin. Inner crust of neutron stars with mass-fitted skyrme functionals. *Phys. Rev. C*, 85:065803, Jun 2012. URL: https://link.aps.org/doi/10.1103/PhysRevC.85.065803, doi:10.1103/PhysRevC.85.065803.

[152] J. M. Pearson, S. Goriely, and N. Chamel. Properties of the outer crust of neutron stars from hartree-fock-bogoliubov mass models. *Phys. Rev. C*, 83:065810, Jun 2011. URL: https://link.aps.org/doi/10.1103/PhysRevC.83.065810, doi:10.1103/PhysRevC.83.065810.

[153] R. Penrose. Gravitational collapse: The role of general relativity. *Riv. Nuovo Cim.*, 1:252–276, 1969. doi:10.1023/A:1016578408204.

[154] R. Penrose. *Singularities and time asymmetry*, pages 581–638. 1980.

[155] Roger Penrose. Gravitational collapse and space-time singularities. *Phys. Rev. Lett.*, 14:57–59, Jan 1965. URL: https://link.aps.org/doi/10.1103/PhysRevLett.14.57, doi:10.1103/PhysRevLett.14.57.

[156] E Poisson. Quadratic gravity as hair tonic for black holes. *Classical and Quantum Gravity*, 8(4):639, apr 1991. URL: https://dx.doi.org/10.1088/0264-9381/8/4/009, doi:10.1088/0264-9381/8/4/009.

[157] Potekhin, A. Y., Fantina, A. F., Chamel, N., Pearson, J. M., and Goriely, S. Analytical representations of unified equations of state for neutron-star matter. *Astronomy and Astrophysics*, 560:A48, 2013. doi:10.1051/0004-6361/201321697.

[158] I. Prasetyo, H. Maulana, H. S. Ramadhan, and A. Sulaksono. 2.6 $M_{\odot}$ compact object and neutron stars in eddington-inspired born-infeld theory of gravity. *Phys. Rev. D*, 104:084029, Oct 2021. URL: https://link.aps.org/doi/10.1103/PhysRevD.104.084029, doi:10.1103/PhysRevD.104.084029.

[159] Chatchai Promsiri, Takol Tangphati, Ekapong Hirunsirisawat, and Supakchai Ponglertsakul. Scalarization of planar anti–de sitter charged black holes in einstein-maxwell-scalar theory. *Phys. Rev. D*, 108:024015, Jul 2023. URL: https://link.aps.org/doi/10.1103/PhysRevD.108.024015, doi:10.1103/PhysRevD.108.024015.

[160] Eugen Radu and Elizabeth Winstanley. Conformally coupled scalar solitons and black holes with negative cosmological constant. *Phys. Rev. D*, 72:024017, Jul 2005. URL: https://link.aps.org/doi/10.1103/PhysRevD.72.024017, doi:10.1103/PhysRevD.72.024017.

[161] Jocelyn S. Read, Benjamin D. Lackey, Benjamin J. Owen, and John L. Friedman. Con-

straints on a phenomenologically parametrized neutron-star equation of state. *Phys. Rev. D*, 79:124032, Jun 2009. URL: https://link.aps.org/doi/10.1103/PhysRevD.79.124032, doi:10.1103/PhysRevD.79.124032.

[162] H. Reissner. Über die Eigengravitation des elektrischen Feldes nach der Einsteinschen Theorie. *Annalen der Physik*, 355(9):106–120, January 1916. doi:10.1002/andp.19163550905.

[163] Clifford E. Rhoades and Remo Ruffini. Maximum mass of a neutron star. *Phys. Rev. Lett.*, 32:324–327, Feb 1974. URL: https://link.aps.org/doi/10.1103/PhysRevLett.32.324, doi:10.1103/PhysRevLett.32.324.

[164] Roger W. Romani, D. Kandel, Alexei V. Filippenko, Thomas G. Brink, and WeiKang Zheng. Psr j0952–0607: The fastest and heaviest known galactic neutron star. *The Astrophysical Journal Letters*, 934(2):L17, jul 2022. URL: https://dx.doi.org/10.3847/2041-8213/ac8007, doi:10.3847/2041-8213/ac8007.

[165] James H. C. Scargill, Máximo Banados, and Pedro G. Ferreira. Cosmology with eddington-inspired gravity. *Phys. Rev. D*, 86:103533, Nov 2012. URL: https://link.aps.org/doi/10.1103/PhysRevD.86.103533, doi:10.1103/PhysRevD.86.103533.

[166] Karl Schwarzschild. On the gravitational field of a mass point according to Einstein's theory. *Sitzungsber. Preuss. Akad. Wiss. Berlin (Math. Phys.)*, 1916:189–196, 1916. arXiv:physics/9905030.

[167] Rajibul Shaikh and Pankaj S. Joshi. Gravitational collapse in (2+1)-dimensional eddington-inspired born-infeld gravity. *Phys. Rev. D*, 98:024033, Jul 2018. URL: https://link.aps.org/doi/10.1103/PhysRevD.98.024033, doi:10.1103/PhysRevD.98.024033.

[168] Y.-H. Sham, L.-M. Lin, and P. T. Leung. Radial oscillations and stability of compact stars in eddington-inspired born-infeld gravity. *Phys. Rev. D*, 86:064015, Sep 2012. URL: https://link.aps.org/doi/10.1103/PhysRevD.86.064015, doi:10.1103/PhysRevD.86.064015.

[169] Irwin I. Shapiro. Fourth test of general relativity. *Phys. Rev. Lett.*, 13:789–791, Dec 1964. URL: https://link.aps.org/doi/10.1103/PhysRevLett.13.789, doi:10.1103/PhysRevLett.13.789.

[170] Stuart L. Shapiro and Saul A. Teukolsky. *Neutron Star Models: Masses and Radii*, chapter 9, pages 264–266. John Wiley & Sons, Ltd, 1983. URL: https://onlinelibrary.wiley.com/doi/abs/10.1002/9783527617661.ch9, arXiv:https://onlinelibrary.wiley.com/doi/pdf/10.1002/9783527617661.ch9, doi:10.1002/9783527617661.ch9.

[171] Graham M Shore. Radiatively induced spontaneous symmetry breaking and phase transitions in curved spacetime. *Annals of Physics*, 128(2):376–424, 1980. URL: https://www.sciencedirect.com/science/article/pii/0003491680903267, doi:10.1016/0003-4916(80)90326-7.

[172] Edward V. Shuryak. Quantum chromodynamics and the theory of superdense matter. *Physics Reports*, 61(2):71–158, 1980. URL: https://www.sciencedirect.com/science/article/pii/0370157380901052, doi:10.1016/0370-1573(80)90105-2.

[173] P.J. Siemens and V.R. Pandharipande. Neutron matter computations in bruckner and variational theories. *Nuclear Physics A*, 173(3):561–570, 1971. URL: https://www.sciencedirect.com/science/article/pii/0375947471909717, doi:10.1016/0375-9474(71)90971-7.

[174] Yu.A. Simonov. The quark compound bag model and the jaffe-low p-matrix. *Physics Letters B*, 107(1):1–4, 1981. URL: https://www.sciencedirect.com/science/article/pii/0370269381911333, doi:10.1016/0370-2693(81)91133-3.

[175] Michael Simpson and Roger Penrose. Internal instability in a reissner-nordström black hole. *International Journal of Theoretical Physics*, 7:183–197, 1973.

[176] Hajime Sotani and Umpei Miyamoto. Properties of an electrically charged black hole in eddington-inspired born-infeld gravity. *Phys. Rev. D*, 90:124087, Dec 2014. URL: https://link.aps.org/doi/10.1103/PhysRevD.90.124087, doi:10.1103/PhysRevD.90.124087.

[177] Hajime Sotani and Umpei Miyamoto. Strong gravitational lensing by an electrically charged black hole in eddington-inspired born-infeld gravity. *Phys. Rev. D*, 92:044052, Aug 2015. URL: https://link.aps.org/doi/10.1103/PhysRevD.92.044052, doi:10.1103/PhysRevD.92.044052.

[178] A. A. Starobinskii. The perturbation spectrum evolving from a nonsingular initially de-sitter cosmology and the microwave background anisotropy. *Soviet Astronomy Letters*, 9:302–304, jun 1983.

[179] A.A. Starobinsky. A new type of isotropic cosmological models without singularity. *Physics Letters B*, 91(1):99–102, 1980. URL: https://www.sciencedirect.com/science/article/pii/037026938090670X, doi:10.1016/0370-2693(80)90670-X.

[180] Alexei A. Starobinsky. Nonsingular model of the universe with the quantum gravitational de Sitter stage and its observational consequences. In *Second Seminar on Quantum Gravity*, 1981.

[181] Leonard Susskind. *The black hole war: My battle with Stephen Hawking to make the world safe for quantum mechanics*. Hachette UK, 2008.

[182] Oliver J. Tattersall, Pedro G. Ferreira, and Macarena Lagos. Speed of gravitational waves and black hole hair. *Phys. Rev. D*, 97:084005, Apr 2018. URL: https://link.aps.org/doi/10.1103/PhysRevD.97.084005, doi:10.1103/PhysRevD.97.084005.

[183] Richard C. Tolman. Static solutions of einstein's field equations for spheres of fluid. *Phys. Rev.*, 55:364–373, Feb 1939. URL: https://link.aps.org/doi/10.1103/

PhysRev.55.364, doi:10.1103/PhysRev.55.364.

[184] Ryoyu Utiyama and Bryce S. DeWitt. Renormalization of a classical gravitational field interacting with quantized matter fields. *Journal of Mathematical Physics*, 3(4):608–618, 07 1962. arXiv:https://pubs.aip.org/aip/jmp/article-pdf/3/4/608/19167505/608_1_online.pdf, doi:10.1063/1.1724264.

[185] D. Vautherin and D.M. Brink. Hartree-fock calculations with skyrme's interaction. *Physics Letters B*, 32(3):149–153, 1970. URL: https://www.sciencedirect.com/science/article/pii/0370269370904582, doi:10.1016/0370-2693(70)90458-2.

[186] Anshuman Verma, Asim Kumar Saha, and Ritam Mallick. Comparison of equations of state for neutron stars with first-order phase transitions: A qualitative study. *The Astrophysical Journal*, 985(1):1, may 2025. doi:10.3847/1538-4357/adcee0.

[187] J.D Walecka. A theory of highly condensed matter. *Annals of Physics*, 83(2):491–529, 1974. URL: https://www.sciencedirect.com/science/article/pii/0003491674902085, doi:10.1016/0003-4916(74)90208-5.

[188] Shao-Wen Wei, Ke Yang, and Yu-Xiao Liu. Black hole solution and strong gravitational lensing in eddington-inspired born–infeld gravity. *The European Physical Journal C*, 75(6):253, Jun 2015. doi:10.1140/epjc/s10052-015-3469-7.

[189] John Archibald Wheeler. The lesson of the black hole. *Proceedings of the American Philosophical Society*, 125(1):25–37, 1981. URL: http://www.jstor.org/stable/986184.

[190] Clifford M. Will. The confrontation between general relativity and experiment. *Living Reviews in Relativity*, 17(1):4, Jun 2014. doi:10.12942/lrr-2014-4.

[191] Elizabeth Winstanley. On the existence of conformally coupled scalar field hair for black holes in (anti-)de sitter space. *Foundations of Physics*, 33(1):111–143, Jan 2003. doi:10.1023/A:1022871809835.

[192] Elizabeth Winstanley. Dressing a black hole with non-minimally coupled scalar field hair. *Classical and Quantum Gravity*, 22(11):2233, may 2005. URL: https://dx.doi.org/10.1088/0264-9381/22/11/020, doi:10.1088/0264-9381/22/11/020.

[193] Kent Yagi, Leo C. Stein, Nicolás Yunes, and Takahiro Tanaka. Post-newtonian, quasi-circular binary inspirals in quadratic modified gravity. *Phys. Rev. D*, 85:064022, Mar 2012. URL: https://link.aps.org/doi/10.1103/PhysRevD.85.064022, doi:10.1103/PhysRevD.85.064022.

[194] Ke Yang, Xiao-Long Du, and Yu-Xiao Liu. Linear perturbations in eddington-inspired born-infeld gravity. *Phys. Rev. D*, 88:124037, Dec 2013. URL: https://link.aps.org/doi/10.1103/PhysRevD.88.124037, doi:10.1103/PhysRevD.88.124037.

[195] Stoytcho S. Yazadjiev, Daniela D. Doneva, Kostas D. Kokkotas, and Kalin V. Staykov. Non-perturbative and self-consistent models of neutron stars in R-squared gravity. *Journal*

of Cosmology and Astroparticle Physics, 2014(06):003–003, jun 2014. URL: https://doi.org/10.1088%2F1475-7516%2F2014%2F06%2F003, doi:10.1088/1475-7516/2014/06/003.

[196] De-Cheng Zou and Yun Soo Myung. Scalarized charged black holes with scalar mass term. *Phys. Rev. D*, 100:124055, Dec 2019. URL: https://link.aps.org/doi/10.1103/PhysRevD.100.124055, doi:10.1103/PhysRevD.100.124055.

[197] Feryal Özel and Paulo Freire. Masses, radii, and the equation of state of neutron stars. *Annual Review of Astronomy and Astrophysics*, 54(1):401–440, 2016. arXiv:https://doi.org/10.1146/annurev-astro-081915-023322, doi:10.1146/annurev-astro-081915-023322.